A smut hybrid provides insights into the regulation of effector genes contributing to tumor formation of *Ustilago maydis*

Inaugural-Dissertation

zur Erlangung des Doktorgrades der Naturwissenschaften
Dr. rer. nat.

der Mathematisch-Naturwissenschaftlichen Fakultät
der Universität zu Köln

vorgelegt von

M. Sc. Janina Werner

geb. 25.06.1994, Kaiserslautern

Köln, Juni 2024

A smut hybrid provides insights into the regulation of effector genes contributing to tumor formation of *Ustilago maydis*

Inaugural-Dissertation

zur Erlangung des Doktorgrades der Naturwissenschaften
Dr. rer. nat.

der Mathematisch-Naturwissenschaftlichen Fakultät
der Universität zu Köln

vorgelegt von

M. Sc. Janina Werner

geb. 25.06.1994, Kaiserslautern

Köln, Juni 2024

Die Untersuchungen der vorliegenden Arbeit wurden im Zeitraum von Februar 2020 bis Mai 2024 am Lehrstuhl für Terrestrische Mikrobiologie der Universität zu Köln unter der Leitung von Herrn Prof. Dr. Gunther Döhlemann durchgeführt.

Erstgutachter:	Prof. Dr. Gunther Döhlemann
Zweitgutachter:	Prof. Dr. Bart Thomma
Prüfungsvorsitzender:	Prof. Dr. Kay Hofmann
Tag der mündlichen Prüfung:	19. September 2024

Erklärung zur Dissertation

gemäß der Promotionsordnung vom 12. März 2020

Hiermit versichere ich an Eides statt, dass ich die vorliegende Dissertation selbstständig und ohne die Benutzung anderer als der angegebenen Hilfsmittel und Literatur angefertigt habe. Alle Stellen, die wörtlich oder sinngemäß aus veröffentlichten und nicht veröffentlichten Werken dem Wortlaut oder dem Sinn nach entnommen wurden, sind als solche kenntlich gemacht. Ich versichere an Eides statt, dass diese Dissertation noch keiner anderen Fakultät oder Universität zur Prüfung vorgelegen hat; dass sie - abgesehen von unten angegebenen Teilpublikationen und eingebundenen Artikeln und Manuskripten - noch nicht veröffentlicht worden ist sowie, dass ich eine Veröffentlichung der Dissertation vor Abschluss der Promotion nicht ohne Genehmigung des Promotionsausschusses vornehmen werde. Die Bestimmungen dieser Ordnung sind mir bekannt. Darüber hinaus erkläre ich hiermit, dass ich die Ordnung zur Sicherung guter wissenschaftlicher Praxis und zum Umgang mit wissenschaftlichem Fehlverhalten der Universität zu Köln gelesen und sie bei der Durchführung der Dissertation zugrundeliegenden Arbeiten und der schriftlich verfassten Dissertation beachtet habe und verpflichte mich hiermit, die dort genannten Vorgaben bei allen wissenschaftlichen Tätigkeiten zu beachten und umzusetzen. Ich versichere, dass die eingereichte elektronische Fassung der eingereichten Druckfassung vollständig entspricht.

Teilpublikation:

Werner, J., Zuo, W. and Doehlemann, G. (2024). CRISPR/Cas9 Ribonucleoprotein-Mediated Mutagenesis in *Sporisorium reilianum*. Bio-protocol 14(8): e4978. DOI: 10.21769/BioProtoc.4978.

(**Chapter 2:** CRISPR/Cas9 Ribonucleoprotein-mediated Mutagenesis in *Sporisorium reilianum*)

_____

Janina Werner

Summary

The smut fungi infect economically important crops such as barley, sorghum, wheat, and maize. The majority of the smuts infect their host systemically, replacing the inflorescences with teliospores. An example is *Sporisorium reilianum*, which can infect maize (*S. reilianum f. sp. zeae*) and sorghum (*S. reilianum f. sp. reilianum*) to cause head smut disease. In contrast, *Ustilago maydis*, the prime model organism of the smuts and a close relative of *S. reilianum*, can form distinct tumors locally at infection sites on both, maize leaves and inflorescences. *U. maydis* and *S. reilianum* have similar genomes and infect the same host, *Zea mays*, providing a promising basis for interspecific hybridization. The objective of this study was to elucidate the molecular mechanisms underlying the different disease progressions observed in *U. maydis* and *S. reilianum*.

An exchange of the mating type genes between the species resulted in the generation of a recombinant hybrid using the mating type system of *S. reilianum* (rUSH). rUSH successfully colonized maize and displayed an *S. reilianum*-like phenotype without the formation of teliospores. RNA sequencing (RNA-seq) was employed to provide insights into the gene expression levels in the binuclear recombinant hybrid strain, which revealed 218 differentially expressed one-to-one effector orthologues in rUSH with three distinct gene expression patterns: *cis*-, *trans*- and hybrid-specific expression. Within these patterns, several downregulated *U. maydis* effector genes were identified mainly residing in gene clusters previously associated with virulence. Therefore, I postulated that *U. maydis* effector genes being downregulated in the non-tumor-forming rUSH may play a role in tumor formation. To test this hypothesis, infection assays were performed with knock-out mutants of the respective effector genes. This resulted in the identification of two novel *U. maydis* virulence factors with a role in tumor formation. As a next step, transcription factors (TFs) that are activated during host infection by *U. maydis* were overexpressed in rUSH to elucidate whether this could lead to a shift towards the *U. maydis* phenotype. Strikingly, the overexpression of the conserved TF Hdp2 of *U. maydis* and *S. reilianum* induced tumor formation in maize seedlings. The utilization of RNA-seq facilitated the identification of five TFs and 41 *U. maydis* effector genes regulated directly or indirectly by Hdp2.

Thus, using rUSH as a tool to investigate the regulation of effector orthologue expression between the two species resulted in the identification of novel virulence factors and the identification of a key TF for tumor formation of *U. maydis*. Future studies aim to elucidate additional elements downstream of Hdp2 to unravel the underlying mechanism of *U. maydis*-induced tumorigenesis.

Abbreviations

AGPs	Arabinogalactan proteins
APS	Ammonium persulfate
ATAC-seq	Transposase-Accessible Chromatin with high-throughput sequencing
bbs	*b*-binding site
Biz1	*b*-dependent zinc finger protein
bE	bEast
bp	Base pairs
BR	Brassinosteroids
BS-seq	Bisulfite sequencing
bW	bWest
cAMP	Cyclic adenosine monophosphate
Cas9	CRISPR-associated protein 9
Cbx	Carboxin
Cce1	Cysteine-rich core effector 1
CDK	Cyclin-dependent kinase
Cds	Coding sequence
ChIP-seq	Chromatin Immunoprecipitation Sequencing
CK	Cytokinin
Clp1	Clampless 1
CR	CRISPR-generated frameshift mutant
CRISPR	Clustered regularly interspaced short palindromic repeats
CW	Cell wall
dpi	Days post inoculation
DTT	Dithiothreitol
ET	Ethylene
ETI	Effector-triggered immunity
Fox1	Forkhead transcription factor 1
GA	Gibberellins
gDNA	Genomic DNA
GO	Gene ontology
GRF1	Growth regulating factor-interacting factor 1
HD	Homeodomain
Hdp2	Homeodomain transcription factor 2
hpi	Hours post inoculation
HR	Homologous recombination
IAA	Auxins (indole-3-acetic acid)
JA	Jasmonic acid
KO	Knock-out
Kb	Kilobases
Log_2FC	Log2 fold change
MAMPs	Microbe-associated molecular pattern
MAPK	Mitogen-activated protein kinase
MCS	Multiple cloning side
Msb2	Multicopy Suppressor of a Budding defect

NLR	Nucleotide-binding leucine-rich repeat receptors
Nlt1	No leaf tumors 1
OE	Overexpression
PAMPs	Pathogen-associated molecular pattern
Pep1	Protein essential during penetration 1
PERK	Proline-rich extensin-like receptor kinase
Pit2	Protein involved in tumors 2
PKA	Protein kinase A
PRE	Pheromone response elements
Prf1	Pheromone response factor 1
PRR	Pattern recognition receptor
PSK	Phytosulphokine
PTI	Pattern-triggered immunity
Rbf1	Regulator of *b*-filament 1
RNAi	RNA interference
RNP	Ribonucleoprotein complex
ROS	Reactive oxygen species
Rsp3	Repetitive secreted protein 3
RT	Room temperature
rUSH	Recombinant *U. maydis* x *S. reilianum* hybrid
rUSH_Umhdp2^{OE}	Recombinant *U. maydis* x *S. reilianum* hybrid overexpressing *Umhdp2* in Um_Smt
rUSH_Srhdp2^{OE}	Recombinant *U. maydis* x *S. reilianum* hybrid overexpressing *Srhdp2* in Um_Smt
SA	Salicylic acid
SAD1	Supressor of apical dominance 1
SCR	Scarecrow
SDS-Page	Sodium dodecyl-sulfate polyacrylamide gel electrophoresis
See1	Seedling efficient effector 1
Sho1	Synthetic High Osmolarity sensitive
Sr_Umt	*S. reilianum U. maydis* mating type mutant
STREME	Sensitive, Thorough, Rapid, Enriched Motif Elicitation
TF	Transcription factor
Tin2	Tumor inducing 2
Tip	TOPLESS-interacting protein
Um_Smt	*U. maydis S. reilianum* mating type mutant
qRT-PCR	Quantitative real-time PCR
WGA	Wheat Germ Agglutinin
wpi	Weeks post inoculation
WT	Wild type
Zfp1	Zinc finger protein 1
ZmGIF1	*Zea mays* GRF1-interacting factor1
ZmSHR1	*Zea mays* short root 1
Δ	Deletion

Table of Contents

Chapter 1: Introduction

1.1 The battlefield: Plants vs. Pathogens

1.1.1 Microbial plant pathogens

Plants are constantly challenged by a multitude of diverse pathogens and can adapt to environmental conditions by genetic regulation or the interaction with other microorganisms (Shen *et al*., 2024). Global climate change and a growing world population threaten sustainable agriculture by shifting the range of pathogens (Jones *et al*., 2024; Seidel *et al*., 2024). An increase in disease outbreaks by altering pathogen evolution and the emergence of new pathogens (Singh *et al*., 2023) are further risks for crop production. However, plant pathogen diseases and pests cause up to 40% yield loss of economically important crops annually (Savary *et al*., 2019; Venbrux *et al*., 2023) and lead to a loss of about 220 billion dollars every year (FAO, 2019). To cope with these challenges, an in-depth understanding of plant-microbe interactions, including the identification of host target genes and breeding for resistance, will be crucial to improve crop yields in the future.

Based on their strategies of nutrient acquisition, plant pathogens can be grouped into three different lifestyles: biotrophic, hemibiotrophic, and necrotrophic (Lo Presti *et al*., 2015). While biotrophic pathogens suppress plant immunity and rely on the living host to acquire nutrients (Lo Presti *et al*., 2015; Xia *et al*., 2020a), necrotrophic pathogens actively induce cell death during early infection stages of infection to feed from dead host cells (Derbyshire & Raffaele, 2023; van Kan, 2006). Hemibiotrophic pathogens initially establish a biotrophic phase with the host which turns into a necrotrophic lifestyle and the uptake of nutrients from the dead host tissue (Horbach *et al*., 2011). The plant host is colonized by a multitude of pathogens, which prompts the plant immune system to recognize the pathogen and initiate a series of defensive responses (Lo Presti *et al*., 2015).

1.1.2 The plant immune system

In response to invaders, plants have developed a variety of defense strategies. These include passive defenses, such as physical barriers (i.e. cuticle, cell wall, stomata) and chemical barriers (i.e. pH, nutrient deprivation, phytoanticipins) as well as active immune defense responses (Priyashantha *et al*., 2023). Plants deploy two layers of immune defense receptors: extracellular membrane-bound receptors for the recognition of apoplastic elicitors and intracellular for cytoplasmic effectors (Boutrot & Zipfel, 2017; Ngou, Jones, *et al*., 2022, Figure 1.1). The first defense response by

the plant is the recognition of molecular signatures of microbes, referred to as microbe-associated molecular patterns (MAMPs) or pathogen-associated molecular patterns (PAMPs), i. e. fungal chitin polymers or bacterial flagellin, by cell-surface pattern recognition receptors (PRRs), which leads to a pathogen-triggered immunity (PTI) and the restriction of pathogen growth (Boutrot & Zipfel, 2017; Couto & Zipfel, 2016; Jones and Dangl, 2006; Ngou, Ding, *et al*., 2022; Zhou & Zhang, 2020). Furthermore, plant-derived immunogenic factors can be recognized by PRRs and can be divided into damage-associated molecular patterns (DAMPs), which are passively released upon damage, and actively released immunomodulatory plant peptides, termed phytocytokines (Hou *et al*., 2021). PRRs are associated with the plasma membrane and are usually receptor-like kinases (RLKs) or receptor-like proteins (RLPs), which lack the kinase domain (Albert *et al*., 2020; Ngou, Ding, *et al*., 2022). Upon elicitor perception by PRRs, typical PTI responses are activated: the production of reactive oxygen species (ROS), the activation of Mitogen-activated protein kinase (MAPK) pathways, callose deposition, transcriptional reprogramming of the host, changes in ion fluxes and more (DeFalco & Zipfel, 2021; Lo Presti *et al*., 2015; Macho & Zipfel, 2014; X. Yu *et al*., 2017). For successful colonization of the host, a pathogen must evade the PTI response by either suppressing or coping with it (Lo Presti *et al*., 2015). Fungal pathogens of different lifestyles secrete secondary metabolites and effectors. These can either kill the host cell to feed the pathogen (hemibiotrophs in the necrotrophic phase and necrotrophs) or suppress the host immune response and manipulate host physiology (biotrophs) (Lo Presti *et al*., 2015). Pathogens have developed strategies to circumvent, manipulate, or disrupt host barriers, regardless of their lifestyle using so-called ‘effectors’ (Remick *et al*., 2023). Effectors are small molecules, secreted during infection which can alter several processes in the host (Hogenhout *et al*., 2009). Although pathogen effectors can suppress PTI, they can also be recognized by intracellular nucleotide-binding leucine-rich repeat receptors (NLRs), which are encoded by plant resistance genes (Lo Presti *et al*., 2015; Ngou, Ding, *et al*., 2022). The perception of effector genes by intracellular nucleotide-binding, leucine-rich repeat (NB-LRR) receptor (NLR) proteins leads to the activation of effector-triggered immunity (ETI) (Jones and Dangl, 2006; Ngou, Ding, *et al*., 2022, Figure 1.1). Compared to PTI, ETI responses are highly specific against adapted pathogens and are qualitatively stronger and faster, leading to localized cell death, which is known as hypersensitive response (Dodds & Rathjen, 2010). However, the strict discrimination between PTI and ETI is increasingly challenged by findings made throughout the last decade (Bentham *et al*., 2020). Today, plant immunity is proposed to be based on the side of microbial recognition, intracellular or extracellular (Dodds *et al*., 2024; van der Burgh & Joosten, 2019; Zhang *et al*., 2020).

In their natural environment, plants are subjected to a multitude of abiotic and biotic stresses. In response, they have evolved an intricate hormone-controlled network that enables them to adapt to

these diverse environmental conditions (Aerts *et al*., 2021). The plant produces a variety of hormones that regulate growth and developmental processes, as well as immunity against abiotic and biotic stresses. Depending on the pathogen's infection style, the phytohormones salicylic acid (SA), jasmonate (JA), and ethylene (ET) are known to play major roles in defense responses (Bari & Jones, 2009; Glazebrook, 2005). While SA is involved in defense responses against biotrophic and hemibiotrophic pathogens, as well as in the establishment of systemic acquired resistance (SAR) (Grant & Lamb, 2006), JA/ET can be associated with the defense against necrotrophic pathogens (Bari & Jones, 2009; Glazebrook, 2005).

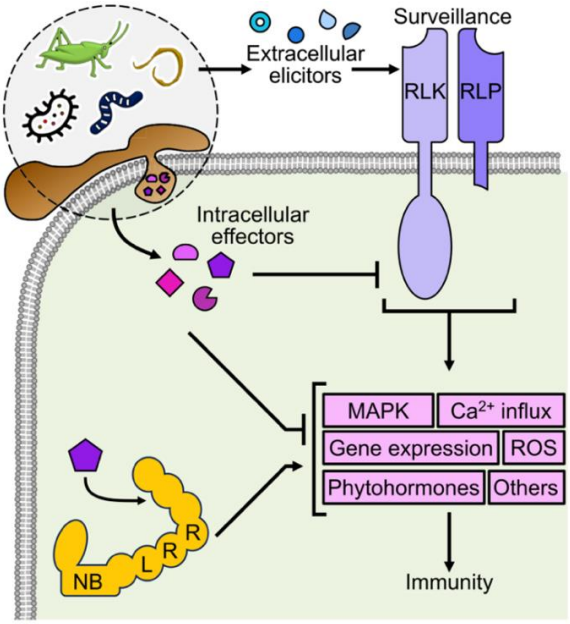

Figure 1.1: Schematic overview of the plant immune system. For the recognition of extracellular elicitors such as conserved molecular patterns, plants use membrane-bound immune receptors such as RLKs and RLPs. Pathogens also secrete intracellular effectors to suppress or manipulate the host. The perception of intracellular effectors by immune receptors, mainly NLRs, leads similarly as for the RLK or RPL recognition to the same downstream responses: MAPK activation, calcium influx, gene expression, ROS, production of phytohormones, and more. Compared to RLK and RLP, NLR responses are generally stronger and lead more often to cell death (Dodds *et al*., 2024).

1.1.3 Manipulation of plant immune system by effectors

Although plant pathogens exhibit diverse infection styles, they share a common trait of secreting effectors to modulate host cellular processes. The co-evolutionary 'arms race' between the defense system of plants and the effector repertoire of pathogens drives the interaction and constant adaptation in plant-microbe interactions (Lanver *et al*., 2017; Uhse & Djamei, 2018). Thus, effector repertoires of plant pathogens can be specialized to particular host species or host cultivars (Bourras *et al*., 2018; Depotter & Doehlemann, 2020). The secretion of effector proteins is crucial for successful colonization and the completion of the life cycle of pathogens (Depotter & Doehlemann, 2020). A multitude of

filamentous pathogens provided evidence for a highly regulated synthesis, secretion, and localization of effectors (Uhse & Djamei, 2018). The expression of effectors was described to act in a spatiotemporal manner during specific infection stages (Hacquard *et al*., 2013; Lanver *et al*., 2018; O'Connell *et al*., 2012), in an organ-specific (Skibbe *et al*., 2010) or in a cell-type specific manner (Matei *et al*., 2018). This implies an activation due to the perception of environmental cues (Lanver *et al*., 2010; Uhse & Djamei, 2018). Effector repertoires comprise highly specific, but also conserved effector genes. It has been demonstrated that conserved effectors are shared among different plant pathogens and are preserved during evolution. This suggests the targeting of conserved structures within the plant immune system. In contrast to conserved effectors that are essential for pathogenesis, accessory effectors are more specific and the pathogen can more easily overcome fitness defects in the case of the absence of the effector (Depotter & Doehlemann, 2020). Examples of conserved effectors are the protein essential during penetration 1 (Pep1) of *Ustilago maydis*, which is conserved among the smuts (Hemetsberger *et al*., 2015), or the necrosis-inducing protein 1 (NIS1) of *Magnaporthe oryzae* which is conserved among the Ascomycota and the Basidiomycota (Irieda *et al*., 2019). A loss of conserved effector genes was shown to have high costs for fungal pathogens, as a mutant of Δ*pep1* in *U. maydis* resulted in a loss of penetration ability (Hemetsberger *et al*., 2012) and Δ*nis1* in *M. oryzae* revealed a reduced virulence on rice and barley, respectively (Irieda *et al*., 2019). In contrast, defects caused by the absence of accessory effectors are easier to overcome. This was demonstrated by the effector Ave1 in *Verticilium dahliae*, revealing a lineage-specific presence/absence in the lineages R2 and VdLS17 (de Jonge *et al*., 2012).

Effectors can be further divided based on their site of action in the extracellular space (apoplastic effectors) or after translocation in the intracellular space (cytoplasmic/nuclear effectors). Extracellular effectors can be for example involved in plant immunity by the inhibition of plant proteases (Mueller *et al*., 2013; Rooney *et al*., 2005), sequestering chitin (De Jonge *et al*., 2010), detoxifying secondary metabolites (Ökmen *et al*., 2013) or in the inhibition of a host peroxidase (Hemetsberger *et al*., 2012). Intracellular effectors are described to act in the innate immune pathways/metabolic pathways, transcription machinery of the host (Zuo *et al*., 2023), hormone pathways (Wang *et al*., 2016; Zhang *et al*., 2021), epigenetic modification (Li *et al*., 2018) and the RNAi machinery (Harris *et al*., 2023). The translocation of effectors into the host cell can take place via the conventional ER-Golgi-dependent secretory pathway with an N-terminal signal (Lo Presti *et al*., 2015) or unconventionally, for effector genes lacking an N-terminal signal peptide (Li *et al*., 2023). For *U. maydis* an effector translocation complex was proposed, which comprises five unrelated conserved effectors and two membrane proteins, all highly expressed during the pathogenic development and crucial for the virulence of *U. maydis* (Ludwig *et al*., 2021).

1.2 The Ustilaginales

The Ustilaginales, or smut fungi, represent the second largest group of plant pathogens within the Basidiomycota. They cause diseases on several cereal crops of the Poaceae family, including maize, wheat, barley, sorghum, and sugarcane (Bakkeren *et al*., 2008; Begerow *et al*., 2004; Zuo *et al*., 2019). Commonly, smuts exhibit a biotrophic lifestyle with a narrow host range, relying on the living host for the uptake of nutrients (Benevenuto *et al*., 2018; van der Linde & Göhre, 2021). The intensive study of smut fungi was driven by the need to understand the causes of a significant reduction in the yields of economically important crops (Bakkeren *et al*., 2008).

The major characteristic among the smuts is the production of massive amounts of dark melanized teliospores, typically in the host floral organs (Bakkeren *et al*., 2008; Morrow & Fraser, 2009; Zuo *et al*., 2019). Thus, the majority of smuts spread systemically in their host, without evident symptoms during the vegetative growth stage. In a later infection stage, they replace the female and male inflorescences with teliospores (Groth, 1967; Laurie *et al*., 2012; Martinez *et al*., 1999). Smut fungi colonize the vascular system until they reach the apical meristem, where symptom development takes place. A well-studied example of the systemic infection is *Sporisorium reilianum*, which is able to infect maize (*Sporisorium reilianum f. sp. zeae*) and sorghum (*Sporisorium reilianum f. sp. reilianum*), respectively. A typical characteristic among the smuts is their dimorphic life cycle (Figure 1.2): a haploid saprophytic yeast-like stage and the pathogenic dikaryotic filament *in planta*. The pathogenesis-related phase is initiated with a successful mating event. The dimorphic life cycle is initiated when teliospores germinate under favorable conditions (Figure 1.2a). Following meiosis, four haploid basidiospores are segregated in the promycelium. After mitosis, they are released and can divide by budding (Lanver *et al*., 2017; Saville *et al*., 2012). Upon encountering a compatible partner, the growth of the haploid basidiospores is facilitated by the perception of pheromones, which initiates the development of conjugation tubes and a process of growth toward the partner (Figure 1.2b). They can fuse and form a dikaryotic cell-cycle arrested filament. On the plant surface, the dikaryotic filament differentiates into a specialized, unmelanized appressoria-like structure (Figure 1.2c), to directly penetrate the plant surface (Figure 1.2d). During the formation of appressoria-like structures, the conserved transmembrane receptors Synthetic High Osmolarity sensitive (Sho1) and Multicopy Suppressor of a Budding defect (Msb2) play a crucial role in the perception of external stimuli (Lanver *et al*., 2010; Liu *et al*., 2011; Perez-Nadales & Di Pietro, 2015; Xia *et al*., 2020b). An exception within the smuts is *Ustilago maydis*, the common corn smut pathogen, which infects all aerial parts of *Zea mays* and teosinte (*Zea mays ssp. parviglumis and ssp. mexicana;* ancestors of maize) (Christensen, 1963), respectively. Unlike the majority of cereal smuts, *U. maydis* forms local tumors in the infection site within 4-7 days and teliospores develop within 2 weeks (Zuo *et al*., 2019, Figure 1.2e+k). Another example of a

tumor-inducing smut pathogen is *Melanopsichium pennsylvanicum* (Figure 1.2l), which infects *Persicaria* species (Sharma *et al*., 2014). Further examples of smuts with distinct characteristics are *Ustilago hordei*, which can form haustoria-like structures during colonization, and *U. bromivora* where the timing of mating is crucial to determine about life or death (Figure 1.2n).

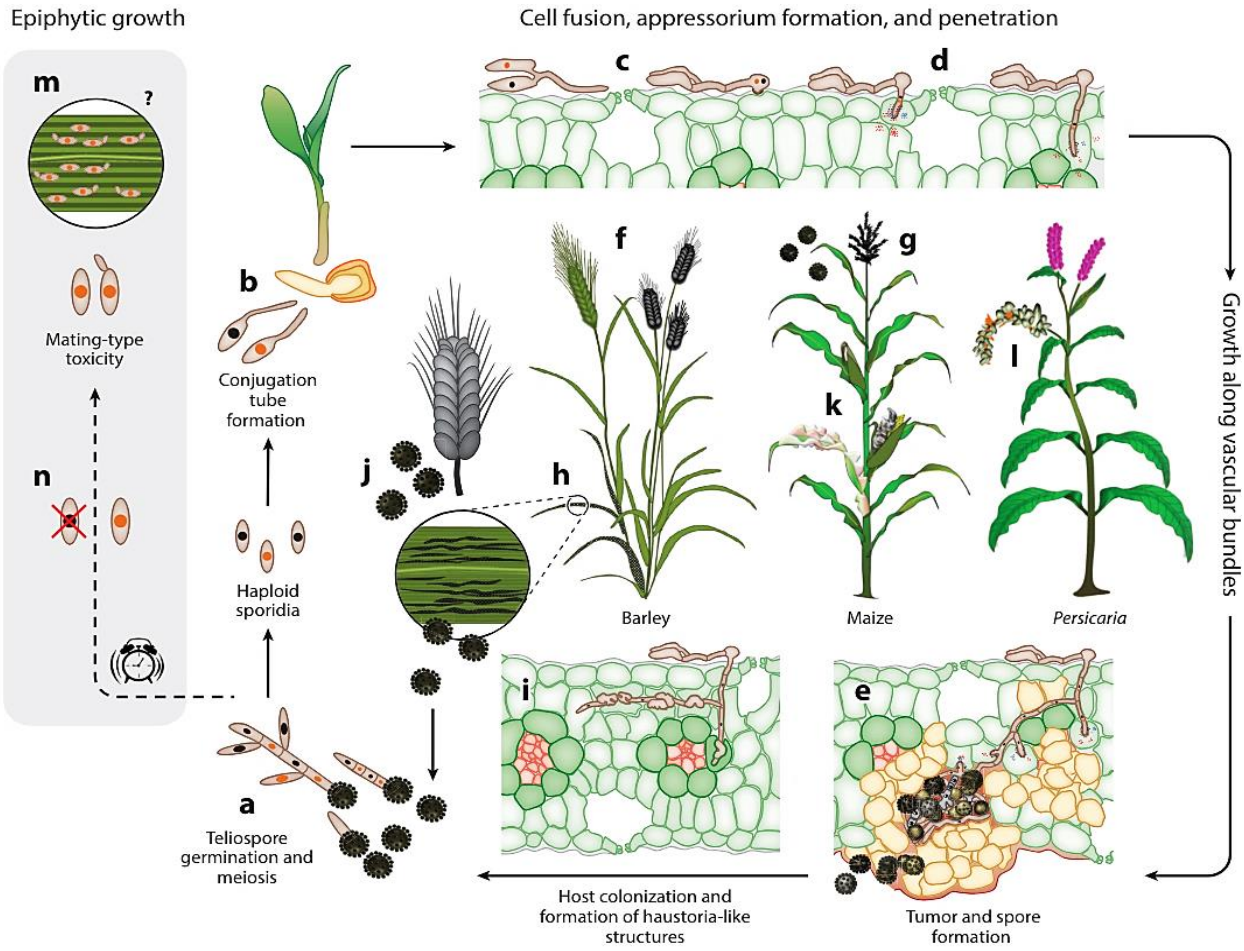

Figure 1.2: The dimorphic life cycle of smut fungi. (a) Under favorable conditions, teliospores germinate and **(b)** release after meiosis four haploid basidiospores. After recognition of a compatible mating partner, the haploid sporidia sense each other through a pheromone-receptor system and grow towards each other, forming a conjugation tube. **(c)** On the plant surface, the two compatible sporidia fuse and form a dikaryotic hyphae. **(d)** Appressoria-like structures are formed to directly penetrate the plant surface. **(e)** During infection, effector genes are secreted to modulate host defense. **(f)** *Ustilago hordei* and **(g)** *Sporisorium reilianum* spread systemically in barley and maize, respectively, and in a late infection stage replace the inflorescences with teliospores. For the majority of the smuts, the sporulation takes place in the floral tissues and rarely in the leaves (strip smut) **(h)**. **(i)** *U. hordei* can form haustoria-like structures during colonization. **(j)** At a late infection stage, sori break open and release teliospores, which under favorable conditions can germinate, where the life cycle starts again. In contrast to the majority of the smuts, *Ustilago maydis* **(k)** and *Melanopsichium pennsylvanicum* **(l)** form local tumors on their host. **(m)** Some smuts were isolated in their anamorphic form and are considered to be epiphytic. **(n)** If two mating types of *Ustilago bromivora* do not mate in a certain time, it was proposed that one of them dies due to mating type toxicity (Figure taken from Zuo *et al*., 2019).

1.2.1 The mating type system of smut fungi

In smut fungi, sex and pathogenic development are tightly linked (Bakkeren *et al*., 2008). Sexual compatibility in smuts requires a self- vs. non-self-recognition (Bakkeren & Kronstad, 1994), which is mediated by the mating type system, comprising two specific loci (Figure 1.3). Different studies of model organisms revealed a high conservation of the mating-dependent signaling network across large phylogenetic distances (Devier *et al*., 2009; Kües, 2000; Li *et al*., 2010; Ohm *et al*., 2010; Vollmeister *et al*., 2012). In smuts, the mating type loci comprise highly conserved genes. Molecular analysis of the mating system in *U. maydis*, *S. reilianum* and *U. hordei* revealed differences in locus structure (Bakkeren *et al*., 2000). In general, mating is regulated by the *a* locus and the *b* locus. In *U. maydis* and *S. reilianum*, the mating type loci *a* and *b* segregate independently and are not physically linked, indicating a tetrapolar mating type system. In contrast, *U. hordei* comprises a bipolar mating type locus (MAT-1 and MAT-2), where the mating type loci are physically linked.

The *a* locus is crucial for cell-cell recognition and encompasses genes encoding for pheromones (*mfa*) and receptors (*pra*) (Bakkeren *et al*., 2008). For *U. maydis* and *U. hordei*, a comparison of the *a* locus revealed two alleles with one pheromone and one receptor (G-protein-coupled seven-transmembrane protein) per locus (Anderson *et al*., 1999; Bakkeren & Kronstad, 1996; Michael Bölker *et al*., 1992) and different sequences of the *a1* (4 kb) and the *a2* loci (>8 kb) (Bakkeren *et al*., 2008). The *a2* locus additionally contains specific genes: *rga2* and *lga2* with a possible role in uniparental inheritance (Bortfeld *et al*., 2004; Urban *et al*., 1996). *S. reilianum* harbors three *a* locus alleles, *a1*, *a2,* and *a3*. While *Sra1* and *Sra2* are syntenic to *a1* and *a2* of *U. maydis* and *U. hordei* with one additional pheromone encoding gene per allele, the *a3* allele encodes for one pheromone receptor and two pheromone genes, which recognize *a1* and *a2* partners, respectively (Schirawski *et al*., 2005). Among the species *U. maydis*, *S. reilianum,* and *U. hordei*, the *a* loci encode for small pheromone precursors of approximately 40 amino acids (aa), which undergo posttranslational modification to yield 9-14 aa mature peptides (Bakkeren *et al*., 2008; Kosted *et al*., 2000; Schirawski *et al*., 2005; Spellig *et al*., 1994). The initiation of the life cycle starts with the recognition of compatible sporidia, which are capable of sensing each other through a pheromone-receptor system on the plant surface, encoded by the *a* locus. The recognition of a compatible mating partner by pheromones results in the formation of conjugation tubes oriented by a pheromone gradient (Snetselaar *et al*., 1996; Spellig *et al*., 1994), and in the fusion of the sporidia (Snetselaar & Mims, 1992) which leads to a G2 cell cycle arrest (Bölker, 2001; García-Muse *et al*., 2003; Spellig *et al*., 1994). Upon perception of the pheromone by the receptor, two signaling cascades are activated: a MAPK- and a cyclic adenosine monophosphate (cAMP)-dependent protein kinase A (PKA) pathway. The MAPK pathway is crucial for mating and virulence (Müller *et al*., 2003) and consists of MAPK kinase kinase Kpp4/Ubc4 (Andrews *et al*., 2000;

Müller *et al*., 2003), the MAPK kinase Fuz7/Ubc5 (Andrews *et al*., 2000) and the MAPK Kpp2/Ubc2 (Mayorga & Gold, 2001; Müller *et al*., 1999). The MAPK- and the PKA- signaling cascades activate the transcription factor (TF) Prf1 by phosphorylation, which is the key player in the activation of *a* locus-regulated genes, harboring pheromone-responsive elements (PREs) (Hartmann *et al*., 1996). Due to several sequence motifs specific for PKA- and MAPK-dependent phosphorylation in Prf1, Hartmann *et al*. (1996) provided further evidence that the signaling of the cascades links the filamentous growth and the pathogenic development. Prf1 can be phosphorylated through the PKA Adr1, which leads to the induction of the *a* genes, while the induction of the *b* genes requires the phosphorylation of the MAPK Kpp2 (Kaffarnik *et al*., 2003).

The multi-allelic *b* locus of the mating type system encodes for the homeodomain (HD) TF subunits, bEast (bE) and bWest (bW). A high synteny of the *b* mating type genes of *U. maydis*, *S. reilianum,* and *U. hordei* MAT-1 has been shown (Bakkeren *et al*., 2008). Two different *b* alleles have been described in *U. hordei*, five different alleles in *S. reilianum,* and at least 19 different alleles of the *b* locus in *U. maydis* (Bakkeren & Kronstad, 1994; Schirawski *et al*., 2005). For the *b* locus, self- vs. non-self-recognition takes place. If different alleles of the *b* locus recognize each other, bE and bW can form a heterodimeric TF complex, and a stable cell-cycle arrested dikaryotic filament is formed (Bölker, 2001). While the C-terminus of diverse *b* alleles is highly conserved and important for DNA binding, the N-terminus is variable and comprises interaction domains, important for the dimerization of the two HD proteins (Gillissen *et al*., 1992; Kronstad & Leong, 1990; Schulz, *et al*. 1990). Since the *b* locus is multi-allelic, several different combinations lead to filament formation and pathogenicity (Kahmann & Bölker, 1996). A total of 345 differentially expressed b-regulated genes were identified (Heimel *et al*., 2010b) and classified into two categories based on their direct or indirect binding. Class 1 of *b*-regulated genes revealed a *bbs* motif in the promoter region, indicating a direct binding of the *b*-heterodimer (Brachmann *et al*., 2001; Romeis *et al*., 2000), while class 2 genes, which comprise the larger group of *b*-regulated genes, are indirectly regulated. Among the class 2 *b*-regulated genes, *rbf1* and other TFs were identified (Heimel *et al*., 2010b), reflecting a hierarchical network of transcriptional regulation downstream of the b-heterodimer. Further, Schirawski *et al*. (2005) showed that both b proteins from *S. reilianum* can functionally replace the b proteins from *U. maydis*. However, the substitution led to reduced virulence as a reduced tumor formation has been observed.

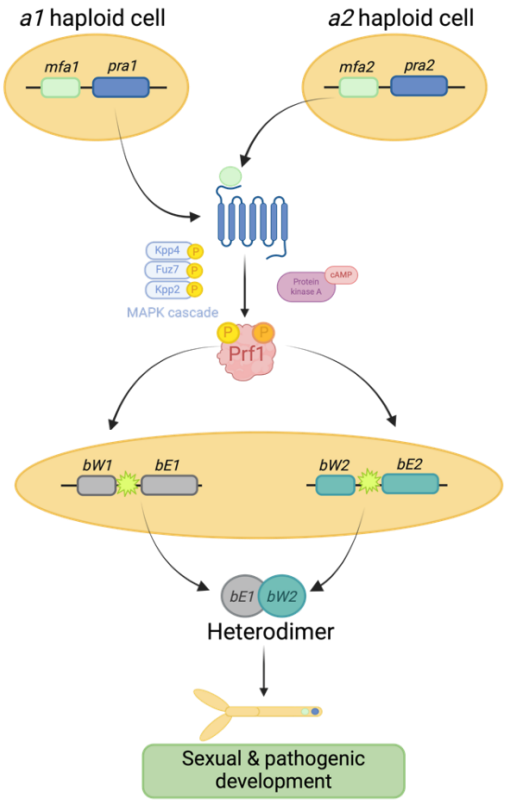

Figure 1.3: The mating type system of *Ustilago maydis and Sporisorium reilianum.* The mating type system can be divided into the *a* locus encoding for precursors of the pheromones (*mfa*) and receptors (*pra*) for recognition of the pheromones, and the *b* locus encoding for a heterodimeric TF complex, consisting of bE and bW important for the pathogenic development *in planta*. Two signaling cascades connect the *a* locus with the *b* locus: a MAPK cascade and a cAMP-dependent PKA. The activation of these signaling cascades leads to the phosphorylation of the TF Prf1 which in turn activates the transcription of the *b* locus (Figure was created with biorender.com).

1.2.2 *Ustilago maydis* - The model organism among the smuts

Ustilago maydis is recognized as one of the top 10 fungal pathogens (Dean *et al*., 2012). Investigations of DNA recombination in *Ustilago* (Holliday, 2004) marked the beginning of it being an excellent model system for studying plant pathogenicity. The rapid development of disease symptoms within two weeks, the ease of cultivation in the laboratory, and the amenability to reverse genetics are the reasons why *U. maydis* has become a model system for further studies (Kahmann *et al*., 2000; Martínez-Espinoza *et al*., 2002; Steinberg & Perez-Martin, 2008).

Furthermore, the transformation and the generation of knock-out (KO) strains in *U. maydis* as well as the generation of the haploid solopathogenic strain SG200 (Bölker *et al*., 1995; Kämper *et al*., 2006) were important steps in the research field. Another breakthrough was the sequencing of the *U. maydis* genome in 2006, which revealed a very compact, gene-dense genome structure with a small number of non-coding insertions and only 6.7% of repetitive sequences (Dutheil *et al*., 2016; Kämper *et al*., 2006).

The small number of introns is likely to reflect the high efficiency of homologous recombination (HR) (Holliday, 2004; Kämper, 2004). Together with the availability of the annotated genome, the availability of microarray and transcriptomic data (Lanver *et al*., 2017) were further steps towards the identification of candidate genes contributing to virulence. The generation of KO mutants was further improved by the establishment of a marker-free CRISPR/Cas9 system in *U. maydis* (Schuster *et al*., 2016; Zuo *et al*., 2020).

1.2.3 Hierarchical network of transcription factors in *Ustilago maydis*

Transcription factors (TFs) can either regulate a small number of genes or act as a master regulator of distinct molecular processes, i.e. during infection. In fungi, only a few master regulators have been reported so far (Heimel *et al*., 2010b; Ruiz-Roldán *et al*., 2015; Tollot *et al*., 2016).

The master regulator of the *b*-filament (Rbf1) in *U. maydis* acts downstream of the heterodimer bE/bW and is directly activated by a *b*-binding site (*bbs*) in the promoter region. The C2H2 zinc finger TF Rbf1 was reported to be required for the regulation of the majority of the *b*-regulated genes as deletion mutants resulted in a loss of pathogenicity (Heimel *et al*., 2010b). Furthermore, the hydrophobicity of the plant surface and the sensing of cutin monomers by Sho1 and Msb2 in *U. maydis* play a pivotal role in the induction of appressoria formation on the plant surface, as well as in the activation of the downstream TFs. In *U. maydis*, a hierarchical network of TFs controls the expression of genes in the sequence of the infection development. Downstream of Rbf1, the homeodomain TF (Hdp2) and the zinc-finger transcription factor (Biz1) regulate the expression of early effector genes (Lanver *et al*., 2014). The underlying mechanism for the activation by Rbf1 is currently unknown, but it is suggested that *rbf1* partially directly regulates the expression of *hdp2* (Jurca, 2021) and the expression of *biz1* indirectly (Ulrich, 2020). Both Biz1 and Hdp2 are essential for the pathogenicity of *U. maydis* and are crucial for the activation of early effector genes (Flor-Parra *et al*., 2006; Heimel *et al*., 2010b). Early effector genes are proposed to deal with the first defense responses of the plant, upon contact of the fungal hyphae with the plant surface (Doehlemann *et al*., 2008).

Biz1 has been described as a TF important for plant penetration, as Δ*biz1* mutants showed a severe reduction in appressoria formation (Flor-Parra *et al*., 2006). Moreover, invading hyphae were arrested in their pathogenic development, suggesting an important role in the regulation of the cell cycle arrest by the downregulation of the mitotic cyclin gene *clb1* (Flor-Parra *et al*., 2006). Clb1 is essential for the G2/M transition in the cell cycle and is required for the distribution of nuclei during cell division of the dikaryon (Heimel *et al*., 2010a). It has been shown, that the interaction of Clb1 with Rbf1 and bW regulates the cell cycle control and ensures the release of the cell cycle arrest during the biotrophic development (Heimel *et al*., 2010a).

Hdp2 belongs to the evolutionary conserved HD TFs. The 60 aa sequence of the HD is a DNA-binding region, including the typical helix-turn-helix (HTH), which determines its role as a TF (Bobola & Merabet, 2017). The expression of *hdp2* was reported to be regulated by Rbf1 upon contact with the leaf surface and by Biz1 after penetration, resulting in the production of two distinct transcripts of *hdp2*, *hdp2*^{L} and *hdp2*^{S}. The expression of the two transcripts is driven by two different promoter regions (Jurca, 2021). It has been demonstrated that Hdp2 is important for the regulation of pathogenicity-related genes since a Δ*hdp2* mutant of *U. maydis* was impaired in tumor formation (Heimel *et al*., 2010b). *In planta* Chromatin Immunoprecipitation Sequencing (ChiP-seq) revealed binding sites for Hdp2 and Biz1 in the same promoter sequences of genes, suggesting an interaction of Hdp2 and Biz1 in the regulation (Jurca, 2021). In contrast to Hdp2 and Biz1, Mrz1 is also involved in the activation of early effector genes, however, it is not crucial for pathogenicity (Zheng *et al*., 2008). During the biotrophic development and disease progression of *U. maydis*, several TFs are activated at different stages of infection. One of these is forkhead transcription factor 1 (Fox1) which was identified to regulate 38 putative effector genes (Zahiri *et al*., 2010). A Δ*fox1* mutant revealed a reduction in virulence and tumor development, reflecting its importance in the regulation of genes important for biotrophic development (Zahiri *et al*., 2010).

For the late disease development of spore formation by *U. maydis*, a TF of the WOPR family, Ros1, was found to regulate 70 late effector genes and to downregulate 128 early effector genes (Tollot *et al*., 2016). Moreover, the differential expression of several b-regulated genes by Ros1 indicated a fundamental change in the regulation of pathogenic development (Tollot *et al*., 2016). Thus, Ros1 was identified as a master regulator of the late disease development of *U. maydis*, leading to a shift from the early to the late effectome (all secreted effector genes of an organism) (Tollot *et al*., 2016). The TF No Leaf Tumors 1 (Nlt1) was found to be important for nuclear fusion, and consequently for tumor induction and spore formation (Lanver *et al*., 2018). *U. maydis* Δ*nlt1* mutants were able to colonize maize leaves, but were attenuated in late proliferation and unable to induce leaf tumors (Lin *et al*., 2021). *S. reilianum*, which does not induce tumors, possesses an orthologue of *nlt1* which is important for the fusion of dikaryotic nuclei in the late infection stage during cob colonization. Furthermore, a regulatory link between *nlt1*, *ros1,* and the effector gene encoding for See1 (seedling efficient effector 1) was proposed to control seedling tumor formation in two stages: *nlt1*-dependent and *nlt1*-independent (Lin *et al*., 2021). In addition, the TF Zpf1 (zinc finger protein 1) has been described to regulate effector genes at various infection stages (Cheung *et al*., 2021). Taken together, the pathogenic development of *U. maydis* is orchestrated by a tightly regulated hierarchical TF network (Figure 1.4).

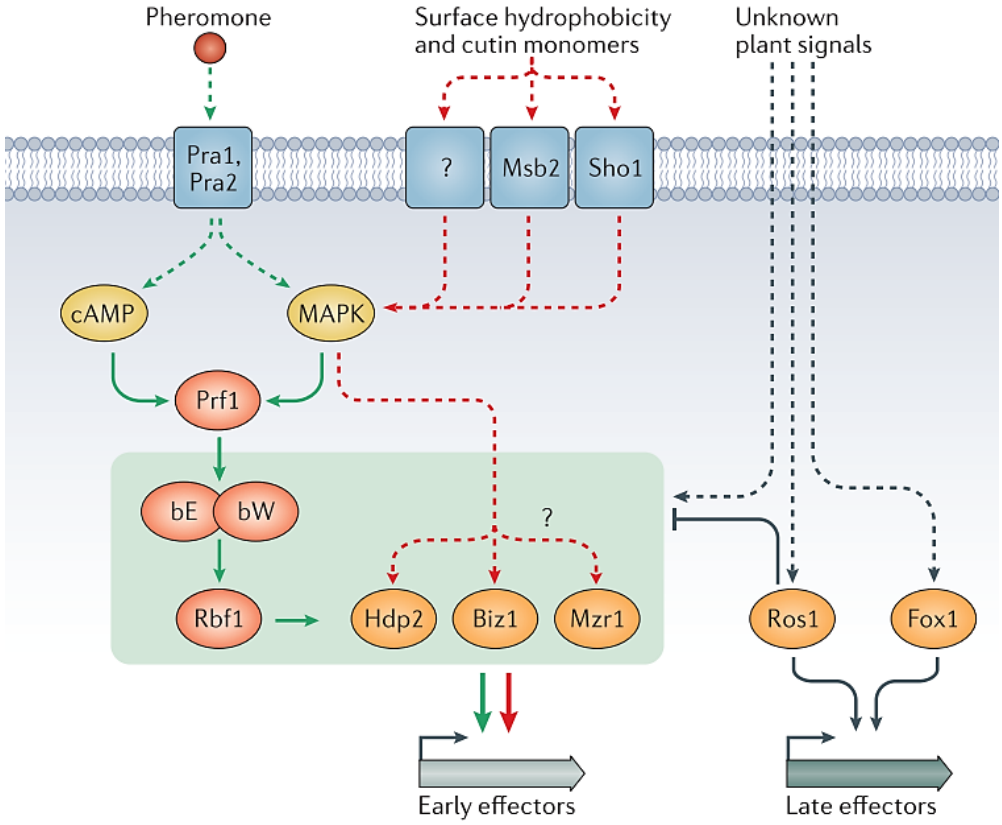

Figure 1.4: Effector gene expression is controlled by a hierarchical network of transcription factors. Left pathway: Recognition of pheromones by the cell surface receptors Pra1 and Pra1 leads to the activation of two conserved signaling pathways: cAMP-dependent PKA and MAPK. The two signaling pathways lead to the phosphorylation of the TF Prf1, which activates the expression of the *b* mating type genes, leading to the formation of the bE-bW heterodimer. bE-bW activates downstream TFs important for the regulation of effector genes. Middle pathway: The perception of the hydrophobicity of the plant surface and cutin monomers by the membrane proteins Msb2 and Sho1 lead to the activation of the MAPK cascade and hence, in the formation of the bE-bW heterodimer. The activation by the pheromones and the plant surface lead together to the activation of expression of the TFs *hdp2* and *biz1*. Hdp2, Biz1, and Mzr1 activate effector genes, when hyphae are present on the leaf surface. The regulation of *mzr1* is still poorly understood. Right pathway: After penetration, the expression of the TFs *ros1* and *fox1* is induced by unknown plant signals which leads to the activation of the late effector gene expression. Ros1 downregulates early effector genes (Figure taken from Lanver *et al*., 2017; modified).

1.2.4 The effector repertoire of *U. maydis*

To enable successful colonization and suppress plant immune responses, *U. maydis* has developed several strategies (Zuo *et al*., 2019), like the reprogramming of the plant metabolism (Djamei *et al*., 2011) or inducing physiological changes for its benefit, i.e. modulating the cell cycle (Redkar *et al*., 2015a; Zuo *et al*., 2023). Genes encoding effectors during the biotrophic development of *U. maydis* are tightly regulated. In total, *U. maydis* encodes 476 small secreted proteins which are predicted effectors, comprising 215 proteins with unknown function (Lanver *et al*., 2018). The genome analysis of *U. maydis* identified 12 clusters encoding for small secreted proteins which comprise

18.2 percent of all predicted secreted proteins of *U. maydis* (Kämper *et al*., 2006). The evolution of effector gene clusters is driven by effector gene duplications and transposable elements (Dutheil *et al*., 2016). In many cases, the KO of individual effector genes did not affect virulence, which suggests that effectors may be functionally redundant or may have a specificity to a certain maize line or maize organ (Schilling *et al*., 2014; Schurack *et al*., 2021; Stirnberg & Djamei, 2016). The majority of the effector genes are co-regulated and are expressed only during infection. For a functional analysis of the cluster, a series of deletion mutants were generated using homologous recombination (HR). Four of the gene cluster mutants revealed a reduction in tumor formation: cluster 5B, 6A, 10A, and 19A. Cluster 6A encodes for five TOPLESS-interacting proteins (Tips) that are involved in the modulation of maize auxin signaling (Bindics *et al*., 2022). Cluster 19A is the largest gene cluster identified and encodes for 24 secreted effector proteins. A deletion mutant of cluster 19A was unable to induce large tumors and failed to develop teliospores. This suggests a potential role for some of the proteins encoded by cluster 19A in tumor formation (Kämper *et al*., 2006). Furthermore, it was found that one cluster 19A effector is responsible for *U. maydis*-induced anthocyanin formation: Tin2 (Brefort *et al*., 2014; Tanaka *et al*., 2014). The 24 secreted proteins of cluster 19A were further separated into sub-deletions for functional analysis (Brefort *et al*., 2014). This identified several genes within cluster 19A that significantly contribute to virulence (Brefort *et al*., 2014).

1.2.4.1 Molecular functions of *U. maydis* effectors

To establish a host interaction, *U. maydis* secretes a plethora of effectors modulating the extracellular plant immunity, contributing to different extends to the pathogen's fitness (Djamei *et al*., 2023). Effectors can be classified according to their genomic location into two categories: core effectors that are essential for the pathogen's virulence, and diversified accessory effectors that reflect a lower cost for the pathogen upon deletion (Depotter & Doehlemann, 2020).

Two examples of core effectors for the early infection phase are Pep1 and Cce1, which are both essential for virulence and have been recently described as part of the cell surface-exposed 'Stp effector complex' (Ludwig *et al*., 2021). Mutant strains of *pep1* or *cce1* lead to the accumulation of H_2O_2 and callose deposition, respectively (Doehlemann *et al*., 2009; Seitner *et al*., 2018). Thus, Pep1 and Cce1 play a vital role in the inhibition of the early immune responses in maize, important for *U. maydis* virulence. Further, the effector Pit2 was identified which is essential for virulence and tumor formation (Mueller *et al*., 2013). Via an inter-kingdom conserved inhibitory motif of 14 amino acids (PID14), Pit2 inhibits apoplastic cysteine proteases to modulate plant immunity by interference with SA-related plant defenses (Misas Villamil *et al*., 2019; Mueller *et al*., 2013). Rsp3, an effector important for virulence and anthocyanin formation contains a conserved virulence-promoting function by shielding fungal hyphae

from maize antifungal proteins (Ma *et al*., 2018). Collectively, apoplastic effectors of *U. maydis* function to prevent the recognition of extracellular immune receptors, the inhibition of systemic immune signals, and the detoxification of host defense compounds (Djamei *et al*., 2023).

After translocation into the host cell, intracellular effectors interfere with several host processes such as intracellular signaling, metabolic regulation, or host transcription machinery. Cmu1, which interacts with the maize cytosolic chorismate mutase ZmCM1, leads to a decrease of chorismate levels in the SA pathway (Djamei *et al*., 2011). Tin2, an example involved in the manipulation of the host metabolism, resides in the virulence cluster 19A (Brefort *et al*., 2014). Tin2 stabilizes the cytoplasmatic maize serine/threonine protein kinase ZmTTK1 to prevent proteosome-dependent degradation (Tanaka *et al*., 2014). ZmTTK1 is involved in the anthocyanin biosynthesis, however, the function is still unknown. *S. reilianum* possesses an orthologue of Tin2, which is absent in *U. hordei* and *Ustilago bromivora*. When *Srtin2* was deleted in *S. reilianum*, a reduction of virulence resulting in a reduced leafy ear structure and spore formation was observed (Tanaka *et al*., 2019). Furthermore, SrTin2 can neither complement the virulence nor the anthocyanin formation of the mutant Δ*tin2* (Tanaka *et al*., 2019). While UmTin2 has a stabilizing function of the interaction with ZmTTK1, SrTin2 suppresses the kinase activity of the maize paralogs of ZmTTK1, ZmTTK2, and ZmTTK3. A computational analysis was conducted to compare the Tin2 proteins of six different smuts to reconstruct the ancestral version of Tin2. The ancestral Tin2 revealed a functional similarity to SrTin2, suggesting a functional conservation of the ancestral Tin2 in *S. reilianum*. This result is consistent with the infection style of the majority of the smuts and suggests that UmTin2 may have undergone neofunctionalization for diversification, potentially leading to the development of tumors (Tanaka *et al*., 2019).

U. maydis is able to reprogram the host cells to proliferate and form tumors. The first leaf-specific, tumor-related effector identified was the effector See1, which is highly expressed in leaves but not in tassel (Redkar *et al*., 2015a; Schilling *et al*., 2014). During leaf infection, See1 reactivates the DNA synthesis in maize which is important for the cell division of tumor cells. *U. maydis* Δ*see1* mutants were reported to be reduced in virulence and failed to induce nuclear division in bundle sheet cells (Redkar *et al*., 2015a). In the plant nucleus, See1 interacts with the highly conserved eukaryotic protein SGT1, which plays a regulatory role in plant immunity and the cell cycle in yeast, respectively. See1 blocks phyosphorylation of maize SGT1, which results in the suppression of phosphorylation of immune responses (Redkar *et al*., 2015). Recently, a combination of proximity labeling using a turbo biotin ligase tag (TurboID) and co-immunoprecipitation identified three ubiquitin–proteasome pathway-related proteins (ZmSIP1, ZmSIP2, and ZmSIP3) as additional targets of See1. It was shown that UmSee1 causes more rapid degradation of a maize cell cycle regulator CDC48 by the maize proteasome, linking See1 with host cell cycle regulation (Shi *et al*., 2023).

Recently, the organ-specific effector Sts2 (Small tumor on seedlings 2) was identified in a differential expression analysis between *U. maydis* and *S. reilianum* (Zuo *et al*., 2021). Sts2 is a functional transcription activator that promotes the division of hyperplasia tumor cells in maize and interacts with a yet uncharacterized maize transcriptional activator, ZmNECAP1 (Zuo *et al*., 2023). The SrSts2 orthologue of *S. reilianum* is unable to functionally replace UmSts2, suggesting neofunctionalization of this tumor-inducing effector, similar as it has been reported previously for UmTin2 (Tanaka *et al*., 2019).

1.2.5 *Ustilago maydis* and its close relative *Sporisorium reilianum f. sp. zeae*

The biotrophic smut fungi *U. maydis* and *S. reilianum* are closely related, infect the same host, *Zea mays*, and share a similar infectious life cycle (Martinez *et al*., 1999; Stoll *et al*., 2005). However, the two pathogens strongly differ in their infection style and the disease symptoms they cause. While *U. maydis* forms distinct tumors, locally to the site of infection, *S. reilianum* systemically colonizes the host and causes symptoms only in the inflorescence, where phyllody is observed and seeds are replaced by teliospores (Ghareeb *et al*., 2011; Zuo *et al*., 2019). *U. maydis*-induced tumorigenesis is initiated when mycelia change from intracellular growth towards the bundle sheet cells (2 dpi) to intercellular growth. Generally, the tumor formation of *U. maydis* is associated with cell enlargement (hypertrophy) and an increase in cell division (hyperplasia) (Flora Banuett & Herskowitz, 1996; Callow & Ling, 1973). Notably, recent studies revealed tumorigenic effectors involved in the development of hypertrophy and hyperplasia tumor cells, respectively (Matei *et al*., 2018; Zuo *et al*., 2023). Within the tumor tissue, a massive proliferation of diploid fungal cells takes place (Banuett, 1995; Feldbrügge *et al*., 2004; Martínez-Espinoza *et al*., 2002). In contrast to *U. maydis*, *S. reilianum* does not form tumors but can induce the formation of teliospores and phyllody in the inflorescences. This phenotype is the result of an alteration in the developmental processes of the inflorescences (Ghareeb *et al*., 2011). During the systemic infection process, *S. relianum* remains in close proximity to the vascular bundles until it reaches the cob primordia (Zuo *et al*., 2021). Symptoms of *S. reilianum* include the development of multiple female inflorescences and the loss of apical dominance, which is mediated by the effector SAD1 (suppressor of apical dominance) (Ghareeb *et al*., 2015).

Comparison of the *U. maydis* and *S. reilianum* genomes disclosed a remarkably high synteny of the genomes with 43 exceptional regions of low sequence conservation and an overall 74.2% amino acid sequence identity of all predicted proteins (Schirawski *et al*., 2010). The average amino acid identity of non-secreted proteins of 76% is distinctly higher compared to the identity of 62% for secreted proteins, suggesting a more rapid evolution of putative effector genes (Schirawski *et al*., 2010).

Gene conversion between the two species indicated that effector orthologues from *U. maydis* and *S. reilianum* exhibited comparable virulence functions (Redkar *et al*., 2015a; Stirnberg & Djamei, 2016). A cross-species transcriptome analysis of *U. maydis* and *S. reilianum* revealed 207 of 335 differentially expressed one-to-one effector orthologues during colonization, suggesting a contribution of these genes to the different disease development of the two smuts (Zuo *et al*., 2021). In a CRISPR/Cas9-mediated gene conversion approach two functionally conserved effector genes (*UMAG_11060* and *UMAG_05306*) were identified within the differentially expressed effector genes, suggesting a possible contribution to the species-specific disease development of *U. maydis* and *S. reilianum*. Generally, this study revealed that the diversification of orthologous effector genes in closely related smut fungi can be caused by the transcriptional regulation of effector genes, as well as by the functional diversification of the effector proteins (Zuo *et al*., 2021). Two differentially expressed effector genes, *tin2,* and *sts2*, have been already identified with different functions between the species (Tanaka *et al*., 2019; Zuo *et al*., 2023). Interestingly, both Tin2 and Sts2 reside in cluster 19A.

Furthermore, the genome comparison between *U. maydis* and *S. reilianum* demonstrated the presence of three putative RNA-dependent RNA polymerase genes as well as homologs of a *dicer* and *argonaute* gene in *S. reilianum*, which are absent in *U. maydis* (Schirawski *et al*., 2010). Since the RNA interference (RNAi) machinery may play a biological role in explaining the difference in the mode of colonization between *S. reilianum* and *U. maydis*, a deletion mutant of the *dicer* gene *sr16838* was generated. However, the deletion mutant was unaffected in virulence and disease development. (Schirawski *et al*., 2010). Collectively, the two closely related smuts provide an excellent model to study the effector orthologues as well as the different disease development in the same host, *Z. mays*.

1.3 Hybridization in filamentous fungi

Hybridization events occur in nature and often result in the emergence of new fungal pathogens. Natural hybridization is defined as a successful mating event in nature between individuals from distinct populations that can be distinguished based on at least one inheritable character (Arnold, 1997). To prevent the transfer of genetic material between fungi, a number of reproductive barriers have evolved. These must be overcome to ensure successful hybridization.

The compatibility barriers associated with hybridization can be categorized into two groups: premating barriers and postmating barriers. The term “premating barriers” is used to describe the geographical, ecological, or temporal isolation of the parental species (Steensels *et al*., 2021). Nevertheless, the drivers of pathogen emergence, such as globalization, climate change, and industrialization (Callaghan & Guest, 2015), have in some instances removed the geographical and ecological barriers (Grabenstein & Taylor, 2018; Mixao & Gabaldón, 2018; Steensels *et al*., 2021). Hybrids can arise

through sexual reproduction or parasexually through the fusion of vegetative cells or hyphae, leading to heterokaryons (multinucleate state) (Kohn, 2005; Steensels *et al*., 2021). A vegetative or somatic incompatibility between two species regulates the self- vs. non-self-recognition process, which, in the event of an incompatibility, activates a series of cellular responses, including cell death. The mating type system as another checkpoint for hybridization allows the existence of two nuclei in the same cell. However, since the mating type system is conserved among large phylogenetic distances, it does not prevent hybridization (Kronstad & Staben, 1997; Olson & Stenlid, 2002).

Postmating barriers are the next checkpoint to overcome for successful hybridization. Hybrids often exhibit reduced viability or sterility, which are influenced by a multitude of factors, and the outcome of hybrids is therefore diverse. With regard to phenotype, hybrids are frequently distinguished by an intermediate phenotype compared to that of the parental species (Greig *et al*., 2002). This is often accompanied by a reduction in fitness, as the recombinant genotypes are less adapted to the parent or novel environments (Barton, 2001). However, hybridization can also result in the outperformance of the parental species, revealing greater biomass, higher speed of development, and fertility than both parents. This effect is called 'heterosis' (Birchler *et al*., 2010; Steensels *et al*., 2021). Generally, hybrids can be homoploid or polyploid, comprising the same ploidy or a higher ploidy as the parental species, respectively (Samarasinghe *et al*., 2020). It is likely that balanced chromosomal inheritance will occur in homoploid hybrids, which will facilitate successful backcrossing. This is further influenced by the divergence of the paired chromosomes in the hybrid (Steensels *et al*., 2021). In addition, the genomes of recently emerged fungal hybrids are relatively unstable, resulting in various genome instabilities, including the deletion or alteration of genetic blocks (D'Angiolo *et al*., 2020).

Interspecific hybridization can be further used between closely related fungi with different hosts to determine host specificity. Backcrossing of a hybrid of the two smut fungi *Ustilago bromivora* and *U. hordei* over several generations with *U. hordei* revealed the formation of spores in *Brachypodium* spp. and three virulence-associated genomic loci of *U. bromivora* (Bosch *et al*., 2019).

The co-occurrence of two nuclei within the same cell can give rise to a phenomenon known as 'transcriptomic shock', which is characterized by alterations in transcriptional regulation and expression levels. So far, several studies investigated the transcriptomic shock in fungi (Cox *et al*., 2014; Hovhannisyan *et al*., 2020; Krogerus *et al*., 2016), however, compared to hybrids in the plant or animal field, the changes in the transcriptome in fungal hybrids are rather mild (Steensels *et al*., 2021). The gene expression in hybrids was reported to reveal maintenance of the absolute gene expression level from parental species (Combes *et al*., 2015; Hovhannisyan *et al*., 2020) or to show a general loss of differential expression in the hybrid compared to the parental species (Behling *et al*., 2022). The transcriptional regulation that occurs subsequent to a transcriptomic shock can result in the rewiring of

transcriptional networks (Behling *et al*., 2022; Tirosh *et al*., 2009). Numerous studies identified *cis*- and *trans*-effects by comparing the gene expression of the homoeologues in the hybrid and the orthologues between the parents (Bell *et al*., 2013; He *et al*., 2012; Shi *et al*., 2012; Tirosh *et al*., 2009). Therefore, interspecific hybridization can be used to disentangle *cis*- vs. *trans*- effects by comparing the gene expression in the hybrid and the gene expression between the orthologues of the parental species. While the differences between the two genomes in the hybrid are caused by *cis*-regulation, the differences in expression between the parental orthologues that are lost in the hybrid reflect *trans*-regulation (Tirosh *et al*., 2009). Notably, hybrid-specific expression was reported in a yeast hybrid, which has been attributed to the emergence of novel *cis*- and *trans*- interactions in the hybrid (Tirosh *et al*., 2009). In general, the transcriptomic changes in the genome before the stabilization and in the long term may be different (Steensels *et al*., 2021). Cox *et al*. (2014) introduced the term "modulon" which encompasses all regulatory mechanisms of gene expression (*cis*/*trans*), posttranslational regulation, TFs, and epigenetics. It was proposed that the differences in orthologous gene expression are caused by the differences in the modulon of each species. Thus, the increase in divergence between the parental species is accompanied by the magnitude of the transcriptome shock (Cox *et al*., 2014). The modulons were subsequently grouped into three categories: (i) modulons that exhibit minimal or no crosstalk due to their significant divergence, which would result in the inheritance of the expression and no alterations in expression, (ii) modulons that are largely similar and compatible, which would minimize the differences in expression compared to the differences observed between the species, and (iii) modulons that target preferentially one of the alleles in the hybrid, leading to a hybrid-specific trend not observed in the parental species, which may be considered a form of transcriptomic shock in the hybrid.

Additionally, hybrid fitness can be further influenced by an interaction between the nuclear genome and the mitonuclear genome (Giordano *et al*., 2018). The inheritance of the mitotype differs across the fungal kingdom, while Basidiomycetes comprise a uniparental inheritance from only one parental species (Basse, 2010), Ascomycetes exhibit a biparental inheritance, resulting in nuclear-mitochondrial chimeras (Barr *et al*., 2005; Steensels *et al*., 2021).

1.4 Interspecific hybridization between *U. maydis* and *S. reilianum*

A prerequisite for successful hybridization is genetic compatibility, which allows mating of distinct species (Åke Olson & Stenlid, 2002). A recent study characterized a hybrid of the haploid strain *U. maydis* strain 521 and the haploid *S. reilianum* strain SRZ2. This hybrid shows that the alteration in gene expression can also alter the virulence. However, the hybrid was unable to exhibit extensive hyphal growth and consequently, its pathogenic development was severely restricted (Storfie & Saville, 2021). From this observation, it was hypothesized that only a change of the mating type genes between the species can lead to a successful hybridization and fungal proliferation inside the host.

In advance of this work, my colleague Weiliang Zuo replaced the mating type genes of the haploid *U. maydis* strain FB1 strain (*Uma1b1*) with the *Sra1b1* mating type genes of *S. reilianum*. Two independent *U. maydis* mating type (**Um_Smt**) strains were generated: FB1_*Sra1b1* #1 and FB1_*Sra1b1* #2. Together with the strain SRZ2 (*Sra2b2*), the Um_Smt mutants were capable of forming filaments, which facilitated the investigation of the different disease developmental processes utilizing the recombinant hybrid of *U. maydis* and *S. reilianum* (**rUSH**).

1.5 Aim of this study

The main objective of this study was to elucidate the molecular basis of the distinct infection styles of *U. maydis* and *S. reilianum* on the same host *Z. mays*. To gain insights into the impact of interspecific hybridization on virulence at all infection stages, and to investigate the expression profile of the hybrid *in planta*, the recombinant hybrid (rUSH) was employed. This was done using RNA sequencing, with a focus on the expression level and regulation of effector genes between the species.

Another objective was to investigate the regulatory basis of effector genes for tumorigenesis of *U. maydis*, utilizing rUSH.

At the beginning of this work, the mutagenesis of *S. reilianum* using CRISPR/Cas9 had not been established. Consequently, another aim of this study was to establish a protocol for CRISPR/Cas9-mediated mutagenesis of *S. reilianum* as a prerequesite to generate a hybrid with the *U. maydis* mating type system (rSUH), and to enable efficient mutagenesis of *S. reilianum* genes.

Chapter 2: CRISPR/Cas9 Ribonucleoprotein-mediated Mutagenesis in *Sporisorium reilianum*

Chapter II was published in BioProtocol on the 20th of April 2024:

Werner, J., Zuo, W. and Doehlemann, G. (2024). CRISPR/Cas9 Ribonucleoprotein-Mediated Mutagenesis in *Sporisorium reilianum*. Bio-protocol 14(8): e4978. DOI: 10.21769/BioProtoc.4978.

2.1 Abstract

Clustered regularly interspaced short palindromic repeats/CRISPR-associated protein 9 (CRISPR/Cas9) has become the state of the art for mutagenesis in filamentous fungi. Here, we describe a ribonucleoprotein complex (RNP)-mediated CRISPR/Cas9 for mutagenesis in *Sporisorium reilianum*. The efficiency of the method was tested in vitro with a cleavage assay as well as *in vivo* with a GFP-expressing *S. reilianum* strain. We applied this method to generate frameshift- and knock-out mutants in *S. reilianum* without a resistance marker by using an auto-replicating plasmid for selection. The RNP-mediated CRISPR/Cas9 increased the mutagenesis efficiency, can be applied for all kinds of mutations, and enables a marker-free genome editing in *S. reilianum*.

2.2 Introduction

The smut fungi consist of more than 1,500 species, being highly economically important due to their infection of relevant crops such as barley, sorghum, wheat, and maize [1]. The majority of smut fungi infect their host systemically through the roots and replace the inflorescences with teliospores without causing symptoms during early infection stages [2,3]. One example of this systemic infection is *Sporisorium reilianum f. sp. zeae*, which is the causal agent of maize head smut. *S. reilianum* is closely related to the intensively investigated model organism *Ustilago maydis*. However, they differ in their mode of infection as well as in the site of symptom development [4,5]. In 2010, a genome sequence of *S. reilianum f. sp. zeae* was published, which, together with the *U. maydis* genome, provided the foundation for systematic identification and genetic manipulation of effector genes contributing to virulence [6,7]. Genome comparison of *U. maydis* and *S. reilianum* revealed conserved effector genes even though they differ drastically in their pathogenesis on the same host, *Zea mays*. To characterize

effector genes and their contribution to virulence, knock-out mutants are generated and compared to the wild type. In the past, *U. maydis* knock-out mutants were generated using PCR-amplified donor templates with resistance markers for gene replacements [8]. Importantly, it was shown that not only the genomic locus but also the integration of resistance markers can negatively influence the expression of reintegrated genes [9]. Recently, the mutagenesis of *U. maydis* was drastically improved with a marker-free approach using clustered regularly interspaced short palindromic repeats/CRISPR-associated protein 9 (CRISPR/Cas9) [10,11] and further developed for a seamless gene conversion approach [12]. In contrast to *U. maydis*, the generation of knockout mutants in *S. reilianum* is still dependent on resistance markers, and multiple gene knockouts are hampered by the limited number (i.e., carboxine, hygromycin, nourseothricin, and phleomycin) of available resistance markers [8]. However, the plasmid-based CRISPR/Cas9 transformation as used in *U. maydis* has not been successful for *S. reilianum*.

CRISPR/Cas9, originating from the adaptive immune system of *Streptococcus pyogenes*, has been broadly adapted to many eukaryotic systems. It is a versatile tool for mutagenesis in various filamentous fungi [13]. The delivery strategies of CRISPR/Cas9 differ between fungal species: (i) stable genomic integration of cas9, (ii) transient delivery of Cas9 where the expression of Cas9 is dependent on selection pressure of a self-replicating plasmid or a telomere vector [10,14], or (iii) ribonucleoprotein complex (RNP)mediated transformation [15,14]. Here, we describe CRISPR/Cas9 applications in *S. reilianum* using an RNPmediated transformation approach. We demonstrate the generation of frameshifts as well as knock-out mutants mediated by RNPs, thereby generally improving the mutagenesis, and, for the first time, enabling a marker-free editing in *S. reilianum*.

2.3 Materials and Reagents

Biological materials

S. reilianum strains were stored at -80 °C in 30% glycerol. For transformation, *S. reilianum* wildtype strains SRZ1 and SRZ2 [7] were used.

Reagents

A. Single-guide RNA (sgRNA) synthesis

1. T4 DNA polymerase (New England Biolabs, catalog number: M0203S), storage: -20 °C
2. NEBuffer™ r2.1 (50 mM NaCl, 10 mM Tris-HCl, 10 mM $MgCl_2$, 100 µg/mL BSA, pH 7.9), storage: -20 °C (New England Biolabs, catalog number: B7202S)
3. dNTPs (DNA) (Carl Roth, catalog number: K039.1), storage: -20 °C

4. NucleoSpin® Gel and PCR clean up (Machery and Nagel, catalog number: 740.609.250), storage: RT
5. HiScribe® T7 High Yield RNA Synthesis kit (New England Biolabs, catalog number: E2040S), storage: -20 °C
6. DNase I (Thermo Fisher, catalog number: EN0521), storage: -20 °C
7. DNase I buffer (Thermo Fisher, catalog number: EN0521), storage: -20 °C
8. RNA Clean & Concentrator 25 kit (Zymo Research, catalog numbers: R1017 and R1018), storage: RT
9. Purple loading dye (New England Biolabs, catalog number: B7024S); ingredients: 2.5% Ficoll®-400, 10 mM EDTA, 0.08% SDS, 0.02% Dye 1, 0.02% Dye 2, pH 8; storage: RT
10. Nuclease-free water, storage: RT

B. Formation of RNP and in vitro cleavage assay

1. EnGen® Spy Cas9 NLS + NEB buffer r3.1 (New England Biolabs, catalog number: M0667)
2. 500 mM Ethylenediaminetetraacetic acid (EDTA) (Carl Roth, catalog number: 8043.2)
3. Proteinase K (Thermo Fisher, catalog number: EO0491)
4. 100 bp ladder (New England Biolabs, catalog number: N3231S)
5. Universal agarose (Bio-Budget, catalog number: 10-35-1020)
6. 1% Ethidium bromide solution (Carl Roth, catalog number: 2218.2)
7. Potato dextrose agar (PDA) plates (39 g/L) (BD, Difco™, catalog number: 213400)
8. Tris base (Sigma, catalog number: 102262896)
9. Acetic acid (VWR, catalog number: 20103.330)
10. EDTA 0.5 M pH 8.0 (Carl Roth, catalog number: 8043.2)

C. Protoplasting and transformation of *S. reilianum*

1. Novozym 234 [Novo Nordisk; Denmark, not available anymore; alternative: lysing enzyme from *Trichoderma harzianum* (Sigma, catalog number: SLBJ0553V)]
2. Sodium citrate (Carl Roth, catalog number. 3580.1)
3. Sorbitol (Sigma, catalog number: 102466217)
4. Citrate acid (Carl Roth, catalog number: X863.2)
5. Sorbitol (Sigma, catalog number: 102466217)
6. Tris-HCl (Carl Roth, catalog number: 9090.3)
7. $CaCl_2$ (Sigma, catalog number: 1002825086)
8. Poly(ethylene glycol) PEG MW3350 (Sigma, P4338, catalog number: 102604683)
9. Bacto™-Yeast-Extract (Thermo Fisher, Gibco, catalog number: 212720)
10. Bacto™Peptone (BD, Difco, catalog number: 211820)

11. Sucrose (Carl Roth, catalog number: 4621.2)
12. Sorbitol (Sigma, catalog number: 102466217)
13. Bacto™-Agar (BD, catalog number: 214030)
14. Potato dextrose agar (PDA) plates (BD, Difco™, catalog number: 213400)
15. Carboxine (5 mg/mL) (Sigma, catalog number: 102085144)
16. Heparin sodium salt from porcine intestinal mucosa (15 mg/mL) (Sigma, catalog number: 1001937695)

Solutions

1. 50× TAE buffer (see Recipes)
2. 1× TAE buffer (see Recipes)
3. SCS buffer (see Recipes)
4. STC buffer (see Recipes)
5. STC/40% PEG (see Recipes)
6. Regeneration agar light (see Recipes)

Recipes

1. 50× TAE buffer

Reagent	Final concentration	Quantity or Volume
Tris base	2 M (v/v)	242.0 g
Acetic acid	2 M (v/v)	57.1 mL
EDTA 0.5 M pH 8.0	10% (v/v)	100.0 mL

2. 1× TAE buffer

Reagent	Final concentration	Quantity or Volume
50× TAE buffer	2% (v/v)	20.0 mL
Deionized water	98% (v/v)	980.0 mL

3. SCS buffer

Reagent	Final concentration	Quantity or Volume
Solution 1:		
Sodium citrate, pH 5	0.6% (w/v)	5.9 ml
Sorbitol	18.2% (w/v)	182.0 g
Solution 2:		
Citrate acid	0.4% (w/v)	4.2 g
Sorbitol	18.2% (w/v)	182.0 g

Solution 1 and 2 are mixed until pH 5.8 is reached (ratio ~5:1) and autoclaved.

4. STC buffer

Reagent	Final concentration	Quantity or Volume
Sorbitol	50% (v/v)	500.0 mL
Tris-HCl, 1 M pH 7.5	1% (v/v)	5.0 mL
$CaCl_2$, 1 M, sterile-filtrated (100 mL total volume is enough)	10% (v/v)	50.0 mL

5. STC/40% PEG

Reagent	Final concentration	Quantity or Volume
STC buffer	60% (v/v)	600.0 mL
Poly(ethylene glycol) PEG, MW3350; sterile filtrated, (50 mL total volume is enough)	40% (w/v)	400.0 g

6. Regeneration agar light

Reagent	Final concentration	Quantity or Volume
Bacto™ yeast extract	1% (w/v)	10.0 g
Bacto™ peptone	0.4% (w/v)	20.0 g
Sucrose	0.4% (w/v)	20.0 g
Sorbitol	18.2% (w/v)	182.2 g
Bacto™ agar	1.5% (w/v)	15.0 g

Laboratory supplies

1. PCR machine (Bio-Rad, model: T100™ Thermal Cycler)
2. Microfuge for PCR tubes (VWR, model: Ministar)
3. Tabletop centrifuge (VWR, model: Microstar 17)
4. 37 °C incubator (Memmert, model: UN110)
5. 28 °C incubator/room
6. Optional: Polyacrylamide gel electrophoresis (SDS-PAGE) equipment (Bio-Rad, model: PowerPac™ Basic, Mini-Protean® Tetra System)
7. Agarose gel electrophoresis equipment
8. Nanodrop (Thermo Scientific, model: Nanodrop 2000c)
9. ChemiDoc™ MP imaging system (or equivalent imaging system), with GFP filter (Bio-Rad, model: Universal Hood III)
10. Geldoc: visualization of DNA by UV radiation using a gel documentation unit (Peqlab/VWR, model: EBOX VX5)

Equipment

1. PCR tubes and 1.5 ml Eppendorf tubes
2. Sterile cut tips (1,000 µL and 20 µL)

2.4 Procedure

A. *In vitro* transcription of sgRNA

1. Design protospacer in CHOPCHOP sgRNA designer (https://chopchop.cbu.uib.no/) using *S. reilianum* as target organism. Choose the protospacer sequence starting with a **G**, which is needed for initiating the transcription by T7 RNA polymerase. If there is no desired protospacer starting with G, add an additional G upstream of the chosen protospacer sequence (21 nt).

2. Add T7 RNA polymerase promoter sequence and overlapping scaffold sequenceupstream and downstream of the chosen protospacer sequence, respectively, and order the gene-specific oligonucleotide (Table 1). In addition, a reverse complementary constant oligonucleotide is needed, which harbors the scaffold and terminator sequence and a 20 nt overlap to the scaffold sequence of the gene-specific oligonucleotide (Table 1).

Table 1. Sequences of oligonucleotides for sgRNA synthesis

Oligo	Sequence
Gene-specific	CAAAATTCCATTCTACAAC**-G**NNNNNNNNNNNNNNNNNNN-GTTTTAGAGCTAGAAATAGCAAG
Constant	AAAAGCACCGACTCGGTGCCACTTTTTCAAGTTGATAACGGACTAGCCTTATTTTAACTTGCTATTTCTAGCTCTAAAAC

Note: The underlined sequence of the constant oligo depicts the overlapping part with the gene-specific oligo.

3. Mix both oligonucleotides in a 1:1 ratio as follows:
1 µL of protospacer oligo 100 µM stock
1 µL of constant oligo 100 µM stock
8 µL of H_2O
10 µL total

4. Anneal the oligos using the following program in PCR machine:
95 °C for 5 min
95 °C to 85 °C at -2 °C/s
85 °C to 25 °C at -0.1 °C/s
4 °C pause

5. Add T4 DNA polymerase to fill in the overhangs:
2.5 µL of dNTPs (10 mM)
2 µL of NEBuffer™ r2.1(10×)
5 µL of H_2O
0.5 µL of T4 DNA polymerase
10 µL total

6. Incubate at 12 °C for 20 min in a PCR machine.
7. Purify the product with a PCR clean-up kit, measure the concentration with Nanodrop, and verify the PCR product on a 2%–3% TAE agarose gel.
8. Use 2 µg of the resulting DNA from above as template and the HiScribe T7 High Yield RNA Synthesis kit for the following reaction (NEB, protocol for small RNAs):
   6 µL of NTPs (25 mM each in stock)
   2 µL of 10× T7 buffer
   1.5 µL of T7 RNA polymerase mix
   X µL of Template (2 µg DNA template, step 6)
   Y µL of nuclease-free H_2O (add to 20 µL)
   20 µL total
9. Flip the tube, vortex shortly, and incubate at 37 °C overnight.
10. The next day, add 14 µL of nuclease-free H_2O, 4 µL of DNase I buffer (10×), and 2 µL of DNase I and incubate at 37 °C for 15 min.
    Caution: Small RNA is easy degradable; work in a RNase-free space and use gloves and a lab coat for all following steps!
11. Purify the resulting sgRNA with the RNA Clean & Concentrator 25 kit and use the manufacturer's protocol (manual, page 5).
    Optional: Check the quality of the RNA on 10% denaturing PAA gel using TBE buffer (89 mM Tris base, 89 mM boric acid, and 2 mM sodium EDTA) and 8 M urea and TBE as running buffer [14].
12. Measure the concentration by Nanodrop and proceed with *in vitro* cleavage assay (section B).
    Pause point: You can freeze the sgRNA at -80 °C and continue the next day; long-term storage of sgRNA is also possible at -80 °C. See Troubleshooting 1.

B. *In vitro* cleavage assay

1. To test the *in vitro* efficiency of the designed sgRNA, mix 1.5 µL of Cas9 (NEB) and ~1.5 µg of the sgRNA (1:1 molar ratio) and incubate it for 10 min at RT (Figure 2.1B).

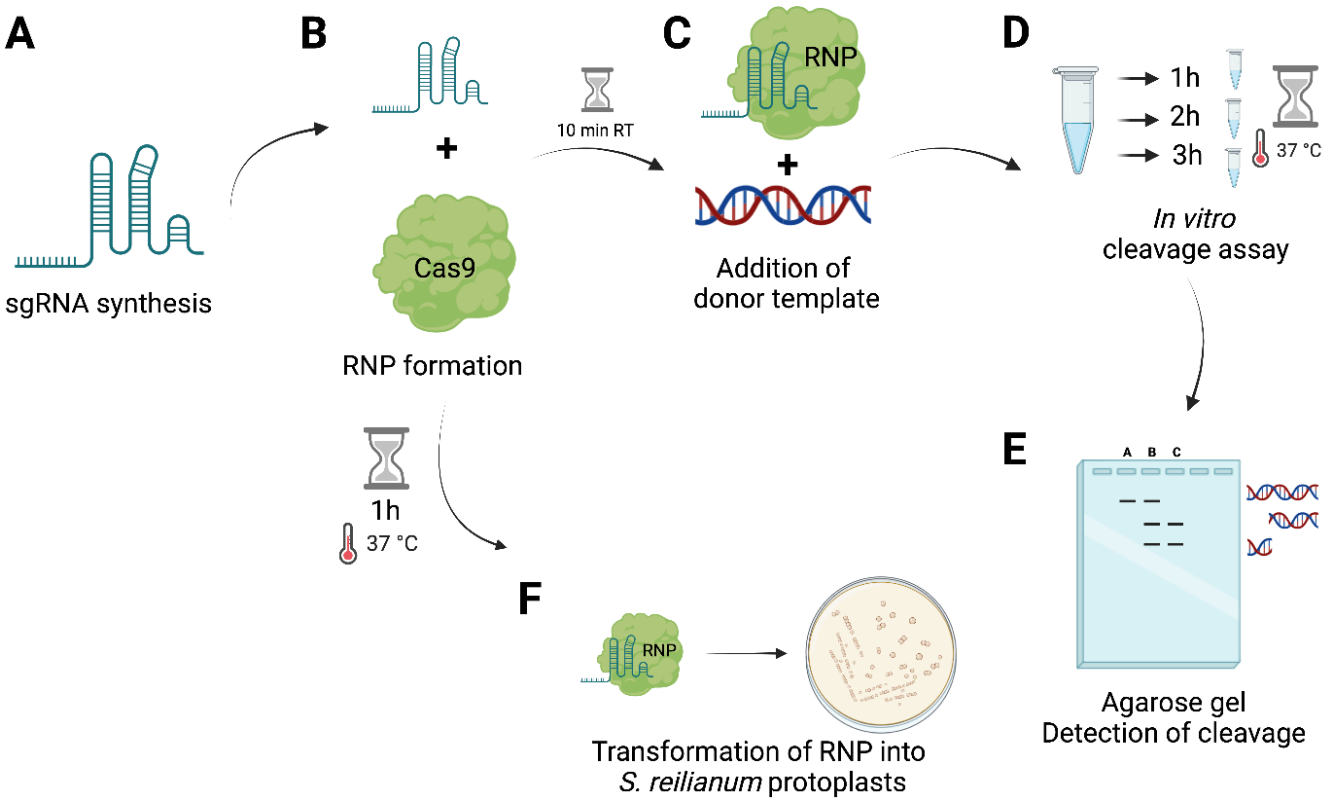

Figure 2.1: Graphical overview of the workflow of ribonucleoprotein complex (RNP)-mediated transformation in ***S. reilianum.*** **(A)** *In vitro* synthesis of sgRNA using T7 HiScribe kit. **(B)** RNP formation of *in vitro*–transcribed sgRNA with *Sp*Cas9. **(C)** Alternatively: To perform an in vitro cleavage assay, incubation at room temperature (RT) for 10 min and subsequent addition of a donor template (amplification of the gene of interest region) and incubation at 37 °C for 3 h is conducted. **(D)** Sampling of 10 µL of reaction mix after 1, 2, and 3 h (or alternatively overnight). **(E)** Visualization of in vitro cleavage on a 1.5% agarose gel using 100 bp ladder. **(F)** RNP incubation for 1 h at 37 °C prior to transformation into *S. reilianum* protoplasts. Figure was created with biorender.com.

2. Afterwards, add 333 ng of a DNA cleavage template (PCR product of the region of interest) (Figure 2.1C).
3. After 1, 2, and 3 h take 10 µL samples (Figure 2.1D) and stop the reaction by adding 1 µL of 500 mM EDTA, pH 8.
4. Subsequently, add 1 µL of proteinase K to the reaction and incubate the reaction mix for 30 min at 50 °C for degradation of Cas9.
5. Stop the reaction by the addition of 1× purple loading dye.
6. After the collection of all samples, check cleavage on an 1.5% agarose gel with 100 bp ladder (stained with ethidium bromide solution) visualized using a Gel-Doc (Figure 2.1E, see Troubleshooting 2).

C. Assembly of RNP for transformation into *S. reilianum*

1. Use 2 µg of the in vitro–transcribed sgRNA targeting the gene of interest and mix it with 6 µg of *Sp*Cas9.
2. Subsequently, add 1× NEBuffer™ 3.1 and water in a minimum volume (Figure 2.1B).
3. After mixing and centrifugation, incubate the reaction for 1 h at 37 °C prior to transformation (Figure 2.1B).

D. Transformation of *S. reilianum*

1. Prepare *S. reilianum* protoplasts using Novozym 234 as described previously [8].
2. For RNP transformation (Figure 2.1E), thaw the protoplasts for 5 min on ice.
3. Add a self-replicating plasmid with antibiotic resistance cassette [e.g., pNEBUC - Carboxine (Cbx); Brachmann *et al*. [8], replicating in *S. reilianum*], the RNP (formed in section C), 1 µL of 15 mg/mL heparin, and, optionally, 1.5 µg of a donor template to the protoplasts (Figure 2.2).

   Note: The self-replicating plasmid is lost when the selection for Cbx resistance is stopped. So far, we could not report an integration into the genome of S. reilianum.
4. Incubate the protoplasts for 10 min on ice.
5. Add 500 µL of STC/40% PEG and resuspend the protoplasts carefully with a tip-cut blue tip until the liquid looks homogenous without clumps (5–8 times pipetting up and down).
6. Incubate the protoplasts for another 15 min on ice.
7. Spread the protoplasts on a regeneration agar light plate with two layers [bottom layer: corresponding selective antibiotic (for pNEBUC—carboxin: 2.5 µg/mL), top layer: without antibiotic resistance].
8. The next day, flip the transformation plate upside down.
9. After four days, use a blue tip to single out transformants from regeneration agar to PDA + Carboxin (2.5 µg/mL) for 2–3 days.
10. Afterwards, transfer a single colony for two days to PDA plates to lose the resistance.
11. Subsequently, DNA is isolated [16] and used for further confirmation (see section E).

E. RNP-assisted homologous recombination to generate a knockout in *S. reilianum*

For the generation of an antibiotic-resistance-free knock-out mutant in *S. reilianum*, a CRISPR/Cas9-mediated homology-directed repair was exploited. To do this, a donor template is generated by cloning the 1 kb homology flanking regions of the target gene into a MOCLO vector TK#1_pAGM1311 by Gibson assembly (Figure 2.2).

1. For the transformation of *S. reilianum* protoplasts (see section D), add the donor template together with a self-replicating plasmid (pNEBUC), the RNP (with a sgRNA against the target region), and 1 µL of heparin.
   Note: The transformation efficiency is high > 100 colonies; if your efficiency is lower, repeat protoplasting and transformation.
2. Transfer obtained transformants as described above (see section C).
3. Isolate DNA of the transformants and the wild type.
4. Conduct a PCR using the forward primer of the left flank and the reverse primer of the right flank (Figure 2.2C) and compare the band sizes to the wild type (Figure 2.2D).
5. Putative positive mutants from PCR are selected for further verification via Southern blot [17,18] using the deletion construct (left flank + right flank), previously used as a donor template, as probe for hybridization.

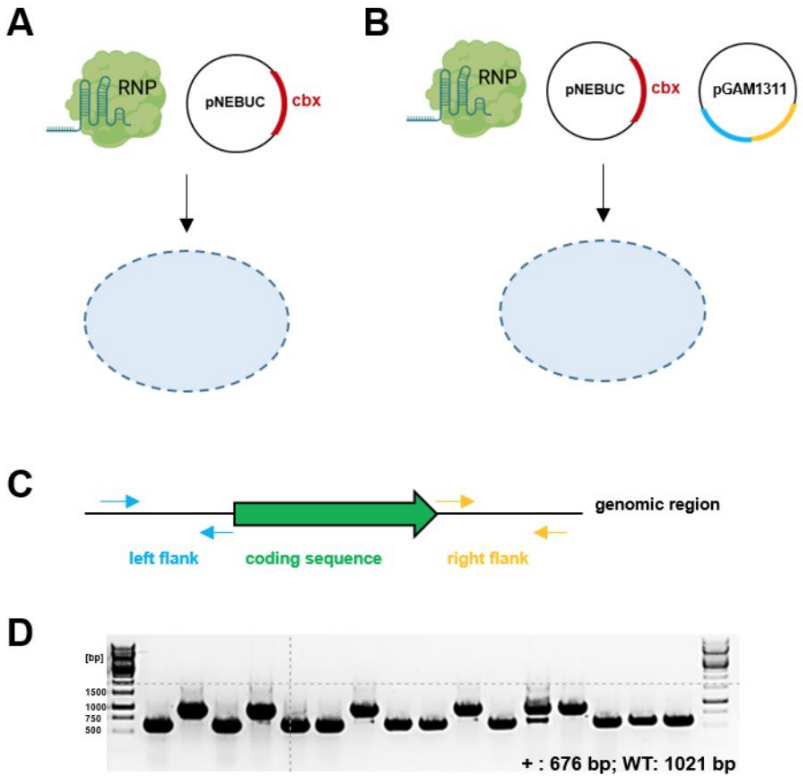

Figure 2.2. Transformation of *S. reilianum* using ribonucleoprotein complex (RNP) with and without a donor template. (A) Generation of frameshift mutants using RNP-mediated transformation. Generated frameshift mutants are screened by sequencing or as described in Figure 2.3 by the loss of fluorescence. **(B)** Generation of knock-out mutants using RNP-assisted homologous recombination with a donor template. **(C)** Donor template design for the generation of a knockout. 1 kb flanking regions of the coding sequence are amplified by PCR with overhangs for Gibson assembly into backbone TK#1_pAGM1311 (MOCLO backbone, Level -1). **(D)** Example of deletion mutant verification PCR using Left Flank (LF) forward primer and Right Flank (RF) reverse primer [expected sizes: WT, 1021 bp; mutant (+), 676 bp; efficiency: 62.5% (10/16)]. The efficiency can vary between different genomic loci. Figure 2.2A and B were created with biorender.com.

2.5 Validation of protocol

The efficiency of the RNP CRISPR/Cas9 can, for instance, be tested with GFP fluorescence as a readout (Figure 2.3). To test the efficiency in *S. reilianum*, a strain harboring a single integration of GFP controlled by pOTEF (constitutive promoter) was generated in the *ip* locus of SRZ2 strain and confirmed via Southern blot (Figure S1.1). For the transformation of *S. reilianum* protoplasts, a sgRNA against GFP together with the Cas9 in a RNP (see section C) and an auto-replicating plasmid (pNEBUC) for selection on regeneration agar was used. Transformants were singled out after four days of incubation at 28 °C on PDA + Cbx (2.5 mg/mL) and, after two days, were transferred to PDA plates and checked for their fluorescence using a Chemi-Doc.

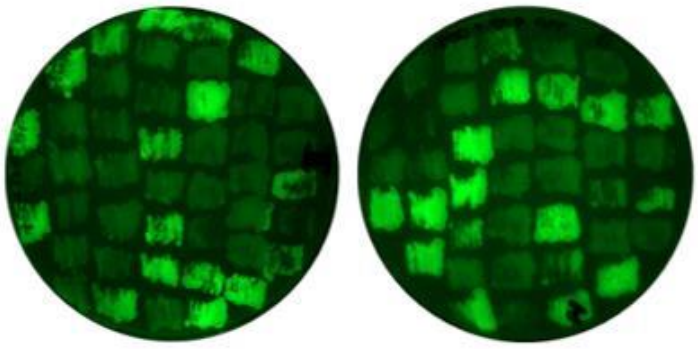

Figure 2.3. GFP as target for ribonucleoprotein complex (RNP)-mediated transformation in *S. reilianum*. An example shows the efficiency of RNPmediated CRISPR/Cas9 transformation in *S. reilianum*. An *S. reilianum* SRZ2 strain expressing GFP under pOTEF promoter was generated. sgRNA+Cas9 targeting GFP coding sequence was transformed, and mutants with frameshift lose the GFP signal. Efficiency for GFP sgRNA: ~41% (34/83).

2.6 General notes and troubleshooting

Troubleshooting

No.	Step	Problem	Suggestion/solution
1	sgRNA synthesis	Low concentration (<500 ng/µL)	Do not proceed with transformation, repeat synthesis; high concentration in minimum volume is needed
2	In vitro cleavage assay	No bands after cleavage	1) Test functionality of Cas9 enzyme (use a control) 2) Design of new sgRNAs

Acknowledgments

This project has received funding from the European Research Council (ERC) under the European Union's Horizon 2020 research and innovation program (grant agreement No. 771035), as well as funding by the Deutsche Forschungsgemeinschaft (DFG, German Research Foundation) under Germany's Excellence Strategy, EXC-2048/1- Project ID: 390686111. This protocol was adapted from previous work [14].

2.7 References

1. **Begerow**, D., Göker, M., Lutz, M. and Stoll, M. (2004). On the evolution of smut fungi on their hosts. Front. Basidiomycote Mycol. 81–98.

2. **Martinez**, C., Roux, C., Jauneau, A. and Dargent, R. (2002). The biological cycle of *Sporisorium reilianum f. sp. zeae*: an overview using microscopy. Mycologia 94(3): 505–514.

3. **Laurie**, J. D., Ali, S., Linning, R., Mannhaupt, G., Wong, P., Güldener, U., Münsterkötter, M., Moore, R., Kahmann, R., Bakkeren, G., *et al*. (2012). Genome Comparison of Barley and Maize Smut Fungi Reveals Targeted Loss of RNA Silencing Components and Species-Specific Presence of Transposable Elements. Plant Cell 24(5): 1733–1745.

4. **Begerow**, D., Stoll, M. and Bauer, R. (2006). A phylogenetic hypothesis of Ustilaginomycotina based on multiple gene analyses and morphological data. Mycologia 98(6): 906–916.

5. **Steinberg**, G. and Perez-Martin, J. (2008). *Ustilago maydis*, a new fungal model system for cell biology. Trends Cell Biol. 18(2): 61–67.

6. **Kämper**, J., Kahmann, R., Bölker, M., Ma, L. J., Brefort, T., Saville, B. J., Banuett, F., Kronstad, J. W., Gold, S. E., Müller, O., *et al*. (2006). Insights from the genome of the biotrophic fungal plant pathogen *Ustilago maydis*. Nature 444(7115): 97–101.

7. **Schirawski**, J., Mannhaupt, G., Münch, K., Brefort, T., Schipper, K., Doehlemann, G., Di Stasio, M., Rössel, N., Mendoza-Mendoza, A., Pester, D., *et al*. (2010). Pathogenicity Determinants in Smut Fungi Revealed by Genome Comparison. Science 330(6010): 1546–1548.

8. **Brachmann**, A., König, J., Julius, C. and Feldbrügge, M. (2004). A reverse genetic approach for generating gene replacement mutants in *Ustilago maydis*. Mol. Genet. Genomics 272(2): 216–226.

9. **Schmitz**, L., Kronstad, J. W. and Heimel, K. (2019). Conditional gene expression reveals stage-specific functions of the unfolded protein response in the *Ustilago maydis*–maize pathosystem. Mol. Plant Pathol. 21(2): 258–271.

10. **Schuster**, M., Schweizer, G., Reissmann, S. and Kahmann, R. (2016). Genome editing in *Ustilago maydis* using the CRISPR–Cas system. Fungal Genet. Biol. 89: 3–9.

11. **Zuo**, W., Depotter, J. R. and Doehlemann, G. (2020). Cas9HF1 enhanced specificity in *Ustilago maydis*. Fungal Biol. 124: 228–234.

12. **Zuo**, W., Depotter, J. R. L., Gupta, D. K., Thines, M. and Doehlemann, G. (2021). Cross-species analysis between the maize smut fungi *Ustilago maydis* and *Sporisorium reilianum* highlights the role of transcriptional change of effector orthologs for virulence and disease. New Phytol. 232(2): 719–733.

13. **Schuster**, M. and Kahmann, R. (2019). CRISPR-Cas9 genome editing approaches in filamentous fungi and oomycetes. Fungal Genet. Biol. 130: 43–53.

14. **Leisen**, T., Bietz, F., Werner, J., Wegner, A., Schaffrath, U., Scheuring, D., Willmund, F., Mosbach, A., Scalliet, G., Hahn, M., *et al*. (2020). CRISPR/Cas with ribonucleoprotein complexes and transiently selected telomere vectors allows highly efficient marker-free and multiple genome editing in *Botrytis cinerea*. PLoS Pathog. 16(8): e1008326.

15. **Foster**, A. J., Martin-Urdiroz, M., Yan, X., Wright, H. S., Soanes, D. M. and Talbot, N. J. (2018). CRISPR-Cas9 ribonucleoprotein-mediated co-editing and counterselection in the rice blast fungus. Sci. Rep. 8(1): 14355.

16. **Hoffman**, C. S. and Winston, F. (1987). A ten-minute DNA preparation from yeast efficiently releases autonomous plasmids for transformaion of *Escherichia coli*. Gene 57: 267–272.

17. **Southern**, E. (1975). Detection of specific sequences among DNA fragments separated by gel electrophoresis. J. Mol. Biol. 98(3): 503–517.

18. **Sambrook**, J., Fritsch, E. F. and Maniatis, T. (1989). Molecular cloning: a laboratory manual (No. Ed. 2). Cold Spring Harbor Laboratory Press.

Chapter 3: Generation and Characterization of a recombinant Hybrid of *Ustilago maydis* and *Sporisorium reilianum* (rUSH)

3.1 Summary

S. reilianum and *U. maydis* are closely related smut fungi that colonize the same host, *Zea mays*. While *S. reilianum* spreads systemically in the host and replaces the female and male inflorescences by teliospores, *U. maydis* forms tumors on all aerial parts of maize. In this study, a recombinant hybrid of *U. maydis* and *S. reilianum* (rUSH) was generated to elucidate the molecular basis of the different disease development of the two species. rUSH was able to form dikaryotic hyphae, proliferate *in planta*, and exhibit a *S. reilianum*-like phenotype. rUSH was used as a tool to elucidate the differences in disease development between the two species. RNA-seq analysis of rUSH revealed 218 differentially expressed effector genes *in planta*, comprising distinct expression patterns: *cis*, *trans,* and hybrid-specific. When these patterns were analyzed in detail, highly expressed *S. reilianum* effector orthologues, as well as downregulated *U. maydis* effector orthologues, were identified in rUSH, compared to their expression levels in the wild type. Within these genes, many genes of the biggest virulence cluster 19A in *U. maydis* were identified, a cluster proposed to be crucial for tumor formation. KO mutants of two of the downregulated effector genes residing in cluster 19A were significantly reduced in pathogenicity, demonstrating their contribution to *U. maydis* virulence. Moreover, a novel *S. reilianum* effector gene was identified as a virulence factor. In addition, 78 putative TFs were identified in rUSH, of which six were selected to generate knockout mutants and to investigate their role in pathogenicity using infection assays. However, none of the mutants exhibited a reduction in virulence.

3.2 Introduction

Smut fungi comprise more than 1,500 species and predominantly infect plants of the Poaceae family (Begerow *et al*., 2004). They are of great economic importance due to their contribution to crop losses each year. The majority of the smuts infect their host systemically without the formation of early infection symptoms and replace the inflorescences of its host with teliospores during a late infection stage (Laurie *et al*., 2012; Martínez-Espinoza *et al*., 2002). One example of systemic infection is the head smut *S. reilianum,* which can infect maize (*S. reilianum f. sp. zeae*) and sorghum (*S. reilianum f. sp. reilianum*), respectively. However, *U. maydis*, the prime model organism and exception within the smuts, can infect all aerial parts of maize and can form tumors locally at infection sites. *S. reilianum* and *U. maydis* are closely related and can infect the same host, *Z. mays*.

During plant-microbe interactions, pathogens secrete a plethora of effector genes to manipulate the host for their benefit and to facilitate host colonization. Evolutionary pressure during the co-evolution of plants and their microbes drives the rapid diversification of effector genes (Franceschetti *et al*., 2017).

The genome data of *U. maydis* (Jörg Kämper *et al*., 2006) and *S. reilianum* (Schirawski *et al*., 2010) provided the basis for the analysis of effector orthologs between the two species, which contribute to the different disease development in maize. In contrast to *S. reilianum*, *U. maydis* possesses no RNAi machinery, which is unique within the smuts (Schirawski *et al*., 2010). RNAi in fungi was described to function in genomic defense, heterochromatin formation, and gene regulation (Dang *et al*., 2011).

Several effectors between *U. maydis* and *S. reilianum* have already been characterized and found to be either functionally conserved, i.e. See1 (Redkar *et al*., 2015b), or revealing different functions in the two species: Tin2 and Sts2 (Tanaka *et al*., 2019; Zuo *et al*., 2023). To understand the differences in the disease progression of the two closely related species and in particular the regulation of effector genes, a cross-species analysis was conducted (Zuo *et al*., 2021). This analysis revealed 207 out of 335 one-to-one effector orthologs being differentially expressed between *U. maydis* and *S. reilianum*. Notably, two effector orthologs with a conserved function were identified, suggesting a contribution of these effectors to the different disease development of *U. maydis* and *S. reilianum*, respectively. Furthermore, *S. reilianum* revealed more fungal biomass at 4 dpi, compared to *U. maydis* (Zuo *et al*., 2021). This suggests a faster proliferation of *S. reilianum* in early infection time points. Nevertheless, the underlying mechanism which determines the different disease development is still poorly understood.

Recently, a fungal hybrid of the haploid strains FB1 (*U. maydis*) and SRZ2 (*S. reilianum*) was used to understand the differences between the two species. However, this resulted in an unstable hybridization event with a lack of fungal proliferation *in planta* (Storfie & Saville, 2021). In previous work, hybridization between *U. maydis* and *S. reilianum* could be achieved by exchanging the mating type genes of the

haploid strain FB1 of *U. maydis* against *Sra1* and *Srb1* of *S. reilianum*. Together with the haploid strain SRZ2, the recombinant hybrid (rUSH) formed filaments on activated charcoal, which served as proof of the initial compatibility of the two species and thus provided the foundation for this study.

The major aim of this chapter was to elucidate the molecular components that influence the different disease development of *U. maydis* and *S. reilianum*. The first objective of this chapter was to investigate the compatibility of the two species for hybridization and the influence of hybridization on virulence at different developmental stages of maize. Another objective was to investigate the gene expression profile of rUSH *in planta* utilizing RNA-seq.

3.3 Results

3.3.1 Generation of a recombinant hybrid of *Ustilago maydis* and *Sporisorium reilianum*

To gain insights into the different disease development of *U. maydis* and *S. reilianum* and to facilitate interspecific hybridization, a recombinant mating type mutant was generated (Figure 3.1). In a two-step transformation, the mating type loci *Uma1* and *Umb1* were replaced in the haploid wild type strain FB1 using CRISPR-assisted HR. Two sgRNAs were designed in the *Uma1* and *Umb1* loci and used together with a donor template carrying the genomic sequence of *Sra1* (*a* locus: *mfa1.2*, *mfa1.3* and *pra1*) or *Srb1* (*b* locus: *bW1* and *bE1*), respectively, in the transformation. After confirmation via Southern blot (Figure S3.1), two independent transformants of FB1_*Sra1b1* were cultured, set to the same OD, and mixed one-to-one (6.9.2) with the corresponding SRZ2 wild type strain of *S. reilianum* (carrying the compatible mating type partner for *Sra2b2*), and further tested for all crucial steps of the biotrophic development *in planta*. Since both independent transformants showed similar results in infection assays with SRZ2, for all further experiments, only one strain named **Um_Smt** (*U. maydis S. reilianum* mating type mutant) was used. The fusion of Um_Smt and SRZ2 was subsequently named **rUSH** (recombinant *U. maydis* x *S. reilianum* hybrid) (Figure 3.1).

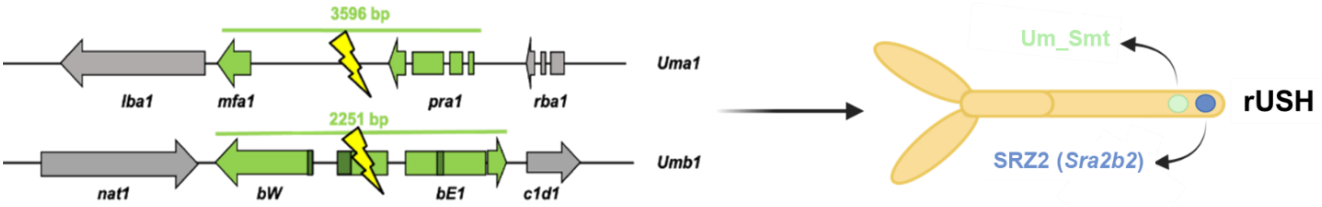

Figure 3.1: Generation of the recombinant *U. maydis* strain Um_Smt. To generate Um_Smt, CRISPR/Cas9-assited homologous recombination (HR) was used. Therefore, sgRNAs cutting within the *a* locus and *b* locus, respectively, were designed and cloned into the pCas9HF1 vector. In addition, a donor template carrying the *a* locus or *b* locus, respectively, was used for the transformation. The resulting mating type mutant was further called Um_Smt and used together with SRZ2 to create rUSH (Um_Smt+SRZ2). rUSH was used for all further experiments.

3.3.2 Proliferation of rUSH *in planta*

To investigate the fungal proliferation of rUSH *in planta*, a nuclear localization signal was added to mcherry and GFP and integrated into the *ip* locus of Um_Smt and SRZ2, respectively. When Um_Smt_mCherry + SRZ2_H1_GFP were mixed one-to-one to a final OD of 1 and dropped on an activated charcoal PD plate (Day & Anagnostakis, 1971), a dikaryotic hyphae could be observed using confocal microscopy. The hyphae carried one green and one red fluorescing nucleus, suggesting that the nuclei were derived from the two different haploid strains of *S. reilianum* (SRZ2) and *U. maydis* (Um_Smt), respectively (Figure 3.2A). Next, the nuclear state of rUSH *in planta* was observed by infecting Um_Smt_H1_mcherry + SRZ2_H1_GFP into 7-day old maize seedlings. FB1_cyto_mcherry + SRZ2_H1_GFP served as a control (Figure 3.2B+C). Similar to the *in vitro* results, a dikaryotic state of the fungal hyphae of rUSH was observed *in planta* at 2 dpi. To elucidate whether rUSH can successfully penetrate the plant tissue, a Calcofluor White staining was conducted on leaves collected at 22 hours post infection (hpi) and analyzed by microscopy (Figure 3.2D). Appressoria-like structures were observed for the wild type of *U. maydis* (FB1+FB2), the wild type of *S. reilianum* (SRZ1+SRZ2), and rUSH.

To investigate the phenotype of rUSH *in planta*, maize seedlings were infected with FB1+FB2, SRZ1+SRZ2, FB1+SRZ2, and rUSH. The phenotypes were observed at 6 days post infection (dpi). While *U. maydis* showed typical infection symptoms such as chlorosis, anthocyanin production, and tumor formation, rUSH and FB1+SRZ2 showed chlorosis and necrotic spots, similar to *S. reilianum*. However, FB1+SRZ2 showed less symptoms compared to rUSH (Figure 1.3.2E). To examine the proliferation of rUSH *in planta* over time, a biomass quantification experiment was conducted. The fungal biomass was measured using the *ppi* gene of *U. maydis* normalized to the *GAPDH* gene of maize. For rUSH, an increase in fungal biomass between 3 dpi and 6 dpi could be observed, while for FB1+SRZ2 no increase over time could be shown (Figure 3.2F). Presumably, the *U. maydis* wild type did not result in an increase in biomass since the leaf area used for the quantification was already fully infected at 3 dpi, similar as reported by Zuo *et al.* (2021). Taken together, rUSH was observed to be capable of mating, forming dikaryotic hyphae, penetrating, and proliferating in maize during the early stages of infection.

To elucidate, whether the mating type system of *U. maydis* can also lead to a successful hybridization, an *S. reilianum* mating type mutant (Sr_Umt) was generated. Therefore, the *S. reilianum* mating type genes *Sra1* and *Srb1* were replaced by *Uma1* and *Umb1* in the SRZ1 background using RNP-mediated CRISPR/Cas9 (see Chapter 2; Figure S3.2A). For the construction of the Sr_Umt strain, two sgRNAs against the *a* and the *b* locus of *S. reilianum* were designed (Figure S3.2C) and tested in an *in vitro* cleavage assay for their on-target efficiency (Figure S3.2B). In a two-step RNP-mediated transformation,

Sra1 and Srb1 were replaced by *Uma1* and *Umb1* (Figure S3.2E), respectively, using a donor template. The transformants of Sr_Umt were verified by Southern blot (Figure S3.2D+F), and for all following experiments, infected along with the compatible mating partner FB2, as the recombinant *S. reilianum* x *U. maydis* hybrid (**rSUH**), into maize seedlings. At 6 dpi, the infected leaves were macerated. To investigate the proliferation of rSUH in maize in more detail, fungal biomass was quantified (Figure S3.2G) and WGA staining for fluorescence microscopy was performed (Figure S3.2H). These experiments resulted in a "clumped" hyphae phenotype (Figure S3.2H), without an increase in biomass between 3 dpi and 6 dpi as it has been shown for rUSH. This suggests incompatibility between the two haploid strains. Therefore, rUSH was used in all further experiments of this study.

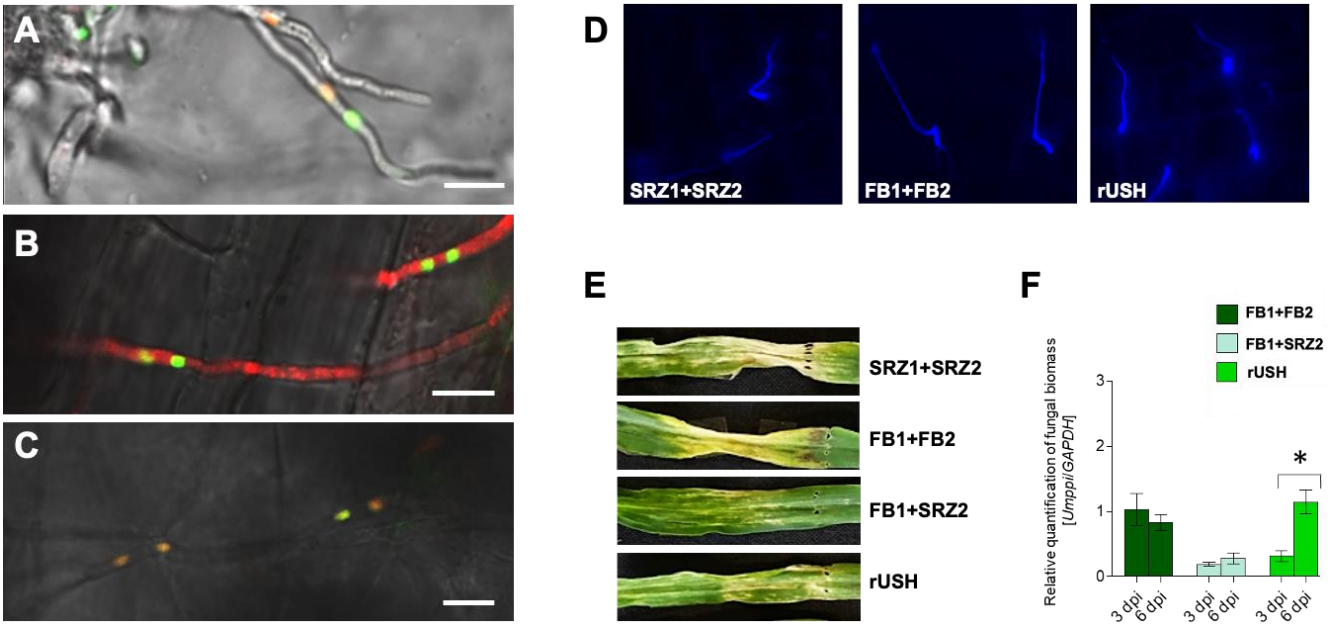

Figure 3.2: Proliferation of rUSH *in planta*. A: Confocal microscopy of Um_Smt_H1_mCherry + SRZ2_H1_GFP on activated charcoal. Scale bar: 10 µM. **B:** Confocal microscopy of 2 dpi maize leaf infected with Um_Smt_mCherry (cytosolic) + SRZ2_H1_GFP. Scale bar: 10 µM. **C:** Confocal microscopy of 2 dpi maize leaf infected with Um_Smt_H1_mCherry + SRZ2_H1_GFP. Scale bar: 10 µM. **D:** Calcofluor white staining of SRZ1+SRZ1 (*S. reilianum* wild type), FB1+FB2 (*U. maydis* wild type), and rUSH. **E**: Phenotype of 6 dpi infected maize leaves of SRZ1+SRZ1 (*S. reilianum* wild type), FB1+FB2 (*U. maydis* wild type), FB1+SRZ2 (control) and rUSH. F: Quantification of fungal biomass at 3 dpi and 6 dpi of infected maize leaves. *GAPDH* (housekeeping gene) of maize and *ppi* of *U. maydis* were used for the quantification of gDNA. Significant differences were calculated based on students t-test (* =$p<0.05$).

S. reilianum systemically infects maize without causing prominent early symptoms. The disease is characterized by a replacement of the inflorescences by teliospores and the formation of phyllody (leafy ear) (Ghareeb *et al*., 2011). To assess the phenotype of rUSH at different time points, FB1+FB2,

SRZ1+SRZ2, and rUSH were used to infect 7-day old maize seedlings of the early flowering maize cultivar Gaspe Flint. The phenotypes were observed three weeks post infection (wpi) (tassel) and eight wpi (ear), respectively (Figure 3.3). rUSH caused a *S. reilianum*-like disease phenotype with leafy ears as the most prominent symptom. However, in none of the performed infection assays (seedling-, tassel-, and ear infection), the formation of teliospores was observed for rUSH (Figure 3.3). Thus, rUSH can colonize different maize organs, it forms *S. reilianum*-like disease symptoms, but is not able to generate teliospores and progeny.

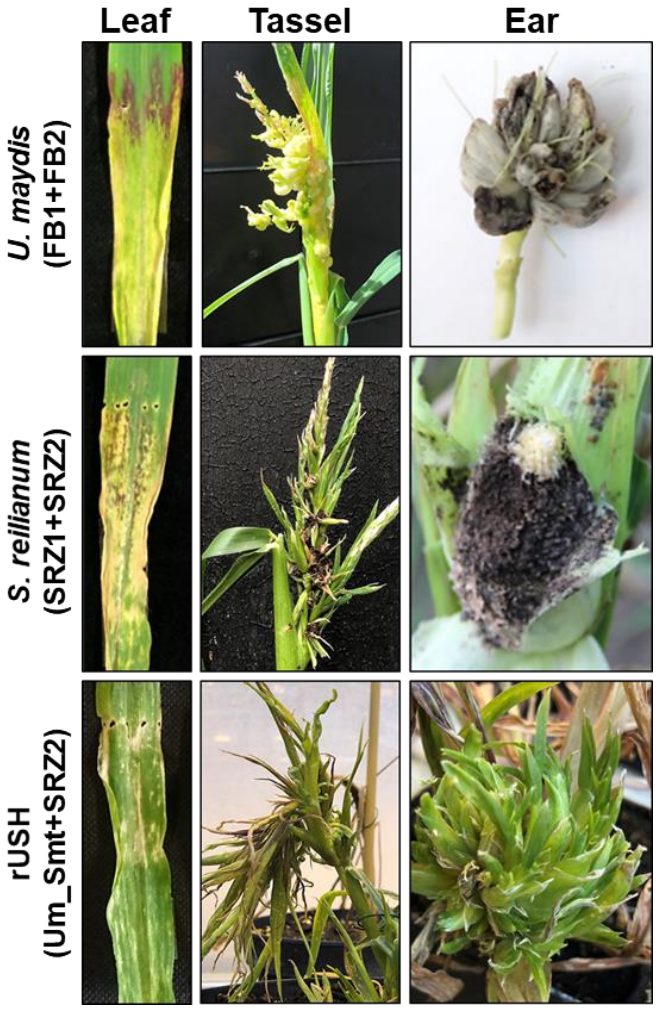

Figure 3.3: Phenotype of the *U. maydis*, *S. reilianum,* and rUSH at all developmental stages of maize. Maize seedlings were infected and grown for 6 days (leaf), 3 weeks (tassel), and 8 weeks (ear) in the greenhouse. Pictures of the ear of maize plants for FB1+FB2 and SRZ1+SRZ2 were taken by Weiliang Zuo, AG Döhlemann.

Since it was proposed that the differential expression of functionally conserved effector genes might contribute to the different phenotypes of *U. maydis* and *S. reilianum* (Zuo *et al*., 2021), the gene expression of effector genes in rUSH was investigated. The expression of two known effector genes,

pit2 (essential virulence factor, highly expressed throughout infection) and *see1* (tumor-related effector, moderate expression with peak at 2 dpi) was quantified via qRT-PCR at 20 hpi, 3 dpi, and 6 dpi (Figure 3.4). For the *U. maydis* orthologues, *Umpit2* and *Umsee1*, the expression was significantly reduced in rUSH at 6 dpi when compared to the *U. maydis* wild type. In contrast, the *S. reilianum* orthologues, *Srpit2* and *Srsee1* were higher expressed in rUSH at 6 dpi, which means a reverse expression of these orthologous genes in rUSH.

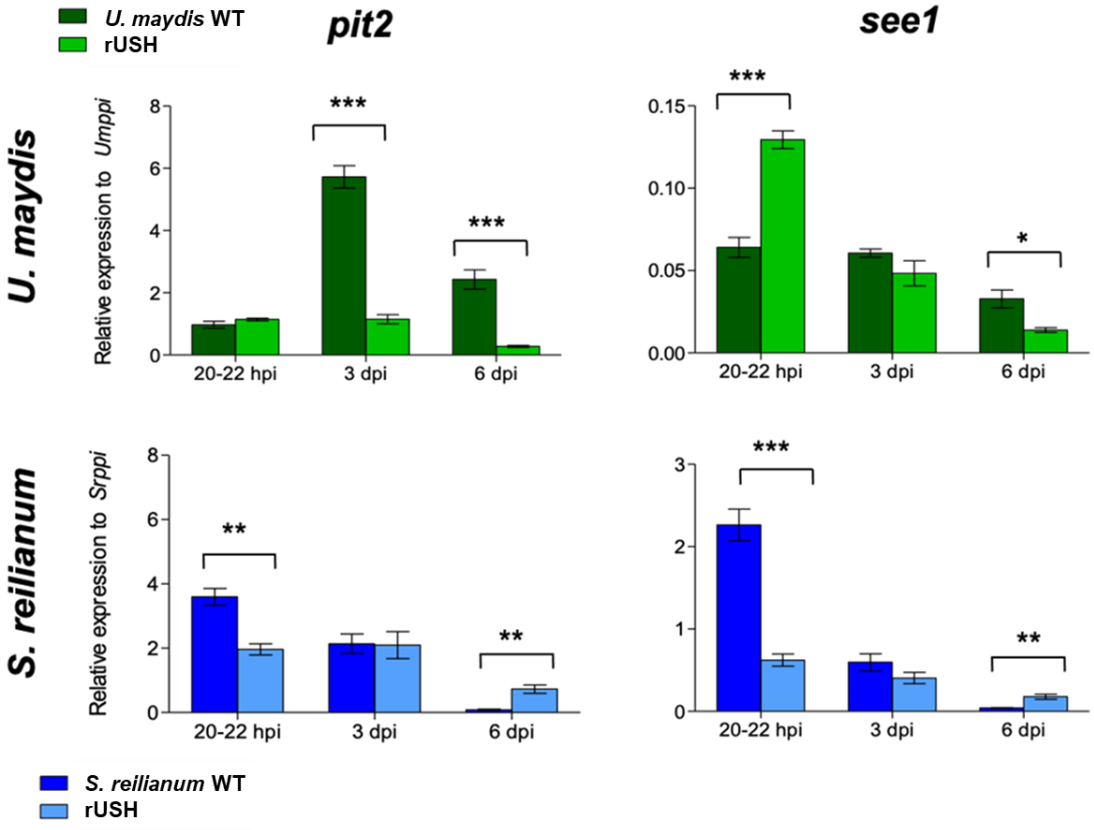

Figure 3.4: Gene expression of the one-to-one effector orthologues *pit2* and *see1* in rUSH. Gene expression of *pit2* and *see1* were measured and normalized to the *ppi* gene of *U. maydis* or *S. reilianum*, respectively. Significant differences were calculated based on students t-test (* =p<0.05, ** =p<0.01, *** =p<0.001).

3.3.3 Downregulation of the *U. maydis* effector orthologues in rUSH

Unlike *U. maydis*, *S. reilianum* possesses a functional RNA silencing machinery (Schirawski *et al*., 2010). Therefore, the reduced expression levels of *U. maydis* orthologues in rUSH compared to FB1+FB2 raised the question, if the expression of *U. maydis* genes in rUSH could be subjected to gene silencing (Figure 3.4). Gene silencing could be caused by different degrees in methylation which can reduce the accessibility of specific genes or through a direct mRNA degradation

by RNAi. To test if the expression of *U. maydis* effector genes is affected by RNAi machinery in rUSH, an *S. reilianum* deletion strain lacking the *dicer* gene (*sr16838*) was generated in the SRZ2 background. A sgRNA targeting the middle part of the coding sequence (cds) of *sr16838* was designed and used for RNP-mediated mutagenesis. The use of 1 kb homology flanks in a donor template enabled an efficient HR in *S. reilianum* (Figure S3.3A). The deletion of *sr16838* was verified by PCR (Figure S3.3B) and Southern blot (Figure S3.3C) before infection of maize seedlings. rUSH and two independent rUSH combinations, lacking the *dicer* gene in the *S. reilianum* SRZ2 strain were used for the infection. Next, qRT-PCR was conducted to investigate the expression of *Umsee1*, *Umnlt1,* and *Umtin2* at 3 dpi and 6 dpi. However, for these three genes, no significant changes in expression levels were observed upon deletion of the Dicer-encoding gene *sr16838* (Figure S3.3D). This suggests that the RNAi machinery of *S. reilianum* does not play a major role in the observed downregulation effect of the tested *U. maydis* orthologues in rUSH.

3.3.4 Expression of *tin2* in rUSH is determined by the promoter

To test if the reduced expression of *U. maydis* in rUSH results from locus-specific silencing, the effector gene *tin2* was used for the following experiment. *Umtin2* functions as a virulence factor and is part of the biggest cluster 19A in *U. maydis*. UmTin2 is translocated to the plant cells and targets ZmTTK1, a protein kinase, leading to anthocyanin formation and the attenuation of lignification (Tanaka *et al.,* 2016). While UmTin2 causes anthocyanin accumulation in maize, for *S. reilianum* no anthocyanin formation is visible during infection (Tanaka *et al*., 2019). In a previous study, the *S. reilianum* orthologue *Srtin2* was found to be expressed at higher levels during maize leaf infection compared to its *U. maydis* one-to-one orthologue (Zuo *et al*., 2021). A qRT-PCR was performed to elucidate the expression level of both *U. maydis* and *S. reilianum tin2* in rUSH. Similar to *Umpit2* and *Umsee1* (Figure 3.4), also *Umtin2* showed a significantly lower expression in rUSH compared to *U. maydis* wild type, while *Srtin2* showed significantly higher expression in rUSH compared to *S. reilianum* wild type (Figure 3.5A+B). Consistent with this expression pattern, rUSH did not induce anthocyanin accumulation in the infected leaf areas.

To investigate the cause for the downregulation of *Umtin2* in rUSH, either the promoter or the coding sequence of the *tin2* orthologue was exchanged (Figure 3.5C+D).

Two strains were generated using CRISPR-assisted HR: one *U. maydis* strain, which expresses *Umtin2* under the control of pro^{Srtin2} in the native locus in the Um_Smt strain and one *S. reilianum* strain in the SRZ2 background, where *Umtin2* is expressed under the control of pro^{Srtin2} in the native locus in *S. reilianum*. When *Umtin2* had been expressed under the control of pro^{Srtin2}, a strong anthocyanin formation was observed (Tanaka *et al*., 2019). Strikingly, anthocyanin was also induced upon rUSH infection when pro^{Srtin2} was used to express *Umtin2* in Um_Smt. The promoter-swap to drive *Umtin2*

expression by pro^{Srtin2} in rUSH abolished the transcriptional repression of *Umtin2* (Figure 3.5C). Similarly, the expression of the *Umtin2* coding sequence in the SRZ2 background was not reduced in the native locus of *S. reilianum* (Figure 3.5D).

These results indicate that the differential expression of *Umtin2* is determined by the promoter and thus, *tin2* expression is *cis*-regulated. To get further insights into this tendency of a downregulation effect and its underlying mechanisms, additional orthologues need to be assessed in the future.

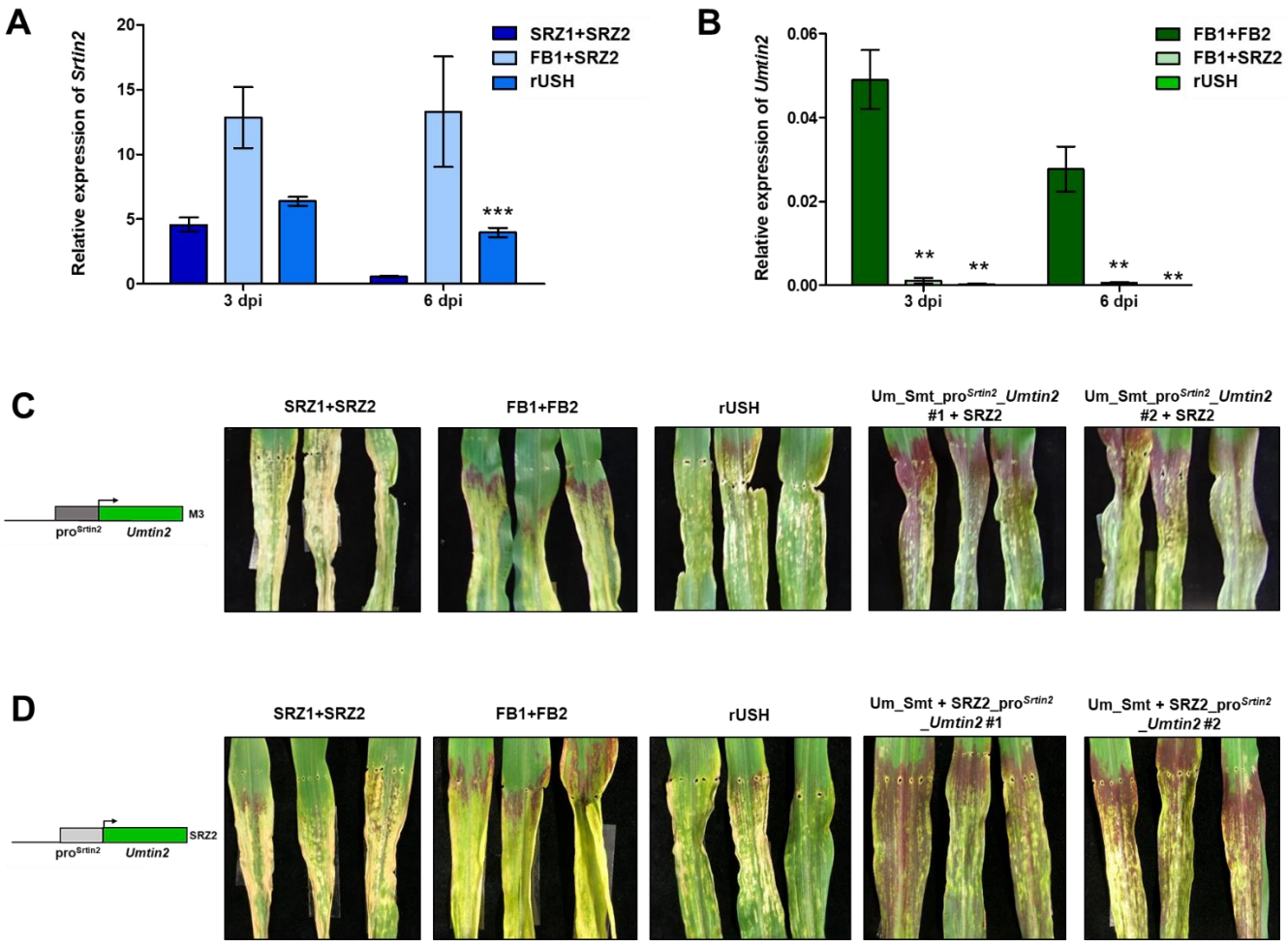

Figure 3.5: The downregulation of the *Umtin2* orthologue in rUSH can be abolished by maintaining the *cis*-regulatory element of the *S. reilianum* orthologue. (A) Relative expression of *Srtin2* compared to *Srppi* in SRZ1+SRZ2, FB1+SRZ2 and rUSH. **(B)** Relative expression of *Umtin2* compared to *Umppi* in FB1+FB2, FB1+SRZ2 and rUSH. **(C,D)** Phenotype assessment of rUSH: pro^{Srtin2} controlling *Umtin2* in Um_Smt **(C)** and pro^{Srtin2} controlling *Umtin2* in *S. reilianum* **(D)**. Plants were grown for 7 days in the walk-in chamber before infection. For the infection assay, strains were grown for 5h at 28°C (200 rpm) and set to an OD of 2 before they were mixed 1:1 to a final OD of 1, and 0.1% (v/v) of Tween was added. Phenotypes were assessed at 6 dpi. Error bars (standard deviation) were calculated from three biological replicates. Significant differences were calculated based on students t-test (* =p<0.05, ** =p<0.01, *** =p<0.001).

3.3.5 RNA-seq analysis of rUSH

To gain a comprehensive insight into the gene expression landscape in rUSH, an RNA-seq experiment was conducted. FB1+FB2, SRZ1+SRZ2, and rUSH were used to infect maize seedlings. Samples were taken at 20 hpi, 3 dpi, and 6 dpi (Figure 3.6). Total RNA was extracted (6.7.13.1) and tested in qRT-PCR for the consistency of the replicates before 3 biological replicates were selected for sequencing. The downstream analysis of the RNA-seq data was conducted as described in 3.5.4. Principal component analysis (PCA) revealed a clustering of the three biological replicates. The wild type of *U. maydis* and *S. reilianum* at 3 dpi and 6 dpi exhibited a greater distance from the other treatments (Figure S3.4).

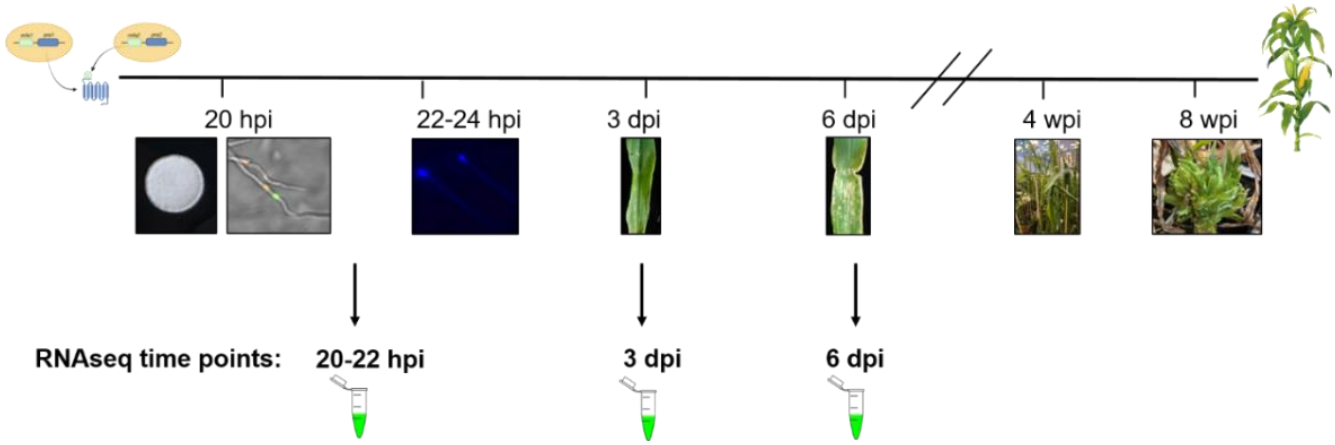

Figure 3.6: Time points of RNA-seq sampling. Samples were taken at 20-22 hpi, 3 dpi, and 6 dpi of FB1+FB2, SRZ1+SRZ2, and rUSH. At 20-22 hpi, fungal material on the plant surface was enriched using liquid latex (see 6.7.13.1). At 3 dpi and 6 dpi, 4 cm of plant material (see 6.7.13) was used for the extraction of total RNA.

First, the obtained relative reads were quantified. In rUSH, similar read counts were observed for both, *U. maydis* and *S. reilianum* at 20 hpi and 3 dpi. At 6 dpi slightly more reads from *U. maydis* were obtained (Figure 3.7B). In a previous study, the differential expression of effector genes between *U. maydis* and *S. reilianum* was proposed to contribute to the different infection modes of the two pathogens (Zuo *et al*., 2021). To test whether the differential effector gene expression explains the *S. reilianum*-like phenotype of rUSH, one-to-one orthologues (determined by Zuo *et al*., 2021) were categorized into effector genes (total number of predicted effector genes: *U. maydis*: 336; *S. reilianum*: 392) and non-effector genes and analyzed for the differential expression. At 3 dpi and 6 dpi the differentially expressed non-effector genes in rUSH were compared to the *U. maydis* wild type (Figure 3.7C). In total, 218 of 336 one-to-one effector orthologues were differentially expressed (log_2FC 1, $p<0.05$). At 3 dpi and 6 dpi, 39 effector genes were exclusively differentially expressed in rUSH, but not in WT (Table S3.1). In rUSH, two effector genes (*UMAG_11915* and *UMAG_12205*) were specifically differentially expressed at 3 dpi and 25 effector genes at 6 dpi, while 12 effector genes were differentially

expressed at both time points (Figure 3.7; gene id of the effector genes: Table S3.1). When the time points of effector gene expression were analyzed individually, at 20 hpi 22, at 3 dpi 38, and at 6 dpi 50 effector genes were exclusively differentially expressed in rUSH and not in the *U. maydis* wild type (Figure S3.5).

In the next step, the RNA-seq data was subjected to further screening of *U. maydis* effector genes that exhibited lower expression in rUSH relative to the wild type (see 3.3.7), *S. reilianum* effector genes that exhibited higher expression in rUSH relative to the wild type (see 3.3.9), as well as differentially expressed genes encoding for TFs, potentially involved in the regulation of effector genes (see 3.3.6). The following sections describe the generation of KO mutants of the three categories previously mentioned, to demonstrate a potential involvement in the observed phenotype.

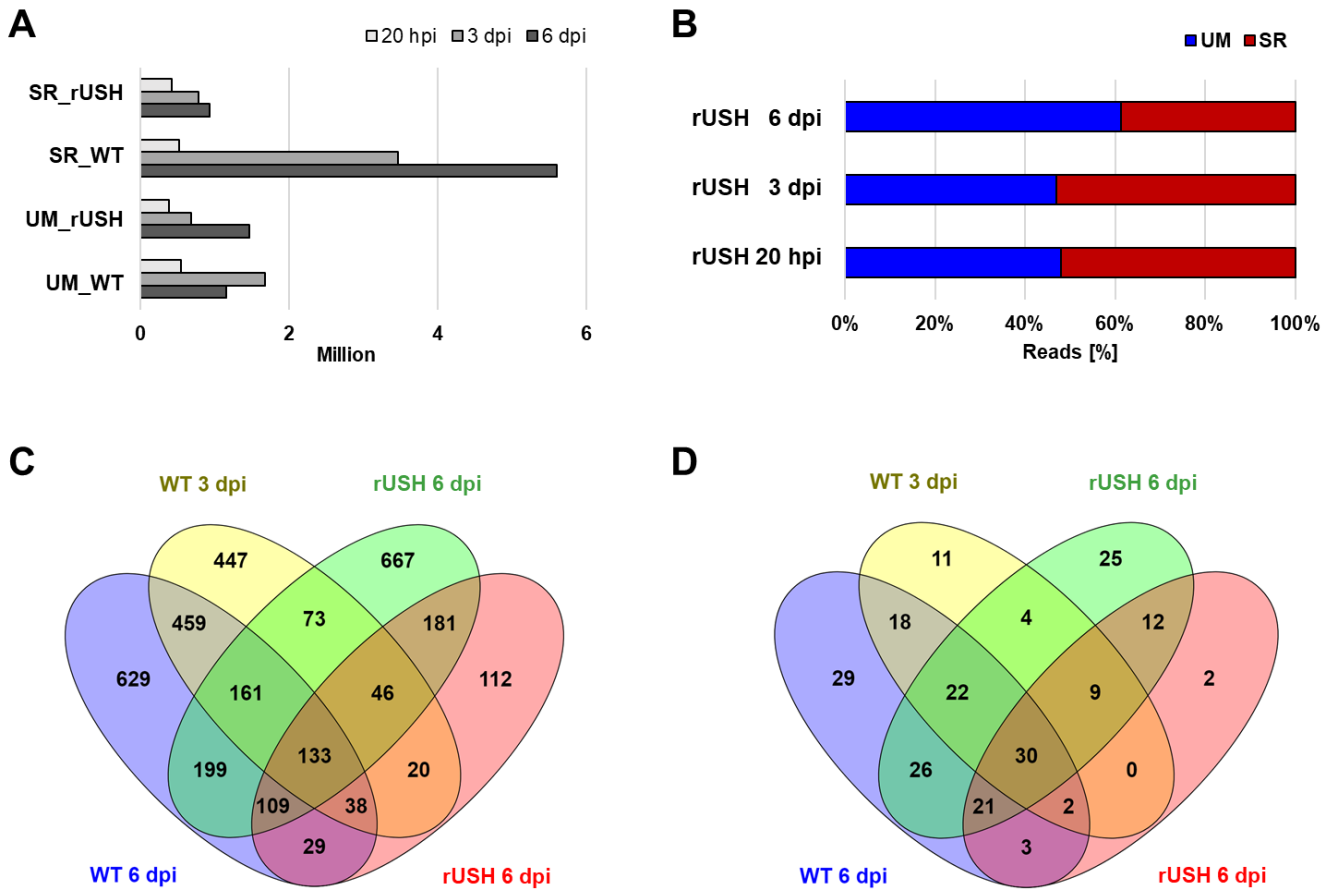

Figure 3.7: RNA-seq analysis of rUSH. (A) Relative reads were obtained from each species at 20 hpi, 3 dpi, and 6 dpi. **(B)** Total reads from *U. maydis* and *S. reilianum* in rUSH at 20 hpi, 3 dpi and 6 dpi. **(C)** Differentially expressed non-effector genes at 3 dpi and 6 dpi. **(D)** Differentially expressed effector genes at 3 dpi and 6 dpi. **(C+D)** Depicted with Venny 2.1.0 (Oliveros, J.C., 2007-2015).

To test the influence of the mating type exchange on the gene expression, an RNA-seq experiment of rUSH and the hybrid FB1+SRZ2 was performed at 3 dpi. The analysis revealed 5,134 and 826 differentially upregulated one-to-one orthologues of *S. reilianum* and *U. maydis*, respectively (Figure S3.6). Among these, 294 *S. reilianum* and 119 *U. maydis* effector genes were identified to be higher expressed in rUSH compared to FB1+SRZ2. The numerous one-to-one orthologues upregulated in rUSH underline the generally higher fitness of rUSH compared to FB1+SRZ2.

3.3.6 Expression of effector genes in rUSH revealed distinct regulation patterns

To get a general overview of the regulation of effector genes between *U. maydis* and *S. reilianum*, the differentially expressed effector genes were grouped into four distinct expression patterns (Figure 3.8A): (**i**) *cis*: the *cis*-regulated expression of effector genes revealed the same differential expression trend between the parental orthologues as well as the orthologues within rUSH, (**ii**) *trans*: a *trans*-regulated expression of effector orthologues was found, where the orthologous genes were significantly higher expressed in one parental WT, but not in rUSH. Notably, two patterns were identified which were hybrid-specific. One of these hybrid-specific expression is the (**iii**) reverse expression of effector orthologues. In this pattern, the orthologous effector genes were significantly higher expressed in one of the parental genomes and showed the opposite expression trend in rUSH (Figure 3.8A). This expression pattern was specifically observed for many effector genes residing in virulence-related gene clusters. Lastly, an orthologue-specific expression (**iv**) was observed, where only one orthologue changes the expression and is either up- or downregulated in rUSH, while the other orthologue shows the same expression trend as between the parents. While the *cis*-regulated effector genes and the *trans*-regulated effector genes were explained by the *cis*-regulatory element in the promoter region and the TF, respectively, the reverse expression was not observed in any other study so far. Therefore, we hypothesized that an interaction between *cis*- and *trans*-regulation may cause this hybrid-specific expression.

Next, the gene expression of previously functionally characterized effector genes was analyzed in rUSH and compared to the wild type (Figure S3.7). The log 2 fold change (log_2FC) (*S. reilianum* / *U. maydis*) of orthologue expression level was calculated between *S. reilianum* and *U. maydis* wild type, and within rUSH. In particular, at 6 dpi an in general higher expression of the *U. maydis* effector orthologue was observed in the wild type, while in the rUSH background, the *S. reilianum* orthologue expression was dominant (Figure S3.7). This can be integrated into the reversed expression pattern, which is in line with the effector gene expressions of *pit2* and *see1* observed in previous results (Figure 3.4). 281 of 336 one-to-one effector orthologues were expressed in rUSH and the wild types, respectively, and revealed

the previously mentioned expression patterns (G1+G3 = *trans*, G2+G4 = reverse, G5+G6= *cis*, G7+G8 = ortholog-specific) (Figure 3.8B).

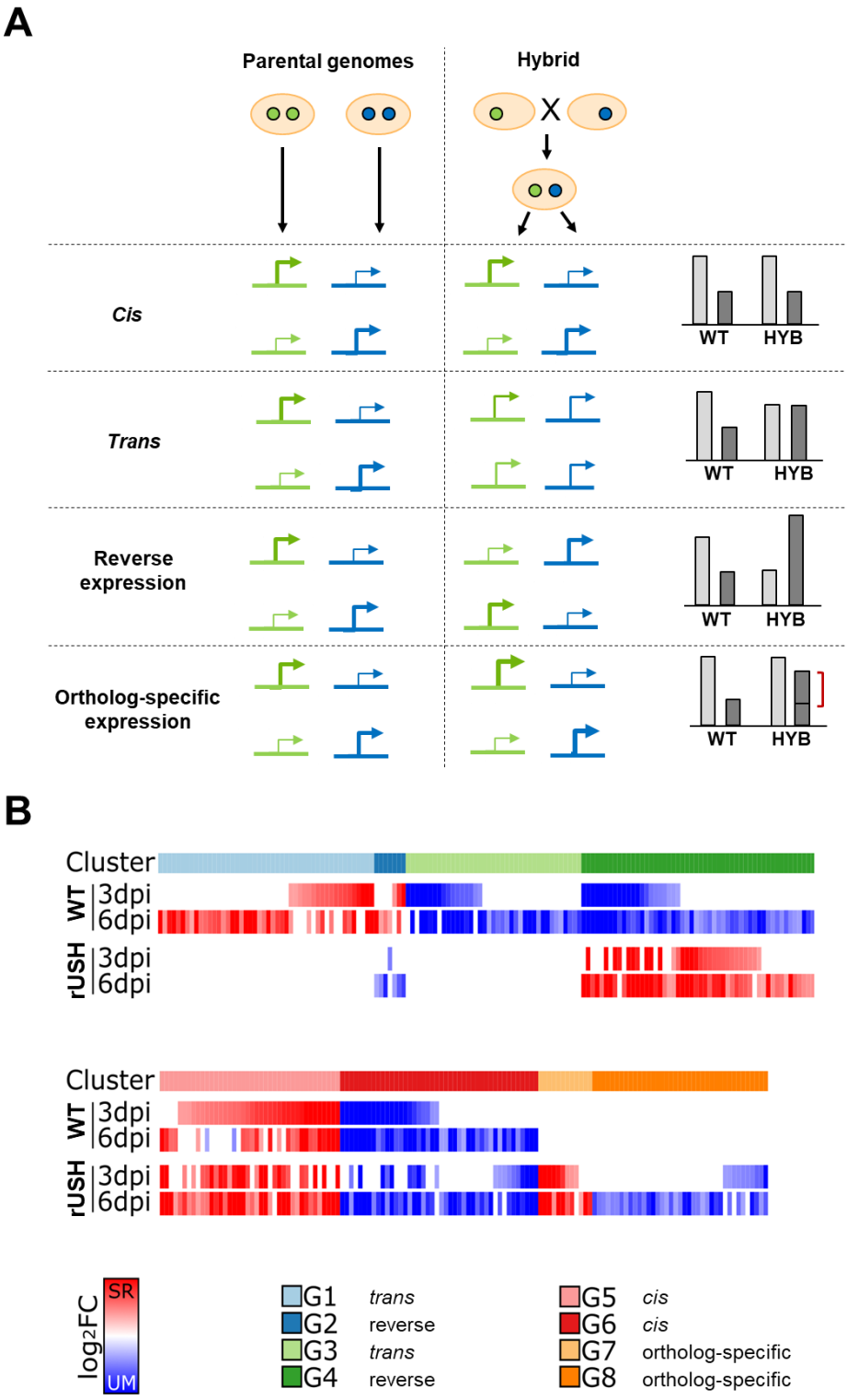

Figure 3.8: Differentially expressed effector genes in rUSH revealed distinct expression patterns. (A) Expression patterns of differentially expressed effector one-to-one effector orthologues in rUSH. Effector genes between the *U. maydis* and *S. reilianum* are differentially expressed and i) *cis*: remains the same expression in rUSH, ii) *trans*: exhibits an equal expression between the two orthologues within rUSH. iii) Reverse expression: shows the opposite expression in rUSH, iv) Orthologue-specific expression: only one orthologue changes the expression within rUSH. The effector gene expression was calculated by dividing the *S. reilianum* transcripts per million (TPM) by *U. maydis* TPM of the wild types FB1+FB2 and SRZ1+SRZ2 (SR_WT / UM_WT) as well as within rUSH (SR_rUSH/UM_rUSH). **(B)** Orthogene clustering was performed based on the expression profiles between WT and rUSH. More specifically, the total expression of each orthogene at 3 and 6 dpi was compared between WT and rUSH, leading to the creation of 8 clusters with the following patterns: G1, higher SR in WT, no difference in rUSH (*trans*-regulated); G2, higher SR in WT, higher UM in rUSH (reverse expression); G3, higher UM in WT, no difference in rUSH (*trans*-regulated); G4, higher UM in WT, higher SR in rUSH (reverse expression); G5, higher SR in WT, higher SR in rUSH (*cis*-regulated); G6, higher UM in WT, higher UM in rUSH (*cis*-regulated); G7, no difference in WT, higher SR in rUSH (orthologue-specific expression); G8, no difference in WT, higher UM in rUSH (orthologue-specific expression).

The RNA-seq results for predicted one-to-one orthologues were further screened for novel TFs, putatively involved in the regulation of genes important for the pathogenicity of *U. maydis*. 78 putative TFs were found to be differentially expressed between *U. maydis* and *S. reilianum* (Figure 3.9). On the one hand, TFs with a higher expression of the *U. maydis* wild type compared to the *S. reilianum* wild type, and on the other hand, TFs which revealed between the wild types a higher *U. maydis* expression compared to the *S. reilianum* orthologue and showed a higher *S. reilianum* expression in rUSH, were chosen as candidates putatively involved in the observed phenotype of rUSH. To further investigate the putative role of these TFs in the control of the regulation of effector genes important for pathogenicity, five were selected for the generation of frameshift mutant strains in *U. maydis* background and tested in infection assays (*UMAG_06257*, *UMAG_10256*, *UMAG_00533*, *UMAG_04262,* and *UMAG_04242*). However, none of the tested mutants showed a different phenotype compared to the wild type of *U. maydis* FB1+FB2 or the solopathogenic strain SG200, respectively (data not shown).

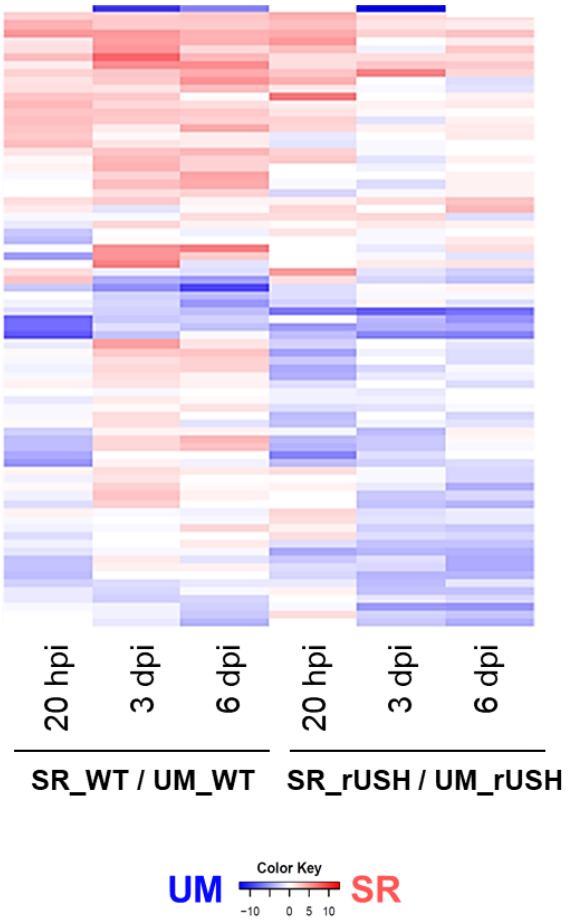

Figure 3.9: Differentially expressed 1:1 orthologous transcription factors between *U. maydis* and *S. reilianum* and in rUSH. *S. reilianum* orthologue expression (TPM) was compared with *U. maydis* orthologue expression between the wild types FB1+FB2 and SRZ1+SRZ2 and within rUSH.

3.3.7 Differentially expressed effector orthologues contribute to fungal virulence and tumorigenesis

The influence of highly expressed *S. reilianum* orthologues in rUSH was tested, to elucidate their contribution to virulence. From the previously mentioned *cis*-regulated expression pattern (Figure 3.8, cluster G5), a highly expressed *S. reilianum* effector gene (higher expression level in rUSH compared to the wild type) was identified. The effector gene with the highest expression among all effector genes of *S. reilianum* in rUSH (*sr16075*) was further tested for its contribution to the *S. reilianum*-like phenotype. Two independent deletion mutants of *sr16075* in SRZ1 and SRZ2 were generated using RNP-mediated HR with a donor template (1 kb flanking regions, see Chapter 2), and verified by PCR and Southern blot (Figure S3.8). In infection assays of 7-day old seedlings of the maize cultivar Gaspe Flint, deletion mutants of *sr16075* showed a reduced virulence compared to the wild type SRZ1+SRZ2 at 8 wpi (Figure 3.10), suggesting a contribution to *S. reilianum* virulence.

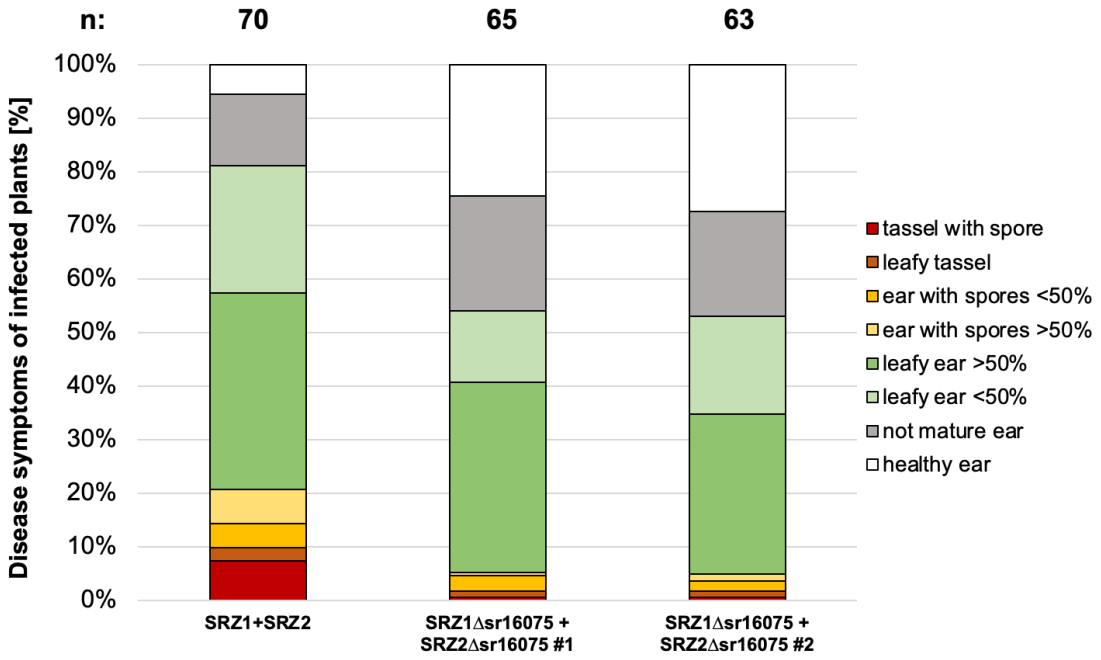

Figure 3.10: Infection of maize cultivar Gaspe Flint with *S. reilianum* wild type SRZ1+SRZ2 and two independent deletion mutants of *sr16075* (SRZ1Δ*sr16075*+SRZ2Δ*sr16075* #1 and SRZ1Δ*sr16075*+SRZ2Δ*sr16075* #2). 7-days old maize seedlings were infected with a final OD of 1 of the mating type combinations. Disease symptoms were scored 8 wpi as described by (Ghareeb *et al*., 2019).

To investigate the *U. maydis* effector gene expression in rUSH, the ratio of transcripts per million (TPM) between the wild types SRZ1+SRZ2 and FB1+FB2 (FC(SR/UM)) was calculated. For the wild type, the expression was divided by two for each gene from each species due to the higher copy number. Notably, an increasing number of up- and downregulated *U. maydis* effector genes was observed from 20 hpi to 6 dpi, while for *S. reilianum* the differentially expressed genes decreased from 20 hpi to 6 dpi, with a similar contribution of up- and downregulated effector genes (Figure 3.11A). As previously stated, the low expression of *U. maydis* effector genes in rUSH may be involved in the formation of tumors caused by *U. maydis*. To investigate this hypothesis, an at least 5-fold decrease of effector gene expression in rUSH compared to the wild type was set as the cut-off (expression in the wild type > 1000 TPM, expression in rUSH < 200 TPM). This revealed 14 downregulated effector genes in rUSH compared to the wild type Figure 3.11B. For seven out of the 14 identified effector genes, frameshift mutants were generated (*UMAG_03749*, *UMAG_05780*, *UMAG_10553*, *UMAG_05928*, *UMAG_04039*, *UMAG_03751* and *UMAG_05312*) and tested in infection assays. At least two independent mutants of each effector gene were compared to the solo-pathogenic strain SG200 for their virulence on maize seedlings. For the majority of the tested effector KO mutants, no difference in virulence could be observed in comparison to SG200.

In contrast, *UMAG_05312* and *UMAG_10553* showed a significant reduction in virulence compared to SG200 at 12 dpi (Figure 3.11C), suggesting a role of these effectors in tumorigenesis of *U. maydis*. Further, *UMAG_05312* and *UMAG_10553* both reside in cluster 19A which was proposed to comprise effector genes important for tumor formation (Brefort *et al*., 2014; Kämper *et al*., 2006). The expression level of both *U. maydis* effectors was found to be lower in rUSH than in the *U. maydis* wild type. Upon detailed examination of the expression patterns, it was observed that the two effector genes, *UMAG_05312* and *UMAG_10553*, exhibited hybrid-specific expression and belong more specifically to the previously described reverse expression pattern.

A

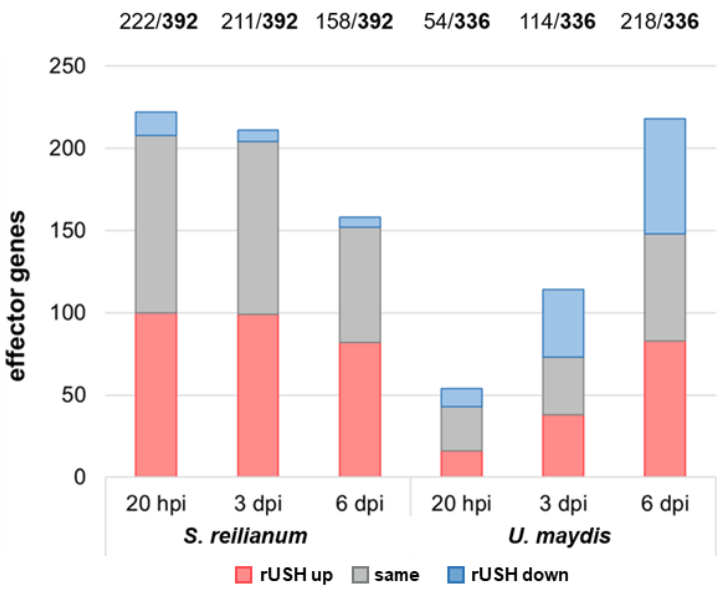

B

Gene ID – effector	WT 6 dpi	rUSH 6 dpi	Description
UMAG_05318	2454.7	112.3	Cluster 19A, Sts2
UMAG_03749	2428.1	32.0	Cluster 10A
UMAG_05780	2412.3	162.1	no
UMAG_10553	1935.7	22.5	Cluster 19A
UMAG_05928	1925.0	56.7	no
UMAG_04039	1655.1	64.3	no
UMAG_03751	1308.0	7.4	Cluster 10A
UMAG_05300	1287.6	168.4	Cluster 19A
UMAG_02533	1267.3	3.2	Cluster 6A
UMAG_05295	1249.9	18.0	Cluster 19A
UMAG_01987	1138.1	187.2	Pep1
UMAG_05312	1134.5	23.3	Cluster 19A
UMAG_05306	1101.5	8.0	Cluster 19A
UMAG_11060	1038.6	87.7	Tip6

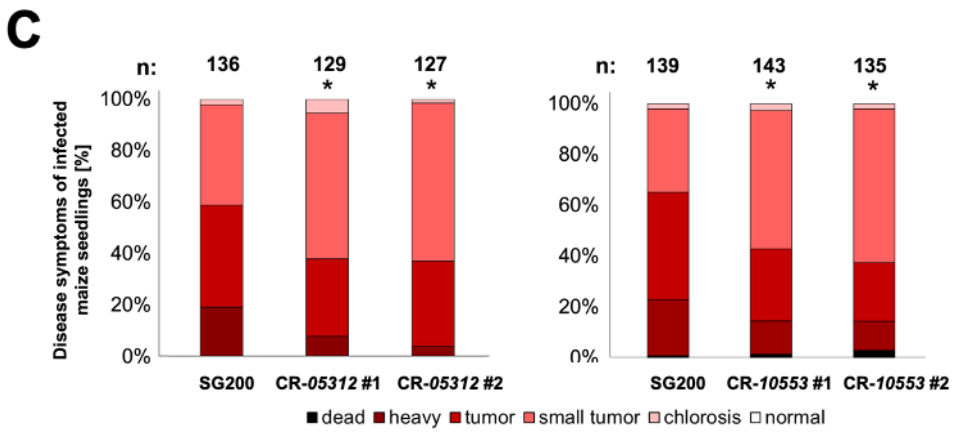

Figure 3.11: Differentially expressed effector genes between wild type *U. maydis* and *S. reilianum* vs. rUSH. **(A)** Log_2FC of effector gene expression was calculated by dividing the *S. reilianum* transcripts per million (TPM) by *U. maydis* TPM of the wild types FB1+FB2 and SRZ1+SRZ2 as well as within rUSH. For the analysis of rUSH, the expression was divided by two, reflecting the existence of only one mating partner of the species, respectively. **(B)** Downregulated 1:1 effector orthologues in rUSH compared to the wild type. TPM: Transcripts per million. **(C)** Infection assay of SG200, SG200:CR-*UMAG_05312*#1, SG200:CR-*UMAG_05312* #2, SG200-CR:*UMAG_10553*#1 and SG200:CR-*UMAG_10553*#2 at 12 dpi. 7-days old maize seedlings were infected with SG200 and mutant strains. Significant differences were calculated based on students t-test (* =p<0.05).

3.3.8 Cluster 19A is crucial for tumor formation of *U. maydis*

The RNA-seq analysis revealed distinct expression patterns of one-to-one effector orthologues (Figure 3.8). Cluster 19A of *U. maydis* comprises 24 effector genes, of which 15 have a one-to-one orthologue in *S. reilianum*. 14 of the 24 effector genes can be assigned to the different expression patterns (*trans*: 5, *cis*: 3, hybrid-specific: 6 (reverse 5, orthologue-specific: 1)). However, the regulation patterns need to be further verified by qRT-PCR in the future. Notably, two neofunctionalized effectors, Tin2 and Sts2 (Tanaka *et al*., 2019; Zuo *et al*., 2023), residing also in cluster 19A were identified with diversified functions in *U. maydis* and *S. reilianum,* respectively. In addition, two novel virulence factors in cluster 19A were identified in this study (see 3.3.7).

Since many cluster 19A effector genes were differentially expressed between rUSH and the wild type, and the cluster is known for diversified functions between *U. maydis* and *S. reilianum*, a contribution to the species-specific adaptation and symptom development of the cluster 19A genes is hypothesized. To test this hypothesis, cluster 19A of *S. reilianum* was deleted in both mating types (SRZ1 and SRZ2) using three sgRNAs with Cas9 in three RNPs together with a donor template (comprising 1 kb of the left flank and 1 kb of the right flank of the cluster) in a single transformation (Figure 3.12A). Before the transformation, the three sgRNAs were tested in an *in vitro* cleavage assay (Figure S3.9A). To introduce cluster 19A of *U. maydis* into the *S. reilianum* cluster 19A deletion mutants of both mating types, it was manually split into four parts (Figure 3.12D). In the complementation 1 to 3, a fluorescence expression

cassette is used to simplify the screening of the transformants to increase the efficiency. To maintain the genomic properties, in the fourth complementation, no fluorescent marker will be used.

First, the deletion mutant of cluster 19A was generated and verified by Southern blot (Figure S3.9B) and further used as a background to integrate the first complementation (Figure 3.12B). Therefore, a sgRNA cutting exactly in the middle of the LF and RF was used to integrate the first complementation (Southern blot: Figure S3.9C+D), which harbor the first seven cluster genes (*UMAG_05294*, *UMAG_05295*, *UMAG_12302*, *UMAG_10553*, *UMAG_10554*, *UMAG_05299* and *UMAG_05300*) and in addition a GFP cassette for screening. When qRT-PCR was performed to check the expression of the first seven genes, no expression of the integrated *U. maydis* genes was observed in the complementation 1 strains. This could be explained by the late expression of these effector genes in *U. maydis* and *S. reilianum*. Three complementation 1 strain combinations (both mating types) were infected along with SRZ1+SRZ2 and the cluster 19A deletion mutant into maize seedlings of the cultivar Gaspe Flint and were grown for eight weeks before scoring of the disease symptoms (Figure S3.10). For the deletion mutant of cluster 19A as well as for the complementation 1 strains, no significant differences to the wild type were observed. However, a slight reduction in virulence was noted for the deletion strain. The complementation 1 strains of both mating types were further used to integrate the complementation 2 construct (Figure 3.12C) by using a donor template, carrying the second complementation (*UMAG_05301*, *UMAG_05302*, *UMAG_05303*, *UMAG_10555*, *UMAG_05305*, *UMAG_05306*, *UMAG_10556*, *UMAG_05308*) and a sgRNA targeting GFP, for the removal of the GFP cassette and efficient screening. The screening for loss of GFP fluorescence and a positive mCherry signal ensured the integration of the second complementation. So far, the complementation 2 strains were generated only in the SRZ2 background, since in the SRZ1 background no transformants could be obtained that harbor only the correct integration. Complementation 2 has not been further tested in qRT-PCR or infection assays. It remains to be elucidated whether a complementation of cluster 19A of *S. reilianum* with cluster 19A of *U. maydis* can induce tumor formation in *S. reilianum*.

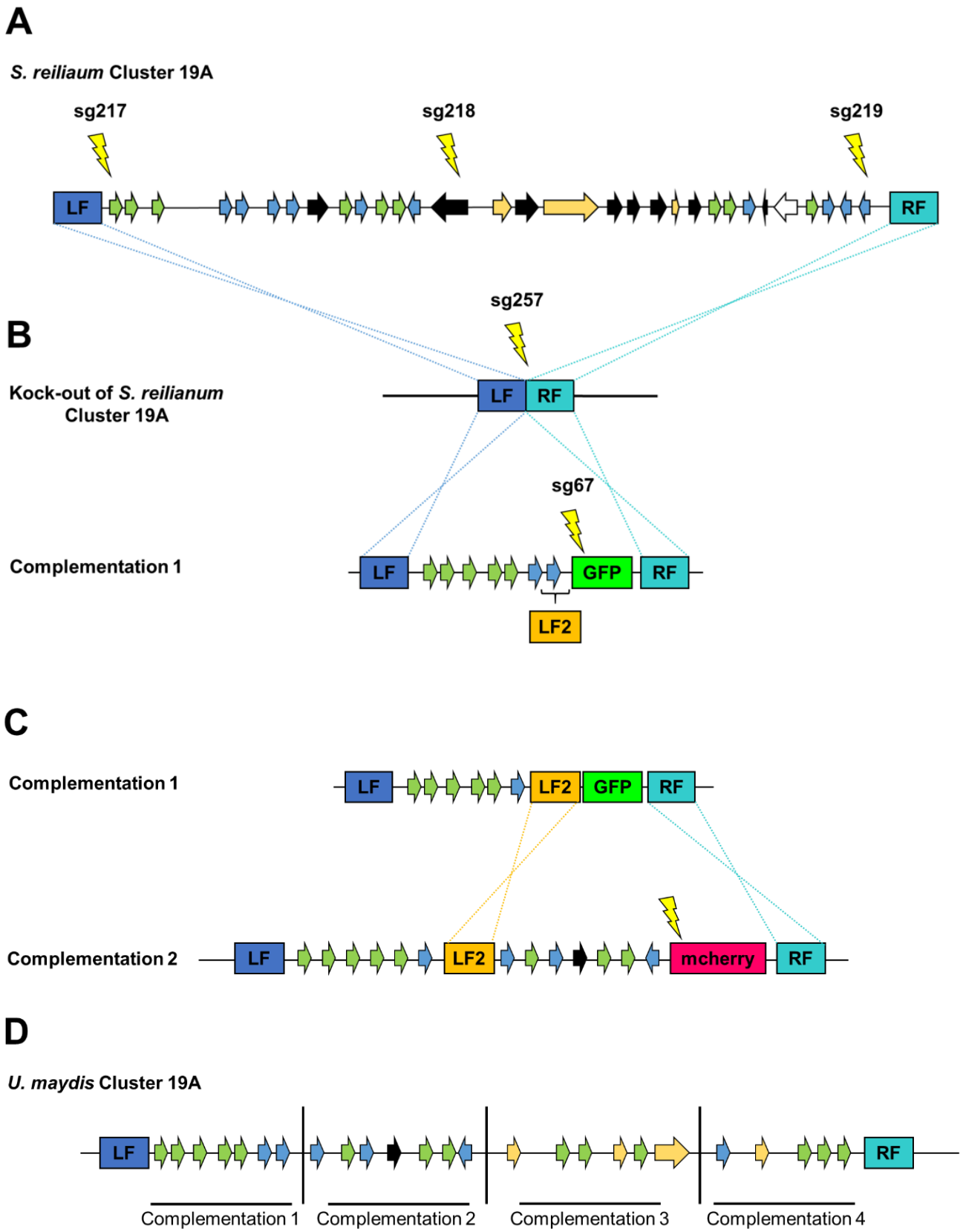
A
S. reiliaum Cluster 19A
sg217
sg218
sg219
LF
RF
B
sg257
Kock-out of S. reilianum Cluster 19A
LF
RF
sg67
Complementation 1
LF
GFP
RF
LF2
C
Complementation 1
LF
LF2
GFP
RF
Complementation 2
LF
LF2
mcherry
RF
D
U. maydis Cluster 19A
LF
RF
Complementation 1
Complementation 2
Complementation 3
Complementation 4

Figure 3.12: Scheme of *S. reilianum* cluster 19A deletion and complementation with *U. maydis* cluster 19A. **(A)** Cluster 19A of *S. reilianum*. Generation of 19A cluster deletion in *S. reilianum* using three sgRNAs in an RNP cutting at the beginning, middle, and end of the cluster. Flashes indicate sgRNAs. Genes in the cluster are represented by colored arrows. The arrow orientation indicates the direction of transcription. Black-colored genes are species-specific genes, yellow-colored genes have homologues in *U. hordei*, blue genes have in *U. maydis* and *S. reilianum*, and green-colored genes are homologues in all three species (Ghareeb *et al*. 2019; modified). **(B)** Deletion of *S. reilianum* cluster 19A using a sgRNA in an RNP cutting right between the LF and RF a repair template containing left flank (LF) and right flank (RF) for homologues recombination. The deletion strain was used to integrate the first complementation. At the end of complementation 1, a GFP cassette was integrated for the screening of mutants. **(C)** Complementation 1 of *U. maydis* cluster 19A in *S. reilianum* Δ19A background was used for the integration of the complementation 2 using a sgRNA against GFP. The complementation 2 construct included a mcherry cassette at the end for the screening of positive mutants (loss of GFP fluorescence and mcherry fluorescent). **(D)** Cluster 19A of *U. maydis* was split into four complementation constructs for a stepwise complementation of the whole cluster due to its size. In the future, complementation 3 will be generated with a GFP cassette and in complementation 4, no fluorescent marker will be included to avoid genomic perturbance.

3.4 Discussion

3.4.1 Compatibility of *U. maydis* and *S. reilianum* for interspecific hybridization

Fungal hybrids need to overcome potential incompatibilities originating from the evolution of the parental species (Hovhannisyan *et al*., 2020). Prior to the successful hybridization of two species, there are two distinct barriers to overcome: premating and postmating barriers (Steensels *et al*., 2021).

In Ustilaginaceae, the sexual life cycle is tightly linked with pathogenicity, which is determined by the compatibility of the mating type system. The high conservation of the mating type systems between *U. maydis* and *S. reilianum* ruled out a premating barrier, leading to successful mating and formation of dikaryotic hyphae. The two species *U. maydis* and *S. reilianum* both infect the same host *Z. mays*, are closely related, and have similar genomes in terms of size and synteny (Schirawski *et al*., 2010). Furthermore, comparative genetics as well as sexual compatibility tests by Kellner *et al*. (2011) revealed compatibility between haploid strains of *U. maydis* and *S. reilianum*, respectively. Thus, the same host, sexual compatibility, and the similar genomes provided an optimal foundation for investigating interspecific hybridization to gain insights into the different disease development of the two species.

The recombinant hybrid rUSH that was generated in this work could increase the biomass during *in planta* colonization and exhibited a *S. reilianum*-like phenotype at the early and the late infection time point. These results are in contrast to the hybrid recently described by Storfie & Saville (2021), which resulted in reduced colonization and virulence during seedling infections in comparison to the parental species. Hence, the improved mating in this study increases the chance of a successful hybridization event, which is very rare in wild type strains. This indicates, that rUSH has overcome premating barriers through the exchange of the mating types, which leads to a higher compatibility of downstream signaling. In contrast to the *S. reilianum*-like phenotype of rUSH, the reported hybrid by Storfie and Saville (2021) revealed chlorosis and a distinct anthocyanin formation.

Notably, in rUSH leafy ears were observed at 8 wpi, which is typical for *S. reilianum,* and was not reported in a previous study where only early time point phenotypes were assessed (Storfie & Saville, 2021). Nevertheless, the absence of teliospore formation in rUSH suggests that rUSH is less stable than the native systems of the wild types or cannot overcome postmating barriers that are needed for further sexual reproduction (Samarasinghe *et al*., 2020). Consequently, no backcrossing with either *U. maydis* or *S. reilianum* was conducted, as shown with a hybrid of *Ustilago bromivora* and *U. hordei* (Bosch *et al*., 2019). To overcome postmating barriers and obtain teliospores in rUSH, future studies should aim to overexpress effector genes, which are important for sporogenesis, or TFs involved in the regulation of genes important for the late infection stage. However, the overexpression (OE) of *ros1*, the master regulator of the late effector genes (Tollot *et al*., 2016), did not result in the formation

of teliospores. Furthermore, when *nlt1* was overexpressed to induce an early karyogamy in rUSH, neither at the early nor at the late stages of development, the formation of teliospores was observed. Therefore, further elements of the transcriptional network or a combination of early and late regulating factors may be needed to induce spore formation in rUSH. Using rSUH resulted in a lack of fungal proliferation and the formation of clump-like structures on the leaf surface during seedling infections. This indicates an incompatibility between Sr_Umt and FB2. However, the factors causing the incompatibility between the two strains and why this combination is unstable, despite the fact that this study shows that rUSH is able to proliferate, remains unknown

3.4.2 Gene expression in rUSH

Generally, gene expression in hybrids is highly dependent on a complex network of *cis*-regulatory elements and *trans*-regulatory factors, which rely on the divergence of the parental species, changes in the chromatin structure and modification as well as RNAi (Combes *et al*., 2015). A major role of the RNAi machinery in the observed downregulation effect of *U. maydis* effector genes in rUSH was disproven since the expression level did not change upon deletion of the *dicer* gene in *S. reilianum*. In rUSH, 218 differentially expressed one-to-one effector orthologues were identified with distinct regulation patterns, probably caused by a so-called “transcriptomic shock”, often observed after the combination of different genomes (Steensels *et al*., 2021). The regulation patterns in rUSH are consistent with the modulons previously described (Cox *et al*., 2014). Modulon 1 corresponds to the *cis*-regulated effector genes observed in this study, modulon 2 to the *trans*-regulated expression, and modulon 3 to the uniquely found hybrid-specific expression.

In this study, approximately half of the effector genes were found to be regulated by *trans*- or *cis*-regulation, while the other half displayed a hybrid-specific expression (reverse and orthologue-specific). The hybrid-specific expression is likely to result from an interaction between *cis*- and *trans*-regulation, which contrasts with previous findings observed for interspecific hybrids, where the gene expression was reported to be equally or more significantly influenced by *cis*-regulation than *trans*-regulation (Hill *et al*., 2021; Runemark *et al*., 2024). In accordance with the findings of this study, a hybrid-specific expression has previously been reported in a yeast hybrid, albeit to a lesser extent than observed in rUSH (Tirosh *et al*., 2009). The *cis*-regulatory elements in the promoter region of the effector gene *Umtin2* were shown to determine the differential expression of *Umtin2* between *U. maydis* and *S. reilianum*. This finding is consistent with a study by Zuo *et al.* (2021), which demonstrated that the differential expression of two one-to-one effector orthologues of *U. maydis* and *S. reilianum*, is also determined by the *cis*-regulatory element in the promoter.

To gain a deeper understanding of the underlying mechanisms that contribute to the observed differences in the gene expression patterns in rUSH, it would be beneficial to employ a combination of an Assay for Transposase-Accessible Chromatin with high-throughput sequencing (ATAC-seq) and Bisulfite sequencing (BS-Seq). This approach could provide further insights into the chromatin accessibility and methylation state of different genomic regions in the wild types and rUSH, which was not further investigated in this study. Additionally, Hi-C could be employed to investigate the proximity of the nuclei, the chromatin structure, and chromosome interactions upon hybridization (Belton *et al*., 2012). This may provide further insights into the contribution of the effector orthologue expression to the observed postmating incompatibility of rUSH.

The identification of new TFs co-regulated with early and late effectors may contribute to understanding the link between the early and late infection phases, which is important for *U. maydis* virulence (Lanver *et al*., 2017). However, frameshift mutants of six of the 78 differentially expressed putative TFs in rUSH did not affect *U. maydis* virulence. This is consistent with the findings of a study in yeast hybrids that revealed only minor differences in TF activity in the hybrid, which was not the primary factor driving the observed differences in gene expression (Hovhannisyan *et al.*, 2020). Furthermore, it was previously described that subtle differences in TF expression might have drastic biological effects (Hovannisyan *et al*., 2020). According to this hypothesis, the differentially expressed TFs in rUSH can be further screened for candidate genes with only minor differences in expression levels between the species.

Several *U. maydis* effector genes were downregulated in rUSH, including the two novel virulence factors (*UMAG_05312* and *UMAG_10553*), identified in this study. The majority of the downregulated effector genes could be associated with the clusters 6A and 19A, previously described to contribute to *U. maydis* virulence (Brefort *et al*., 2014; Kämper *et al*., 2006). This suggests a subgenome-specific expression of certain genomic regions, which is consistent with a previous study in *Agaricus bisporus*, where the dominant expression of genes in one karyallele was observed to colocalize in subchromosomal regions (Gehrmann *et al*., 2018). In the future, the generation of multiple mutants in *U. maydis* could be tested to elucidate whether an additive effect of the effector genes in cluster 19A on tumor formation can be observed. Furthermore, the replacement of the diversified cluster 19A of *S. reilianum* by *U. maydis* cluster 19A will shed light on the role of cluster 19A in tumor formation and may generate a *S. reilianum* strain that causes tumor formation in *Z. mays*.

3.5 Material and Methods

For a detailed description of the buffer compositions, the oligonucleotides used and the plasmids generated in this study (see Chapter 6 – Appendix, General Material and Methods).

3.5.1 Strains, growth conditions, and plant infections

For RNA-seq analysis and infection, the compatible isolates of *U. maydis* (FB1 and FB2), *S. reilianum* (SRZ1+SRZ2), and the recombinant hybrid (rUSH) were used. Infection assays of effector candidate gene KOs were conducted with the solopathogenic strain SG200 or FB1+FB2, respectively. CRISPR mutants were generated for *U. maydis* and *S. reilianum* as previously described (Schuster *et al*., 2016; Werner *et al*., 2023; Zuo *et al*., 2020). In the absence of a donor template, CRISPR mutagenesis was performed as described by Zuo *et al*. (2021). The oligonucleotides used for the generation of the CRISPR-plasmids are listed in table 6.7**.** The resulting *U. maydis* strains were sent for sequencing to confirm a premature stop codon. For strains generated by CRISPR-assisted HR, Southern blot was performed (see 6.7.11)

All strains were grown in $YEPS_{light}$ liquid medium and at 28°C and 200 rpm shaking or on potato dextrose agar plates (PD). All generated mutant strains in this study were cultivated in the same way and are listed in Table 3.1 (*U. maydis* strains) and 3.2 (*S. reilianum* strains). For cloning the *Escherichia coli* strain Top10 was used and cultivated in dYT liquid medium or on YT plates, supplemented with the corresponding antibiotics. The generated plasmids in this study are listed in table 6.3. For infection assays, maize plants were grown under controlled conditions of 16 h light at 28°C and 8 h darkness at 22°C. Maize seedlings of the cultivar Golden Bantham (RNA-seq, *U. maydis* infections) and Gaspe Flint (*S. reilianum* infections) were infected with an OD_{600} of 1 of a 1:1 mixture of compatible mating partners (see Figure 6.3) or the solopathogenic strain SG200. For rUSH, 0.1% Tween was added before infection. Disease symptoms were assessed for *U. maydis* at 12 dpi (see Table 6.23) and for *S. reilianum* at 8 wpi (Figure 6.4).

Table 3.1: *U. maydis* strains used and generated in this study. MI: Multiple integration into *ip* locus. SI: Single integration into *ip* locus. CR: CRISPR-generated frameshift mutant.

Strain (Genotype)	Usage	Reference
FB1	Maize infection, transformation	Banuett & Herskowitz, 1989
FB2	Maize infection, transformation	Banuett & Herskowitz, 1989
SG200	Maize infection, transformation	(Bölker *et al*., 1995) Kämper *et al*., 2006
FB1_*Sra1b1* (short: M3)	Maize infection, transformation	Weiliang Zuo, AG Döhlemann
Tin2 promoter exchange		

FB1_*Sra1b1*_M3_psr10057_*UMAG_05302*_#3 FB1_*Sra1b1*_M3_psr10057_*UMAG_05302*_#4	Maize infection	This study
Histon1 tagged strain for nuclear localization of mcherry		
FB1_Sra1b1_M3_H1_mCherry#22	Maize infection, microscopy	This study
Generation of Transcription factor frameshift mutants using CRISPR/Cas9		
FB1:CR-*UMAG_00533* #1 FB1:CR-*UMAG_00533* #2 FB1:CR-*UMAG_00533* #8 FB2:CR-*UMAG_00533* #1 FB2:CR-*UMAG_00533* #2 FB2:CR-*UMAG_00533* #4	Frameshift mutant of *UMAG_00533* (putative TF)	This study
FB1:CR-*UMAG_02462* #2 FB1:CR-*UMAG_02462* #4 FB1:CR-*UMAG_02462* #5 FB2:CR-*UMAG_02462* #1 FB2:CR-*UMAG_02462* #2	Frameshift mutant of *UMAG_02462* (putative TF)	This study
FB1:CR-*UMAG_04242* #2 FB1:CR-*UMAG_04242* #3 FB2:CR-*UMAG_04242* #3 FB2:CR-*UMAG_04242* #5 FB2:CR-*UMAG_04242* #8	Frameshift mutant of *UMAG_04242* (putative TF)	This study
SG200:CR-*UMAG_06257* #1 SG200:CR-*UMAG_06257* #7 SG200:CR-*UMAG_06257* #8	Frameshift mutant of *UMAG_06257* (putative TF)	Bachelor thesis Kerstin Lehnen, this study
SG200:CR-*UMAG_10256* #6 SG200:CR-*UMAG_10256* #13 SG200:CR-*UMAG_10256* #16	Frameshift mutant of *UMAG_10256* (putative TF)	Bachelor thesis Kerstin Lehnen, this study
Generation of effector candidate frameshift mutants (Downregulated in rUSH)		
SG200:CR-*UMAG_05312* #1 SG200:CR-*UMAG_05312* #3 SG200:CR-*UMAG_05312* #4	Frameshift mutant of *UMAG_05312*	This study
SG200:CR-*UMAG_03751* #3 SG200:CR-*UMAG_03751* #4	Frameshift mutant of *UMAG_03751*	This study
SG200:CR-*UMAG_10553* #1 SG200:CR-*UMAG_10553* #2 SG200:CR-*UMAG_10553* #8	Frameshift mutant of *UMAG_10553*	This study
SG200:CR-*UMAG_05928* #3 SG200:CR-*UMAG_05928* #5 SG200:CR-*UMAG_05928* #8	Frameshift mutant of *UMAG_05928*	This study
SG200:CR-*UMAG_04039* #1 SG200:CR-*UMAG_04039* #3 SG200:CR-*UMAG_04039* #6	Frameshift mutant of *UMAG_04039*	This study
SG200:CR-*UMAG_05780* #1 SG200:CR-*UMAG_05780* #2 SG200:CR-*UMAG_05780* #5	Frameshift mutant of *UMAG_05780*	This study

Table 3.2: *S. reilianum* strains generated and used in this study.

Strain (Genotype)	Usage	Reference
SRZ1	Maize infection, transformation	Schirawski *et al*., 2010
SRZ2	Maize infection, transformation	Schirawski *et al*., 2010
Histon1 tagged strain for nuclear localization of GFP		
SRZ2_H1_GFP#9	Maize infection, microscopy	This study
Generation of *dicer* mutants in *S. reilianum*		

SRZ2_Δ*sr16838*_#7 SRZ2_Δ*sr16838*_#15	Maize infection, qRT-PCR	This study
Generation of effector gene mutants in *S. reilianum*		
SRZ1Δ*sr16075* #3 SRZ1Δ*sr16075* #14 SRZ2Δ*sr16075* #3 SRZ2Δ*sr16075* #5	Maize infection	This study
Generation of Cluster 19A mutants		
SRZ1Δ19A #1 SRZ1Δ19A #2 SRZ1Δ19A #12 SRZ2Δ19A #3 SRZ2Δ19A #9 SRZ2Δ19A #16	Maize infection, transformation	Master thesis, Vanessa Volz
SRZ1Δ19A #1+Comp1#1 SRZ1Δ19A #1+Comp1#2 SRZ1Δ19A #1+Comp1#6 SRZ2Δ19A #3+Comp1#4 SRZ2Δ19A #3+Comp1#5 SRZ2Δ19A #3+Comp1#8	Maize infection, transformation	Master thesis, Vanessa Volz
SR92_Cluster19AComp2 #10 SR92_Cluster19AComp2 #19 SR92_Cluster19AComp2 #21	Maize infection	This study

3.5.2 Staining and microscopy

For the observation of the formation of appressoria-like structures as well as for WGA-AlexaFlour 488 staining, a Nikon Eclipse Ti Inverted Microscope and the Nikon NIS-ELEMENTS software (Düsseldorf, Germany) were used. For Calcoflour white staining, infected maize leaf sections were cut at 20-24 hpi, washed in $H2O_{deion.}$, and incubated for 30-60 s in Calcoflour working solution (1:100 dilution of the stock solution in 0.2 M Tris-HCl (pH 8.0). Subsequently, leaves were washed with $H2O_{deion.}$ and observed using the DAPI filter of the Nikon Eclipse Ti Inverted microscope. Pictures were taken with a HAMAMATSU camera. For the visualization of nuclear-localized signals, the confocal microscope Leica TCS SP8 Confocal Laser Scanning was used (Leica, Bensheim, Germany). GFP was excited at 488 nm and detected at 490-540 nm, while mCherry was excited at 561 nm and detected at 580-660 nm. The analysis of the microscopy pictures was performed using the Leica LAS X.Ink software.

3.5.3 DNA and RNA preparation and qRT-PCR

Three maize infections were conducted from three independent fungal cultures. The compatible haploid *U. maydis* and *S. reilianum* cells from cultures with OD_{600} of 0.8 were mixed in a 1:1 ratio before infection. 4 cm-long sections (1 cm below the infection side) of the third leaf were collected from at least 13 individual plants (see Figure 6.2). At 20 hpi liquid latex was applied to the infected maize leaves, dried, and used for RNA extraction. At the 3 dpi and 6 dpi the plant material was used as described above. The plant tissue and the frozen latex were ground into a fine powder using liquid nitrogen. Total RNA

was extracted using TRIzol (Thermo Fisher, Waltham, USA) according to the manufacturer's protocol. Subsequently, a DNase I digest was performed (Thermo Fisher) and the samples were sent to Novogene (UK) for RNA-seq. For qRT-PCR cDNA was synthesized using RevertAid First Strand cDNA Synthesis kit (Thermo Fisher). The qRT-PCR was performed using a GoTaq qPCR mix (Promega) and a CFX96 Real-Time PCR Detection System (BioRad).

DNA of *U. maydis* and *S. reilianum* was prepared using lysis buffer (Table 6.12) and subsequently purified using a MasterPure Complete DNA and RNA Purification Kit (Epicenter, Madison, USA). For biomass quantification, the DNA was isolated using maize extraction buffer (Table 6.11) and the purification kit mentioned earlier. For biomass quantification (gDNA) $2^{\Delta Ct}$ ($Ct^{ZmGAPDH}$ - Ct^{Umppi}) and for relative gene expression $2^{\Delta Ct}$ (Ct^{Umppi} – Ct^{GOI}) were calculated. For statistical analysis, a student's t-test was conducted.

3.5.4 RNA-sequencing data analysis

RNA libraries were prepared by Novogene using an Illumina TruSeq Stranded mRNA kit (Illumina, SanDiego, CA, USA), and paired-end sequencing was performed on a HiSeq4000 platform (Figure 3.13). Reads of three biological replicates were filtered using the Trimmomatic software 0.39 and standard settings. They were mapped to a reference assembly using BOWTIE2 (version 2.3.4.1) (Langmead & Salzberg, 2012). The reference genomes of *U. maydis* (Kämper *et al*., 2006) and *S. reilianum* (Schirawski *et al*., 2010) were combined prior to mapping to ensure a right genome assignment. Reads were counted to *U. maydis* and *S. reilianum* using HTseq-count (version 2.0.4) (Anders *et al*., 2015). The edgeR package was used for statistical analysis of differential gene expression (counts per million, CPM) and Excel was used to calculate the transcripts per million (TPM) normalized to the different gene lengths between the species. Afterward, one-to-one orthologues were determined using the parameters from (Zuo *et al*., 2021). For the comparison between the wild type strains SRZ1+SRZ2 (SR) and FB1+FB2 (UM), the fold change FC(SR/UM) was calculated by dividing the *S. reilianum* transcripts per million (TPM) by *U. maydis* TPM of the wild types. The same analysis was conducted for the orthologous genes in rUSH (log_2FC 1, $p<0.05$).

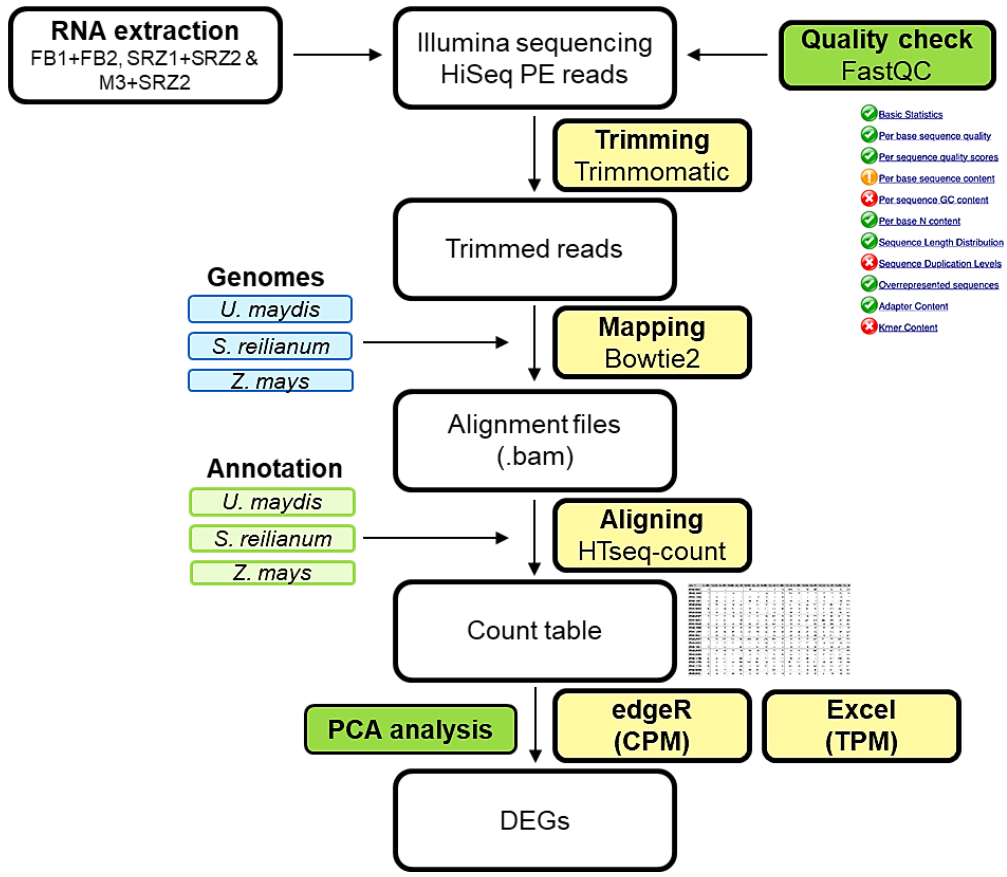

Figure 3.13: RNA-seq analysis workflow. RNA libraries were prepared using an Illumina TruSeq Stranded mRNA kit (Illumina, SanDiego, CA, USA), and paired-end sequencing was performed on a HiSeq4000 platform with Novogene (UK). Reads of three biological replicates were filtered using the Trimmomatic software and standard settings. They were mapped to a reference assembly using BOWTIE2 (version 2.3.4.1). The reference genomes of *U. maydis* (Kämper *et al*., 2006) and *S. reilianum* (Schirawski *et al*., 2010) were combined prior to mapping. Reads were counted to the *U. maydis* and *S. reilianum* loci using HTseq-count (version 2.0.4). The edgeR package was used for statistical analysis of differential gene expression (counts per million, CPM) and Microsoft Excel was used to calculate the transcripts per million (TPM) normalized to the different gene lengths between the species.

3.6 References

Anders, S., Pyl, P. T., & Huber, W. (2015). HTSeq-A Python framework to work with high-throughput sequencing data. *Bioinformatics*, *31*(2), 166–169. https://doi.org/10.1093/bioinformatics/btu638

Banuett, F., & Herskowitz, I. (1989). Different a alleles of *Ustilago maydis* are necessary for maintenance of filamentous growth but not for meiosis . *Proceedings of the National Academy of Sciences*, *86*(15), 5878–5882. https://doi.org/10.1073/pnas.86.15.5878

Begerow, D., Göker, M., Lutz, M., & Stoll, M. (2004). On the evolution of smut fungi on their hosts. *Frontiers in basidiomycote mycology*, 81-98.

Belton, J. M., McCord, R. P., Gibcus, J. H., Naumova, N., Zhan, Y., & Dekker, J. (2012). Hi-C: A comprehensive technique to capture the conformation of genomes. *Methods*, *58*(3), 268–276. https://doi.org/10.1016/j.ymeth.2012.05.001

Bosch, J., Czedik-Eysenberg, A., Hastreiter, M., Khan, M., Güldener, U., & Djamei, A. (2019). Two is better than one: Studying *Ustilago Bromivora-Brachypodium* compatibility by using a hybrid pathogen. *Molecular Plant-Microbe Interactions*, *32*(12), 1623–1634. https://doi.org/10.1094/MPMI-05-19-0148-R

Brefort, T., Tanaka, S., Neidig, N., Doehlemann, G., Vincon, V., & Kahmann, R. (2014). Characterization of the Largest Effector Gene Cluster of *Ustilago maydis*. *PLoS Pathogens*, *10*(7). https://doi.org/10.1371/journal.ppat.1003866

Combes, M. C., Hueber, Y., Dereeper, A., Rialle, S., Herrera, J. C., & Lashermes, P. (2015). Regulatory divergence between parental alleles determines gene expression patterns in hybrids. *Genome Biology and Evolution*, *7*(4), 1110–1121. https://doi.org/10.1093/gbe/evv057

Cox, M. P., Dong, T., Shen, G. G., Dalvi, Y., Scott, D. B., & Ganley, A. R. D. (2014). An Interspecific Fungal Hybrid Reveals Cross-Kingdom Rules for Allopolyploid Gene Expression Patterns. *PLoS Genetics*, *10*(3). https://doi.org/10.1371/journal.pgen.1004180

Day, P. R., & Anagnostakis, S. L. (1971). Corn Smut Dikaryon in Culture. *Nature New Biology*, *231*, 1971.

Franceschetti, M., Maqbool, A., Jiménez-Dalmaroni, M. J., Pennington, H. G., Kamoun, S., & Banfield, M. J. (2017). Effectors of Filamentous Plant Pathogens: Commonalities amid Diversity. *Microbiology and Molecular Biology Reviews*, *81*(2). https://doi.org/10.1128/mmbr.00066-16

Gehrmann, T., Pelkmans, J. F., Ohm, R. A., Vos, A. M., Sonnenberg, A. S. M., Baars, J. J. P., Wösten, H. A. B., Reinders, M. J. T., & Abeel, T. (2018). Nucleus-specific expression in the multinuclear mushroom-forming fungus *Agaricus bisporus* reveals different nuclear regulatory programs. *Proceedings of the National Academy of Sciences of the United States of America*, *115*(17), 4429–4434. https://doi.org/10.1073/pnas.1721381115

Ghareeb, H., Becker, A., Iven, T., Feussner, I., & Schirawski, J. (2011). *Sporisorium reilianum* infection changes inflorescence and branching architectures of maize. *Plant Physiology*, *156*(4), 2037–2052. https://doi.org/10.1104/pp.111.179499

Ghareeb, H., Zhao, Y., & Schirawski, J. (2019). *Sporisorium reilianum* possesses a pool of effector proteins that modulate virulence on maize. *Molecular Plant Pathology*, *20*(1), 124–136. https://doi.org/10.1111/mpp.12744

Hill, M. S., Vande Zande, P., & Wittkopp, P. J. (2021). Molecular and evolutionary processes generating variation in gene expression. *Nature Reviews Genetics*, *22*(4), 203–215. https://doi.org/10.1038/s41576-020-00304-w

Hovhannisyan, H., Saus, E., Ksiezopolska, E., Gabaldón, T., Krogerus, K., Arvas, M., De Chiara, M., Magalhães, F., Mattinen, L., Oja, M., Vidgren, V., Yue, J. X., Liti, G., & Gibson, B. (2020). Ploidy influences the functional attributes of de novo lager yeast hybrids. *Applied Microbiology and Biotechnology*, *100*(3), 7203–7222. https://doi.org/10.1007/s00253-016-7588-3

Kämper, J., Kahmann, R., Bölker, M., Ma, L. J., Brefort, T., Saville, B. J., Banuett, F., Kronstad, J. W., Gold, S. E., Müller, O., Perlin, M. H., Wösten, H. A. B., De Vries, R., Ruiz-Herrera, J., Reynaga-Peña, C. G., Snetselaar, K., McCann, M., Pérez-Martín, J., Feldbrügge, M., … Birren, B. W. (2006). Insights from the genome of the biotrophic fungal plant pathogen *Ustilago maydis*. *Nature*, *444*(7115), 97–101. https://doi.org/10.1038/nature05248

Langmead, B., & Salzberg, S. L. (2012). Fast gapped-read alignment with Bowtie 2. *Nature Methods*, *9*(4), 357–359. https://doi.org/10.1038/nmeth.1923

Lanver, D., Tollot, M., Schweizer, G., Lo Presti, L., Reissmann, S., Ma, L. S., Schuster, M., Tanaka, S., Liang, L., Ludwig, N., & Kahmann, R. (2017). *Ustilago maydis* effectors and their impact on virulence. *Nature Reviews Microbiology*, *15*(7), 409–421. https://doi.org/10.1038/nrmicro.2017.33

Laurie, J. D., Ali, S., Linning, R., Mannhaupt, G., Wong, P., Güldener, U., Münsterkötter, M., Moore, R., Kahmann, R., Bakkeren, G., & Schirawski, J. (2012). Genome comparison of barley and maize smut fungi reveals targeted loss of RNA silencing components and species-specific presence of transposable elements. *Plant Cell*, *24*(5), 1733–1745. https://doi.org/10.1105/tpc.112.097261

Martínez-Espinoza, A. D., García-Pedrajas, M. D., & Gold, S. E. (2002). The Ustilaginales as plant pests and model systems. *Fungal Genetics and Biology*, *35*(1), 1–20. https://doi.org/10.1006/fgbi.2001.1301

Redkar, A., Villajuana-Bonequi, M., & Doehlemann, G. (2015). Conservation of the *Ustilago maydis* effector See1 in related smuts. *Plant Signaling and Behavior*, *10*(12). https://doi.org/10.1080/15592324.2015.1086855

Runemark, A., Moore, E. C., & Larson, E. L. (2024). Hybridization and gene expression: Beyond differentially expressed genes. *Molecular Ecology*, *February*, 1–18. https://doi.org/10.1111/mec.17303

Schirawski, J., Mannhaupt, G., Münch, K., Brefort, T., Schipper, K., Doehlemann, G., Di Stasio, M., Rössel, N., Mendoza-Mendoza, A., Pester, D., Müller, O., Winterberg, B., Meyer, E., Ghareeb, H., Wollenberg, T., Münsterkötter, M., Wong, P., Walter, M., Stukenbrock, E., … Kahmann, R. (2010). Pathogenicity determinants in smut fungi revealed by genome comparison. *Science*, *330*(6010), 1546–1548. https://doi.org/10.1126/science.1195330

Schuster, M., Schweizer, G., Reissmann, S., & Kahmann, R. (2016). Genome editing in *Ustilago maydis* using the CRISPR-Cas system. *Fungal Genetics and Biology*, *89*, 3–9. https://doi.org/10.1016/j.fgb.2015.09.001

Storfie, E. R. M., & Saville, B. J. (2021). Fungal Pathogen Emergence : Investigations with an *Ustilago maydis* × *Sporisorium reilianum* Hybrid. *Journal of Fungi*, *7*(672).

Tanaka, S., Schweizer, G., Rössel, N., Fukada, F., Thines, M., & Kahmann, R. (2019). Neofunctionalization of the secreted Tin2 effector in the fungal pathogen *Ustilago maydis*. *Nature Microbiology*, *4*(2), 251–257. https://doi.org/10.1038/s41564-018-0304-6

Tirosh, I., Reikhav, S., Levy, A. A., & Barkai, N. (2009). A yeast hybrid provides insight into the evolution of gene expression regulation. *Science*, *324*(5927), 659–662. https://doi.org/10.1126/science.1169766

Werner, J., Zuo, W., & Doehlemann, G. (2023). CRISPR/Cas9 Ribonucleoprotein-Mediated Mutagenesis in *Sporisorium reilianum*. Bio-protocol 14(8): e4978. https://doi.org/10.21769/BioProtoc.4978.

Zuo, W., Depotter, J. R., & Doehlemann, G. (2020). Cas9HF1 enhanced specificity in *Ustilago maydis*. *Fungal Biology*, *124*(3–4), 228–234. https://doi.org/10.1016/j.funbio.2020.02.006

Zuo, W., Depotter, J. R. L., Gupta, D. K., Thines, M., & Doehlemann, G. (2021). Cross-species analysis between the maize smut fungi *Ustilago maydis* and *Sporisorium reilianum* highlights the role of transcriptional change of effector orthologs for virulence and disease. *New Phytologist*. https://doi.org/10.1111/nph.17625

Zuo, W., Depotter, J. R. L., Stolze, S. C., Nakagami, H., & Doehlemann, G. (2023). A transcriptional activator effector of *Ustilago maydis* regulates hyperplasia in maize during pathogen-induced tumor formation. *Nat Commun,* 14, 6722 (2023). https://doi.org/10.1038/s41467-023-42522-w

Chapter 4: Expression of tumor-inducing effectors in *Ustilago maydis* is controlled by a key transcriptional regulator

4.1 Summary

U. maydis induces locally distinct tumors on maize, while its close relative *S. reilianum* spreads systemically in the host and does not induce tumor formation. Previous work indicated that the regulation and functional diversification of effectors is linked with pathogen lifestyle. Here, we make use of a recombinant hybrid of *U. maydis* and *S. reilianum* (rUSH) to identify transcriptional regulators and effectors that orchestrate tumor formation.

In *U. maydis*, a hierarchical network of TFs determines the expression of effector genes throughout the pathogen's life cycle. Deletion of several TFs has been described to result in an avirulent phenotype, reflecting their importance in the regulation of pathogenicity-related genes. rUSH revealed a *S. reilianum*-like phenotype without the formation of teliospores. To test whether the phenotype of rUSH is determined by species-specific activity of TFs, known transcriptional regulators of *U. maydis* were overexpressed in rUSH. Overexpression of a single *U. maydis* TF, *hdp2,* enabled rUSH to induce the formation of plant tumors in maize leaves. This suggests a crucial role of UmHdp2 in the regulation of genes important for tumorigenesis of *U. maydis*. We found that not only UmHdp2 but also SrHdp2 lead to the induction of tumor formation in rUSH. This indicates a high conservation between the Hdp2 proteins of the two species, which was further confirmed by the native replacement of *Umhdp2* with *Srhdp2* in *U. maydis*. To elucidate the downstream targets of Hdp2, an RNA-sequencing analysis was performed. This analysis revealed 41 *U. maydis* effector genes, which are directly and indirectly regulated by UmHdp2 and five genes encoding proteins with a predicted DNA-binding function. The identification of a distinct gene set linked with tumorigenesis represents a major step toward the understanding of the evolution of fungal-induced tumor formation.

4.2 Introduction

In plant pathogenic fungi, the infection strategies are often specialized and require precisely coordinated molecular regulation (John *et al*., 2022) at specific time points during infection (Toruño *et al*., 2016). The smut fungi consist of more than 1,500 species and infect mainly members of the Poaceae family, such as barley, wheat, sorghum, and maize (Begerow *et al*., 2004). *U. maydis*, the prime model system among the smuts, can form locally distinct tumors on the site of infection on all aerial parts of *Zea mays* within 2 weeks (Zuo *et al*., 2021). A characteristic among the smuts is their dimorphic lifestyle: the haploid yeast-like stage and the dikaryotic hyphae for the biotrophic development *in planta* (Kämper *et al*., 2006).

The molecular mechanisms underlying the developmental processes and the virulence of diverse fungi are frequently regulated by TFs (John *et al*., 2022; Van Der Does & Rep, 2017). Since in smut fungi, sexual and pathogenic development are tightly linked (Bakkeren *et al*., 2008), the expression of the genes encoding for TFs was further investigated. TFs tightly regulate the expression of effector genes. In particular, organ-specific effectors require a precise and site-specific expression (Lanver *et al*., 2017). In *U. maydis*, a tight regulation of gene expression through a hierarchical network of TFs, known as the *b* cascade, is crucial. Effector gene expression takes place in different waves during the pathogenic development of *U. maydis* in the host. The *b* cascade is activated after a successful mating event of two compatible haploid partners, which leads to the induction of the expression of the genes encoding for the two HD TFs bE and bW. bE and bW can form a heterodimer TF complex which activates genes important for the pathogenic development, including the master regulator Rbf1. Rbf1 in turn can activate the downstream TFs Biz1 and Hdp2 that are crucial for the regulation of the expression of early effectors. The signal that triggers the activation of effector gene expression and involved TFs is currently unknown (Lanver *et al*., 2017). However, it has been shown that the expression of some effector genes is induced upon supplementation of glucose and malate in *in vitro* assays (Kretschmer *et al*., 2022). Similar to Rbf1 and Biz1, Hdp2 was found to be crucial for the pathogenic development of *U. maydis*, as KO mutants resulted in an avirulent strain unable to form tumors (Heimel *et al*., 2010b; Lanver *et al*., 2014).

A fungal hybrid of *S. reilianum* and *U. maydis* was reported to result in a lack of fungal proliferation. However, when *rbf1* and *hdp2* were overexpressed in the hybrid, a rare induction of tumor formation was observed in infected maize seedlings (Storfie & Saville, 2021). Recently, *in planta* ChIP-seq revealed the presence of two transcripts of *hdp2* resulting in two protein isoforms Hdp2^{S} and Hdp2^{L}, which are regulated by two different promoters. Rbf1 controls the early expression of *hdp2* via the first promoter, while *biz1* takes over the regulation of the second promoter after plant penetration (Jurca, 2021).

In previous work, a recombinant hybrid of *U. maydis* and *S. reilianum* (rUSH) was generated and used as a tool to understand the differences in the disease development of the two species on the same host, *Z. mays*. The analysis of the recombinant hybrid revealed a successful formation of a dikaryotic filament, penetration, proliferation in the plant, and a *S. reilianum*-like phenotype at all developmental stages, without the formation of tumors. Furthermore, this study elucidated three distinct expression patterns of effector genes in rUSH compared to the wild types: *cis*-, *trans*- and hybrid-specific, and revealed based on these patterns novel virulence factors of *U. maydis* and *S. reilianum* (see Chapter 3).
In this chapter, I overexpressed the TFs of *U. maydis* in rUSH to elucidate their role in the regulation of tumorigenic effector genes of *U. maydis*. Furthermore, we performed a motif enrichment analysis to identify specific binding sites for the effector gene expression pattern, previously observed in rUSH.

4.3 Results

4.3.1 *S. reilianum* dominates expression of transcription factors in rUSH

To elucidate the role of TFs in the observed *S. reilianum*-like phenotype of rUSH, the expression levels of the TFs were analyzed and compared to those of *U. maydis* and *S. reilianum* wild type.
Since the mating type system of *S. reilianum* was used in rUSH and is known to be important to initiate the pathogenic development, the expressions of the known downstream TFs of the b cascade were analyzed. For all TFs, a higher expression of the *S. reilianum* orthologue compared to the *U. maydis* orthologue was observed in rUSH (Figure 4.1). This is in line with the *S reilianum*-like phenotype of rUSH (Chapter 3). To elucidate whether a higher expression of the corresponding *U. maydis* TF in rUSH could shift the phenotype towards tumor formation, the genes encoding for the TFs Rbf1, Biz1, Hdp2, Fox1, Ros1, and Nlt1 were overexpressed in Um_Smt. The promoter pro^{Umcmu1} was chosen for the OE due to its high expression during the biotrophic development *in planta* (Figure S4.4). Only for the OE of *biz1*, no positive transformants could be generated using pro^{Umcmu1}. The mutants overexpressing *hdp2*, *rbf1*, *fox1*, *ros1,* and *nlt1* were tested for their role in virulence in infection assays of maize seedlings (Figure S4.2, Southern blot *hdp2* OE: Figure S4.1). Only one TF showed a change in the phenotype and revealed the formation of small tumors: Hdp2. This suggests a role of Hdp2 in the regulation of effector genes contributing to tumor formation. Interestingly, the formation of tumors after infections with the OE of *hdp2* in rUSH (rUSH_Umhdp2^{OE}) was already visible at 3 dpi, although it is normally observed at 4-6 dpi. This suggests that the OE of *hdp2* using the pro^{Umcmu1} may result in excessively early and intense induction of downstream genes that are crucial for tumor formation. In a qRT-PCR, the relative expression of *Umhdp2* was measured in FB1+FB2, in rUSH and rUSH_Umhdp2^{OE} (Figure S4.3). The level of *Umhdp2* expression was significantly higher in rUSH_Umhdp2^{OE} compared to rUSH and the

wild type. This suggests that a certain threshold of Hdp2 may be required for the regulation of tumor formation. In rUSH, this threshold may need to be higher as the downstream *U. maydis* effector genes are downregulated compared to the *U. maydis* wild type.

Consequently, for rUSH_Umhdp2^{OE}, two distinct promoters were employed, regulating the expression of effector genes that exhibited a lower level of expression (*UMAG_02196*) or a delayed and reduced expression profile (*UMAG_05312*) compared to *Umcmu1* (Figure S4.4). The coding sequence of *Umhdp2* was cloned with 1 kb of the promoter sequence of the effector genes into the *ip* locus of Um_Smt and infected together with SRZ2 into maize seedlings. While rUSH using pro^{UMAG_02196} for OE of *Umhdp2* revealed rare small tumors at 6 dpi, no tumor formation was observed in rUSH with pro^{UMAG_05312} (preliminary data, not shown).

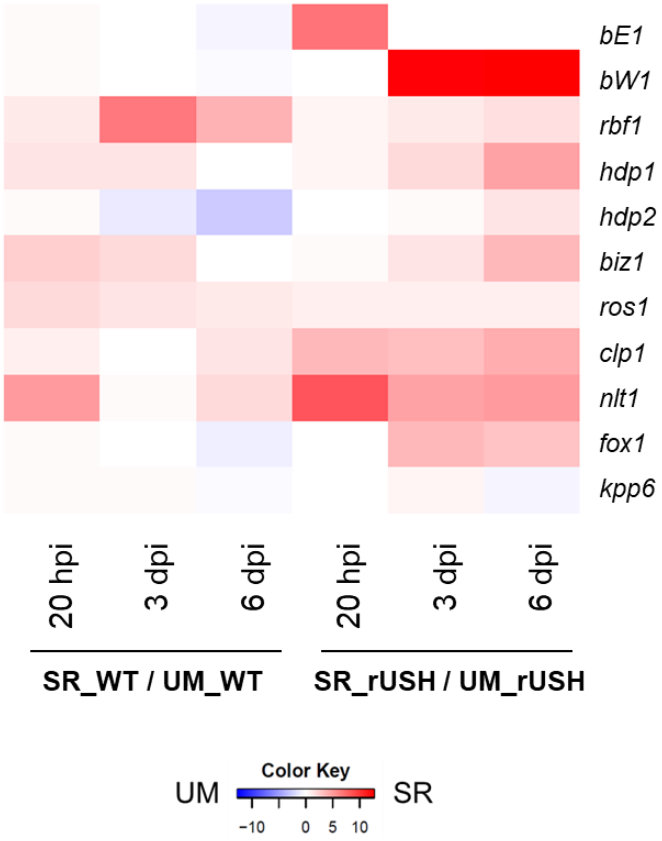

Figure 4.1: Expression of transcription factors in the wild types and rUSH. Log_2FC was calculated by dividing the *S. reilianum* transcripts per million (TPM) by *U. maydis* TPM of the wild types FB1+FB2 and SRZ1+SRZ2 (SR_WT / UM_WT) as well as within rUSH (SR_rUSH/UM_rUSH).

4.3.2 Hdp2 is conserved among the smut fungi

Since rUSH_Umhdp2^{OE} revealed tumor formation, the conservation of Hdp2 among the smuts was investigated. A phylogenetic tree of the Hdp2 proteins of *U. maydis*, *S. reilianum*, *Sporisorium scitamineum, Ustilago loliicola, U. bromivora, Ustilago tritici, Ustilago nuda, U. hordei* and *M. pennsylvanicum* was generated (Figure 4.2A) and revealed a high conservation of Hdp2 among the smuts. To test for functional conservation, *Srhdp2* was overexpressed in Um_Smt to elucidate whether SrHdp2 can also regulate effector genes, that contribute to tumor formation. Similar to rUSH_Umhdp2^{OE}, pro^{cmu1} was used to control the expression of *Srhdp2* in the *ip* locus of the Um_Smt strain (Southern blot: Figure S4.5). Together with SRZ2, the resulting hybrid (rUSH_Srhdp2^{OE}) was infected in 7-day old maize seedlings and the phenotype was observed. After 6 dpi, the formation of small tumors was visible for rUSH_Srhdp2^{OE}, supporting the predicted conservation of Hdp2 between *U. maydis* and *S. reilianum* (Figure 4.2B).

4.3.3 Overexpression of *hdp2* revealed induced effector gene expression in rUSH

To test the regulation of effector genes by Hdp2, the known motif for Hdp2 “ATGAA” (Jurca, 2021) was searched in the promoter region of effector genes (500 bp upstream of the start codon) of *U. maydis* and *S. reilianum*. The ATGAA motif was identified in 186 promoter sequences of *U. maydis* effector genes and 149 promoter regions of *S. reilianum* effector genes (Table S4.1). Two of the *U. maydis* effector genes with predicted Hdp2 binding sites in their promoter region, *tip6,* and *pit2*, were selected to test their regulation by Hdp2. *tip6* and *pit2* were tested in qRT-PCR to compare the gene expression level in rUSH and rUSH_Umhdp2^{OE}. *tip6* revealed five binding motifs for Hdp2, while in the promoter region of *pit2* two motifs were found (Figure 4.2C). When the gene expression level was compared between rUSH and in rUSH_Umhdp2^{OE}, for both effector genes a significantly higher expression could be observed in rUSH_Umhdp2^{OE} (Figure 4.2D). However, the measured expression of the tested effector genes could not be correlated with the abundance of sequence motifs in the promoter region.

Next, the presence of the HA-tagged UmHdp2 and SrHdp2 proteins was analyzed in the OE mutant strains (rUSH_Umhdp2^{OE} and rUSH_Srhdp2^{OE}). At 6 dpi, plant material was collected, enriched using anti-HA magnetic beads, and analyzed via western blot with an anti-HA antibody. However, no clear signal could be detected using different amounts of plant material (data not shown).

In a study by Kretschmer *et al*. (2022), effector gene expression was enabled *in vitro,* when *U. maydis* were cultured in a minimal medium supplemented with glucose and malate (see 6.8.4). Induced effector genes comprised *Umcmu1.* Since *pro^{Umcmu1}* was used for the OE of *Umhdp2* and *Srhdp2* in rUSH, an *in vitro* induction was performed to test the presence of Hdp2. Hence, rUSH_Umhdp2^{OE} and rUSH_Srhdp2^{OE} were grown for 72h in a minimal medium supplemented with 1% glucose and

0.5% malate (see 6.8.4) before detection of UmHdp2 and SrHdp2 by western blot (Figure 4.2E). In addition to the expected bands at 118 kDa (UmHdp2) and 111 kDa (SrHdp2), several other bands with different intensities were detected, suggesting a processing of Hdp2 and the presence of potentially unspecific bands.

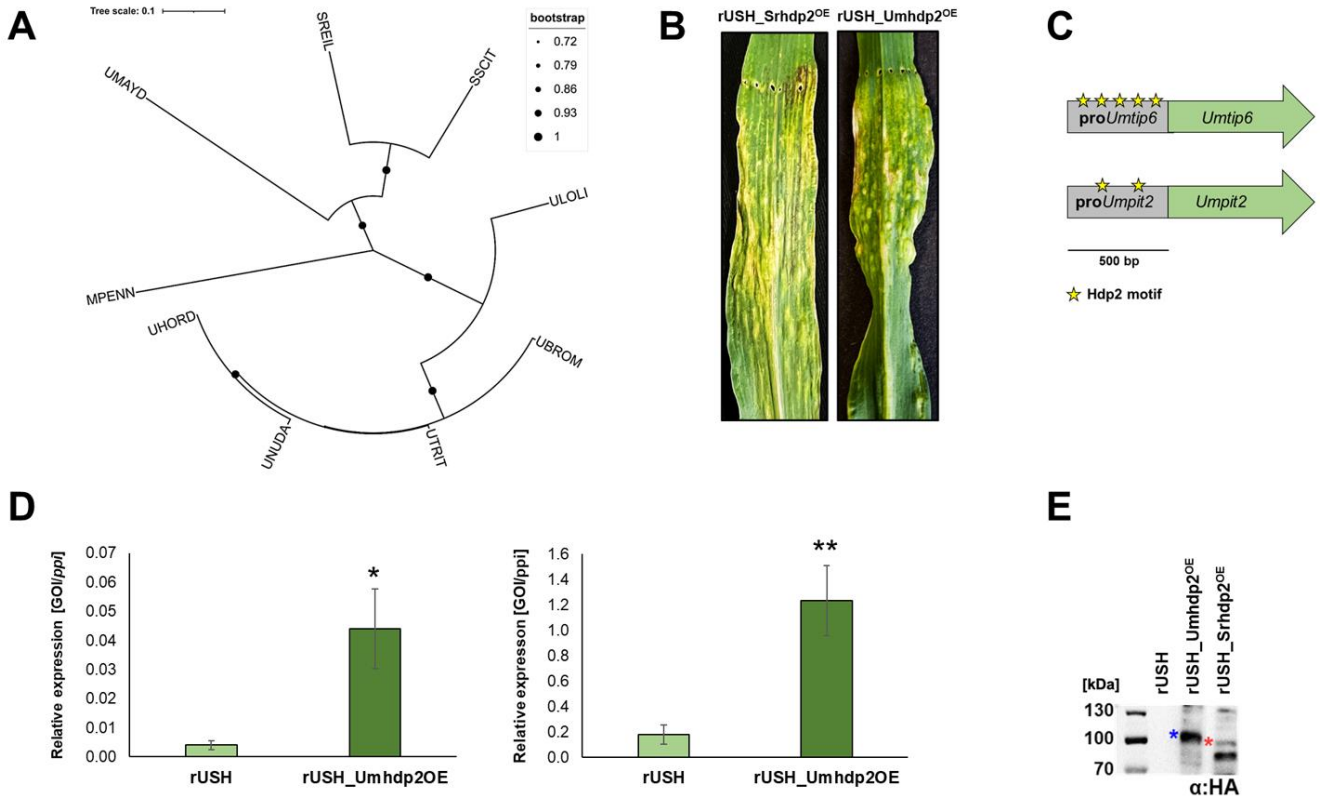

Figure 4.2: Overexpression of the conserved transcription factor Hdp2 in rUSH leads to tumor formation. **(A)** Phylogenetic analysis of Hdp2 among smut fungi. Hdp2 protein sequences were aligned using MUSCLE and a Maximum-Likelihood tree was constructed using MEGA X. Bootstrapping was performed with 100 iterations. **(B)** The phenotype of rUSH_Srhdp2^{OE} and rUSH_Umhdp2^{OE} at 6 dpi. **(C)** Hdp2 motifs in the 500 bp promoter region of *Umtip6* (*UMAG_11060*) and *Umpit2* (*UMAG_01375*). Yellow stars indicate Hdp2 binding sites. **(D)** Relative gene expression of *Umtip6* and *Umpit2* was normalized to *Umppi* and measured in rUSH and rUSH_Umhdp2^{OE}. Significant differences were calculated based on students t-test (* =p<0.05, ** =p<0.01). **(E)** Anti-HA western blot of *in vitro*-induced production of UmHdp2 and SrHdp2. Expected sizes: UmHdp2: 118 kDa, SrHdp2: 111 kDa.

4.3.4 UmHdp2 is crucial for virulence and can be functionally replaced by SrHdp2

To test the importance of UmHdp2 in the regulation of pathogenicity-related genes, a deletion of *Umhdp2* was generated in the SG200 background. Therefore, a donor template consisting of the 1 kb upstream and 1 kb downstream region of *Umhdp2* was designed and used together with the pCas9HF1 plasmid with a sgRNA, which cuts approximately in the middle of the cds of *Umhdp2*, in a transformation.

Three independent mutants were verified by Southern blot and used to infect 7-day old maize seedlings. At 6 dpi and 12 dpi the disease symptoms were assessed as described in Table 6. (Figure 4.3). All three independent deletion mutants revealed a significant reduction in virulence, showing no symptoms or chlorosis, which is in line with a previous study of Δ*hdp2* by Heimel *et al*., (2010b).

Since conservation of Hdp2 among the smuts was predicted using the software Mega X (Kumar *et al.*, 2018) (Figure 4.2A), we tested whether SrHdp2 can functionally replace UmHdp2 in *U. maydis*. Therefore, we replaced the cds of *Umhdp2* under the control of the native promoter pro^{Umhdp2} against the cds of *Srhdp2.* In a CRISPR-assisted HR, pCas9HF1 with the previously mentioned sgRNA of *Umhdp2,* as well as a donor template with 1 kb homology flanks and the cds for *Srhdp2* were used for the replacement. The resulting mutant was verified by Southern blot and, along with the deletion mutants of Δ*Umhdp2*, used to infect 7-day old maize (Figure 4.3). The replacement of the cds of *Umdhp2* against *Srhdp2* revealed a functional conservation of Hdp2 between *U. maydis* and *S. reilianum*, since no difference in the phenotype compared to SG200 was observed at 6 dpi (Figure 4.3A) and 12 dpi (Figure 4.3B).

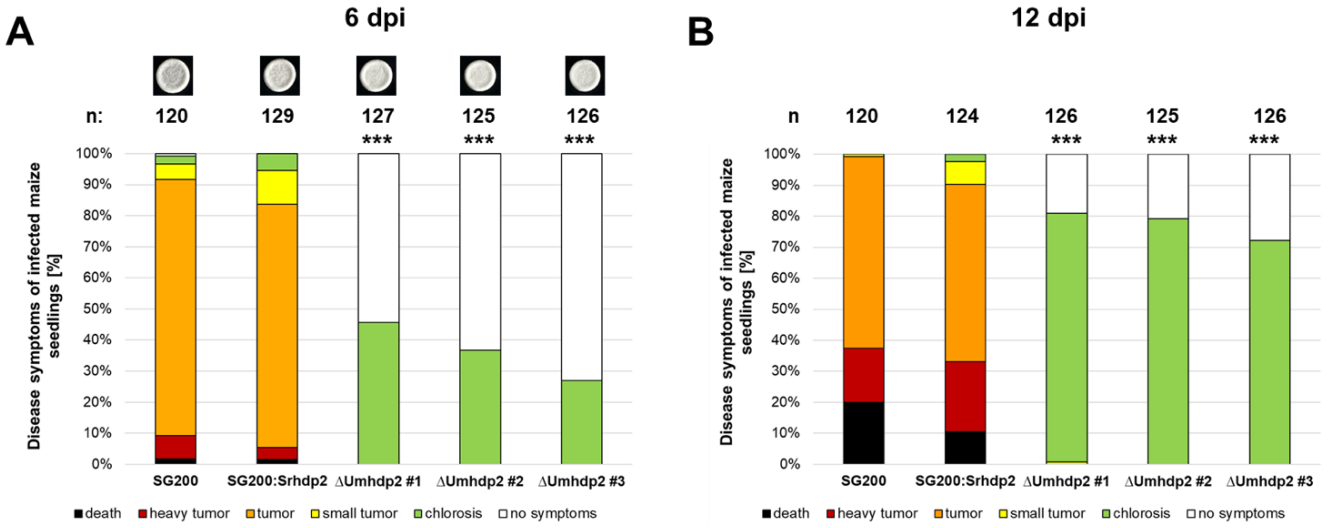

Figure 4.3: Disease symptoms of 7-day old maize seedlings infected with SG200, SG200:Srhdp2, SG200Δ*Umhdp2* #1, SG200Δ*Umhdp2* #2, SG200Δ*Umhdp2* #3 after (A) 6 dpi and (B) 12 dpi. Scoring of disease symptoms was performed as described in 6.9.3. The data represents three independent biological replicates. Significant differences were calculated based on students t-test (* =p<0.05, ** =p<0.01, *** =p<0.001). n = total number of plants. Used strains were tested on activated charcoal (above the bar chart in A). The figure was modified from Katharina Stein (Bachelor thesis).

4.3.5 Motif enrichment analysis revealed distinct transcription factor binding motifs

To elucidate whether the observed expression pattern of effector genes in rUSH can be linked to specific TFs, a motif enrichment analysis of the effector gene promoters (500 bp upstream of the start codon) was performed. Therefore, the total expression of each of the 281 orthogenes (prediction of

Dr. Georgios Saridis) was compared between WT and rUSH at 3 dpi and 6 dpi, leading to the creation of eight clusters with distinct patterns (G1-G8, Figure 4.4A). Based on the expression patterns, G1 and G3 were attributed to *trans*-regulation, G5 and G6 to *cis*-regulation, G2 and G4 to reverse expression and G7 and G8 to the orthologue-specific expression (Figure 4.4A, Table S4.2). For three of the clusters (G3, G4, and G7), specific motifs were enriched. In the case of G3 which contains effector orthologues highly expressed in the WT of *U. maydis* but exhibits no differential expression in rUSH, the binding motif "GTGGG" known for Biz1 was identified (Figure 4.4B). For the reverse expression of the effector genes in cluster G4, motifs for Biz1 ("GTGGG") and Hdp2 ("ATGAAG") were identified, and for the cluster G7, showing no differential expression between the WT and a higher expression of the *S. reilianum* orthologue, a yet unidentified motif was found (Figure 4.4B).

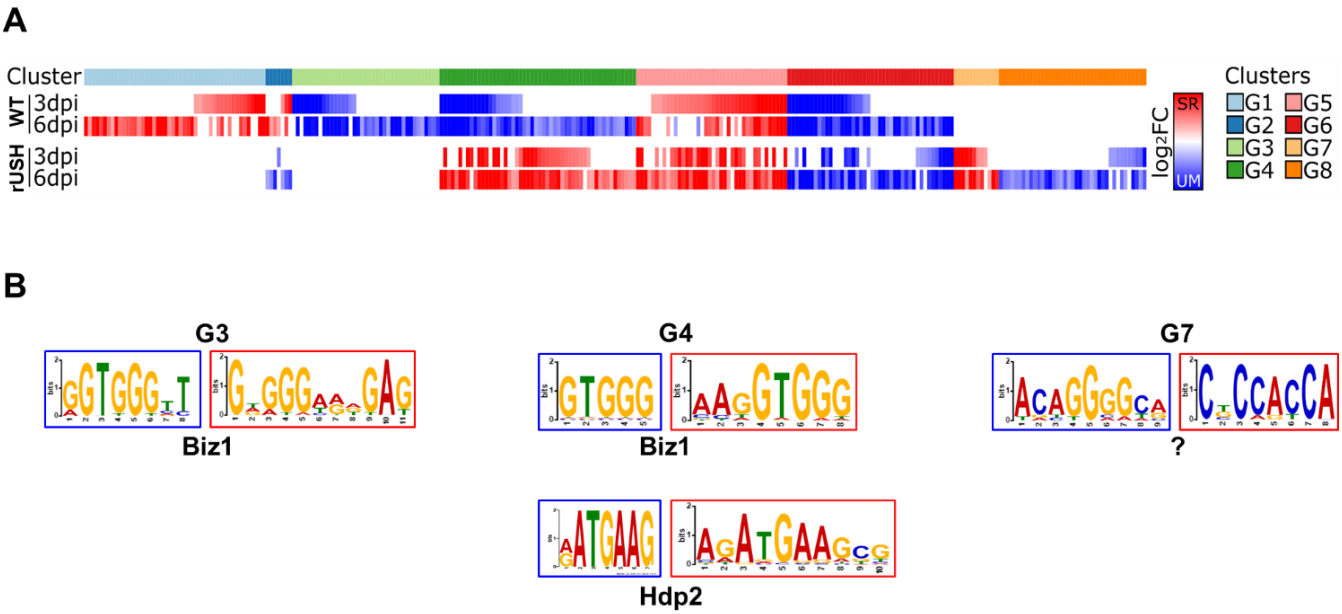

Figure 4.4: Motif enrichment analysis of 500 bp promoter sequence of differentially expressed effector one-to-one orthologues. (A) Orthogene clustering was performed based on the expression profiles between WT and rUSH. The total expression of each orthogene at 3 and 6 dpi was compared between WT and rUSH and led to the generation of 8 clusters with the following patterns: G1, higher SR in WT, no difference in rUSH; G2, higher SR in WT, higher UM in rUSH; G3, higher UM in WT, no difference in rUSH; G4, higher UM in WT, higher SR in rUSH; G5, higher SR in WT, higher SR in rUSH; G6, higher UM in WT, higher UM in rUSH; G7, no difference in WT, higher SR in rUSH; G8, no difference in WT, higher UM in rUSH. **(B)** 500 bp promoter regions (upstream of the start codon) were used in the software STREME (Bailey, 2021) with the specific option „any number of occurrences" to identify effector genes with specific sequence motifs in the promoter sequence. The motifs for Biz1 and Hdp2 were found. The analysis was performed by Dr. Georgios Saridis.

4.3.6 RNA-seq analysis of rUSH_Umhdp2^{OE} and rUSH_Srhdp2^{OE} compared to rUSH

The conserved TF Hdp2 was identified in previous experiments as a major player in tumor formation of *U. maydis*. The reverse expressed effector genes, which were previously associated with virulence clusters of *U. maydis*, were enriched in the motif regulated by Hdp2 and Biz (G4). rUSH_Umhdp2^{OE} and rUSH_Srhdp2^{OE} induced the induction of small tumors in maize seedlings. To gain insights into the target genes activated by Hdp2 and, in particular, the Hdp2-activated genes in rUSH, an RNA-seq experiment was conducted. 7-days old maize seedlings of the cultivar Golden Bantam were infected with rUSH, rUSH_Umhdp2^{OE}, and rUSH_Srhdp2^{OE}. Samples were collected at 3 dpi and analyzed by RNA-seq.

4.3.6.1 *U. maydis* effector genes were activated upon *hdp2* overexpression in rUSH

The RNA-seq analysis revealed for *U. maydis* the activation of a higher number of one-to-one effector genes compared to non-effector genes rUSH_Umhdp2OE and rUSH_Srhdp2OE. This is in contrast with the *S. reilianum* genes upregulated in rUSH_Umhdp2^{OE} and rUSH_Srhdp2^{OE}-infected plants, where more non-effector genes than effector genes were activated (Figure 4.5A).

In rUSH_Umhdp2^{OE}, 53 upregulated *U. maydis* genes, comprising 41 effector genes and 12 non-effector genes compared to rUSH were identified (log_2FC 1, p-value <0.05). This indicated a regulation of those effector genes by UmHdp2. Next, the promoter regions of the effector genes were examined for the presence of the “ATGAA” Hdp2 motif. This resulted in the identification of the binding motif of Hdp2 in the 500 bp promoter region (upstream of the start codon) of ten effector genes and none in the promoter region of non-effector genes (Figure 4.5B+C). For the remaining effector genes, an indirect activation is hypothesized, since the “ATGAA” motif was not identified in their promoter region. The upregulated effector genes comprise 21 effector genes organized in gene clusters (Figure 4.5B) and 20 that were not associated with clusters (Figure 4.5C). From the effector genes in clusters, five were identified to reside in cluster 6A and 13 in cluster 19A; two clusters known for their contribution to virulence. In addition, three core effector genes were identified, out of which two comprise the Hdp2 motif three times in their promoter region: *UMAG_12226* and *UMAG_00781*, which indicates a direct regulation of these effectors by Hdp2. The upregulated non-effector genes in rUSH_Umhdp2^{OE} revealed five genes with a functional DNA-binding domain, including the already characterized TF UmFox1 and three putative TFs *UMAG_02591*, *UMAG_04998* and *UMAG_01573*. These genes comprise an M-type MADS, a bZIP, and a Zn(2)-C6 fungal-type binding domain, respectively.

Next, the upregulated genes in rUSH_Srhdp2^{OE} compared to rUSH were analyzed. 48 upregulated *U. maydis* genes were identified, including 36 effector genes and 12 non-effector genes. Within the

36 effector genes, 11 were attributed to cluster 19A and 5 to cluster 6A. The 88 upregulated *S. reilianum* genes in rUSH_Srhdp2^{OE} comprise 18 effector genes and 70 non-effector genes.

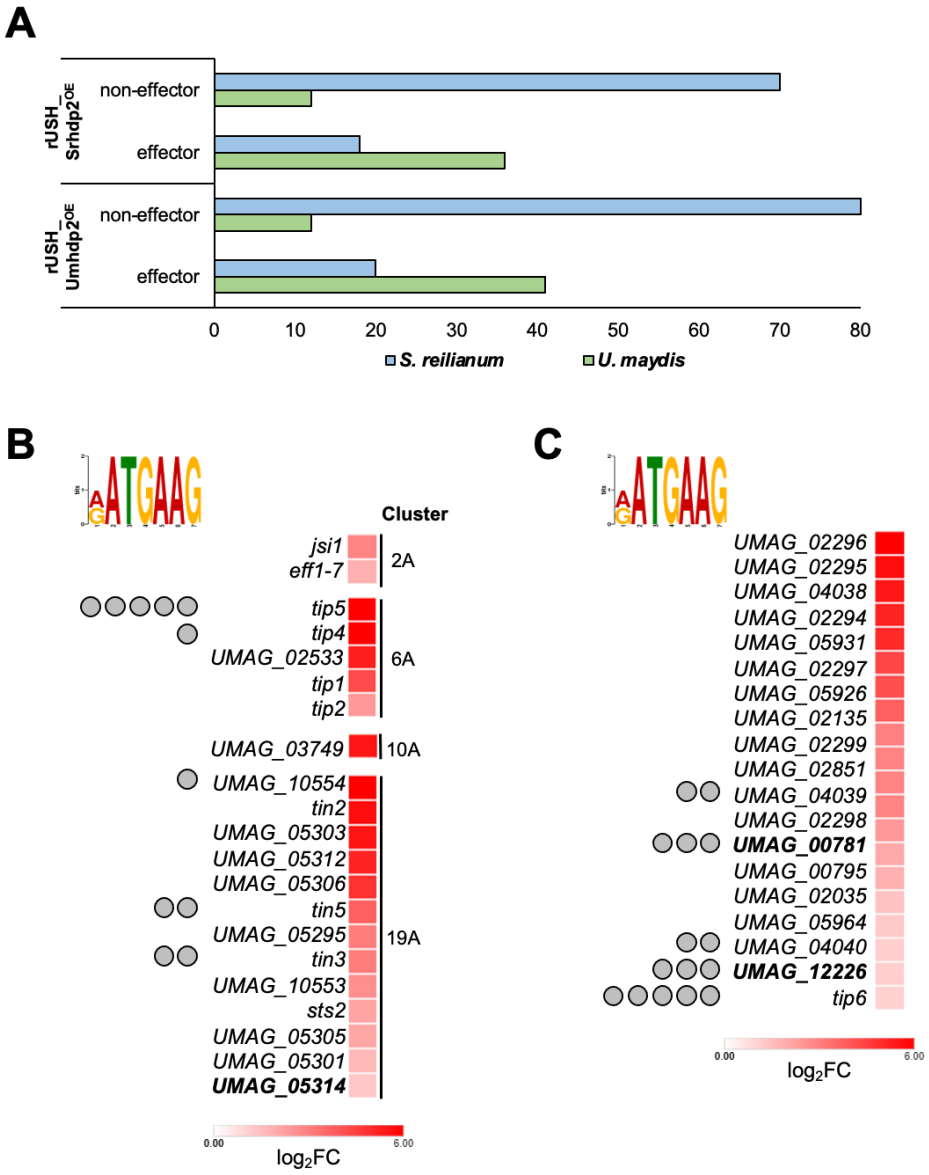

Figure 4.5: RNA-seq revealed differentially expressed effector and non-effector genes in rUSH_Umhdp2OE and rUSH_Srhdp2^{OE} compared to rUSH. (A) Upregulated effector and non-effector genes of *U. maydis* and *S. reilianum* in rUSH_Umhdp2^{OE} and rUSH_Srhdp2^{OE} compared to rUSH. **(B)** Upregulated *U. maydis* effector genes in rUSH_Umhdp2OE compared to rUSH are located in effector clusters. **(C)** Upregulated *U. maydis* effector genes in rUSH_Umhdp2OE compared to rUSH that are not located in effector clusters. Grey circles indicate the binding sites for Hdp2. Core effectors are highlighted in bold. Hdp2 motif: "ATGAAG", previously identified motif: "ATGAA" (Jurca, 2021).

To investigate whether the same effector genes of *U. maydis* and *S. reilianum* are activated by UmHdp2 and SrHdp2, rUSH_Umhdp2^{OE} (41) and rUSH_Srhdp2^{OE} (36) were analyzed in detail (Figure 4.6A+B). This analysis revealed 32 *U. maydis* effector genes upregulated upon UmHdp2 and SrHdp2, 9 uniquely

in rUSH_Umhdp2^{OE} (*UMAG_11060* (*tip6*), *UMAG_12226, UMAG_04040, UMAG_05964, UMAG_05314, UMAG_00781, UMAG_02298, UMAG_02135, UMAG_10554*) and 4 exclusively in rUSH_Srhdp2^{OE} (Figure 4.6C). Similarly, the upregulated *S. reilianum* effector genes of rUSH_Umhdp2^{OE} (20) and rUSH_Srhdp2^{OE} (18) were investigated (Figure 4.6C). This resulted in the upregulation of 17 *S. reilianum* effector genes in rUSH_Umhdp2^{OE} and rUSH_Srhdp2^{OE}, respectively. Three *S. reilianum* effector genes were uniquely upregulated in rUSH_Umhdp2^{OE} and one in rUSH_Srhdp2^{OE} (Figure 4.6C).

Next, the presence of one-to-one orthologues between the upregulated *U. maydis* and *S. reilianum* effector genes, observed in rUSH_Umhdp2^{OE} compared to rUSH, was investigated. In this comparison, eight shared upregulated one-to-one effector orthologues were identified (Figure 4.6D). This suggests a diversification of effector orthologue regulation by Hdp2 during the speciation of *U. maydis* and *S. reilianum*.

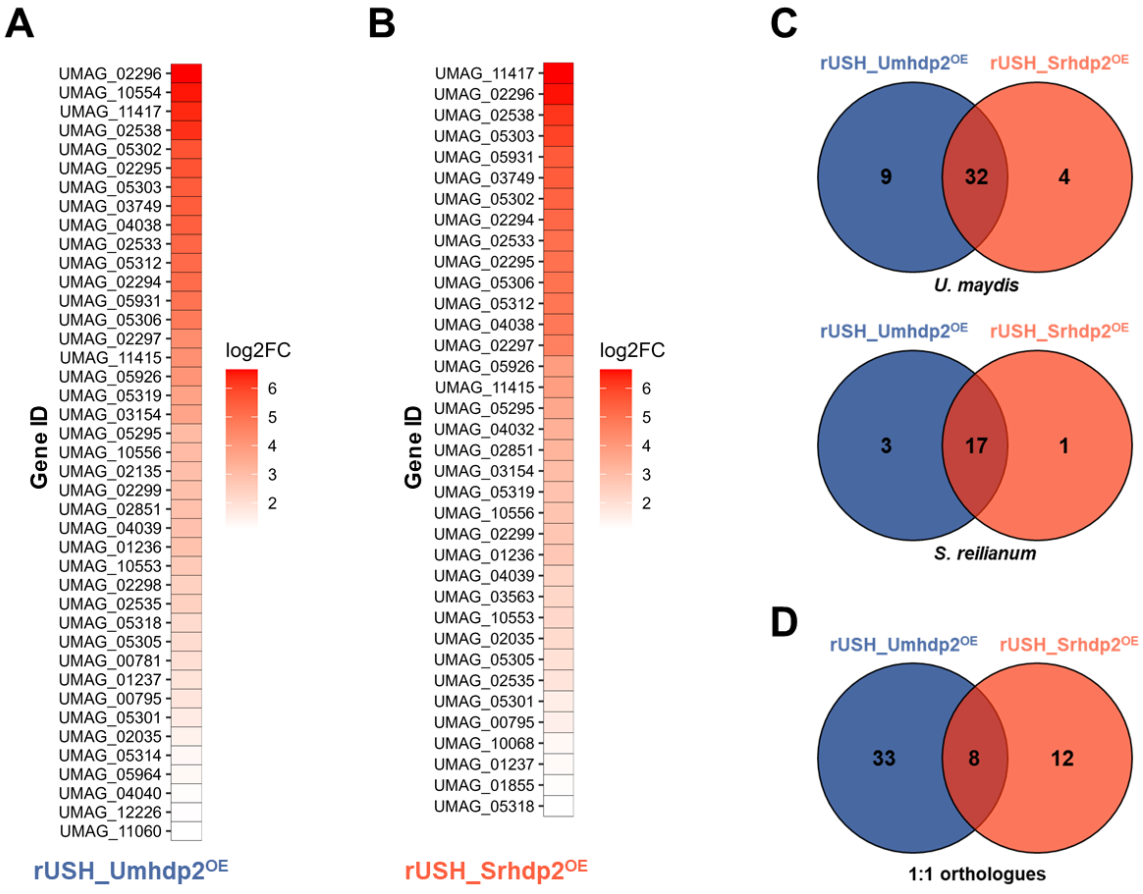

Figure 4.6: Upregulated effector genes in rUSH_Umhdp2^{OE} and rUSH_Srhdp2^{OE} compared to rUSH at 3 dpi. **(A)** Upregulated *U. maydis* effector genes between rUSH_Umhdp2^{OE} and rUSH. **(B)** Upregulated *U. maydis* effector genes between rUSH_Srhdp2^{OE} and rUSH. **(C)** Intersection of 41 upregulated *U. maydis* effector genes in rUSH_Umhdp2^{OE} and the 36 upregulated *U. maydis* effector genes in rUSH_Srhdp2^{OE}. **(D)** Intersection of one-to-one orthologues among the upregulated *U. maydis* and *S. reilianum* genes in rUSH_Umhdp2^{OE} vs. rUSH.

4.3.6.2 rUSH_Umhdp2^{OE} and rUSH_Srhdp2^{OE} reveal maize genes important for leaf tumor development in maize

To identify genes putatively involved in the reprogramming of cellular processes in *Z. mays* by rUSH, the upregulated maize genes in rUSH_Umhdp2^{OE} and rUSH_Srhdp2^{OE} were screened. Compared to rUSH, in total, 1145 and 1384 maize genes were upregulated in rUSH_Umhdp2^{OE} and rUSH_Srhdp2^{OE}, respectively. While 674 upregulated genes were shared between rUSH_Umhdp2^{OE} and rUSH_Srhdp2^{OE}, in rUSH_Umhdp2^{OE} 471 and rUSH_Srhdp2^{OE} 710 maize genes were uniquely upregulated (Figure 4.7A). The shared upregulated maize candidate genes were further grouped into different categories based on their function, including groups such as potentially involved in tumorigenesis (cell division, cell expansion, cell elongation and cell growth), cell wall (CW) loosening, sugar metabolism, cysteine-rich receptor-like kinases (CRKs), general defense, Glutathione-S-transferases (GSTs), cytochrome P450 (CYPs), WRKY TFs, undescribed genes, and others (Figure 4.7B). Compared to the genes putatively involved in tumorigenesis and genes related to phytohormonal pathways that add up to almost 10% of the investigated 674 genes, a similar number of genes was identified as putatively involved in plant defense responses and the secondary metabolism (Fig. 4.7B). Presumably, these relations are different in the wild types due to the varying levels of virulence.

Among the 674 shared upregulated genes, 36 *Z. mays* genes that may be utilized by *U. maydis* to induce tumor formation were identified (Figure 4.6B; green). Within this category, eight genes involved in cell expansion such as expansins and arabinogalactans, three genes involved in cell elongation (*ZmGIF1* (growth-regulating-factor-interacting factor 1(GRF1)-interacting factor 1), Proline-rich Extensin-like Receptor Kinase 7 (*PERK7*) and BREVIS RADIX-like (BRXL) 4), 18 genes involved in the regulation of cell division, such as cyclins and cyclin-dependent kinases (CDKs) and seven genes involved in cell growth (Cytokinin-dehydrogenases and phytosulphokines (PSKs) were identified (Figure 4.7C). *ZmGIF1* (*Zm00001eb056300*) and *ZmSHR1* (Short Root 1*, Zm00001eb326020)* have been previously reported to be activated for tumorigenesis of *U. maydis* (Zuo *et al*., 2023) and are also upregulated in rUSH_Umhdp2^{OE}. Furthermore, 28 of the identified maize genes are related to phytohormonal pathways, including IAA, ABA, JA, and ET, that are known to be important for plant growth and development. These genes were not further investigated in this study.

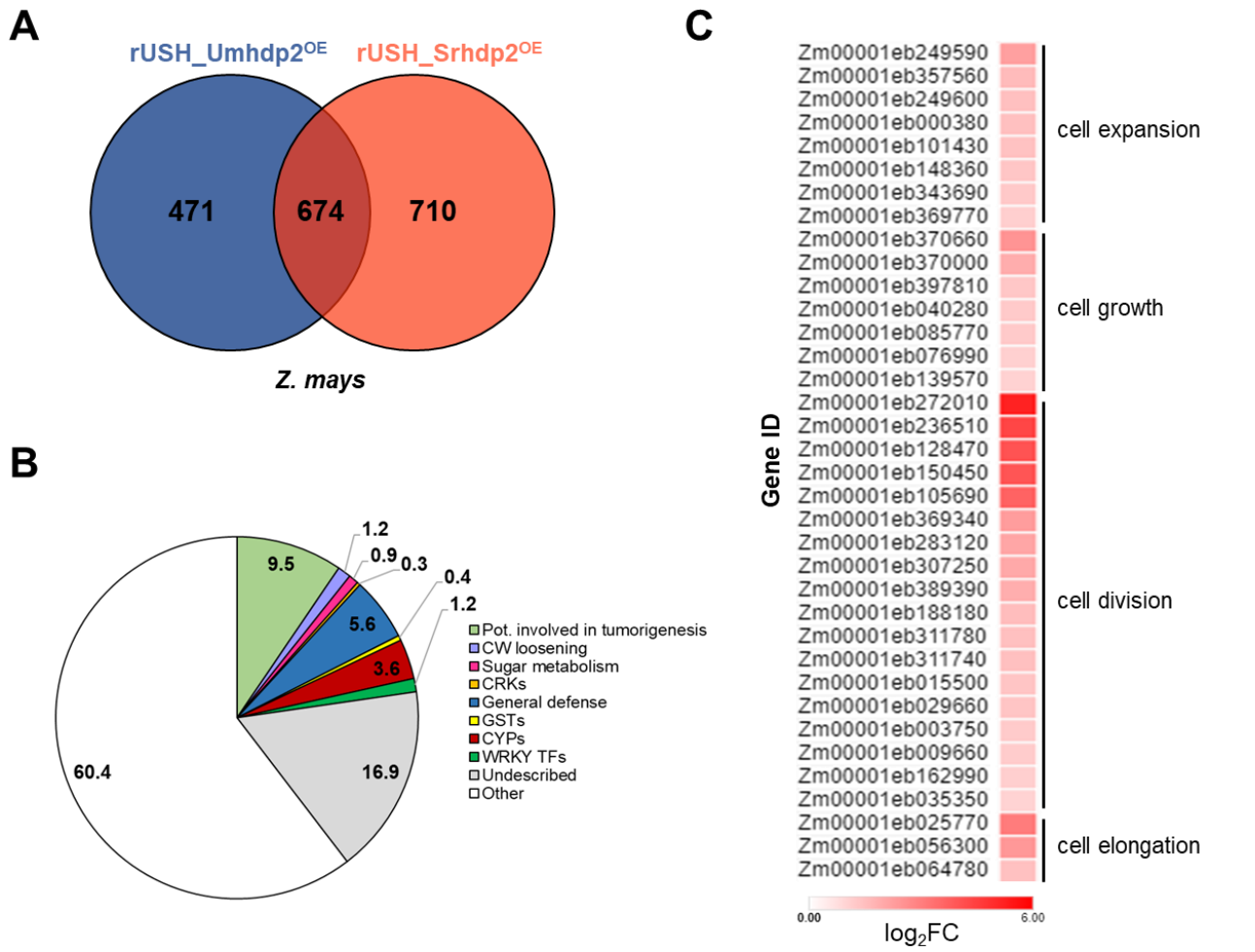

Figure 4.7: Upregulated maize genes in rUSH_Umhdp2^{OE} and rUSH_Srhdp2^{OE} compared to rUSH. (A) Intersection of upregulated maize genes in rUSH_Umhdp2^{OE} and rUSH_Srhdp2^{OE}. **(B)** Upregulated maize genes can be grouped into different categories: potentially involved in tumorigenesis (cell division, cell expansion, cell elongation, and cell growth), cell wall (CW) loosening, sugar metabolism, Cysteine-rich receptor-like kinases (CRKs), General defense, Glutathione-S-transferases (GSTs), Cytochrome P450 (CYPs), WRKY TFs, undescribed maize genes and others. **(C)** Heatmap of upregulated maize genes (log_2FC, $p<0.05$) in rUSH_Umhdp2^{OE} and rUSH_Srhdp2^{OE} compared to rUSH, involved in cell expansion, cell growth, cell division and cell elongation. The software MORPHEUS was used for the generation of the heatmap.

4.4 Discussion

4.4.1 The HD TF Hdp2 is crucial for tumorigenesis

For the expression of pathogenicity-related genes of fungi, a coordinated regulation at a distinct time point during infection is crucial (John *et al*., 2022). The expression of effector genes in smut fungi is highly dependent on a tight regulation of a TF cascade. When the expression of pathogenicity-related TFs was investigated in rUSH, a generally higher expression of the *S. reilianum* TF orthologue was observed. It has been previously reported that constitutively expressed TFs involved in *U. maydis* pathogenesis enhanced the virulence in a *U.maydis* X *S. reilianum* hybrid, while the expression of individual effectors did not (Storfie & Saville, 2021). To shift the *S. reilianum*-like phenotype of rUSH towards *U. maydis*, six *U. maydis* TFs (rbf1, *hdp2*, *biz1*, *fox1*, *ros1* and nlt1) were overexpressed. Only the OE of *hdp2* altered the *S. reilianum*-like phenotype and led to the induction of small tumors in rUSH. This is in line with the recently published hybrid of *U. maydis* strain 521 and *S. reilianum* SRZ2. In laboratory conditions, the hybrid formed anthocyanin and, on rare occasions, small tumors during leaf infection when the TFs *rbf1* and *hdp2* were overexpressed (Storfie & Saville, 2021). In contrast to the previously mentioned hybrid, no visible phenotypical change was observed upon *rbf1* OE in rUSH in this study. This difference may be attributed to the different promoters used in this study (pro^{Umcmu1}) and the study by Storfie & Saville (2021) (pro^{OTEF}), as well as to the different genetic backgrounds, which may result in varying expression timing and level.

The genes encoding for the TFs Hdp2 and Biz1 are transcriptionally induced by the cell-surface proteins Sho1 and Msb2. This provides evidence for an induction of early effectors by Biz1 and Hdp2 (Lanver *et al*., 2018). The phenotype of the generated *U. maydis* Δ*hdp2* deletion mutants showed a significant reduction in virulence, reflecting the importance of Hdp2 for tumor formation of *U. maydis*. This is consistent with previous studies by Heimel *et al.* (2010b) and Lanver *et al.* (2014), which demonstrated that Δ*hdp2* resulted in an avirulent strain that was unable to form penetration structures. The filamentous growth of the deletion strains was not affected in Δ*hdp2* mutants, which is also consistent with previous studies (Heimel *et al*., 2010b; Lanver *et al*., 2014).

In *U. maydis*, HD TFs have been described to control the dimorphic growth, sexual cycle, and pathogenicity (Schulz *et al.*, 1990). In this study, Hdp2 has been identified as a key transcriptional regulator for tumor induction in *U. maydis*. Across the kingdom of Fungi, important roles in developmental processes have been assigned to HD proteins, i. e. in *Botrytis cinerea* (Schamber *et al*., 2010), *Magnaporthe oryzae* (Liu *et al*., 2010), *Schizophyllum commune* (Ohm *et al*., 2011) and *Ustilaginoidea virens* (Yu *et al*., 2019). However, the functional analyses of the

majority of the HD proteins in filamentous fungi remain to be elucidated in the future (Vonk & Ohm, 2018).

When *Umhdp2* was replaced by *Srhdp2* in the solopathogenic strain SG200, a functional conservation was shown. This observed conservation is also consistent with the tumor formation of rUSH_Umhdp2^{OE} and rUSH_Srhdp2^{OE}. However, due to the different infection modes of *U. maydis* and *S. reilianum*, the effector genes regulated by Hdp2 may have functionally diverged between the species and are crucial for tumor induction by *U. maydis*. The different function of the downstream genes of Hdp2 in *U. maydis* and *S. reilianum* was further confirmed by an *S. reilianum* strain with the replacement of *Umhdp2* against *Srhdp2* in the native locus. This mutant was not capable of tumor formation in maize, reflecting the different functions as well as the different regulation of disease development.

To correlate the different expression patterns observed in rUSH with specific binding motifs, a motif enrichment analysis was conducted. In the reverse expression pattern, enrichment for the binding sites recognized by Hdp2 and Biz1 was identified in the 500 bp upstream region of the cds. This implements a co-regulation of these effector genes by Hdp2 and Biz1, which is consistent with previous results of ChIP-seq data (Jurca, 2021). However, the timing of the binding of Hdp2 and Biz1 is still poorly understood. Furthermore, it remains unclear whether both TFs can simultaneously bind to the promoter region of the same effector gene and whether the activation of expression needs a certain threshold of Hdp2 before activation, as it was previously described for Biz1 (Ulrich, 2020).

4.4.2 RNA-seq revealed direct and indirect regulated *U. maydis* effector genes by Hdp2

To shed light on the target genes that are regulated by Hdp2, an RNA-seq experiment was conducted. 41 and 36 *U. maydis* one-to-one effector orthologues were upregulated in rUSH_Umhdp2^{OE} or rUSH_Srhdp2^{OE}, respectively, suggesting a contribution of these genes to the observed tumor formation in rUSH.

The occurrence of the *U. maydis* cluster 6A or 19A effector genes among the upregulated genes reflects their previously reported importance in virulence (Brefort *et al*., 2014; Kämper *et al.*, 2006). This suggests that the diversification of these genomic regions during evolution may have resulted in different effector functions in *U. maydis* and *S. reilianum*, which is consistent with the findings of two neofunctionalized effectors in cluster 19A: Tin2 and Sts2 (Tanaka *et al*., 2019; Zuo *et al*., 2023). When the expression of the corresponding *S. reilianum* one-to-one effector orthologues of the upregulated *U. maydis* genes in rUSH_Umhdp2^{OE} or rUSH_Srhdp2^{OE} were observed in the *S. reilianum* wild type (RNA-seq, Werner *et al*., unpublished) for some genes, no expression was observed. This suggests on the one hand that the *S. reilianum* effector orthologues may have retained the function of tumor formation during speciation of the two species, but are not expressed during *S. reilianum* infection. On

the other hand, the *U. maydis* effector genes may have gained a specialized function in tumor formation during evolution.

SrHdp2 was shown to maintain the function of UmHdp2 in SG200 infection assays. This suggests the functional conservation of Hdp2 between the species. However, an amino acid identity of about 58% indicates variations on protein level, which is supported by the observed differences in the upregulated downstream targets in rUSH_Umhdp2^{OE} and rUSH_Srhdp2^{OE}. In addition, Hdp2 is possibly post-translationally modified, which may result in alterations in protein function or the acquisition of an additional function of UmHdp2 in *U. maydis*. This is consistent with what has been reported for human and mouse HD TFs, where the activity of individual TFs has been reported to be shaped by different post-translational modifications within a conserved TF family (Reichlmeir *et al*., 2021). Further, yet undescribed *U. maydis*-specific mediators or factors required for the UmHdp2-mediated initiation of effector gene transcription may contribute to observed differences in downstream targets.

At least one binding site for Hdp2 was found in the promoter region of 10 out of 41 upregulated *U. maydis* effector genes. This suggests that Hdp2 can directly and indirectly activate effector genes. The indirect regulation may be mediated by an intermediate TF situated between Hdp2 and the effector genes. For the identification of such a TF putatively acting downstream of Hdp2, a KO of the three identified TFs in rUSH_Umhdp2^{OE} (*UMAG_02591*, *UMAG_04998,* and *UMAG_01573*) was conducted in SG200, followed by an infection assay to assess the contribution of these TFs to *U. maydis* pathogenicity.

4.4.3 Hdp2 modulates leaf tumor development in maize

When the gene ontology (GO) terms of the shared upregulated maize genes of rUSH_Umhdp2^{OE} and rUSH_Srhdp2^{OE} were analyzed in detail, maize genes important for general defense were observed. This may be explained by a different spatiotemporal expression of *hdp2* or by an excessively high expression of *hdp2* in rUSH_Umhdp2^{OE} and rUSH_Srhdp2^{OE}-infected maize plants in comparison to the wild type. The observed differences in virulence between rUSH_Umhdp2^{OE} and *U. maydis* wild type suggest an enhanced suppression of plant defense responses in the *U. maydis* wild type compared to rUSH_Umhdp2^{OE}. This could further explain why tumors of rUSH_Umhdp2^{OE}- and rUSH_Srhdp2^{OE}-infected maize seedlings cannot develop further. Nevertheless, the precise mechanism underlying the upregulation of defense genes in rUSH_Umhdp2^{OE}- and rUSH_Srhdp2^{OE}-infected plants compared to the *U. maydis* wild type remains unclear.

Furthermore, 36 maize genes putatively involved in cell cycle and cell cycle-related processes, such as cell division and cell enlargement, were identified. Among the genes involved in cell division, genes encoding for cyclins and CDKs were found. In plants, a distinct regulation of cell division during plant development is crucial (Renaudin *et al*., 1996). CDKs are known to be crucial for the regulation of cell

cycle progression in eukaryotes allowing the transition from G1/S to G2/M phases (Nigg, 1995; Norbury & Nurse, 1992; Shimotohno *et al*., 2021). The activity of CDKs has been reported to be dependent on the binding of cyclins (Renaudin *et al*., 1996). Therefore, the presence of cyclins and CDKs suggests an interaction of the downstream targets of Hdp2 with the plant cell cycle for the manipulation of leaf development in maize. However, whether the identified cyclins and CDKs are manipulated during infection and directly interact with the effectors encoded by the upregulated effector genes in rUSH_Umhdp2^{OE} or rUSH_Srhdp2 ^{OE} remains to be elucidated in the future.

Additionally, genes encoding for putative maize expansins and AGPs were identified among the upregulated genes after infection with rUSH_Umhdp2^{OE} and rUSH_Srhdp2^{OE}. Expansins and AGPs are associated with cell expansion. The manipulation of plant AGPs was described to alter several biological processes, e. g. cell division and cell expansion (Majewska-Sawka & Nothnagel, 2000). Therefore, AGPs may be possible interaction targets of *U. maydis* effectors, secreted for the manipulation of maize leaf development, favoring tumorigenesis.

Moreover, cytokinin-dehydrogenases were identified among the upregulated maize candidate genes. CKs are phytohormones involved in several plant processes such as root and shoot branching, leaf development, and cell division (Mok, 1994). The CK level is regulated by a homeostasis between synthesis and metabolism. Cytokinin-dehydrogenases catalyze the degradation of CKs by cleaving their oxidative side chain (Schmülling *et al*., 2003). Using mass spectrometry, the production of fungal-derived CKs has been reported in *U. maydis* (Bruce *et al*., 2011) which possibly explains the upregulation of maize cytokinin dehydrogenases during *U. maydis* infection to maintain CK homeostasis *in planta*. It has been hypothesized, that *U. maydis*-derived CKs (Bruce *et al*., 2011) and manipulation of plant CKs by *U. maydis* (Mills & Van Staden, 1978) may be associated with the initiation or maintenance of tumor formation during pathogenicity. Consistent with these findings, CKs were described to be important for the signaling during gall formation in the endophyte *Ustilago esculenta* and its host *Zizania latifolia* (He *et al.*, 2020).

In addition, phytosulpohokines (PSKs), generally known to function in plant growth, have been identified among the upregulated maize candidates. PSKs have been previously reported in maize for their role in cell division in low-density suspension cultures and plant tissue differentiation (Lorbiecke *et al*., 2005; Yang *et al*., 2000), and are therefore interesting candidates for manipulation by *U. maydis*. Moreover, PERKs that are known to be involved in plant growth and development were identified (Borassi *et al*., 2016; Invernizzi *et al*., 2022). In Arabidopsis, PERKs were reported to be involved in the negative regulation of root growth and the modulation of root cell elongation (Bai *et al*., 2009; Humphrey *et al*., 2015). The involvement of PERKs in the cell growth and in particular the cell

elongation, suggest a putative function of the identified ZmPERK7 in the manipulation of the leaf development during colonization by *U. maydis*.

Furthermore, BRXL4 was identified in rUSH_Umhdp2^{OE} and rUSH_Srhdp2^{OE}, compared to rUSH. In Arabidopsis, BRXL4 regulates cell elongation and proliferation in roots and shoots (Beuchat *et al*., 2010; Mouchel *et al*., 2004), which may suggest a putative role of BRXL4 in the cell elongation during the *Ustilago*-induced development of tumor cells. Additionally, *ZmGIF1* and *ZmSHR1* were identified, which have been previously found to be downregulated in a frameshift mutant of *Umsts2* in comparison to SG200. Since the mutant of *sts2* resulted in the impairment of the further development of a leaf tumor, a role of these genes in maize leaf development was suggested (Zuo *et al*., 2023). *sts2* is upregulated in rUSH_Umhdp2^{OE} and rUSH_Srhdp2^{OE} and was shown in a previous study to activate the expression of *ZmGIF1* and *ZmSHR1* via its transactivation motif (Zuo *et al*., 2023). The identification of ZmGIF1 and ZmSHR1 in two independent RNA-seq analyses as putative maize targets of *U. maydis* that are involved in tumorigenesis (this study; Zuo *et al*., 2023) renders them interesting candidates to investigate the underlying mechanism during leaf tumor development of *U. maydis*.

Taken together, the RNA-seq analysis of rUSH_Umhdp2^{OE} and rUSH_Srhdp2^{OE} revealed promising maize candidate genes, encoding for cyclins, CDKs, expansins, AGPs, cytokinin-dehydrogenases, and more. These genes play a putative role in the regulation of plant cellular processes that are manipulated by *U. maydis* during tumorigenesis. However, the *U. maydis* genes that activate the maize candidate genes, the underlying mechanism, and the distinct role of these genes during *U. maydis* pathogenicity remain to be elucidated in future studies.

4.5 Material and Methods

For a detailed description of the buffer compositions, the oligonucleotides used and the plasmids generated in this study (see Chapter 6 – Appendix, General Material and Methods).

4.5.1 Strains, growth conditions, and plant infections

For RNA-seq analysis and infection, the compatible isolates of *U. maydis* (FB1 and FB2), the recombinant hybrid (Um_Smt+SRZ2, rUSH), as well as the *hdp2* OE strains rUSH_Umhdp2^{OE} and rUSH_Srhdp2^{OE} were used. All strains were grown in YEPSlight liquid medium and at 28°C and 200 rpm shaking or on potato dextrose agar plates (PD). CRISPR mutants were generated for *U. maydis* and *S. reilianum* as previously described (Schuster *et al*., 2016; Werner *et al*., 2023; Zuo *et al*., 2020). All generated mutant strains in this study were cultivated in the same way and are listed in Table 4.1 (*U. maydis* strains) and 4.2 (*S. reilianum* strains). For cloning the *Escherichia coli* strain Top10 was used and cultivated in dYT liquid medium or on YT plates, supplemented with the corresponding antibiotics. The generated plasmids in this study are listed in table 6.3. For infection assays, maize plants were grown under controlled conditions in 16h light at 28°C and for 8 h darkness at 22°C. Maize seedlings of the cultivar Golden Bantham were infected with an OD_{600} of 1 of a 1:1 mixture of compatible mating partners or SG200. For rUSH, 0.1% Tween was added before infection. Disease symptoms for the OE strains were assessed at 6 dpi.

Table 4.1: *U. maydis* strains used in this study.

Strain (Genotype)	Usage	Reference
FB1	Maize infection, transformation	Banuett & Herskowitz, 1989
FB2	Maize infection, transformation	Banuett & Herskowitz, 1989
FB1_*Sra1b1* (short: M3)	Maize infection, transformation	Weiliang Zuo, AG Döhlemann
Generation of TF overexpression strains		
M3_proCmu1_hdp2_2xHA #1	Multiple integrations of Umhdp2 into *ip* locus of M3	This study
M3_proCmu1_hdp2_2xHA #12	Single integration of Umhdp2 into *ip* locus of M3	This study
M3_proCmu1_rbf1_MI#2	Overexpression of *Umrbf1* in M3	This study
M3_proCmu1_nlt1_2xHA #3	Overexpression of Umnlt1 in M3	This study
M3_proCmu1_fox1_MI#1	Overexpression of *Umfox1* in M3	This study
M3_proCmu1_ros1_2xHA_MI #2	Overexpression of *Umros1* in M3	This study
Understanding the role of the TF Hdp2 in tumor formation		
M3_Srhdp2_repl_#9 M3_Srhdp2_repl_#10		This study
M3_OE_Srhdp2_2xHA MI#10 M3_OE_Srhdp2_2xHA MI#11	RNA-seq	This study
SG200_Srhdp2_repl #3	Maize infection	Bachelor thesis, Katharina Stein

SG200_KO_Umhdp2_#3 SG200_KO_Umhdp2_#4 SG200_KO_Umhdp2_#5	Maize infection	Bachelor thesis, Katharina Stein
Overexpression of *Umhdp2* using different promoters		
M3_pro02196_Umhdp2_2xHA MI #1 M3_pro02196_Umhdp2_2xHA MI #5	Maize infection	This study
M3_pro05312_Umhdp2_2xHA MI #3		This study

Table 4.2: *S. reilianum* strains used in this study

Strain (Genotype)	Usage	Reference
SRZ1	Maize infection, transformation	Schirawski *et al*., 2010
SRZ2	Maize infection, transformation	Schirawski *et al*., 2010
Understanding the role of the TF Hdp2 in tumor formation		
SRZ1_Umhdp1_#11 SRZ2_Umhdp1_#7	Maize infection	This study
Overexpression of the RF Srhdp2 in *S. reilianum*		
SRZ2_psr16064_Srhdp2_2xHA #4, MI	Maize infection, SRZ2_psr16064_Srhdp2_2xHA #4, MI for RNA-seq	Bachelor thesis Katharina Stein, this study

4.5.2 DNA and RNA preparation and qRT-PCR

Three maize infections were conducted from three independent fungal cultures. The compatible haploid *U. maydis* and *S. reilianum* cells from cultures with OD_{600} of 0.8 were mixed in a 1:1 ratio before infection. 4 cm-long sections (1 cm below the infection side) of the third leaf were collected from at least 13 individual plants. At 20 hpi liquid latex was used to enrich the fungal material, for the 3 dpi and 6 dpi time points the plant material was sampled as described above. The plant tissue and the frozen latex was ground into a fine powder using liquid nitrogen. Total RNA was extracted using TRIzol (Thermo Fisher, Waltham, USA) according to the manufacturer's protocol. Subsequently, a DNase I digest was performed (Thermo Fisher) and the samples were sent to Novogene (UK) for RNA-seq. For qRT-PCR cDNA was synthesized using RevertAid First Strand cDNA Synthesis kit (Thermo Fisher). The qRT-PCR was performed using a GoTaq qPCR mix (Promega) and a CFX96 Real-Time PCR Detection System (BioRad). DNA of *U. maydis* and *S. reilianum* was prepared using lysis buffer (Table 6.12) and subsequently purified using a MasterPure Complete DNA and RNA Purification Kit (Epicenter, Madison, USA). For relative gene expression, $2^{\Delta Ct}$ (Ct^{Umppi} – Ct^{GOI}) was calculated. For statistical analysis, a student's t-test was conducted.

4.5.3 RNA-seq- and motif enrichment analysis

The sample preparation was conducted as mentioned in Chapter 3 with slight modifications. A 4 cm-long section of the 3rd leaf from 10 individual maize plants of 3 dpi was collected for each sample. Total RNA was extracted as described in Chapter 3. RNA libraries were prepared by Novogene using an Illumina TruSeq Stranded mRNA kit (Illumina, SanDiego, CA, USA), Illumina paired-end (PE) 150 sequencing

was performed on a HiSeq4000 platform. The standard bioinformatical analysis of the RNA-seq data was conducted by Novogene (DE). Reads were filtered to exclude low-quality reads and reads containing adapters. For the alignment, the software HISAT2 (version 2.0.5) and the combined reference genome from previous RNA-seq for *U. maydis* (Kämper *et al*., 2006), *S. reilianum* (Schirawski *et al.*, 2010) and *Z. mays* (Hufford *et al*., 2021) was used (Chapter 3). The counting of the reads was conducted using featureCounts (version 1.5.0-p3), and for the subsequent analysis of the differentially expressed genes, the R package DESeq2 (version 1.20.0) was used. To identify upregulated *U. maydis*, *S. reilianum,* and *Z. mays* candidates, the log_2FC was calculated, and genes of a log_2FC>1 (p-value < 0.05) were considered as upregulated and genes of a log_2FC<1 (p-value < 0.05) were considered as downregulated. Hdp2 Protein sequences were aligned using MUSCLE (Edgar, 2004), and a Maximum-Likelihood tree was constructed with the software MEGA X (Kumar *et al*., 2018). To extract the promoter sequences, the 500 regions upstream from the transcription start site was considered a promoter. For the extraction of promoter coordinates for the effector genes, the annotation files (GFF3 or GTF) along with the chromosome fasta files were used and the tool flank from bedtools was run with the following parameters: -l 500 -r 0 and -s, considering the gene orientation (Quinlan & Hall, 2010). Thereafter, the generated coordinates were used as input for the extraction of the promoter sequences in fasta format using bedtools getfasta. The promoter sequences were used for motif enrichment analysis of the effector gene promoters (500 bp) was conducted by the online tool STREME (Bailey, 2021). Heatmaps were generated with the online tool MORPHEUS (https://software.broadinstitute.org/morpheus).

4.5.4 Protein extraction and pull-down of *in vitro* induction samples

To test the production of the Hdp2-HA protein in rUSH_Umhdp2^{OE} and rUSH_Srhdp2^{OE}, the *in vitro* induction described by (Kretschmer *et al*., 2022) was used. Therefore, a 3 ml YEPSlight overnight culture was inoculated and incubated at 28°C and 200 rpm. On the next day, the OD_{600} of the fungal cultures was set to 0.3 in 5 ml minimal medium and minimal medium supplemented with glucose and malate (see 6.8.4) for both mating partners. After three washing steps, the pellet was resolved minimal medium with glucose and malate and incubated for 72 h at 28°C and 200 rpm. After 72 h, the culture was pelleted, and the pellet was then washed twice with sterile $H2O_{deoin}$. and used for protein extraction. Using extraction buffer (see 6.8.1) pellets were resuspended and incubated on ice for 30 min, centrifuged twice at 16,000 g, 4 °C for 30 min. 10 µl of anti-HA magnetic beads (Pierce) were added into each supernatant, and incubated for 1 h at 4 °C with end-to-end rotation. Subsequently, the beads were washed three times with extraction buffer and used for SDS-PAGE (see 6.8.2) followed by western blot (see 6.8.3) using an anti-HA antibody.

4.6 References

Bai, L., Zhang, G., Zhou, Y., Zhang, Z., Wang, W., Du, Y., Wu, Z., & Song, C.-P. (2009). Plasma membrane-associated proline-rich extensin-like receptor kinase 4, a novel regulator of Ca2+ signaling, is required for abscisci acid responses in *Arabidopsis thaliana*. *The Plant Journal*, *60*, 314–327.

Bailey, T. L. (2021). STREME: accurate and versatile sequence motif discovery. *Bioinformatics*, *37*(18), 2834–2840. https://doi.org/10.1093/bioinformatics/btab203

Bakkeren, G., Kämper, J., & Schirawski, J. (2008). Sex in smut fungi: Structure, function and evolution of mating-type complexes. *Fungal Genetics and Biology*, *45*(SUPPL. 1). https://doi.org/10.1016/j.fgb.2008.04.005

Banuett, F., & Herskowitz, I. (1989). Different *a* alleles of *Ustilago maydis* are necessary for maintenance of filamentous growth but not for meiosis. *Proceedings of the National Academy of Sciences*, *86*(15), 5878–5882. https://doi.org/10.1073/pnas.86.15.5878

Begerow, D., Göker, M., Lutz, M., & Stoll, M. (2004). On the evolution of smut fungi on their hosts. *Frontiers in basidiomycote mycology*, 81-98.

Beuchat, J., Scacchi, E., Tarkowska, D., Ragni, L., Strnad, M., & Hardtke, C. S. (2010). BRX promotes Arabidopsis shoot growth. *New Phytologist*, *188*(1), 23–29. https://doi.org/10.1111/j.1469-8137.2010.03387.x

Borassi, C., Sede, A. R., Mecchia, M. A., Salgado Salter, J. D., Marzol, E., Muschietti, J. P., & Estevez, J. M. (2016). An update on cell surface proteins containing extensin-motifs. *Journal of Experimental Botany*, *67*(2), 477–487. https://doi.org/10.1093/jxb/erv455

Brefort, T., Tanaka, S., Neidig, N., Doehlemann, G., Vincon, V., & Kahmann, R. (2014). Characterization of the Largest Effector Gene Cluster of Ustilago maydis. *PLoS Pathogens*, *10*(7). https://doi.org/10.1371/journal.ppat.1003866

Bruce, S. A., Saville, B. J., & Emery, R. J. N. (2011). *Ustilago maydis* Produces Cytokinins and Abscisic Acid for Potential Regulation of Tumor Formation in Maize. *Journal of Plant Growth Regulation*, *30*(1), 51–63. https://doi.org/10.1007/s00344-010-9166-8

Edgar, R. C. (2004). MUSCLE: Multiple sequence alignment with high accuracy and high throughput. *Nucleic Acids Research*, *32*(5), 1792–1797. https://doi.org/10.1093/nar/gkh340

He, Q., McLellan, H., Boevink, P. C., & Birch, P. R. J. (2020). All Roads Lead to Susceptibility: The Many Modes of Action of Fungal and Oomycete Intracellular Effectors. *Plant Communications*, *1*(4), 100050. https://doi.org/10.1016/j.xplc.2020.100050

Heimel, K., Scherer, M., Vranes, M., Wahl, R., Pothiratana, C., Schuler, D., Vincon, V., Finkernagel, F., Flor-Parra, I., & Kämper, J. (2010). The transcription factor rbf1 is the master regulator for b-mating type controlled pathogenic development in *Ustilago maydis*. *PLoS Pathogens*, *6*(8), 17–18. https://doi.org/10.1371/journal.ppat.1001035

Hufford, M. B., Seetharam, A. S., Woodhouse, M. R., Chougule, K. M., Ou, S., Liu, J., Ricci, W. A., Guo, T., Olson, A., Qiu, Y., Coletta, R. Della, Tittes, S., Hudson, A. I., Marand, A. P., Wei, S., Lu, Z., Wang, B., Tello-Ruiz, M. K., Piri, R. D., … Dawe, R. K. (2021). De novo assembly, annotation, and comparative analysis of 26 diverse maize genomes. *Science*, *373*(6555), 655–662. https://doi.org/10.1126/science.abg5289

Humphrey, T. V., Haasen, K. E., Aldea-Brydges, M. G., Sun, H., Zayed, Y., Indriolo, E., & Goring, D. R. (2015). PERK-KIPK-KCBP signalling negatively regulates root growth in *Arabidopsis thaliana*. *Journal of Experimental Botany*, *66*(1), 71–83. https://doi.org/10.1093/jxb/eru390

Invernizzi, M., Hanemian, M., Keller, J., Libourel, C., & Roby, D. (2022). PERKing up our understanding of the proline-rich extensin-like receptor kinases, a forgotten plant receptor kinase family. *New Phytologist*, *235*, 875–884.

John, E., Singh, K. B., Oliver, R. P., & Tan, K. C. (2022). Transcription factor lineages in plant-pathogenic fungi, connecting diversity with fungal virulence. *Fungal Genetics and Biology*, *161*. https://doi.org/10.1016/j.fgb.2022.103712

Jurca, M. (2021). Die Charakterisierung des Transkriptionsfaktors Hdp2 und dessen Rolle in der biotrophen Phase von *Ustilago maydis*. *PhD Thesis*.

Kämper, J., Kahmann, R., Bölker, M., Ma, L. J., Brefort, T., Saville, B. J., Banuett, F., Kronstad, J. W., Gold, S. E., Müller, O., Perlin, M. H., Wösten, H. A. B., De Vries, R., Ruiz-Herrera, J., Reynaga-Peña, C. G., Snetselaar, K., McCann, M., Pérez-Martín, J., Feldbrügge, M., … Birren, B. W. (2006). Insights from the genome of the biotrophic fungal plant pathogen *Ustilago maydis*. *Nature*, *444*(7115), 97–101. https://doi.org/10.1038/nature05248

Kretschmer, M., Damoo, D., Sun, S., Lee, C. W. J., Croll, D., Brumer, H., & Kronstad, J. (2022). Organic acids and glucose prime late-stage fungal biotrophy in maize. *Science*, *376*(6598), 1187–1191. https://doi.org/10.1126/science.abo2401

Kumar, S., Stecher, G., Li, M., Knyaz, C., & Tamura, K. (2018). MEGA X: Molecular evolutionary genetics analysis across computing platforms. *Molecular Biology and Evolution*, *35*(6), 1547–1549. https://doi.org/10.1093/molbev/msy096

Lanver, D., Berndt, P., Tollot, M., Naik, V., Vranes, M., Warmann, T., Münch, K., Rössel, N., & Kahmann, R. (2014). Plant Surface Cues Prime *Ustilago maydis* for Biotrophic Development. *PLoS Pathogens*, *10*(7). https://doi.org/10.1371/journal.ppat.1004272

Lanver, D., Müller, A. N., Happel, P., Schweizer, G., Haas, F. B., Franitza, M., Pellegrin, C., Reissmann, S., Altmüller, J., Rensing, S. A., & Kahmann, R. (2018). The biotrophic development of *Ustilago maydis* studied by RNA-seq analysis. *Plant Cell*, *30*(2), 300–323. https://doi.org/10.1105/tpc.17.00764

Lanver, D., Tollot, M., Schweizer, G., Lo Presti, L., Reissmann, S., Ma, L. S., Schuster, M., Tanaka, S., Liang, L., Ludwig, N., & Kahmann, R. (2017). *Ustilago maydis* effectors and their impact on virulence. *Nature Reviews Microbiology*, *15*(7), 409–421. https://doi.org/10.1038/nrmicro.2017.33

Liu, W., Xie, S., Zhao, X., Chen, X., Zheng, W., Lu, G., Xu, J. R., & Wang, Z. (2010). A homeobox gene is essential for conidiogenesis of the rice blast fungus *Magnaporthe oryzae*. *Molecular Plant-Microbe Interactions*, *23*(4), 366–375. https://doi.org/10.1094/MPMI-23-4-0366

Lorbiecke, R., Steffens, M., Tomm, J. M., Scholten, S., Von Wiegen, P., Kranz, E., Wienand, U., & Sauter, M. (2005). Phytosulphokine gene regulation during maize (*Zea mays* L.) reproduction. *Journal of Experimental Botany*, *56*(417), 1805–1819. https://doi.org/10.1093/jxb/eri169

Majewska-Sawka, A., & Nothnagel, E. A. (2000). Update on Extracellular Matrix The Multiple Roles of Arabinogalactan Proteins in Plant Development. *Society*, *122*(January), 3–9.

Mills, L. J., & Van Staden, J. (1978). Extraction of cytokinins from maize, smut tumors of maize and *Ustilago maydis* cultures. *Physiological Plant Pathology*, *13*(1), 73–80. https://doi.org/10.1016/0048-4059(78)90076-0

Mok, M.C. (1994) Cytokinin and Plant Development—An Overview. In: Mok, D.W.S. and Mokeds, M.C., Eds., Cytokinin: Chemistry, Activity and Function, CRC Press, Boca Raton, 155-166.

Mouchel, C. F., Briggs, G. C., & Hardtke, C. S. (2004). Natural genetic variation in Arabidopsis identifies BREVIS RADIX, a novel regulator of cell proliferation and elongation in the root. *Genes and Development*, *18*(6), 700–714. https://doi.org/10.1101/gad.1187704

Nigg, E. A. (1995). Cyclin-dependent protein kinases Key regulators of the eukaryotic cell cycle. *BioEssays*, *17*(6), 471–480.

Norbury, C., & Nurse, P. (1992). Animal cell cycles and their control. *Annual Review of Biochemistry*, *61*, 441–470. https://doi.org/10.1146/annurev.biochem.61.1.441

Ohm, R. A., de Jong, J. F., de Bekker, C., Wösten, H. A. B., & Lugones, L. G. (2011). Transcription factor genes of *Schizophyllum commune* involved in regulation of mushroom formation. *Molecular Microbiology*, *81*(6), 1433–1445. https://doi.org/10.1111/j.1365-2958.2011.07776.x

Quinlan, A. R., & Hall, I. M. (2010). BEDTools: a flexible suite of utilities for comparing genomic features. Bioinformatics (Oxford, England), 26(6), 841–842. https://doi.org/10.1093/bioinformatics/btq033

Reichlmeir, M., Elias, L., & Schulte, D. (2021). Posttranslational Modifications in Conserved Transcription Factors: A Survey of the TALE-Homeodomain Superclass in Human and Mouse. *Frontiers in Cell and Developmental Biology*, *9*(March), 1–10. https://doi.org/10.3389/fcell.2021.648765

Renaudin, J. P., Doonan, J. H., Freeman, D., Hashimoto, J., Hirt, H., Inzé, D., Jacobs, T., Kouchi, H., Rouzé, P., Sauter, M., Savouré, A., Sorrell, D. A., Sundaresan, V., & Murray, J. A. H. (1996). Plant cyclins: A unified nomenclature for plant A-, B- and D-type cyclins based on sequence organization. *Plant Molecular Biology*, *32*(6), 1003–1018. https://doi.org/10.1007/BF00041384

Schamber, A., Leroch, M., Diwo, J., Mendgen, K., & Hahn, M. (2010). The role of mitogen-activated protein MAP kinase signalling components and. *Molecular Plant Pathology*, *11*(1), 105–119.

Schirawski, J., Mannhaupt, G., Münch, K., Brefort, T., Schipper, K., Doehlemann, G., Di Stasio, M., Rössel, N., Mendoza-Mendoza, A., Pester, D., Müller, O., Winterberg, B., Meyer, E., Ghareeb, H., Wollenberg, T., Münsterkötter, M., Wong, P., Walter, M., Stukenbrock, E., … Kahmann, R. (2010). Pathogenicity determinants in smut fungi revealed by genome comparison. *Science*, *330*(6010), 1546–1548. https://doi.org/10.1126/science.1195330

Schmülling, T., Werner, T., Riefler, M., Krupková, E., & Bartrina Y Manns, I. (2003). Structure and function of cytokinin oxidase/dehydrogenase genes of maize, rice, Arabidopsis and other species. *Journal of Plant Research*, *116*(3), 241–252. https://doi.org/10.1007/s10265-003-0096-4

Schulz, B., Banuett, F., Dahl, M., Schlesinger, R., Schäfer, W., Martin, T., Herkowitz, I., Kahmann, R. (1990). Erratum: The b alleles of *U. maydis*, whose combinations program pathogenic development, code for polypeptides containing a homeodomain-related motif (Cell 60, (295-306), 1990). *Cell*, *60*(3), 521. https://doi.org/10.1016/0092-8674(90)90744-y

Schuster, M., Schweizer, G., Reissmann, S., & Kahmann, R. (2016). Genome editing in *Ustilago maydis* using the CRISPR-Cas system. *Fungal Genetics and Biology*, *89*, 3–9. https://doi.org/10.1016/j.fgb.2015.09.001

Shimotohno, A., Aki, S. S., Takahashi, N., & Umeda, M. (2021). Regulation of the Plant Cell Cycle in Response to Hormones and the Environment. *Annual Review of Plant Biology*, *72*, 273–296. https://doi.org/10.1146/annurev-arplant-080720-103739

Storfie, E. R. M., & Saville, B. J. (2021). Fungal Pathogen Emergence : Investigations with an *Ustilago maydis* × *Sporisorium reilianum* Hybrid. *Journal of Fungi*, *7*(672).

Tanaka, S., Schweizer, G., Rössel, N., Fukada, F., Thines, M., & Kahmann, R. (2019). Neofunctionalization of the secreted Tin2 effector in the fungal pathogen *Ustilago maydis*. *Nature Microbiology*, *4*(2), 251–257. https://doi.org/10.1038/s41564-018-0304-6

Toruño, T. Y., Stergiopoulos, I., & Coaker, G. (2016). Plant-Pathogen Effectors: Cellular Probes Interfering with Plant Defenses in Spatial and Temporal Manners. *Annual Review of Phytopathology*, *54*, 419–441. https://doi.org/10.1146/annurev-phyto-080615-100204

Ulrich, J. (2020). Die kombinatorische Regulation eines Transkriptions- Netzwerks reguliert die Pflanzeninfektion von *Ustilago maydis*. *PhD Thesis*.

Van Der Does, H. C., & Rep, M. (2017). Adaptation to the Host Environment by Plant-Pathogenic Fungi. *Annual Review of Phytopathology*, *55*, 427–450. https://doi.org/10.1146/annurev-phyto-080516-035551

Vonk, P. J., & Ohm, R. A. (2018). The role of homeodomain transcription factors in fungal development. *Fungal Biology Reviews*, *32*(4), 219–230. https://doi.org/10.1016/j.fbr.2018.04.002

Werner, J., Zuo, W., & Doehlemann, G. (2023). CRISPR/Cas9 Ribonucleoprotein-Mediated Mutagenesis in *Sporisorium reilianum*. Bio-protocol 14(8): e4978. https://doi.org/10.21769/BioProtoc.4978.

Yang, H., Matsubayashi, Y., Hanai, H., & Sakagami, Y. (2000). Phytosulfokine-α, a peptide growth factor found in higher plants: Its structure, functions, precursor and receptors. *Plant and Cell Physiology*, *41*(7), 825–830. https://doi.org/10.1093/pcp/pcd009

Yu, J., Yu, M., Song, T., Cao, H., Pan, X., Yong, M., Qi, Z., Du, Y., Zhang, R., Yin, X., & Liu, Y. (2019). A homeobox transcription factor UvHOX2 regulates chlamydospore formation, conidiogenesis, and pathogenicity in *Ustilaginoidea virens*. *Frontiers in Microbiology*, *10*(JUN), 1–15. https://doi.org/10.3389/fmicb.2019.01071

Zuo, W., Depotter, J. R., & Doehlemann, G. (2020). Cas9HF1 enhanced specificity in *Ustilago maydis. Fungal Biology*, *124*(3–4), 228–234. https://doi.org/10.1016/j.funbio.2020.02.006

Zuo, W., Depotter, J. R. L., Gupta, D. K., Thines, M., & Doehlemann, G. (2021). Cross-species analysis between the maize smut fungi *Ustilago maydis* and *Sporisorium reilianum* highlights the role of transcriptional change of effector orthologs for virulence and disease. *New Phytologist*. https://doi.org/10.1111/nph.17625

Zuo, W., Depotter, J. R. L., Stolze, S. C., Nakagami, H., & Doehlemann, G. (2023). A transcriptional activator effector of *Ustilago maydis* regulates hyperplasia in maize during pathogen-induced tumor formation. *Nat Commun,* 14, 6722 (2023). https://doi.org/10.1038/s41467-023-42522-w

Chapter 5: General discussion and future perspectives

5.1 Interspecific hybridization

In the evolution of plant pathogens, hybridization plays a critical role in the emergence and adaptation of new pathogens (Brasier, 2000; Brasier, 2001). Generally, hybridization combines the genetic material of evolutionary diverged species in the same cell, leading to novel interactions of the genes and genomes (Samarasinghe *et al*., 2020). However, the extent to which each nucleus contributes to the phenotype in a hybrid and the regulatory processes at the nuclear level remain poorly understood. The varying levels of mRNA from each nucleus may also result in varying functional outcomes (Gehrmann *et al*., 2018). The basidiomycetes *U. maydis* and *S. reilianum* are closely related and infect the same host, *Z. mays*. This provides the perfect basis for interspecific hybridization. Despite a co-occurrence of both species in the same field, the two pathogens were not observed on the same plant (personal communication: Weiliang Zuo). To our knowledge, no natural hybrids of *U. maydis* and *S. reilianum* species have been identified. This may also be explained by the instability of the hybridization event between *U. maydis* 521 and SRZ2, in which the resulting hybrid was unable to proliferate *in planta* (Storfie & Saville, 2021). This is further supported by the absence of fungal proliferation of FB1+SRZ2, as well as by the RNA-seq data of this study, in which the expression of effector genes in rUSH to FB1+SRZ2 was compared. The RNA-seq analysis revealed numerous effector and non-effector genes upregulated in rUSH, thus reflecting the general differences in fitness levels.

Due to differences between the parental species and their low survival rate, interspecific hybrids are uncommon in nature and make up less than 0.1% of a typical population (Mallet, 2005, 2007). The relationship between parental genetic divergence and phenotypic variation in hybrids is still poorly understood. A recent study examined the mating of fungal *Cryptococcus* strains with up to 15% sequence divergence. The resulting phenotypes were either similar to one of the parents, intermediate, or distinct from the parental species (You & Xu, 2021). Due to genomic incompatibilities of separately evolved alleles, hybrids may suffer from negative fitness effects (Stukenbrock *et al*., 2016). However, the rare findings of natural hybrids suggest that fitness deficiencies can be compensated under certain conditions (Greig *et al*., 2002). In contrast to the parental species, interspecific hybrids can also exhibit increased virulence and outcompete the parental species, comprising broader host ranges and possessing the ability to inhabit new niches (Gabaldón, 2020; Schardl & Craven, 2003) as it was demonstrated for several natural and laboratory-generated strains of *Phytophtera* species (Kroon *et al*., 2012).

With the mating type exchange, rUSH is able to proliferate *in planta* and induce *S. reilianum*-like symptoms in the inflorescences, without the formation of teliospores. Since the different timing of karyogamy might also influence the hybridization event (Steensels *et al*., 2021), *nlt1* was overexpressed in rUSH to induce a nuclear fusion. However, no change in rUSH phenotype was observed upon *nlt1* OE, suggesting that the different timing of karyogamy between *U. maydis* and *S. reilianum* as well as a possible incompatibility between Nlt1 from the two species, could be the causal factors. Whether an exchange of the "early" *nlt1* of *U. maydis* in *S. reilianum* SRZ2 can achieve an early-induced nuclear fusion in rUSH, and therefore lead to tumor formation, remains to be elucidated.

5.2 Gene regulation in fungal hybrids

In interspecific hybridization, two genomes are combined in a single cell, resulting in the intertwining of diverse cellular processes, including gene regulation. Generally, gene regulation controls the timing, location, and amount of a gene product in response to environmental changes. The regulation of gene expression involves DNA sequences, regulatory proteins, RNA molecules, and epigenetic modifications (Mack & Nachman, 2017). In this study, distinct gene regulation patterns of effector genes could be identified, comprising *cis*, *trans,* and hybrid-specific expression, which is consistent with previous studies (Combes *et al.*, 2015; Tirosh *et al*., 2009). Commonly, hybridization leads to the combination of two genomes and regulatory networks in the same cellular context (Combes *et al*., 2015; Landry *et al*., 2007). Based on the similarities of the two species, a compatibility of the TFs and TF binding sites between the two species is likely (Combes *et al.*, 2015). Nevertheless, the combination of two genomes upon hybridization can also result in an incompatible network of regulatory elements (Landry *et al*., 2007; Mack & Nachman, 2017; Sriswasdi *et al*., 2019). In particular, the extent of divergence between the *cis*- and *trans*-effects of two species has a significant influence on the gene expression in hybrids (Combes *et al*., 2015). In this study, approximately half of the effector genes in rUSH were found to exhibit *cis*- or *trans*-regulation, while the other half exhibited hybrid-specific expression, likely due to *cis*- and *trans*- interactions. However, the underlying mechanisms of the combination and the compatibility of the two parental regulatory networks in rUSH remain to be investigated.

In natural hybrids of the Basidiomycota *Trichosporon*, the correlation of gene expression within species was found to be higher than the correlation between different species (Sriswasdi *et al*., 2019). The question of whether this is due to a rapid evolution of the transcriptional network or to a slow divergence of homeolog expression in the hybrid was further investigated by analyzing the presence of TF genes and their binding sites. The analysis demonstrated the presence of shared TF binding sites between

homeologs in the two hybrids, suggesting that these sites contribute to the concerted transcriptional activity observed in the hybrids (Sriswasdi *et al*., 2019).

Moreover, the *S. reilianum*-like phenotype observed in rUSH could be attributed to the dominant expression of *S. reilianum* genes, which may be the result of a nuclear imbalance in rUSH. In plants, the level of gene expression can range from OE to intermediate expression, and to complete silencing of different alleles (Botet & Keurentjes, 2020). Nevertheless, the impact of hybridization events on the transcriptome and allele-specific imbalance is much more pronounced in animals and plants compared to fungal studies, where the effects are more moderate (Hovhannisyan *et al*., 2020). These differences in the nuclei can lead to effects on regulatory mechanisms of transcription, such as TF binding efficiencies, transcription efficiency, differences in mRNA stability, epigenetic factors, and the phenotype (Gehrmann *et al*., 2018), which need to be further investigated in rUSH in the future. A study of the mushroom-forming fungus *Agaricus bisporus* examined a nucleus-specific expression of genes and concluded that the differential regulation occurs at the gene level and not on a specific locus, chromosome, or nuclear level. This study further revealed that the expression affects different functional groups of genes and that epigenetic factors play a crucial role in the regulation of the different expression (Gehrmann *et al*., 2018).

The influence of methylation on the gene expression level in rUSH was not tested in this study. In *U. maydis* very little is known regarding the chromatin modification of gene expression regulation during infection. However, DNA methylation may not play an important role in the regulation of gene expression in *U. maydis* due to the absence of any methyl transferase homolog (Elías-Villalobos *et al*., 2019). Notably, histone deacetylates have been reported to play a crucial role in the virulence of plant pathogenic fungi. In *U. maydis*, two histone deacetylates, Hos2 and Clr3, important for the dimorphic switch and the pathogenicity of *U. maydis* have been identified (Elías-Villalobos *et al*., 2015). In the RNA-seq data of rUSH, the expression levels of *hos2* and *clr3* did not change in rUSH compared to the wild type. Nevertheless, the influence of epigenetic modification on gene regulation in rUSH needs to be assessed in the future.

In addition to epigenetic modifications, mitochondrial ncRNAs or transposable elements influence gene expression in hybrids (Runemark *et al*., 2024). However, in *U. maydis*, very few repetitive sequences were observed in the genome analysis (Kämper *et al*., 2006). The interaction between the nuclear genome and the mitochondrial genome is important, since in Basidiomycetes only one of the parental mitotypes is inherited (uniparental), influencing the hybrids' characteristics (Steensels *et al*., 2021). Since the mitotype inheritance was shown to be mediated by the genes *rga2* and *lga2* in the *a2* mating type locus of smut fungi (Fedler *et al*., 2009), an influence of *S. reilianum* mitochondrial DNA on the observed gene expression in rUSH is likely. An effect of mito-nuclear interactions on hybrid fitness was

shown in yeast hybrids (Olson & Stenlid, 2001; Zeyl *et al*., 2005). This is in line with the gene expression data of the fungal hybrid *Heterobasidion irregulare* X *Heterobasidion annosum*, which revealed an interplay of nuclear genes with the mitotype, accompanied by a reduction in the saprobic growth of the pathogen (Giordano *et al*., 2018). Nevertheless, the impact of the mitotype of the inherited mitochondria on gene expression was not further explored in rUSH in this study, and its implications remain to be elucidated in future research.

5.3 Hdp2 is a key transcriptional regulator for tumorigenesis of *U. maydis*

In general, HD TFs such as Hdp2 bind *in vitro* to short AT-rich sequences. However, the accessibility of the binding of HD TFs *in vivo* is dependent on several additional elements, including the chromatin structure and landscape, as well as the shape of the DNA double helix (Bobola & Merabet, 2017). HD TFs in filamentous fungi have been first identified in the mating type loci, important for sexual development, but were also found to play a crucial role during the fungal development, i.e. in the development of fruiting bodies in Ascomycota and Basidiomycota (Vonk & Ohm, 2018). In the ascomycete *Botrytis cinerea*, a HD TF encoded by the BcHOX8 was shown to be crucial for filamentous growth and conidiation (Schamber *et al*., 2010). In *M. oryzae*, several HD TFs reflected the importance in hyphal growth, conidiation, and appressoria formation (Liu *et al*., 2010). Similarly, for the basidiomycete *S. commune* two out of eleven identified HD proteins were functionally characterized and involved in the development of the fruiting body (Ohm *et al*., 2011). Furthermore, in *Ustilaginoidea virens*, responsible for false smut in rice, the importance of an HD TF with homology to *M. oryzae* in clamydospore formation was elucidated (Yu *et al*., 2019). Nevertheless, the function of the majority of HD proteins in filamentous fungi, as well as the impact of putatively post-translational modifications of HD TFs on fungal development, remain to be elucidated (Vonk & Ohm, 2018).

In rUSH, *Umhdp2* is downregulated compared to the *U. maydis* wild type. This suggests that the low level of *Umhdp2* expression and the putative compensation by *Srhdp2* expression in rUSH were sufficient to activate effector genes that are important for “basic” virulence. However, for pathogenicity-related effectors, the required level of *Umhdp2* for the activation of expression may need to be higher. Furthermore, the OE of *hdp2* in rUSH may contribute to a higher fitness level and a higher biomass, leading to the activation of tumorigenic effectors contributing to tumor induction.

In rUSH_Umhdp2^{OE}, tumor formation in all infected maize seedlings was observed at 3 dpi. This is in contrast to the hybrid of *U. maydis* 521 and *S. reilianum* SRZ2, where the formation of small tumors was observed only in rare events after 14 dpi upon infection with OE strains of *Umhdp2* (Storfie & Saville, 2021). One difference between rUSH and the previously mentioned hybrid is the use of different promoters for the OE. In this study, *pro^{Umcmu1}* was used for the OE, while in the publication

of Storfie & Saville (2021), pro^{OTEF} was used. Nevertheless, the observed differences in phenotype and tumor abundance may be partially attributed to the use of only the *S. reilianum* mating type system in rUSH, or the use of different haploid *U. maydis* strains. The mating type system in rUSH may result in a higher degree of compatibility between downstream responses during a successful hybridization event and the formation of small tumors upon *hdp2* OE in all infected plants.

5.4 Pathogen-induced tumor development in plants

Tumors were described to appear on all plant organs (roots, leaves, stems, and floral organs) (Ahuja, 1998). Tumor cells in plants can be either induced by pathogens or in rare cases, spontaneously occur in certain plant hybrids or mutants (Dodueva *et al*., 2020). The presence of hypertrophy and hyperplasia as well as high vascularization in tumor cells is similar between animals and plants (Dodueva *et al*., 2020; Ullrich & Aloni, 2000). However, tumor development between plants and animals evolved independently (Meyerowitz, 2002). Consistent with previous findings, the tumor development induced by *U. maydis* is accompanied by plant cell enlargement and increased cell division. The onset of tumor formation of rUSH_Umhdp2^{OE} at 3 dpi is early compared to the wild type of *U. maydis*, where the onset of tumor formation has been reported to begin around 4 dpi (Doehlemann *et al*., 2008; Lanver *et al*., 2018). This may be attributed to the high expression of the promoter pro^{Umcmu1} during the biotrophic development.

When plant cells differentiate into tumor cells, changes in the phytohormones and deregulation of the cell cycle were observed (Dodueva *et al*., 2020). Plants use complex signaling cascades of phytohormones as a defense mechanism against invaders (Schenk *et al*., 2000). JA, SA, and ET are known to be important for the defense of plants. However, abrisic acid (ABA), auxins (indole-3-acetic acid; IAA), cytokinins (CKs), brassinosteroids (BRs), gibberellins (GA), and stringolactones, are known to be involved in plant growth and development, beyond their roles in defense responses. Pathogens have developed various strategies to exploit the host's hormone signaling for their benefit, which includes the promotion of colonization and disease development (Kazan & Lyons, 2014). The modulation of phytohormone signaling is of great importance in the context of tumor formation by certain pathogens. For instance, in *U. maydis*, several effector genes target TOPLESS to interfere with the hormonal signaling in maize (Bindics *et al*., 2022; Darino *et al*., 2021; Navarrete *et al*., 2022). Pathogens can also synthesize phytohormones to modulate plant responses and enhance virulence (Lopez *et al*., 2008). In rUSH_Umhdp2^{OE}, only small tumors were observed. These tumors did not develop into larger tumors that are usually observed upon *U. maydis* infection on maize seedlings. Therefore, it would be of interest to test on a cellular level which tumor cells are present in rUSH_Umhdp2^{OE} and at which stage of infection rUSH stops the further development of a tumor. It has

been demonstrated that gall- or tumor-inducing phytobacteria, secrete IAAs and CKs, which are reported to play a role in the initiation of gall formation and modulation of plant development (Kazan & Lyons, 2014), e. g. *Rhodococcus fascians*, requires CK for its development of the leafy gall disease (Stes *et al*., 2011). In the case of *U. maydis*, it has been demonstrated that fungal-derived auxin is not a crucial factor in the formation of tumors (Kämper *et al*., 2006; Reineke *et al*., 2008). However, testing of various maize mutants suggested that tumor formation in *U. maydis* is influenced by other phytohormones such as gibberellins (Walbot & Skibbe, 2010). To investigate the contribution of phytohormones to tumor formation in rUSH_Umhdp2^{OE}, the level of the phytohormone CK could be measured and compared to its level in rUSH since CK-related genes were identified among the upregulated maize genes. Whether Hdp2 activates downstream genes involved in the modulation of phytohormones required for tumor enlargement remains to be elucidated. In particular, numerous auxin-, ET- and ABA/JA-related genes were identified to be upregulated in rUSH_Umhdp2^{OE} and rUSH_Srhdp2^{OE} compared to rUSH, rendering them interesting candidates for tumor enlargement. Moreover, *U. maydis* uses cell-type specific genes to induce hypertrophy tumor cells (Redkar *et al*., 2015a) or hyperplasia tumor cells (Zuo *et al*., 2023). Nevertheless, the fundamental process by which cell-type-specific genes are activated remains elusive (Doehlemann *et al*., 2008). Additionally, the observed differences in tumor formation between the wild type and rUSH_Umhdp2^{OE} may provide insights into the function of the downstream targets activated by Hdp2. While the role of Hdp2 in the pathogenicity of *U. maydis* has been previously reported (Heimel *et al*., 2010b; Lanver *et al*., 2014), the central and elemental role of Hdp2 in the regulation of genes crucial for tumorigenesis of *U. maydis*, was firstly described in this study.

5.5 Hdp2 modulates expression of maize genes putatively involved in leaf tumor development

The OE of the gene encoding for the TF Hdp2 in rUSH led to the induction of small tumors in maize leaves upon seedling infections. This indicates a modulation of maize genes involved in leaf developmental processes. An RNA-seq analysis of rUSH_Umhdp2^{OE} and rUSH_Srhdp2^{OE} in comparison to rUSH revealed the presence of upregulated maize genes that may be involved in *U. maydis*-induced leaf tumor formation. These genes are associated with functions related to cell growth, cell division, cell expansion, and cell enlargement.

Cyclins and CDKs were identified among the upregulated maize genes. These genes are known for their importance in the regulation of cell division (Renaudin *et al*., 1996). Deregulation of the cell cycle was reported as a common hallmark in human cancer research. Changes in CDK expression lead to uncontrolled proliferation as well as genomic instability (Malumbres & Barbacid, 2009).

Furthermore, recent studies in human cancer research indicated that several classes of CDKs are not crucial for the mammalian cell cycle and revealed the requirement of specific CDKs for specific cell types (Malumbres & Barbacid, 2009). It is not known whether the function of CDKs in *U. maydis*-induced tumorigenesis in maize is similar to that reported in human cancers. ZmGIF1 and ZmSHR1 were previously reported to be involved in cell division in maize (Zuo *et al*., 2023) and were identified in the RNA-seq in this study. ZmGIF1 binds to Unbranched3 and regulates the meristem size and branching in the tassel of maize (Li *et al*., 2022). This is consistent with findings in Arabidopsis, where an OE of *GIF1* resulted in a higher level of cell division (Lee *et al*., 2009). In maize, ZmSHR1 was described to play a role in the Kranz development in maize leaves, including bundle sheet and mesophyll cells (Slewinski *et al*., 2014). *At*SHR1 interacts with Scarecrow (SCR) and regulates the development of the endodermis in root and shoot (Helariutta *et al*., 2000; Nakajima *et al*., 2001; Vatén *et al*., 2011). OE of *AtSHR1* or *OsSHR1* in both, rice and Arabidopsis roots resulted in additional cortical cell layers, suggesting a conserved function of *SHR1* among land plants (Henry *et al*., 2017).

The identification of expansins and AGPs among the maize candidate genes suggests the manipulation of these genes by *U. maydis* during tumorigenesis. Expansins have been first described in cucumber hypocotyls for a pH-dependent plant cell wall-loosening (McQueen-Mason *et al*., 1992). It has been hypothesized that expansins are always involved in changes in cell growth and cell wall modification and are therefore putative targets for *U. maydis* effectors. The same applies to the cell wall glycoproteins AGPs that play a role in maintaining cell wall structure and signaling (Ma & Johnson, 2023). In conclusion, these maize genes are interesting candidates for manipulation by *U. maydis* for leaf development during tumorigenesis.

5.6 Future perspective of the project

In this study, the recombinant hybrid rUSH was used as a tool to shed light on the underlying mechanisms and molecular elements that contribute to the different disease development of *U. maydis* and *S. reilianum*. rUSH revealed an increase of fungal biomass during *in planta* proliferation, a *S. reilianum*-like phenotype, but no teliospores to complete the life cycle. Thus, future work aims to elucidate unknown elements contributing to the postmating incompatibilities in rUSH and elements that influence the completion of the life cycle, i.e. epigenetic factors or mito-nuclear interactions.

The RNA-seq analysis of rUSH revealed 218 differentially expressed one-to-one orthologues with distinct regulation patterns including *cis*-, *trans*- and hybrid-specific regulation. Following these patterns in the hybrid with association of the *S. reilianum*-like phenotype, I was able to identify novel virulence factors of *U. maydis* and *S. reilianum* that contribute to the different disease progressions of the two species. Within the hybrid-specific reverse expression in rUSH, many effector genes associated with

the virulence cluster 19A could be identified, which include the two novel virulence factors *UMAG_05312* and *UMAG_10553*. The findings in this study are consistent with previous work, which showed that cluster 19A is essential for *U. maydis* virulence (Brefort *et al*., 2014; Kämper *et al*., 2006). The differences in disease development of *U. maydis* and *S. reilianum*, as well as the identification of different regulation patterns of effector gene expression, the neofunctionalization of the effectors Tin2 and Sts2 (Tanaka *et al*., 2019; Zuo *et al.*, 2023), plus the finding of novel virulence factors, led to the hypothesis that tumor formation is encoded in the virulence cluster 19A of *U. maydis*, which has undergone diversification from *S. reilianum* cluster 19A during speciation.

Furthermore, the gene encoding for the TF UmHdp2 was downregulated in rUSH, which led to the identification of Hdp2 as a key TF for the onset of tumor induction by *U. maydis*. Hdp2 regulates 13 of 24 cluster 19A genes directly and indirectly. This suggests that additional factors are situated between Hdp2 and are participating in the regulation of tumorigenic effector genes (Figure 5.1). Thus, the upregulated effector genes without binding motifs for Hdp2 can be further screened in a motif enrichment analysis to identify a putative binding motif for a yet undescribed TF in future studies. Consequently, identified *U. maydis* non-effector genes identified in rUSH_Umhdp2^{OE} with a predicted DNA-binding motif may be investigated in the future for their potential contribution to the regulation of effector genes crucial for tumor formation. The induction of small tumors in maize seedlings by rUSH_Umhdp2^{OE} requires further investigation at the cellular level by transverse sectioning using paraplast-embedded leaf-tumor samples for microscopy (Matei *et al*., 2018). A comparison of the tumor formation in the wild type of *U. maydis* with rUSH_Umhdp2^{OE} may provide insights into the tumor cell type. It might also elucidate the regulation of cell-type specific effectors as well as the time point at which further tumor development in rUSH is blocked. Additional factors crucial for the development of a normal tumor after the onset of tumor induction by UmHdp2 remain to be elusive. An OE of *ros1* could be generated in the rUSH_Umhdp2^{OE} background, to also cover the regulation of the late effector genes. This may be necessary for the further development of the small “non-developing” tumors observed in rUSH_Umhdp2^{OE}.

Taken together, the utilization of rUSH enabled us to identify the two major forces in the induction of tumorigenesis of *U. maydis*: the effector genes encoded in cluster 19A and the TF Hdp2. With this knowledge and the completion of the replacement of *S. reilianum* cluster 19A with *U. maydis* cluster 19A, we will shed light on the different disease progressions of *U. maydis* and *S. reilianum* on maize, and putatively generate a tumor-inducing *S. reilianum* strain in the future.

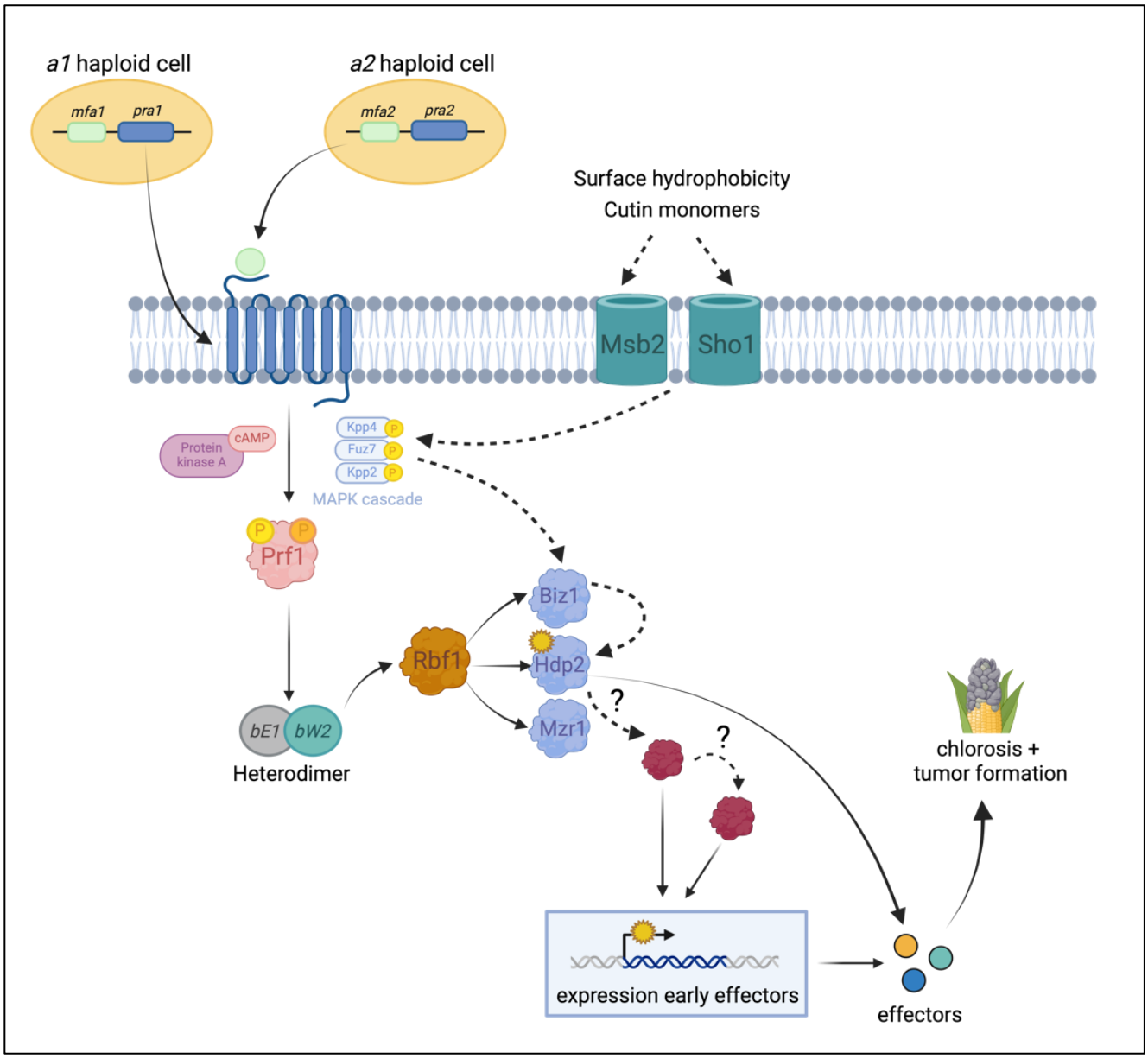

Figure 5.1: Working model of the tumor induction by Hdp2 in rUSH. Upon recognition of the pheromone (encoded by *mfa*) by the receptor (encoded by *pra*), two signaling cascades are activated leading to the phosphorylation of the transcription factor Prf1. P: Phosphorylation. Prf1 activates the expression of the genes encoding for the heterodimeric TFs bE1 and bW2 in the *b* locus. bE1/bW2 heterodimer activates the transcription of the major regulator Rbf1, which in turn activates the genes encoding for Biz1, Hdp2 and Mzr1, regulating the transcription of early effector genes. The cell surface proteins Msb2 and Sho1 perceive external stimuli that lead to the activation of the MAPK cascade. OE (yellow sun) of *hdp2* leads to the induction of effector genes contributing to chlorosis and tumor formation in rUSH. Genes downstream of Hdp2 can be either directly or indirectly regulated by Hdp2. The indirect regulation of effector genes by Hdp2 is still poorly understood, but it is hypothesized to be controlled by an additional TF acting downstream of Hdp2.

Chapter 6: Appendix - General Material and Methods

6.1 Materials and source of supply

6.1.1 Chemicals

All chemicals used in this study were acquired from Difco (Augsburg, Germany), GE Healthcare Life Science (Freiburg, Germany), Invitrogen (Carlsbad, USA), Merck (Darmstadt, Germany), Roche (Mannheim, Germany), Roth (Karlsruhe, Germany), and Sigma-Aldrich (St. Louis, USA) unless stated otherwise.

6.1.2 Buffers and solutions

Buffers, media, and solutions were prepared with $H_2O_{deoin.}$ unless stated otherwise, and autoclaved for at least 20 min at 121 °C. Heat-sensitive solutions, i. e. containing high sugars, were filter-sterilized (0.2 µm pore size, GE Health Care Life Science, Freiburg, Germany). The composition of all buffers, media, and solutions are indicated in the respective methods.

6.1.3 Enzymes

Used enzymes in the experiments of this study are listed in Table 6.1.

Table 6.1: Enzymes used in this study.

Enzyme	Company	Usage
Restriction enzymes	New England Biolads (NEB) Ipswich, USA)	Restriction digests
Phusion® High Fidelity DNA Polymerase	NEB (Ipswich, USA)	Amplification of PCR products
KOD Hot Start Polymerase	Sigma-Aldrich, Merck	Amplification of PCR products
GoTaq® Green Master Mix	Promega GmbH (Madison, USA)	Amplification of PCR products
GoTaq® qPCR Master Mix	Promega GmbH (Madison, USA)	qRT-PCR
T4 DNA Polymerase	NEB (Ipswich, USA)	sgRNA synthesis
HiScribe® T7 High Yield RNA Synthesis Kit	NEB (Ipswich, USA)	sgRNA synthesis
NEBuilder® HiFi DNA Assembly Master Mix	NEB (Ipswich, USA)	Gibson assembly, cloning
Novozyme234	Novo Nordisk (Copenhagen, Denmark)	Degradation of fungal cell wall, protoplasting

6.1.4 Commercial kits

All commercial kits used in this study are listed in Table 6.2.

Table 6.2: Commercial kits used in this study.

Kit	Company	Usage
NucleoSpin® Plasmid Kit	Macherey-Nagel (Düren, Germany)	Extraction of plasmid DNA
NucleoSpin® gel and PCR Clean-up Kit	Macherey-Nagel (Düren, Germany)	PCR clean-up and gel-extraction of nucleic acids
MasterPure™ Complete DNA and RNA Purification Kit	Epicenter (Madison, USA)	Clean-up of genomic DNA for biomass quantification
TURBO DNA-free™ Kit	Ambion®/ Thermo Fisher Scientific (Waltham, USA)	Enzymatic degradation of DNA after RNA extraction; *in vitro* synthesis of sgRNA
RevertAid H Minus First Strand cDNA Synthesis Kit	Thermo Fisher Scientific, (Waltham, USA)	Synthesis of cDNA
RNA Clean and Concentrator™-25 Kit	Zymo Research (USA)	Clean-up of sgRNAs

6.2 Microorganisms, Plasmids and Oligonucleotides

6.2.1 *Escherichia coli* strain

For the amplification of plasmids and cloning of new constructs the *E. coli* K-12 strain Top10/DH10β [F- *mcrA Δ(mrr-hsd RMS-mcrBC) Φ80lacZΔM15 ΔlacX74 nupG recA1 araDΔ139 Δ(ara98leu)7697 galK16 galE15*(GalS) *rpsL*(Str^R) *endA1 λ*-] was used.

6.2.2 Generated plasmids

All generated plasmids are listed in Table 6.3. The following backbones were used for cloning of new constructs:

1. **p123** (Aichinger *et al*., 2003)

The plasmid backbone was used for cloning of complementation constructs containing cbx resistance and enabling integration into the *U. maydis ip locus* via homologous recombination. For this, the plasmids were linearized via SspI, BsrGI, or AgeI before the transformation of *U. maydis*.

2. **pAGM1311, MOCLO Toolkit, plasmid #1, Level -1**

Plasmid containing a MCS was used for the generation of KO and cds replacement constructs due to its size and the blue-white selection.

3. **pCas9HF1** (Zuo *et al*., 2020)

Self-replicating plasmid derived from pMS73 (Schuster *et al*., 2016) harboring a cbx resistance for transient selection. Cas9 was replaced by the high-fidelity variant Cas9HF1.

4. pNEB_SrCbx

Plasmid contains the cbx resistance cassette for *S. reilianum* and was used for overexpression in *S. reilianum* (Weiliang Zuo, AG Döhlemann).

Table 6.3: Plasmids generated in this study. KO: knock-out.

Backbone	Plasmid	Usage	Reference
pAGMBII1311	pAGMBII1311_SRZ1_Uma1_#3	rUSH – using *U. maydis* mating type system	This study
pAGMBII1311	pAGMBII1311_SRZ1_Umb1_#4	rUSH – using *U. maydis* mating type system	This study
pNEB_SrCbx	pNEB_SrCbx_GFP_Cl#1	Single integration of GFP for Establishment of RNP in *S. reilianum*	This study
pAGMBII1311	pAGM1311_SRZ2_psr10057_*UMAG 05302*_cds#6	Cds replacement of *tin2*	This study
pCas9HF1	pAGM1311_FB1_psr10057_*UMAG_ 05302*_prom#1	promoter replacement of *tin2*	This study
pNEB_SrCbx	pNEB_SrCbx_H1_GFP_Cl#1		This study
p123	p123_pactin_*rbf1*_2xHA #1	Overexpression of TF *rbf1*	This study
p123	p123_pactin_*hdp2*_2xHA #3	Overexpression of TF *hdp2*	This study
p123	p123_pACTIN_*nlt1*_2xHA_#3	Overexpression of TF *nlt1*	This study
p123	p123_pOTEF_*nlt1*_2xHA_#3	Overexpression of TF *nlt1*	This study
p123	p123_proCmu1_*nlt1*_2xHA #27	Overexpression of TF *nlt1*	This study
pCas9HF1	pCas9HF1_*UMAG_00533* #1	Frameshift mutant	This study
pCas9HF1	pCas9HF1_*UMAG_02462* #1		This study
pCas9HF1	pCas9HF1_*UMAG_04242* #1		This study
pCas9HF1	pAGM1311_ΔSR19A#1	KO of Cluster 19A in *S. reilianum*	Master thesis, Vanessa Volz
p123	p123_proCmu1_*fox1*_2xHA #1	Overexpression of TF *fox1*	This study
p123	p123_proCmu1_*rbf1*_2xHA #2	Overexpression of TF *rbf1*	This study
p123	p123_proCmu1_*hdp2*_2xHA #7	Overexpression of TF *UmHdp2*	This study
pAGM1311	pAGM1311_Δ*sr16075* #1	KO of sr16075 in *S. reilianum*	This study
pAGM1311	pAGM1311_UM19A_Compl1	Complementation1 of *U. maydis* Cluster 19A in *S. reilianum*	Master thesis, Vanessa Volz
pCas9HF1	pCas9HF1_*UMAG_06257*	Frameshift mutant	This study
pCas9HF1	pCas9HF1_*UMAG_10256*		This study
pCas9HF1	pCas9HF1_*UMAG_10626*		This study
pCas9HF1	pCas9HF1_*UMAG_05312*		This study
pCas9HF1	pCas9HF1_*UMAG_03749*		This study
pCas9HF1	pCas9HF1_*UMAG_03751*		This study
pCas9HF1	pCas9HF1_*UMAG_10553*		This study
pCas9HF1	pCas9HF1_*UMAG_05928*		This study
pCas9HF1	pCas9HF1_*UMAG_04039*		This study
pCas9HF1	pCas9HF1_*UMAG_05780*		This study
p123	p123_proCmu1_*ros1*_2xHA	Overexpression of TF Ros1	This study

pAGM1311	pAGM1311_Cluster19A_Comp2_1st half #13	Complementation 2.1 of *U. maydis* Cluster 19A in *S. reilianum*	This study
p123	p123_proCmu1_*biz1*_2xHA_#3	Overexpression of TF *biz1*	This study
pAGM1311	pGAM1311_UmCluster19A_Comp2_complete #60	Complementation 2 of *U. maydis* Cluster 19A in *S. reilianum*	This study
p123	pCas9HF1_*Umhdp2* #3	CRISPR plasmid for HR-assisted KO of *Umhdp2*	This study
pAGM1311	pAGM1311_KO_*Umhdp2* #2	Donor Template for KO	This study
pAGM1311	pAGM1311_*Srhdp2*_repl.	Replacement of *Umhdp2* against *Srhdp2* in *U. maydis*	This study
p123	p123_proCmu1_*Srhdp2*_2xHA	Overexpression of TF *Srhdp2*	This study
pAGM1311	pAGM1311_*Umhdp2*_Donor_Cl#1	Replacement of *Srhdp2* against *Umhdp2* in *S. reilianum*	This study
pNEB_SrCbx	pNEB_SrCbx_*sr16075_Umhdp2* #2	Overexpression of TF *Umhdp2*	This study
pNEB_SrCbx	pNEB_SrCbx_*sr16075_Srhdp2* #7	Overexpression of TF *Srhdp2*	This study
pNEB_SrCbx	pNEB_SrCbx_pro^{sr16064}_*Srhdp2*_2xHA #2	Overexpression of TF *Srhdp2*	This study
p123	p123_pro^{UMAG_02196}_*Umhdp2*_2xHA #3	Overexpression of TF *Umhdp2*	This study
p123	p123_pro^{UMAG_05312}_*Umhdp2*_2xHA #1		This study

6.3 Cultivation of microorganisms

6.3.1 Cultivation of *E. coli*

The media for the cultivation of *E. coli* strains are listed in Table 6.4.

Table 6.4: Media for the cultivation of *E. coli*.

Medium	Components	Amount
dYT	Trypton Yeast extract NaCl	1.6 % (w/v) 1.0 % (w/v) 0.5 % (w/v)
YT agar	Trypton Yeast extract NaCl Bacto™ Agar	0.8 % (w/v) 0.5 % (w/v) 0.5 % (w/v) 1.2 % (w/v)

6.3.2 Cultivation of smut fungi

The media for cultivation of *U. maydis* and *S. reilianum* were prepared using $H_2O_{deoin.}$ and are listed in Table 6.5.

Table 6.5: Media for the cultivation of *U. maydis* and *S. reilianum*.

Medium	Components	Amount	Used for
$YEPS_{light}$	Yeast extract Bacto™ peptone Sucrose	1 % (w/v) 0.4 % (w/v) 0.4 % (w/v)	*U. maydis, S. reilianum*
PD agar	Potato dextrose agar	3.9 % (w/v)	
PD agar + 1% activated charcoal	Potato dextrose agar Activated charcoal	3.9 % (w/v) 1 % (w/v)	
$Regeneration_{light}$ agar	Yeast extract Bacto™ peptone Sucrose Sorbitol Agar	1 % (w/v) 2 % (w/v) 2 % (w/v) 18.2 % (w/v) 1.4 % (w/v)	

6.3.3 Generation of Glycerol stocks

For a long-term storage of *E. coli* strains an overnight culture of the positive colony was inoculated in 5 ml of dYT with the respective antibiotic and the next day diluted 1:1 with 60% Glycerol and stored at -80°C. For fungal strains, an overnight culture of the positive colony was inoculated in 3 ml $YEPS_{light}$ medium and diluted the following day to an OD_{600} of 0.2 and grown for 4-5 hours to an OD600 of 0.8 – 1, prior to the mixture with 60% Glycerol and the storage at -80°C.

6.4 Used antibiotics and fungicides

In this study used antibiotics and fungicides are listed in Table 6.6.

Table 6.6: Antibiotics and Fungicides used for the cultivation of microorganisms.

Antibiotic/Fungicide	Concentration	Usage
Antibiotics		
Carbenicillin (Carb) Kanamycin (Kan)	100 µg/mL 50 µg/mL	selection of *E. coli*
Fungicide		
Carboxin (Cbx)	2 µg/ml *U. maydis* 2.5 µg/ml *S. reilianum*	selection of *U. maydis* and *S. reilianum* strains respectively

6.5 Oligonucleotides

All the oligonucleotides used in this study were purchased from Sigma-Aldrich (Darmstadt, Germany) or Eurofins (Luxemburg). The names, sequences, and usage of the different oligonucleotides are listed in Table 6.7.

Table 6.7: Oligonucleotides used for cloning, qRT-PCR, and sgRNA synthesis in this study. TF: Transcription factor. RNP: Ribonucleoprotein. T7 promoter sequence for RNP. Protospacer sequence. Scaffold sequence. OE: overexpression. KO: knock-out. Comp: Complementation.

Name	Sequence	Usage
Cloning		
JW107_Sra1_LF_F	TGCATGCCTGCAGGTCGACTACTACTGTTG CTGACCGTGAC	Generation of recombinant rSHU strain SRZ1_*Uma1b1*
JW108_Sra1_LF_R	TACAGCGCTGTTTCTCGTATTGAGCTTCTC TTGTGATGTTCG	
JW109_Uma1.1_F	AACATCACAAGAGAAGCTCAATACGAGAAA CAGCGCTGTA	
JW110_Uma1.1_R	GGGGATCTGAAGCGGCCTAGTTTCGTTATT TCGTGGCATCTG	
JW111_Uma1.2_F	CAGATGCCACGAAATAACGAAACTAGGCCG CTTCAGATCCCC	
JW112_Uma1.2_R	AAAGAGTGCCCTCAGCATGAATGCTCGACC ATATCACGCC	
JW113_Sra1_RF_F	GGCGTGATATGGTCGAGCATTCATGCTGAG GGCACTCTTT	
JW114_Sra1_RF_R	AAAACGACGGCCAGTGAATTACCCCAAAAC GCTCGAGAAC	
JW115_Srb1_LF_F	TGCATGCCTGCAGGTCGACTGGCCGCTGCG AACGGCGAGAC	
JW116_Srb1_LF_R	TTTCTACTGCGTTTGGCTGAGGTAGGATGT GCTGGTTGC	
JW117_UmbE1_F	CGCAACCAGCACATCCTACCTCAGCCAAAC GCAGTAGAAA	
JW118_UmbE1_R	GGTAGTGGTGGTAGCGTCATTCTGATTTGA GAGGCCAAAG	
JW119_UmbW1_F	CTTTGGCCTCTCAAATCAGAATGACGCTAC CACCACTACC	
JW120_UmbW1_R	ATACAAAGGGAATCGAAAAATCAGGCAAGC GAGAAAGAAT	
JW121_Srb1_RF_F	ATTCTTTCTCGCTTGCCTGATTTTTCGATT CCCTTTGTAT	
JW122_Srb1_RF_R	AAAACGACGGCCAGTGAATTCGCTGTTTGA AGGTTGAGAC	
JW152_SR1_Uma1_F	GAGCCTCTACGAGCGAATTTGTG	Proof of right genomic integration of *Uma1*
JW153_SR1_Uma1_R	CATCTTGCTCACCGGCTAGAATG	
JW154_SR1_Uma1_gen_INS_F	TGGCCCTTTGACGATAGTCTCC	
JW155_SR1_Uma1_gen_INS_R	CGGGATGTCAGCACTCTTACTC	
JW174_SRZ1_a1_Probe_R	TCGGCGCCTTTATCGAAGTC	Probe for Southern Blot
JW175_SRZ1_a1_Probe_F2	CAGCTCGGACCTGTCTTGTTG	
KF_SrCbx_GFP_NotI_F	TTAAGGATCCGGCGCGCCGCGCATGCCTGC AGGTCGAAAT	Cloning of single integrated GFP strain in *S. reilianum ip* locus
KF_SrCbx_GFP_NotI_R	CCACTAGTTCTAGAGCGGCCCATCGATGAA TTCTCATGTT	
KF_SrCbx_GFP_SacII_SphI_F	GATTACGCCAAGCTTGCATGGCATGCCTGC AGGTCGAAAT	
KF_SrCbx_GFP_SacII_SphI_R	ACTAGTTCTAGAGCGGCCGCCATCGATGAA TTCTCATGTT	
JW157_Prom_repl_LF_F	TGCATGCCTGCAGGTCGACTCGTCGAGCTC TATGGGGTTG	Generation of *Srtin2* promoter replacement construct
JW158_Prom_repl_LF_R	ACCATGTCAAGTCTGTACTCAGCTTCTAGA GCGTTGAATA	

JW159_sr10057_Prom_F	GAGTACAGACTTGACATGGTGCAG	
JW160_sr10057_Prom_R	CTTGGCGGATAGTGTGTGTAAGAG	
JW161_Prom_repl_RF_F	CTCTTACACACACTATCCGCCAAGATGAATAGACTTCAGTCCTACAC	
JW162_Prom_repl_RF_R	TTGTAAAACGACGGCCAGTGAAGAAGCGAGTGTGATAGGGA	
JW163_cds_Umtin2_repl_LF_F	TGCATGCCTGCAGGTCGACTAGTCTTTCTACCACCTTACTC	Generation of *Umtin2* cds replacement construct
JW164_cds_Umtin2_repl_LF_R	TAGGACTGAAGTCTATTCATCTTGGCGGATAGTGTGTGTAAGAG	
JW165_cds_Umtin2_F	ATGAATAGACTTCAGTCCTACAC	
JW166_cds_Umtin2_R	TCAAAGAGGGAAGCGAGGG	
JW167_cds_Umtin2_repl_RF_F	TCCCTCGCTTCCCTCTTTGAACTCGCAAAGCTGCTCGCCACC	
JW168_cds_Umtin2_repl_LF_R	TTGTAAAACGACGGCCAGTGCTGCCGGTCCGAGGCGGTCC	
JW281_*sr16838*_LF_F	TTGCATGCCTGCAGGTCGACTGCTCGCTTGCTGCTGTCCTT	Generation of *dicer* KO in *S. reilianum*
JW282_*sr16838*_LF_R	GGGTGGGGAGACGTGAAGGA	
JW283_*sr16838*_loLF_F	TTGCATGCCTGCAGGTCGACTAACTTCTGTGCGACACAGGAAC	
JW284_*sr16838*_RF_F	TCCTTCACGTCTCCCCACCCGGTAGGGGAGGAGTGGATGTTG	
JW285_*sr16838*_RF_R	TAAAACGACGGCCAGTGAATTGTTCAGCGCCAAACGCAAACC	
JW286_*sr16838*_loRF_R	TAAAACGACGGCCAGTGAATTTCTGGCGCCCGAATGCTTTGAG	
7433_JW290_*sr16838*_Probe_F	GGTAGGGGAGGAGTGGATGTTG	Probe for Southern Blot
7434_JW291_*sr16838*_Probe_R	CTGCCTCGTTCGCATTCTCC	
7895_JW307_proCmu1_F	ATTGTACTGAGAGTGCACCAAGATTCACATTTCGCCTCACGC	pro^{Cmu1} for OE constructs
7896_JW308_proCmu1_R	CTCAAAGGAGCTTGATTCATCGTAACCTAGAGCTCTTGCAG	*Nlt1* OE in rUSH
7897_JW309_nlt1_F_proCmu1	TGCAAGAGCTCTAGGTTACGATGAATCAAGCTCCTTTGAGTG	
7898_JW310_nlt1_R_proCmu1	GAACATCGTATGGGTACCATGCACCGCGTTCTACTTGTTCTG	
8065_JW311_proCmu1_R_hdp2	CTCTGCGGTCGTTGTGACATCGTAACCTAGAGCTCTTGCAG	*Hdp2* OE in rUSH
8066_JW312_hdp2_cds_F	CTGCAAGAGCTCTAGGTTACGATGTCACAACGACCGCAGAG	
8067_JW313_hdp2_cds_R	AACATCGTATGGGTACCATGCGGGTTCAGCAGCGGCAGCGT	
8068_JW314_proCmu1_R_rbf1	ACTAGTTCCAAGATGTCCATCGTAACCTAGAGCTCTTGCAG	*Rbf1* OE in rUSH
8069_JW315_rbf1_cds_F	CTGCAAGAGCTCTAGGTTACGATGGACATCTTGGAACTAGTG	
8070_JW316_rbf1_cds_R	AACATCGTATGGGTACCATGCGGCGCTCTGCAGTTGAGAGG	
8071_JW317_proCmu1_R_fox1	TGGGACTTGGCCCAGTACATCGTAACCTAGAGCTCTTGCAG	*Fox1* OE in rUSH
8072_JW318_fox1_cds_F	CTGCAAGAGCTCTAGGTTACGATGTACTGGGCCAAGTCCCAC	

8073_JW319_fox1_cds_R	AACATCGTATGGGTACCATGCACGCCTCGAGATAGGGTTAG	
9183_JW_proCmu1_ros1_F	GCAGCTTGGTGTGAACCCATCGTAACCTAGAGCTCTTGCAG	*Ros1* OE in rUSH
9184_JW_ros1_cds_F	CTGCAAGAGCTCTAGGTTACGATGGGTTCACACCAAGCTGCTAC	
9185_JW_ros1_cds_R	AACATCGTATGGGTACCATGCCGGCACAGGTCTCGTCAACAC	
9321_JW_proCmu1_R_biz1	CCGTGTGCTAAGCATCGACATCGTAACCTAGAGCTCTTGCAG	*Biz1* OE in rUSH
9322_JW_biz1_cds_F	CTGCAAGAGCTCTAGGTTACGATGTCGATGCTTAGCACACGG	
9323_JW_biz1_cds_R	AACATCGTATGGGTACCATGCCCAACGACGGCTGGTGTGACC	
8150_JW328_sr16075_LF_F	TGCATGCCTGCAGGTCGACTAAAGCGTTAATGCGGTACAA	Generation of *sr16075* KO
8151_JW334_sr16075_LF_R	ACGCGAGACGCAAGCGCACCTGTTGCGCTGTGCGTGTCGG	
8152_JW335_sr16075_RF_F	CCGACACGCACAGCGCAACAGGTGCGCTTGCGTCTCGCGTCG	
8153_JW336_sr16075_RF_R	AAAACGACGGCCAGTGAATTCGCGCTGGGCGCGCTCAACG	
8202_VV_19A_LF_F	TGCATGCCTGCAGGTCGACTGTCGTTTCATTGTTCTCGATTC	KO of Cluster 19A in *S. reilianum*
8204_VV_19A_RF_F	GGCGAGCTTCTCTCTCTAGCTTTGGCGGCTTGGCGTGTCT	
8205_VV_19A_RF_R	AAAACGACGGCCAGTGAATTCAGTGCCCTTGCGATCCAAG	
8206_VV_19A_LF_R2	TCACTGCTTCCTCCAACTCAGCTAGAGAGAGAAGCTCGCC	
8209_VV_19A_beg_F	TAAGCGAACCGGCTCTGAAGG	PCR templates for *in vitro* cleavage assay, Cluster 19A deletion
8210_VV_19A_beg_R	ACGACGGAGATAGCCAGGAAG	
8211_VV_19A_mid_F	CTTGTCCAGCCATTGTCTGTC	
8212_VV_19A_mid_R	TCGGCGTGGGAAACGGATAG	
8213_VV_19A_end_F	CCTTTGACCTCCGCTGTTGC	
8214_VV_19A_end_R	AAGTTGTGGTTGCGCTAGACG	
8276_VV_before_19A_F2	AACTTTCTGCTCCGGTTCCTC	PCR, deletion *Sr*19A
8277_VV_after_19A_R	CCTGCATGACGGTTCGTTTCG	
8282_JW344_sr16075_F	ATGAAGCCGCATCCTCCGTG	PCR, deletion *sr16075*
8283_JW345_sr16075_R	TGTGCAGGATGAGGGCAAGAG	
8286_VV_UM19A1_C1_LF_R	GCGTTTGAGCAGCTTTTGTCGCTAGAGAGAGAAGCTCGCC	Generation of complementation 1 construct of *U. maydis* cluster 19A in *S. reilianum*
8287_VV_UM19A1_C1_F1_F	GGCGAGCTTCTCTCTCTAGCGACAAAAGCTGCTCAAACGC	
8288_VV_UM19A1_C1_F1_R	CAGCACGTCTCTGAGTACAATTCACGATTTGTTGGCAAAA	
8289_VV_UM19A1_C1_F2_F	TTTTGCCAACAAATCGTGAATTGTACTCAGAGACGTGCTG	
8290_VV_UM19A1_C1_F2_R	CTCCCTCGCCCTATCGCACAAGACGCAAGCTTAGGACCAA	
8291_VV_UM19A1_C1_F3_F	TTGGTCCTAAGCTTGCGTCTTGTGCGATAGGGCGAGGGAG	

8292_VV_UM19A1_C1_F3_R	ATTTCGACCTGCAGGCATGCGAGGGTACGATAGACTGACT	
8293_VV_UM19A1_C1_F4_F	AGTCAGTCTATCGTACCCTCGCATGCCTGCAGGTCGAAAT	
8294_VV_UM19A1_C1_F4_R	AGACACGCCAAGCCGCCAAACATCGATGAATTCTCATGTTTG	
8295_VV_UM19A1_C1_RF_F	AACATGAGAATTCATCGATGTTTGGCGGCTTGGCGTGTCT	
8320_VV_UM19A1_C1FA_R	AATACGAGGTCGAAAATGAGTGATCAATATGGCTGTTTAC	Split of complementation 1 plasmid (Cluster 19A)
8321_VV_UM19A1_C1FB_F	GTAAACAGCCATATTGATCACTCATTTTCGACCTCGTATT	
8322_VV_UM19A1_C1FB_R	CGACAGACGGTCTGCTCGATCCATACATCGTTGCTTCTTC	
8323_VV_UM19A1_C1FC_F	AGAAGAAGCAACGATGTATGGATCGAGCAGACCGTCTGT	
8324_VV_UM19A1_C1FC_R	TCATACTTAGTCCATCGGTCCTCTTGATCTCGGTCAAAGC	
8325_VV_UM19A1_C1FD_F	GCTTTGACCGAGATCAAGAGGACCGATGGACTAAGTATG	
8326_VV_UM19A1_C1FD_R	ATTGACCACGGTGGAGACTGGTAGTGGAGCATCAGGTAG	
8327_VV_UM19A1_C1FE_F	GCTACCTGATGCTCCACTACCAGTCTCCACCGTGGTCAATG	
8604_VV_KOsg_templ_FW	TCCTCAACACTCACGAAGTC	PCR template *in vitro* cleavage assay, Cluster 19A comp.
8605_VV_KOsg_templ_RW	CAATAACGCCGAACGACAGG	
9416_JW_procmu1_Srhdp2_F	ATTGTACTGAGAGTGCACCAAGATTCACATTTCGCCTCACG	OE *Srhdp2* in rUSH
9417_JW_proCmu1_Srhdp2_R	CTCTGCGGACGTTGCGACATCGTAACCTAGAGCTCTTGCAGTTC	
9418_JW_Srhdp2_cds_F	TGCAAGAGCTCTAGGTTACGATGTCGCAACGTCCGCAGAG	
9419_JW_Srhdp2_cds_R	AACATCGTATGGGTACCATGCCTCCTGCTCACCTCCAGCAGA	
9420_JW_Umhdp2_LF_F	TGCATGCCTGCAGGTCGACTGTGGGTGGGACCAGAGGCAAAAG	Deletion construct for *Umhdp2*
9421_JW_Umhdp2_LF_R	CGTGCGATGTAAGCCGAGTCGTTGGTTACAAAGTGAATGC	
9422_JW_Umhdp2_RF_F	GCATTCACTTTGTAACCAACGACTCGGCTTACATCGCACG	
9423_JW_Umhdp2_RF_R	AAAACGACGGCCAGTGAATTAAGGCGTGTTTGAACCTAGAC	
9424_JW_Umhdp2_LF_Srhdp2_R	CTCTGCGGACGTTGCGACATGTTGGTTACAAAGTGAATGC	Native replacement of *Umhdp2* by *Srhdp2* in *U. maydis*
9425_JW_Srhdp2_cds_F	GCATTCACTTTGTAACCAACATGTCGCAACGTCCGCAGAG	
9426_JW_Srhdp2_cds_comp_R	CGTGCGATGTAAGCCGAGTCTCACTCCTGCTCACCTCCAG	
9427_JW_Srhdp2_comp_RF_F	CTGGAGGTGAGCAGGAGTGAGACTCGGCTTACATCGCACG	
9510_Srhdp2_LF_F	TGCATGCCTGCAGGTCGACTGTGTTGCACATGAAGTCATC	Replacement of *Srhdp2* by *Umhdp2* in *S. reilianum*
9511_Srhdp2_LF_R	CTCTGCGGTCGTTGTGACATGTTTGGCGCCAGGGGGAAAG	

9512_Umhdp2_cds_F	CTTTCCCCCTGGCGCCAAACATGTCACAACGACCGCAGAG	
9513_Umhdp2_cds_R	GATCAAGCAACGAACAGCCCTTAGGGTTCAGCAGCGGCAG	
9514_Srhdp2_RF_F	CTGCCGCTGCTGAACCCTAAGGGCTGTTCGTTGCTTGATCG	
9515_Srhdp2_RF_R	AAAACGACGGCCAGTGAATTCTGCTTCTTCTTCTTTCGATCC	
9698_pNEB_SrCbx_Tnos_R	ATACAGAGCAGCCGTCAACGTC	Generation of *Srhdp2* OE in *S. reilianum*
9699_Comp2_F3_R_1123	AGAGAAGACACGCCAAGCCGCCAAATTTGTCTCTGTCCGCTCAGGAGGCCGAATAG	
9700_Comp2_Cl19A_RF_F1123	TTTGGCGGCTTGGCGTGTCTTCTCT	
2992_F-Level-0	CGTTATCCCCTGATTCTGTGGATAAC	
2993_R-Level-0	GTCTCATGAGCGGATACATATTTGAATG	
9760_JW_psr16064_F	TTAAGGATCCGGCGCGCCGCGTCGATGTTGCAACGATGAC	Generation of *Srhdp2* OE in *S. reilianum*
9761_JW_psr16064_R	CTCTGCGGACGTTGCGACATTGTTGTGTGAGCGAGTTGTAG	
9762_JW_Srhdp2_F	TACAACTCGCTCACACAACAATGTCGCAACGTCCGCAGAG	
9790_JW_proUMAG_02196	ATTGTACTGAGAGTGCACCAATGTAGAAGAGCGAGCGTCC	OE of *Umhdp2* in rUSH
9791_JW_proUMAG_02196_hdp2_R	CTCTGCGGTCGTTGTGACATTGCTCGAAACATTGTCGCTC	
9792_JW_hdp2_F_02196	GAGCGACAATGTTTCGAGCAATGTCACAACGACCGCAGAG	
9793_JW_pro2196_biz1_R	CCGTGTGCTAAGCATCGACATTGCTCGAAACATTGTCGCTC	OE of *Umbiz1* in rUSH
9794_JW_biz1_cds_F	GAGCGACAATGTTTCGAGCAATGTCGATGCTTAGCACACGG	
9795_JW_pro_05312_F	ATTGTACTGAGAGTGCACCACCAACAAGCTCAGAGTCAGTC	OE of *Umhdp2* in rUSH
9796_JW_pro05312_R_Umhdp2	CTCTGCGGTCGTTGTGACATCTACGTTGAAGGCCTCTTGC	
9797_JW_pro05312_Umhdp2_F	GCAAGAGGCCTTCAACGTAGATGTCACAACGACCGCAGAG	
9798_pro05312_Umbiz1_R	CCGTGTGCTAAGCATCGACATCTACGTTGAAGGCCTCTTGC	OE of *Umbiz1* in rUSH
9799_JW_biz1_pro05312_F	GCAAGAGGCCTTCAACGTAGATGTCGATGCTTAGCACACGG	
9800_JW_pro02196_Srhdp2_R	CTCTGCGGACGTTGCGACATTGCTCGAAACATTGTCGCTCA	OE of *Srhdp2* in rUSH
9801_JW_Srhdp2_F_pro02196	GAGCGACAATGTTTCGAGCAATGTCGCAACGTCCGCAGAG	
9802_JW_pro05213_Srhdp2_R	CTCTGCGGACGTTGCGACATCTACGTTGAAGGCCTCTTGC	OE of *Srhdp2* in rUSH
9803_JW_Srhdp2_pro05312_F	GCAAGAGGCCTTCAACGTAGATGTCGCAACGTCCGCAGAG	
Sequencing		
JW127_Sra1_F_seq	GCGATAGTGCAGCTCGAGTAG	Sequencing of *Uma1* and *Umb1* donor templates
JW128_Sra1_R_seq	CGAGCTGCGTACTGTGTCTTG	
JW129_SRZ1_Uma1_seq2	TCGCACTACCGCGAACATCAC	
JW130_SRZ1_Uma1_seq3	TCGGCAACCCTTCGTATCCC	

JW131_SRZ1_Uma1_seq4	TGGAGCTAGATCCGCAGTTG	
JW132_SRZ1_Umb1_seq1	GTGGGCCAAGGGTGTTGTAG	
JW133_SRZ1_Umb1_seq2	ATGGCGCTTCGCTACTGTGG	
JW134_SRZ1_Umb1_seq3	TTGACGGGCTGCGCACAAAG	
JW135_SRZ1_Umb1_seq4	TCATACCAAGCCCATCGACAG	
JW177_Tin2_seq_F	GCGCCAGGTTTAGGAGTCAG	Sequencing *tin2*
JW277_hdp2_cds_F	ATGTCACAACGACCGCAGAG	Sequencing *hdp2*
JW278_hdp2_seq2	CAAATTGCGCATGCCTGAACG	
JW279_hdp2_seq3	TGCCGCTTCGTTGGACATGTG	
JW280_hdp2_seq4	ACGGTTTCGATGGCCACAAGG	
9343_JW_biz1_seq	AAGATGCGAACCACGGCTTCC	Sequencing of biz1
8116_JW320_proCmu1_seq	AGACGAGTTGGAGCGAAACG	Sequencing of pro^{cmu1}
7435_JW292_*sr16838*_seq1_F	GCTCGCTTGCTGCTGTCCTT	Sequencing of *dicer* (SR)
7436_JW293_*sr16838*_seq2_F	CGCACCACCAACCACTATCAC	
8154_JW337_UMAG_00533_F	TTACCACTCTCGGCCATGGG	Sequencing of TF KO
8155_JW338_UMAG_00533_R1	ATGAGACCGGGCAGCGATTG	
8156_JW339_UMAG_00533_R2	ACCCGCAACATCATTCAAGC	
8157_JW340_UMAG_02462_F	AAGAAGTCGCCCTGTCACCG	Sequencing of TF KO
8158_JW341_UMAG_02462_R	TGTCCAACGTGCTGTGAAAG	
8159_JW342_UMAG_04242_F	CTCGCTTGGGACTTGTCCTTG	Sequencing of TF KO
8160_JW343_UMAG_04242_R	TGGTGCAGGCAGAGTAGAATG	
8776_KRL_UMAG_10626_F	AGTCAAAGTGGAGGGCCAAAC	Sequencing of TF KO
8777_KRL_UMAG_10626_R	TGGATGCGTTCCGTTCAAGTC	
8785_JW_UMAG_06257_F	CTTGCGTGTAGCTAGGGCTTG	Sequencing of TF KO
8786_JW_UMAG_06257_R	TTATGGCTGCCAGGTCCAGAG	
8791_JW_UMAG_10256_F	CTCGCCAAGTGCCATCTCAAG	Sequencing of TF KO
8792_JW_UMAG_10256_R	CACATTGAACACGGTGGAGGG	
9201_JW_proCmu1_seq	TTTGCAGACGAGCGTGGAATG	
9202_JW_ros1_cds_seq	CATGATGGATCCGCATGCAAG	Sequencing of *ros1* OE construct
9203_JW_ros1_cds_seq2	CAGCATCCCTCAATGCATAGC	
X_JW_ros1_seq3	TCGTCTTCGTCGGTCCCTTAC	
9447_JW_Srhdp2_seq	CCGCAAGAAGCGCAACAAGTG	Sequencing of *Srhdp2* OE construct
9448_JW_Srhdp2_seq2	TTGGCCTGGTCAACAGTATGC	
9516_Srhdp2_seq3	TTGACTTTGGCACGGCGGTTC	
9517_Srhdp2_seq4	AAAGGATCGCCTGTGGACGAG	
qRT-PCR		
rt-ppi-F-2	ACATCGTCAAGGCTATCG	Biomass quantification
rt-ppi-R-2	AAAGAACACCGGACTTGG	
Sr_ppi_RT_Fw	ACGGCAAGCACGTCGTCTTC	Biomass quantification
Sr_ppi_RT_Rv	CTTGGTCTTGCCCGAGTTGG	
GAPDH-RT-for	CTTCGGCATTGTTGAGGGTTTG	Biomass quantification
GAPDH-RT-rev	TCCTTGGCTGAGGGTCCGTC	
JW69_UMAG_05302_qP_F	ACGGAAAGTGGGCAGAAAG	Expression of *Umtin2*
JW70_UMAG_05302_qP_R	TGTTAGGCGAACGAGACTG	
JW71_sr10057_qP_F	TCAACCCCGAATGTCTGGAA	Expression of *Srtin2*
JW72_sr10057_qP_R	AGAATGTTACGGGCTAGCGA	
pit2_rt_rv	AGGATCTGTCGGCATGACC	Expression of *Umpit2*
pit_rt_fw	CAAGAATCCGCCTGCCAAC	

SrPit2RT_fw	TCAGGATCCCGGAAGAC	Expression of *Srpit2*
SrPit2RT_rv	GGACGTACTGCCAATCG	
OAli17_um11060_qRT_fw	CAGAGCTCGTTCAGCATAC	Expression of UMAG_11060
OAli18_um11060_qRT_rv	CCTGTTGCGACCATACTTC	
8837_JW_Umhdp2_qRT_F2	ATACACTGCGCATCGACACT	Expression of *Umhdp2*
8838_JW_Umhdp2_qRT_R2	CATCCCAGCCGTTAAAAGCG	
JW215_UMAG_02239_qPCR_F2	GCGCACAGAGCAACAAAACA	Expression of *Umsee1*
JW216_UMAG_02239_qPCR_R2	TGAACTCGCCTTCTCCTTGC	
JW217_sr13434_qPCR_F1	GCCTCTACACTCGTTTCGCT	Expression of *Srsee1*
JW218_sr13434_qPCR_R1	TCGGGATTTGAGCTTGTGCT	
sgRNA synthesis		
JW123_Sra1 sgRNA	AAGCTAATACGACTCACTATAGACTCGTGC GCTCTTTACGTGTTTTAGAGCTAGAAATAG CAAG	Replacement of *Sra1* against *Uma1*
JW124_Srb1 sgRNA	AAGCTAATACGACTCACTATAGCCAATCGG AGATGGTCGAGGGTTTTAGAGCTAGAAATA GCAAG	Replacement of *Srb1* against *Umb1*
JW169_sgRNA_Srtin2_1	AAGCTAATACGACTCACTATAGCCTCACTG ACGTACGAGCGGTTTTAGAGCTAGAAATAG CAAG	Replacement of *Srtin2* against *Umtin2*
JW170_sgRNA_Srtin2_2	AAGCTAATACGACTCACTATAGGGGAAAAC ATCCAAAGTATGTTTTAGAGCTAGAAATAG CAAG	Replacement of *Srtin2* against *Umtin2*
JW171_sgRNA_Umtin2_prom_1	AAGCTAATACGACTCACTATAGGGAGAAAG AGTACGTATCGGTTTTAGAGCTAGAAATAG CAAG	Replacement of pro^{Umtin2} against pro^{Srtin2}
JW172_sgRNA_Umtin2_prom_2	AAGCTAATACGACTCACTATAGGAGATTAC TCGGAGAGACAGTTTTAGAGCTAGAAATAG CAAG	Replacement of pro^{Umtin2} against pro^{Srtin2}
JW289_sgRNA3 *sr16838*	AAGCTAATACGACTCACTATAGCACGTGCC CGTGAAGAACAGTTTTAGAGCTAGAAATAG CAAG	Deletion of *dicer*
209_JW321_sgRNA_UMAG_00533_beg	CAAAATTCCATTCTACAACGCCGAATCGAT ACCAACACAGTTTTAGAGCTAGAAATAGC	KO of UMAG_00533
210_JW322_sgRNA_UMAG_02462	CAAAATTCCATTCTACAACGTATTTGTCGA CGGACCCGGGTTTTAGAGCTAGAAATAGC	KO of UMAG_02462
211_JW323_sgRNA_UMAG_04242	CAAAATTCCATTCTACAACGAACTCGGTTT TGAGAGTGGGTTTTAGAGCTAGAAATAGC	KO of UMAG_04242
216_JW332_sgRNA_16075_mid	AAGCTAATACGACTCACTATAGTCGCGCGA GAAGGCCGACAGTTTTAGAGCTAGAAATAG CAAG	Deletion *sr16075* RNP
262_JW_UMAG_10256_sgRNA	CAAAATTCCATTCTACAACGTCCGTGTTGG CAAAGCTGGGTTTTAGAGCTAGAAATAGC	KO of UMAG_10256
264_JW_UMAG_06257_sgRNA	CAAAATTCCATTCTACAACGTAAGCATCTC TGGGCTGAGGTTTTAGAGCTAGAAATAGC	KO of UMAG_06257
278_JW_UMAG_10626	CAAAATTCCATTCTACAACGACCAACGCAG TCAAAGTGGAGTTTTAGAGCTAGAAATAGC	KO of UMAG_10626
286_JW_UMAG_05312_new	CAAAATTCCATTCTACAACGTGCTCGCAGA CCTAACTAAGTTTTAGAGCTAGAAATAGC	KO UMAG_05312
287_JW_UMAG_03749_new	CAAAATTCCATTCTACAACGTTACCAACTT CGGTAGATGGTTTTAGAGCTAGAAATAGC	KO UMAG_03749
288_JW_UMAG_03751_new	CAAAATTCCATTCTACAACGGCGAACGAAG ATTCGTCTGGTTTTAGAGCTAGAAATAGC	KO UMAG_03751
289_JW_UMAG_10553	CAAAATTCCATTCTACAACGTGAAAGTGTG AAGCTGACGGTTTTAGAGCTAGAAATAGC	KO UMAG_10553

290_JW_UMAG_05928	CAAAATTCCATTCTACAACGCATGTGTATTGGGCACAGAGTTTTAGAGCTAGAAATAGC	KO of UMAG_05928
291_JW_UMAG_04039	CAAAATTCCATTCTACAACGTGCTGCTTGTTGTCCGTCTGTTTTAGAGCTAGAAATAGC	KO of UMAG_04039
303_JW_sgRNA_Umhdp2	CAAAATTCCATTCTACAACGCTGACAACTTTGGGCTGGTGTTTTAGAGCTAGAAATAGC	Deletion of Umhdp2
309_JW_sgRNA_Srhdp2	AAGCTAATACGACTCACTATAGCACTGCGCAGCTCCTCGTAGTTTTAGAGCTAGAAATAGCAAG	Umhdp2 repl.
217_VV_sgRNA_19A_beg	AAGCTAATACGACTCACTATAGATGCTGAGATTGCCGTCGTGTTTTAGAGCTAGAAATAGCAAG	Deletion of Sr19A
218_VV_sgRNA_19A_mid	AAGCTAATACGACTCACTATAGCATACATGCTGATGTCTGCGTTTTAGAGCTAGAAATAGCAAG	Deletion of Sr19A
219_VV_sgRNA_19A_end	AAGCTAATACGACTCACTATAGGATGATCCTCATCAGAAAGGTTTTAGAGCTAGAAATAGCAAG	Deletion of Sr19A
257_VV_sgLF_RF	AAGCTAATACGACTCACTATAGCGAGCTTCTCTCTCTAGCTTGTTTTAGAGCTAGAAATAGCAAG	Complementation 1 of Um19A in *S. reilianum*

6.5 Microbiology methods

6.5.1 Competent *Escherichia coli* cells

Before starting to prepare competent *E. coli* cells, all media and equipment needed to be cooled down to 4°C, and steps were conducted on ice in the cold room. A 15-20 ml dYT pre-overnight culture was started from a single colony and the next day 2 ml of this culture was used to inoculate a 100 ml dYT liquid culture which was subsequently incubated for 2 – 2.5 hours at 37°C and 200 rpm until the culture reached an OD_{600} of around 0.6. Afterward, cells are transferred to centrifugation tubes and incubated for 30 min on ice in the cold room. *E. coli* cells were centrifuged for 8 min at 3,000 rpm and 4°C and the supernatant was discarded. Next, 1/3 (33 ml) of the cells are resuspended with cold RF1 solution (Table 6.) using a glass pipette, followed by an incubation of ice in the cold room for 30 min. Subsequently, cells were centrifuged again for 8 min at 3,000 rpm and 4°C, the supernatant was discarded and the cells were resuspended in 5 ml (1/20 of the original volume) of cold RF2 solution (Table 6.8). After the transfer to a Falcon tube, the cells rested for 30 min at 0°C. In the meantime, 1.5 ml reaction tubes were prepared and cooled down using liquid nitrogen. Lastly, 50-100 µl of the cells were aliquoted in the pre-cooled reaction tubes and frozen at -80°C for further use.

Table 6.8: Solutions used for the preparation of competent *E. coli* cells.

Solutions	Composition
RF1 solution	100 mM RbCl 50 mM MnCl2·4H2O 30 mM Potassium acetate1 10 mM CaCl2 ·2H2O 15% (w/v) Glycerol pH 5.8 (adjusted with glacial acetic acid) sterile-filtered
RF2 solution	10 mM MOPS2 10 mM RbCl 75 mM CaCl2 x 2 H2O 15% (w/v) Glycerol pH 5.8 (adjusted with NaOH) sterile-filtered

6.5.2 Transformation of *E. coli*

1-5 ng of plasmid DNA or the Gibson assembly reaction (5 µl, see 6.7.8) was added to 50 µl of the competent cells (see 6.5.1) and incubated on ice for 30 min. Afterward, the reaction tubes were then placed in a thermo block at 42 °C for 45 s to heat shock the cells, followed by an incubation on ice for 2 min. Subsequently, 700 µl dYT is added and the cells are incubated for 30 min at 37°C with 200rpm shaking. Lastly, the cells were plated on YT plates containing the respective antibiotics (see 0) for selection and incubated overnight at 37°C.

6.5.3 Protoplast preparation of *U. maydis* and *S. reilianum*

An overnight culture of the *U. maydis*/ *S. reilianum* was prepared and incubated at 28 °C and 200 rpm. The next day, the culture was diluted in 55 ml to an OD_{600} of 0.2 (*U. maydis*) or 0.25 (*S. reilianum*) and shaken for 3.5 h at 28 °C and 200 rpm until a final OD_{600} of 0.6 – 0.8 was reached. Subsequently, the culture was centrifuged at 3,500 rpm for 10 min, the supernatant discarded and the pellet was resuspended in 25 ml SCS (RT). After another centrifugation step for 10 min at 3,500 rpm, the supernatant was discarded and the pellet was resuspended in 2 ml of SCS buffer containing 7 mg/ml of Novozyme 234 (see 0) previously filtered through a 0.2 µm filter for sterilization. The cells were incubated at RT for 5 min until approximately 40% of the cells formed protoplasts (checked by microscope). Subsequently, the enzymatic activity was stopped by the addition of 10 ml of ice-cold SCS buffer and centrifuged at 2,400 rpm for 5 min at 4 °C. The supernatant was discarded and the pellet was carefully resuspended in 10 ml of ice-cold SCS and the cells were centrifuged at 2,400 rpm for 5 min at 4 °C. This step was repeated twice before the pellet was then resuspended in 10 ml of ice-cold STC buffer and the cells were centrifuged again at 2,400 rpm for 5 min at 4°C. Lastly, the pellets were resuspended in 500 µl of ice-cold STC buffer and stored in 50 µl aliquots in pre-cooled 1.5 ml reaction tubes, before they were

stored at -80°C for transformation. All buffers used for the preparation of protoplasts are listed in Table 6.9.

Table 6.9: Buffers for protoplasting of *U. maydis* and *S. reilianum*.

Solution	Components	Amount
SCS buffer	Sodium citrate, pH 5 Sorbitol diluted in sterile $H_2O_{deion.}$	20 mM 1 M
STC buffer	Tris-HCl, pH 7.5 $CaCl_2$ Sorbitol	10 mM 100 mM 1 M
SCS/Novozym	SCS Novozym	99.65 % 0.35 %
STC/PEG	STC PEG	60 % 40 %

6.5.4 Transformation of *U. maydis* and *S. reilianum*

Before the transformation, Reg_{light} agar plates were prepared in 2 layers each 10 ml. The bottom layer contains the selective fungicide cbx in a double concentration (see Table 6.10) and after drying of the bottom layer for ~10 min, the top layer is poured without the addition of a fungicide. For the transformation of *U. maydis* and *S. reilianum* protoplasts, 50 µl of protoplasts were either freshly used after the preparation or thawn on ice for 5 min, before 1.5-3-5 µg of DNA was added to the cells (depending on the transformation approach, see Table 6.10) in a minimal volume (max. 10 µl) and 1 µl of heparin (1 mg/ml). After an incubation of 10 min on ice, 500 µl of STC-PEG was added to the protoplasts and resuspended by pipetting up and down with a tip-cut blue tip until the reaction mix looked homogeneous without the formation of clumps. After another incubation of 15 min on ice, the protoplasts were gently spread on the 2-layered Reg agar light plates and incubated for 3-5 days at 28°C until colonies were visible. Afterward, colonies were transferred for 2 days onto PDA+Cbx plates for singling out. After 2 days, one single colony was transferred to PDA plates and incubated for 2 days prior to DNA extraction.

Table 6.10: Amount of DNA used for the transformation approaches.

Transformation approach	DNA type	Amount
Integration into *ip* locus	Linearized Plasmid DNA	1.5 µg
CRISPR frameshift	Circular Plasmid DNA	3.5 µg
CRISPR-mediated HR	Circular Plasmid DNA	1.5 µg + 1.5 µg
RNP-mediated HR	Circular Plasmid DNA	1.5 µg

6.6 Molecular Microbiology methods

6.6.1 DNA isolation from infected maize tissue

For the extraction of genomic DNA (gDNA) from infected maize tissue, 4 cm leaf sections of at least 10 independent leaves were taken and frozen in liquid nitrogen. After grinding, 800 µl of Maize extraction buffer was added to ~200 mg of the powder and incubated for 20 min at 65°C. After letting the samples cool down to room temperature (RT), 800 µl of ROTI®phenol/chloroform/isoamyl alcohol were added and mixed by inverting the tubes for 2 min by hand. Afterward, samples were centrifuged at 12,000 rpm for 8 min and the aqueous phase was transferred to a new 1.5 ml reaction tube, containing 600 µl of 100% isopropanol (0.7 V). The samples are inverted until the DNA is visible. Subsequently, the samples were centrifuged for 5 min at 4°C, the supernatant was discarded and 200 µl of 70% Ethanol was used for washing of the DNA pellet. After another centrifugation of 5 min at 13,300 rpm at 4°C, the remaining Ethanol was removed using a yellow tip and the pellets were dried for 10 min at RT before they were dissolved in 35 µl TE-buffer and frozen at -20°C or directly continued with the clean- up of the DNA. For the preparation of 1 L DNA maize extraction buffer see Table 6.11.

Table 6.11: Composition of buffers used for gDNA extraction of infected maize leaves.

Buffer	Components
Maize extraction buffer	0.5 M EDTA 1 M Tris-HCl 100 mM NaCl SDS After autoclaving add 3 ml β-mercaptoethanol
TE buffer	10 mM Tris base 1 mM Na_2-EDTA* $2H_2O$

6.6.2 Clean-up of isolated DNA from infected maize leaves for biomass quantification

The samples described in 6.6.1 above used and 1 µl of RNase was added to each sample. Afterwards, the samples were incubated for 30 min at 37 °C. 14 µl of TE buffer and 50 µl of 2x T and C Lysis solution were added to each sample and the reaction tubes were placed on ice for 3-5 min. 100 µl of MPC Protein Precipitation Reagent was added and the reaction tubes were vortexed for 10 s followed by a centrifugation for 10 min at 10,000g and 4 °C to get rid of cell debris. The supernatant was transferred to a new 1.5 ml reaction tube, 200 µl of ice-cold isopropanol was added and the reaction tubes were inverted 30-40 times for precipitation. Subsequently, the DNA was pelleted by centrifugation for 30 min at 10,000 g and 4 °C (Caution: pour isopropanol without losing the pellet). The pellet was washed 2 times with 500 µl

70% Ethanol and the remaining Ethanol was removed using a yellow tip. After drying for 10 min at RT, the pellet was resuspended in 35 µl TE buffer and the concentration was measured via Nano drop. 150 ng of the DNA were used for biomass quantification of fungal material.

6.6.3 DNA isolation from *U. maydis* or *S. reilianum* culture

For the isolation of gDNA from *U. maydis*, a modified version of the protocol from Hoffman and Winston (1987) was used. 2 ml of a thickly grown overnight culture of *U. maydis* was pelleted at 13,300 rpm for 1 min in a 2 ml reaction tube. After discarding the supernatant, ~ 0.3 g glass beads (0.4-0.6 mm), 500 µl *Ustilago* lysis buffer, and 500 µl ROTI®phenol/chloroform/Isoamyl alcohol (Roth) were added to the pellet (Table 6.12). The reaction tube was then incubated for 10 min on a Vibrax-VXR shaker (IKA, Staufen, Germany) at 2,500 rpm. Subsequently, the samples were centrifuged for 10 min at 13,300 rpm for the separation of phases. 400 µl of the upper aqueous phase containing the extracted DNA was transferred to a fresh 1.5 ml reaction tube and precipitated by the addition of 280 µl of 100% Isopropanol (0.7 V) and centrifugation at 13,000 rpm for 10 min. The supernatant was discarded, the DNA pellet was washed with 500 µl 70% EtOH for 10 min at 13,300 rpm and afterward remaining EtOH was removed with a yellow tip after another centrifugation at 13,000 rpm. After letting the pellet dry for 10 min at room temperature, the pellet was finally dissolved in 80-100 µl nuclease-free water and dissolved in a Thermomixer (Eppendorf, Hamburg, Germany) at 37 °C, 650 rpm for 30 min and stored at -20 °C.

Table 6.12: Composition of reagents used for isolation of gDNA from *U. maydis* and *S. reilianum*.

Buffer	Composition
Ustilago lysis buffer	10 mM Tris HCl, pH: 8.0 100 mM NaCl 1 mM Na_2-EDTA 1% SDS 2% (v/v) Triton
ROTI® phenol/chloroform/Isoamyl alcohol	50% (v/v) Phenol (equilibrated in TE buffer) 50% (v/v) Chloroform

6.6.4 Polymerase chain reaction

In this study the following polymerases were used: Phusion® High Fidelity DNA Polymerase and KOD Hot Start Polymerase for Cloning and GoTaq® Green Master Mix for colony PCRs. The components of PCR programs are listed in Table 6.13 and Table 6.14, respectively.

Table 6.13: PCR reaction mixture of Phusion® High Fidelity DNA Polymerase, KOD Hot Start Polymerase, and GoTaq® Green Master Mix.

PCR reaction mixture	Components	Amount
Phusion® High Fidelity DNA Polymerase	$H_2O_{deion.}$	62 % (v/v)
	5 x HF buffer (NEB)	20 % (v/v)
	Primer, FW (10 µM)	5 % (v/v)
	Primer, RV (10 µM)	5 % (v/v)
	DNTPs (10 mM)	5 % (v/v)
	Phusion polymerase (NEB)	1 % (v/v)
	Template DNA	2 % (v/v)
KOD Hot Start Polymerase	$H_2O_{deoin.}$	42 % (v/v)
	2 x KOD Master Mix (Merck)	50 % (v/v)
	Primer, FW (10 µM)	3 % (v/v)
	Primer, RV (10 µM)	3 % (v/v)
	Template DNA	2 % (v/v)
GoTaq® Green Master Mix	$H_2O_{deion.}$	30 % (v/v)
	2 x GoTaq® Green Master Mix	50 % (v/v)
	Primer, FW (10 µM)	10 % (v/v)
	Primer, RV (10 µM)	10 % (v/v)

Table 6.14: PCR program for Phusion® High Fidelity DNA Polymerase, KOD Hot Start Polymerase, and GoTaq® Green Master Mix.

Steps	Temperature [°C]	Duration [sec]	Cycles
Phusion® High Fidelity DNA Polymerase			
Steps	**Temperature [°C]**	**Duration [sec]**	**Cycles**
Initial denaturation	98	60	1
Denaturation	98	10	35
Annealing	X	30	
Elongation	72	2 kb/min	
Final elongation	72	X	1
Storage	4	∞	1
KOD Hot Start Polymerase			
Steps	**Temperature [°C]**	**Duration [sec]**	**Cycles**
Initial denaturation	95	120	1
Denaturation	95	20	35
Annealing	X	10	
Elongation	70	2-3 kb/min	
Final elongation	70	X	1
Storage	4	∞	1
GoTaq® Green Master Mix			
Steps	**Temperature [°C]**	**Duration [sec]**	**Cycles**
Initial denaturation	95	120	1
Denaturation	95	20	35
Annealing	X	10	
Elongation	72	1 kb/min	
Final elongation	72	X	1
Storage	4	∞	1

6.6.5 Gel electrophoresis

The separation of DNA of restriction digests, PCR products, and Southern blots were visualized on agarose gels (Table 6.15) supplemented with ethidium bromide. The agarose concentration

ranges from 0.9% (Southern blot), 1% (restriction digests and fragment separation till 500 bp) to 2% for fragments smaller than 500 bp using gel electrophoresis. Therefore, samples were prepared with 6x Loading dyes from either TriTrack (Thermo Fisher Scientific, Waltham, USA) for larger fragments or Purple Loading Dye (NEB). DNA was visualized using UV radiation using a gel documentation unit (Peqlab/VWR, Radnor, USA).

Table 6.15: Buffers used for gel electrophoreses of DNA.

Buffer	Composition	Amount
50% TAE buffer	$H_2O_{deion.}$ 2 M Tris 2 M acetic acid 0.5 M EDTA, pH 8	60.09 % (v/v) 24.2 % (w/v) 5.71 % (v/v) 10 % (v/v)
1% TAE buffer	$H2O_{deion.}$ 50 x TAE	98 % (v/v) 2 % (v/v)
6x DNA Loading Dye	Sucrose Bromophenol blue In TE buffer	50 % (w/v) 5.1 % (v/v)

6.7.6 DNA Ladder

Depending on the expected size of the DNA fragments, (>500 bp) GeneRuler 1 kb (Thermo Fisher Scientific) or (<500 bp) the 100 bp ladder (NEB) was used.

6.7.7 DNA purification

Purification of DNA fragments was conducted using the NucleoSpin® gel and PCR Clean-up kit (Macherey-Nagel, Düren, Germany) kit following the manufactures instructions.

6.7.8 Gibson assembly

Gibson assembly of DNA fragments was performed using NEBuilder® HiFi DNA Assembly Master Mix (NEB, Ipswich, USA). Therefore, the fragments were amplified using Phusion® High Fidelity DNA Polymerase or KOD Hot Start Polymerase, respectively (Table , Table 6.). The used backbone needed to be linearized according to the planned overhangs before it was used in a Gibson assembly reaction. After the clean-up of the DNA fragments and the linearized backbone using the NucleoSpin® gel and PCR Clean-up kit (Macherey-Nagel, Düren, Germany), the concentration of the fragments was assessed using Nanodrop and for the fragments and the backbone, a 2:1 ratio was used for fragment sizes above 300 bp. For fragments below 300 bp, a 5:1 ratio (fragment to backbone) was used. 100 ng of the linearized backbone was used per reaction. After all, components were mixed accordingly in a volume of 2.5 µl, 2.5 µl of 2x NEBuilder® HiFi DNA Assembly Master Mix was added and the reaction was incubated

depending on the fragment number and size between 15 and 60 min at 50°C in a PCR thermo cycler. Subsequently, the Gibson assembly reaction (5 µl) was transformed into competent *E. coli* Top 10 cells (see 6.5.2).

6.7.9 Sequencing of plasmids and PCR products

Sequencing of plasmids and PCR products was done by Eurofins (GATC, Luxemburg) and visualized using the software Clone Manager 9.

6.7.10 Restriction digest

In this study, different restriction digests were performed for verification of generated constructs (6.7.10.1), preparative digestion for cloning and smut transformation, respectively (6.7.10.2), and restriction digests of gDNA for verification of correct insertions in *U. maydis* and *S. reilianum*, respectively (6.7.10.3).

6.7.10.1 Analytical digest for verification of generation constructs

To verify new constructs, analytical digests were performed using 500 ng of the purified Plasmid DNA, 0.5 µl of the respective enzyme (NEB), and 2 µl of the corresponding enzyme buffer in a total volume of 20 µl. After 1 hour of incubation at 37°C, 5 µl of Purple Loading Dye was added and 100 ng was loaded on a 1% agarose gel.

6.7.10.2 Preparative digestion

For cloning new constructs using Gibson assembly, the plasmids needed to get linearized first. Therefore, 5 - 10 µg of the plasmid were digested overnight with 1 µl of the respective endonuclease in a final volume of 100 µl. The constructs for smut transformation for the integration into the *ip* locus were digested overnight using 10 - 15 µg of the plasmid with 1 µl of the respective endonuclease in a final volume of 200 µl.

6.7.10.3 Restriction digest of gDNA for Southern blot

For the verification of the correct genomic integration, Southern blots were performed. Therefore, the DNA of smut transformants as well as the control was extracted (see 6.6.3) and 20 µl was used for the digestion with an appropriate endonuclease. In a total volume of 200 µl, 159.5 µl of nuclease-free water, 20 µl of the endonuclease-specific buffer, and 0.25 µl of the respective endonuclease were added and incubated at 37°C overnight.

6.7.11 Southern blot

The correct integration into specific genomic loci was detected using Southern blot (Southern, 1975). All the buffers used for Southern blot are listed in Table 6.16.

6.7.11.1 Design and amplification of Southern hybridization probe

For the specific probe used for the detection of southern blots 1-2 kb of the locus of interest is amplified using digoxigenin (DIG)-labelled dNTPs (Roche, Mannheim, Germany) following the manufacturer's instruction (Roche, Mannheim, Germany) in a PCR reaction using Phusion® High Fidelity DNA Polymerase (Table 6.16). For deletion constructs, the donor template containing the left homology flank and right homology flank was used for amplification of the hybridization probe, and an endonuclease cutting in the cds and outside of the homology flanks was used for the restriction digest, revealing one band for the mutant and 2 bands for the respective control.

Table 6.16: PCR conditions and program for the amplification of Southern hybridization probes.

PCR condition	PCR program	
10 µl 5x Phusion HF buffer	98°C	30 s
5 µl DIG labeling mix (Roche)	98°C	10 s
0,5 µl Forward primer	60-72°C	30 s
0,5 µl Reverse primer	72°C	30 s/kb – 35 cycles
100 ng Plasmid DNA template	72°C	5-10 in
1 µl Phusion polymerase	4°C	∞
50 µl total volume		

6.7.11.2 Precipitation of digested DNA

After the restriction digest (see 6.7.10.3) a precipitation step was conducted by the addition of 20 µl 3 M sodium acetate (Mini III buffer) and 150 µl isopropanol (0.7 V). The reaction tubes were inverted several times and incubated at -20°C for 30 min. Subsequently, the reaction tubes were centrifuged at 13,000 rpm for 30 min at 4°C, the supernatant was discarded and the pellet was washed with 70% Ethanol and after vortexing again centrifuged at 13,000 rpm for 15 min at 4°C. After removing the Ethanol, the samples were centrifuged at 13,000 rpm for 1 min at 4 °C, and remaining Ethanol was removed using a yellow tip. Afterwards, the pellets were dried for 10 min before 20 µl of 1x TriTrack loading dye was added and the samples were dissolved in a thermo block at 37°C for 30 min at 650 rpm.

6.7.11.3 Blotting and detection of Southern blot

After the precipitation of the DNA, the samples were loaded on a freshly prepared 0.9% agarose gel containing ethidium bromide and ran for 2 h at 110 V in 1% TAE buffer to ensure a clear separation of the DNA. To compare the sizes, 2.5 µl of a 1 kb DNA Ladder (Thermo Fisher

Scientific, Waltham, USA) was used. After 2 h, the gel was visualized using UV radiation in a gel documentation unit (Peqlab/VWR, Radnor, USA) and transferred upside down (slots down) into a small bowl containing 0.125 M HCl for depurination for 15 min until the bromphenol blue band of the loading dye turned yellow. Afterward, the HCl was discarded and replaced for 15 min by Southern transfer buffer until the loading dye front was blue again before the gel was incubated for 30 min in a renaturation buffer. For blotting, 20x SSC buffer was used. Therefore, a bridge of Whatman paper (1 gel: 38 cm x 12 cm; 2 gels: 38 cm x 24 cm) and 5 Whatman paper per gel (10 cm x 12 cm) were wetted in 20x SSC buffer and stacked (see Figure 6.1). For blotting of the DNA overnight a transfer membrane ROTI®Nylon plus (Roth) (10 cm x 12 cm) was used. On the next day, the blot was carefully removed from the gel and the DNA was cross-linked in an ultraviolet cross-linker for 2.5 min (Amersham Biosciences, Little Chalfont, UK) before the membrane was incubated in 20-30 ml hybridization buffer in a hybridization oven (UVP HB-1000 Hybridizer, Ultra-violet products Ltd., Cambridge, UK) with turning at 65 °C for 1.5 - 2 h. For the detection of nucleic acids digoxigenin (DIG)- labeled DNA probes were used (see 6.7.11.1). DIG-labeled PCR products were added to 45 ml hybridization buffer and boiled for 15 min for denaturation. The membrane was incubated in the probe-containing hybridization buffer in a hybridization oven with turning at 65 °C overnight. On the third day, the probe was collected for further use and the membrane was washed two times for 15 min with southern wash buffer at 65 °C. Afterwards, the membrane was then incubated in DIG wash buffer for 5 min at RT, before 50 ml DIG buffer 2 was added for 30 min at RT. The DIG buffer 2 was discarded and the membrane incubated in 50 ml antibody solution for 30 min at RT in the hybridization oven. Subsequently, the membrane was washed 2 times for 15 min with DIG wash buffer prior to equilibration of the membrane for 5 min with DIG buffer 3 at RT. Lastly, the membrane was incubated in a square petri dish with 2.5 ml CDP-star solution for 5-10 min (*U. maydis*: 5 min, *S. reilianum*: 10 min) at 37 °C, before the CDP-star was collected for further use using a blue pipette. The blot was detected in a ChemiDocTMMP (Bio-Rad Laboratories GmbH, Hercules; USA) using a signal accumulation mode for 1 to 600 s and the ImageLab program of Bio-Rad. All buffers used for Southern blot are listed in Table 6.17.

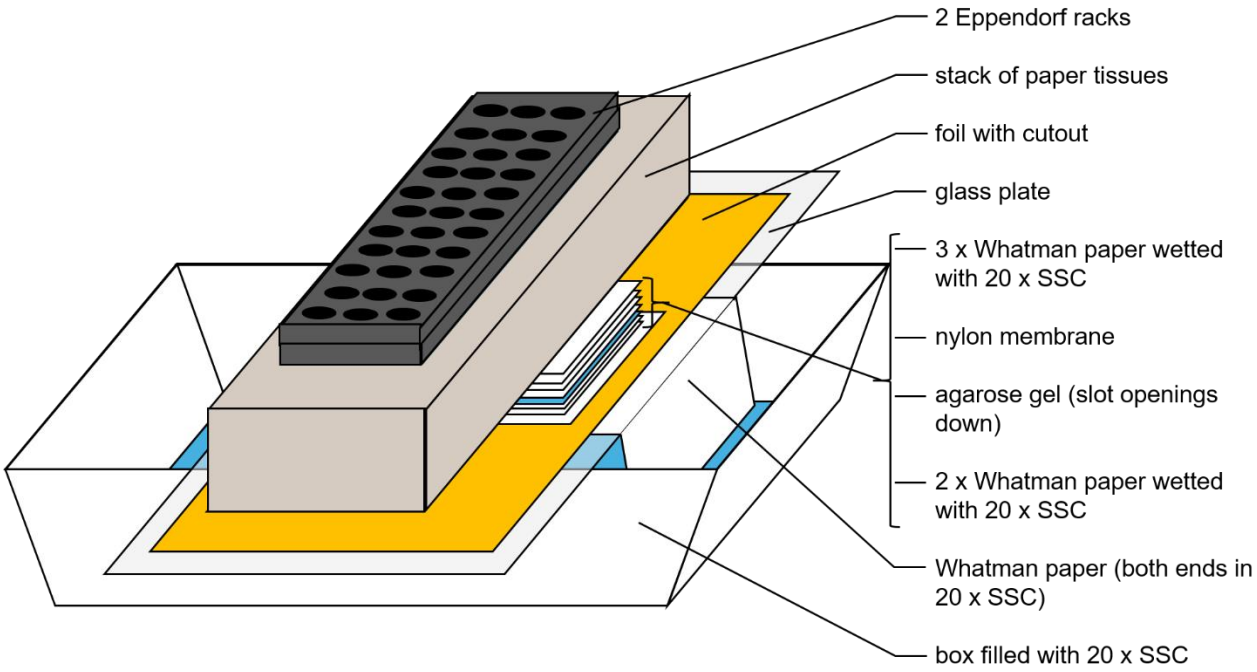

Figure 6.1: Assembly of Southern blot (Source: Bachelor thesis – Katharina Stein, AG Döhlemann).

Table 6.17: Buffers used for Southern blot.

Buffer/solution	Component	Amount
0.125 M HCl	HCl (37%)	1.04 % (v/v)
Transfer buffer	0.5 M NaOH 1.5 M NaCl	
Renaturation buffer	1,5 M NaCl 282 mM Tris-HCl 218 mM Tris base	
20 x SSC buffer	3 M NaCl 0.3 M Sodiumcitrate * $H_2O_{deoin.}$	17.53 % (w/v) 8.82 % (w/v)
Southern hybridization buffer	1 M $NaPO_4$, pH 7 20 % SDS	50 % (v/v) 35 % (v/v)
Southern wash buffer	1 M $NaPO_4$, pH 7 20 % SDS	10 % (v/v) 5 % (v/v)
DIG buffer 1	Maleic acid 5 M NaOH pH 7	1.16 % (w/v) 3 % (v/v)
DIG buffer 2	Skimmed milk powder DIG buffer 1	1 % (w/v) 99 % (v/v)
DIG buffer 3	1 M Tris-HCl, pH 9.5 5 M NaCl 1 M $MgCl_2$	10 % (v/v) 2 % (v/v) 5 % (v/v)
DIG wash buffer	Tween 20 DIG buffer 1	0.3 % (v/v) 99.7 % (v/v)
DIG antibody solution	Anti-DIG antibodies (150 U) DIG buffer 2	0.01 % (v/v) 99.99 % (v/v)
CDP star solution	CDP star DIG buffer 3	1 % (v/v) 99 % (v/v)

6.7.12 Total RNA extraction

For the isolation of total RNA, plant material was homogenized using liquid nitrogen, a mortar, and a pestle. ~200-500 mg of plant material was filled into a nuclease-free 2 ml reaction tube and frozen at -80 °C. For the extraction, the reaction tubes were taken from -80°C, and subsequently 1 ml of TRIzol™ Reagent was added. The reaction tubes were then incubated for 2 min on a Vibrax-VXR shaker (IKA, Staufen, Germany) at 2,500 rpm followed by an incubation for 5 min at RT. Afterward, 200 µl Chloroform was added and the samples were incubated again for 2 min on a Vibrax-VXR shaker. Reaction tubes were then spun down for phase separation for 15 min at 12.000 g and 4°C. After centrifugation, the upper/aqueous phase (600 µl) was transferred to a new 1.5 ml reaction tube, 400 µl of 100% Isopropanol was added, and the tubes were inverted several times and incubated for 10 min at RT. After incubation, the samples were centrifuged for 10 min at 12.000g at 4°C and the supernatant was discarded (Be careful to not lose the pellet!). Subsequently, 1 ml of 75% Ethanol (mixed with nuclease-free water) was added to the samples for washing, samples were vortexed and centrifuged for 10 min at 12.000 g at 4 °C. After discarding the Ethanol, another centrifugation for 10 min at 12.000 g and 4 °C was conducted and the remaining Ethanol was removed using a 200 µl pipette. After the pellets were dried for 10-15 min at RT, 50 µl of nuclease-free water was added to the pellet and the reaction tubes were incubated for 15 min at 55°C to dissolve the pellet. After dissolving the pellet, keep the RNA always on ice and proceed with DNase treatment (see 6.7.14; Invitrogen) or freeze it immediately at -80°C.

6.7.13 Sample preparation for RNA-seq

The sample preparation differences between the two RNA-seq analyses conducted in this study are further described in 6.7.13.1 and 6.7.13.2.

6.7.13.1 1st RNA-seq experiment: rUSH vs. wild type

For RNA sample preparation, the first cm after infection side was skipped and a 4 cm long section of the 3rd leaf (Figure) from more than 14 individual maize plants of 3 dpi and 6 dpi were collected for each sample. For the 20 h time point, the first cm after infection side was skipped and an around 1.5 – 2 cm long section of the 3rd leaf from more than 14 individual maize plants was collected for each sample. For the latex material, the 3rd leaf of at least 30 maize plants was fixated to the table to apply a thin layer of liquid latex on it. When the latex layer was dry, it was removed using a tweezer and subsequently frozen in liquid nitrogen. To generate biological replicates of infected samples, four plant infections were conducted from four independent plates

and fungal cultures. For each infection, more than 80 plants were inoculated for each pathogen. The compatible haploid *U. maydis* and *S. reilianum* cells from cultures with OD_{600} of 1 were spun down, suspended in water to reach an OD_{600} of 2, and mixed in a 1:1 ratio to get a final OD_{600} of 1 for infection. This was similarly done for rUSH infections, *U. maydis* strain FB1_Sra1b1_M3 was set to an OD_{600} of 2 and mixed 1:1 with the compatible mating partner SRZ2 of *S. reilianum* to a final OD_{600} of 1. Before infection, 0.1% of Tween was added to each culture. The plant tissues and latex material were ground to a fine powder using liquid nitrogen. Afterward, RNA samples were prepared using TRIZOL (Thermo Fisher, Waltham, USA) according to 0 (Total RNA extraction) and followed by DNase I digestion (Thermo Fisher, Waltham, USA).

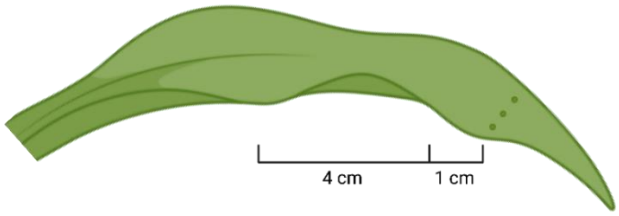

Figure 6.2: RNA sample preparation from infected maize leaves. Dots mark the infection side. The first centimeter of infected leaf area was skipped and the following 4 cm section was used for grinding and RNA extraction.

6.7.13.2 2nd RNA-seq analysis: Overexpression of *hdp2* in rUSH

The sample preparation was conducted as mentioned in 6.7.13.1 with slight modifications. A 4 cm long section of the 3rd leaf from 10 individual maize plants of 3 dpi was collected for each sample.

6.7.14 DNase treatment

To remove DNA contamination in the isolated RNA samples, a DNase I digest was conducted using the TURBO DNA-free™ Kit according to the manufacturer's instructions.

6.7.15 cDNA synthesis

cDNA synthesis was performed using the RevertAid H Minus First Strand cDNA Synthesis Kit, according to the manufacturer protocol. The cDNA was synthesized in a PCR thermocycler for 1 h at 42°C, followed by the inactivation at 70°C for 5 min.

6.7.16 Quantitative real time PCR

For the quantitative real-time PCR (qRT-PCR), the cDNA (see 6.7.15) was diluted 1:100 for each reaction using the GoTaq® qPCR Mastermix (Promega, Heidelberg, Germany) protocol as described by the manufacturer's instructions. 5 µl of diluted cDNA was added to each master mix

to achieve a total volume of 20 µl. All used qRT-PCR primers were tested in their efficiency using different dilutions of cDNA. The performed qRT-PCRs were carried out using an iCycler system (Bio-Rad, Hercules, USA) with the following program:

1. 95 °C - 2 min
2. 95 °C - 30 s - steps 2 to 4 were repeated in 45 cycles
3. 62 °C - 30 s
4. 72°C – 30 s

After the qRT-PCR, the melting curves were checked to confirm the specificity of the reaction. The threshold cycles were determined using the Bio-Rad CFX Manager™ software (version 3.1) and the relative expression values were calculated using the $2^{-\Delta Ct}$ method.

6.7.17 Ribonucleoprotein-mediated CRISPR/Cas9 in *S. reilianum*

sgRNA synthesis, *in vitro* cleavage assays, and the RNP formation for RNP-mediated transformation in *S. reilianum* were performed as described in (Werner *et al*., 2024) – BioProtocol (Chapter 2).

6.8 Protein and biochemical assays

6.8.1 Protein extraction from smut-infected maize leaves

To extract protein from infected maize leaves, a 4-cm section of the infected area (see Figure 6.2) was harvested and frozen in liquid nitrogen. The plant material was ground to fine powder using liquid nitrogen and around 1 mg was transferred into 2 ml reaction tubes (half full of powder). The samples can be at that point stored at -80°C or be used for the extraction. Therefore, 1.6 ml of extraction buffer (Table 6.19) was added, and the samples were vortexed and incubated for 30 min on ice. Afterward, the samples were centrifuged for 30 min at 13,300 rpm and 4°C, the supernatant was transferred to a new 2 ml reaction tube and centrifuged again for 30 min at 13,300 rpm and 4°C. 100 µl of the supernatant was mixed with 20 µl of 6x Lämmli buffer and boiled for 10 min at 95°C as input (IN) sample. To capture the protein of interest, HA-magnetic beads (Table 6.18) were equilibrated in a cold extraction buffer and collected using a magnetic rack (Dynamac 2) before the remaining supernatant from the previous step was transferred into the reaction tube containing the beads. The reaction tube with the extracted proteins and the beads were incubated at 4°C with constant rotation for 1-1.5 h. Afterward, the reaction tubes were placed on a magnetic rack for 2 min to capture the beads bound to the protein of interest, and the supernatant was discarded. The beads were washed four times with 800 µl extraction buffer, the

supernatant was discarded and 100 µl 2x loading dye was added. Subsequently, the samples were boiled for 10 min at 95°C, spun down, and placed again on a magnetic rack. 20 µl of the supernatant was loaded on an SDS gel.

Table 6.18: Used HA beads and antibody for the detection of tagged proteins in maize-infected samples.

HA pull-down	
Pierce™ Anti-HA Magnetic Beads	Thermo Scientific
HA-HRP antibody	Roche, 1:2000 dilution

Table 6.19: Composition of lysis buffer and sample buffer for protein extraction and loading.

Buffer	**Components**	**Amount**
Extraction buffer	Tris-HCl, pH: 8.5 NaCl Glycerol EDTA IGEPAL CA-630 DTT PMSF Pierce Protease Inhibitor	50 mM 150 mM 10 % (v/v) 10 mM 1 % 1 mM 1 mM 1 tablet/50 ml
2x Lämmli buffer	4% SDS 20% Glycerine 10% 2-Mercaptoethanol 0.004% Bromphenol blue 0.125 M Tris HCl, pH ca. 6.8.	4 % 20 % 10 % 0.004% 0.125 M

6.8.2 SDS polyacrylamide gel electrophoresis

To separate proteins in a sample based on their molecular weight sodium dodecyl sulfate-polyacrylamide gel electrophoresis (SDS-PAGE) was used according to (Laemmli, 1970). The SDS reagent binds to the proteins, unfolds them, and applies a negative charge. Further, a reducing agent dithiothreitol (DTT) is usually added to break the disulfide bonds of the proteins. The separation of proteins using an electric field occurs in a polyacrylamide medium. Thereby, the molecular weight determines the separation as well as the speed of the movement through the gel. While smaller proteins move faster, larger proteins encounter more resistance and move therefore slower. The SDS protein gels can be divided into two parts (Table 6.20), a stacking, and a resolving gel. The stacking gel ensures a gathering of all proteins at the before the demarcation line (80 V for 20 min). Afterwards, the machine is set to a constant voltage of 120 V for another 1.5 h. The resolving gel serves for the separation of the proteins based on their molecular weight. Depending on the protein size, the percentage of the resolving gel can vary between 8% and 15%. The samples were prepared in Lämmli Loading dye. To determine the molecular weight of

the proteins, PageRuler Prestained Protein Ladder (Thermo Fisher Scientific, Düsseldorf, Germany) was used.

Table 6.20 Composition of Resolving and stacking gel for 10% gels.

Solution	Components	Amount
Resolving gel	$H_2O_{deoin.}$	39.56 % (v/v)
	30 % Acrylamide	33.37 % (v/v)
	1.5 M Tris, pH 8.8	25.03 % (v/v)
	10 % SDS	1 % (v/v)
	10 % APS	1 % (v/v)
	TEMED	0.04 % (v/v)
Stacking gel	$H_2O_{deoin.}$	65.39 % (v/v)
	30 % Acrylamide	19.95 % (v/v)
	1.0 M Tris, pH 6.8	12.57 % (v/v)
	10 % SDS	1 % (v/v)
	10 % APS	1 % (v/v)
	TEMED	0.1 % (v/v)

6.8.3 Western Blot

For the detection of specific proteins separated by SDS-PAGE, a semi-dry Trans-Blot Turbo transfer system from Bio-Rad (Munich, Germany) was used to transfer the proteins on a nitrocellulose membrane. Therefore, the SDS gel as well as 2 Whatman papers (8.5 to 6.5 cm) were wetted in Western blot transfer buffer (Table 6.21) and the nitrocellulose membrane was activated for 3-5 min in 100% Methanol. For the assembly of the western blot, one Whatman paper is placed on the Trans-Blot system, followed by the membrane, the SDS gel, and another Whatman paper. Air bubbles were removed by rolling gently over the assembled stack before the gels were transferred to the machine for 30 min at 1.3 A and 25 V (for one gel) or 2.5 A and 25 V (for two gels). After blotting, the membrane was incubated for 1 h in a 3% blocking solution before the HA-HRP antibody was added for 1 h at RT or overnight at 4°C in the cold room. After 3 washing steps of 15 min using TBST, the western blot was detected using either SuperSignal™ West Pico PLUS Chemiluminescent Substrate or a 1:1 mixture of SuperSignal™ West Pico PLUS Chemiluminescent Substrate and SuperSignal™ West Femto Maximum Sensitivity Substrate (Thermo Fisher, USA) on a ChemiDoc™ MP machine (Bio-Rad, Hercules, USA).

Table 6.21: Buffers used for western blot.

Buffer	Composition
Western blot transfer buffer	25 mM Tris-HCl, pH 10.4 192 mM glycine 15 % (v/v) methanol
TBST	50 mM Tris-HCl, pH 7.5 150 mM NaCl 0.1 % (v/v) Tween 20
Blocking solution	3 % (v/v) skim milk powder in TBST
Antibody solution	3 % (v/v) skim milk powder in TBST+HA-HRP

6.8.4 Protein extraction from cell pellets using *in vitro* induction

Since the protein extraction from plant material was not successful for the TF Hdp2, the *in vitro* induction described by (Kretschmer *et al*., 2022) was used for the proof of expression. Therefore, a 3 ml $YEPS_{light}$ overnight culture was inoculated and incubated at 28°C and 200 rpm. On the next day, the OD_{600} of the fungal cultures was set to 0.3 and 0.8 in 5 ml minimal medium and minimal medium supplemented with glucose and malate for both mating partners. After setting the OD_{600}, the culture was spun down for 10 min at 3,500 rpm, the supernatant was discarded and the pellet was three times washed with 500 µl sterile minimal medium (Table 6.) by pipetting up and down with a cropped tip and a centrifugation of 10 min at 3,500rpm. Subsequently, the pellet was resolved in 5 ml sterile minimal medium (Table 6.22) or sterile minimal medium with glucose and malate and incubated for 72 h at 28°C and 200 rpm. After 72 h, 2 ml of the culture was centrifuged for 10 min at 3,500 rpm and the supernatant discarded. The pellet was washed twice with sterile $H_2O_{deoin.}$ and stored at -80 °C or immediately used for protein extraction (see 6.8.1).

Table 6.22: Media used for *in vitro* induction of effector gene expression.

Medium / solution	Components	Amount
Trace elements	H_3BO_4	0.006 % (w/v)
	$MnCl_2 * 4H_2O$	0.014 % (w/v)
	$ZnCl_2$	0.04 % (w/v)
	Na_2MoO_4	0.004 % (w/v)
	$FeCl_3 * 6H_2O$	0.01 % (w/v)
	$CuSO_4 * 5H_2O$	0.04 % (w/v)
Salt solution	KH_2PO_4	1.6 % (w/v)
	Na_2SO_4	0.4 % (w/v)
	KCl	0.8 % (w/v)
	$MgSO_4 * 7H_2O$	0.2 % (w/v)
	$CaCl_2 * 2H_2O$	0.1 % (w/v)
Minimal medium	NH_4NO_3	0.3 % (w/v)
	Salt solution	6.25 % (v/v)
	Trace elements	0.8 % (v/v)
	pH: 7	
Minimal medium with glucose and malate	NH_4NO_3	0.3 % (w/v)
	Salt solution	6.25 % (v/v)
	Trace elements	0.8 % (v/v)
	Glucose	1 % (w/v)
	Malate	0.5 % (w/v)
	pH: 7	

6.9 Plant assays using *Zea mays*

6.9.1 Cultivation of *Zea mays*

For infection assays of *U. maydis* the maize cultivar Golden Bantham was used, while for *S. reilianum*, an early flowering maize line Gaspe Flint was used. Maize was grown in a

greenhouse or phytochamber at 28 °C on a long day period (16 h light) with ~50% (greenhouse) or 40% (walk-in chamber) humidity, respectively, and an 8 h night period at 22 °C in VMV800 soil (Einheitserde®, Sinntal, Germany).

6.9.2 Smut infection of *Zea mays* seedlings

7-days old maize seedlings were infected with *U. maydis* or *S. reilianum* strains. Therefore, overnight cultures of the respective strains were inoculated in 10 ml $YEPS_{light}$ medium at 28°C and 200 rpm. On the next day, the cultures were diluted in 55 ml $YEPS_{light}$ medium to an OD_{600} of 0.2 (*U. maydis*) or 0.25 (*S. reilianum*), respectively, and shaken for 4.5-5 h at 28°C and 200 rpm. The OD600 was measured and set to 1 or 2 depending on the infection assay. When the solopathogenic strain SG200 was used, cultures were set to OD_{600} of 1, and for mating type partners such as FB1, FB2, SRZ1, and SRZ2 an OD_{600} of 2 was set, before the cultures were mixed 1:1 to reach a final OD_{600} of 1. Similarly, the mixture of the cultures for rUSH was conducted (Figure 6.3).

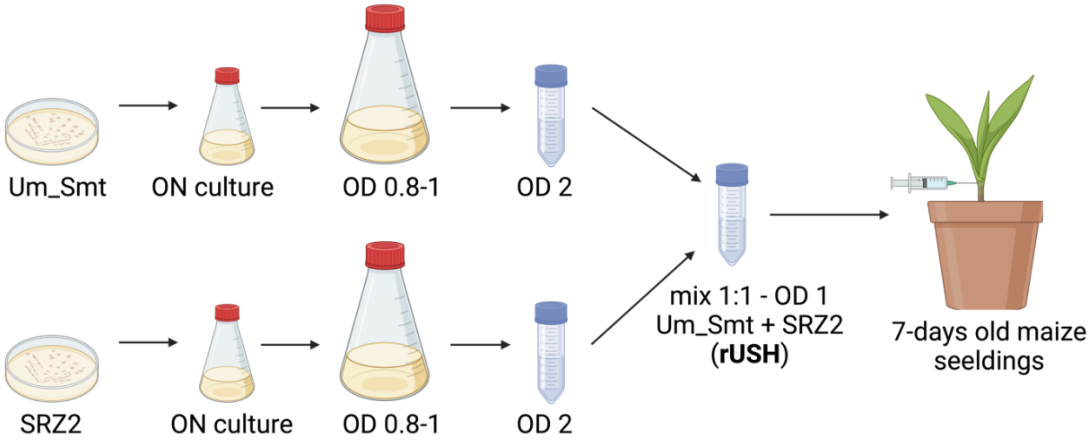

Figure 6.3: Infection of rUSH into maize seedlings. Strains were cultivated separately on PDA plates. For infection 10 ml $YEPS_{light}$ overnight cultures were inoculated with the fungal material and incubated overnight at 28°C and 200 rpm. On the next day, the OD_{600} was measured and set to an OD_{600} of 0.2 (*U. maydis*) or 0.25 (*S. reilianum*) and grown for 4-5 hours until a OD_{600} of 0.8 to 1 was reached. After centrifugation, the OD_{600} was set to 2 and the individual cultures of FB1_*Sra1b1* and SRZ2 were mixed 1:1 to a final OD_{600} of 1 for infection into 7-dyas old maize seedlings (Figure was created with BioRender).

6.9.3 Phenotype assessment of *U. maydis* infections

Virulence assays of *U. maydis* were performed as described in (Redkar & Doehlemann, 2016) and disease symptoms were classified as described in Table 6.23. The disease indexes were 9, 7, 5, 3, 1, and 0. These correspond to dead, heavy tumor, tumor, small tumor, chlorosis, and normal symptom, respectively. The number of infected plants of each replicate was multiplied by

the corresponding disease index, and the sum was divided by the total number of plants used for the replicate of infection to calculate an average disease index for each strain. Student's t-test was used to test the significance of the disease index from three biological replicates.

Table 6.23: Disease symptoms of *U. maydis* infected maize plants. Pictures were taken at 6 dpi. Pictures of no symptoms and death were taken by Katharina Stein.

Category	Description	Example
No symptoms	Plants without any symptoms	
Chlorosis	Plants without tumors but with discoloration	
Small tumor	Plants with small tumors	
Tumor	Plants with bigger tumors	
Heavy tumor	Plants with heavy tumors that affect the entire stalk	
Death	Dead plants	

6.9.4 Phenotype assessment of *S. reilianum* infections

Virulence assays of *S. reilianum* were conducted using the maize cultivar Gaspe Flint. 7-days old seedlings were infected with a syringe as described by (Redkar & Doehlemann, 2016). The disease symptoms were scored according to (Ghareeb *et al*., 2019; Figure 6.4).

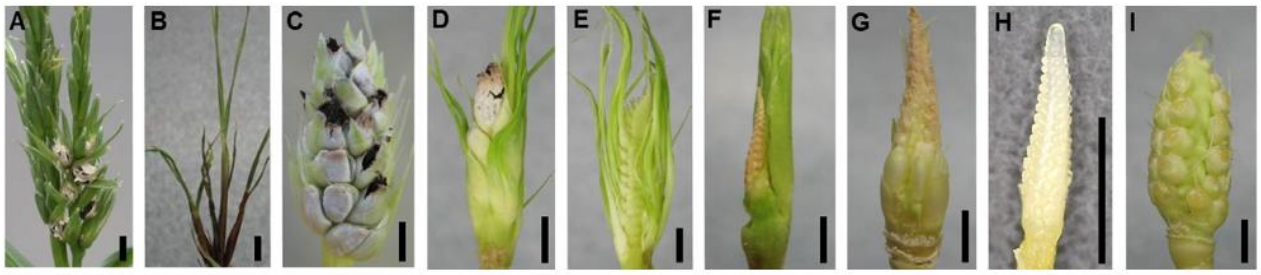

Figure 6.4: The assessment of the *S. reilianum* phenotype was performed as described by Ghareeb *et al*. (2019).

6.10 Microscopy

6.10.1 Fluorescence microscopy

For the observation of the formation of appressoria-like structures as well as for WGA-AlexaFlour 488 staining, a Nikon Eclipse Ti fluorescence microscope was used.

6.10.2 Confocal microscopy

To investigate the nuclear state of rUSH on charcoal plates (Day & Anagnostakis, 1971) and *in planta*, the confocal microscope Leica TCS SP8 Confocal Laser Scanning was used (Leica, Bensheim, Germany). GFP was excited at 488 nm and detected at 490-540 nm, while mCherry was excited at 561 nm and detected at 580-660 nm. The analysis of the microscopy pictures was performed using the Leica LAS X.Ink software.

6.11 Staining methods

6.11.1 Calcofluor white staining

For the observation of the formation of appressoria-like structures. Calcoflour white staining was performed. Therefore, infected maize-leaves were cut after 20-24 hpi. The leaves were cut and washed in $H_2O_{deion.}$ Afterwards, the leaves were incubated for 30-60 s in the Calcoflour working solution (1:100 dilution of the stock solution in 0.2 M Tris-HCl (pH 8.0). The working solution can be stored for 1 year in the fridge (4°C) in the dark. Subsequently, the leaves were washed again with H_2O_{deion} and observed using the DAPI filter of the Nikon Eclipse Ti Inverted microscope.

Calcofluor stock solution: 10 mg/ml (Fluorescent Brightener 28 in DMSO)

6.11.2 WGA staining

Fungal infected leaves were collected and destained in 100 % ethanol for 2 days at RT or 24 h at 37°C. For the staining, the leaves were incubated in 10 % KOH at 85 °C for 3 - 4 h, depending on the age of the leaves. Afterwards, the samples were washed with 1xPBS buffer (Table 6.24) until a pH of 7.4 was achieved (measurement with pH stripes). The leaf parts were vacuum infiltrated with the staining solution three times at 250 mbar containing WGA-AF488 (Wheat Germ Agglutinin, Alexa Flour 488) and propidium iodide for fungal and plant cell wall staining (Table 6.26; Doehlemann *et al*., 2009). The staining solution was collected and the samples were stored in the dark at 4 °C until microscopy. A Nikon Eclipse Ti Inverted microscope and the Nikon NIS-ELEMENTS software were used for microscopy. Pictures were taken with a HAMAMATSU camera. Filters with excitation 458 nm and emission 470 - 490 nm were used for WGA-AF488 and 561 nm excitation and 590 - 603 nm emission were used for propidium iodide observation.

Table 6.24: Composition of PBs buffer and WGA-AF488 staining solution.

Buffer/solution	Composition
10x PBS buffer	1.37 M NaCl 27 mM KCl 100 mM Na2HPO4: 18 mM KH2PO4: pH 7.4
Staining solution	20 µg/ml Propidium Iodide 10 µg/ml WGA-AF488 0.02 % Tween20 in 1x PBS (pH 7.4)

6.12 Bioinformatical analysis

6.12.1 Software

Sequences from *U. maydis* and *S. reilianum* were obtained from Ensembl Fungi (https://fungi.ensembl.org/index.html). Sequences were imported into Clone Manager 9 for further steps such as *in silico* cloning, planning of restriction digests and visualization of sequencing results. For qRT-PCR and the analysis of primer efficiency the software Bio-Rad CFX Manager™ (version 3.1) was used. For illustration of figures PowerPoint, Excel, BioRender and GraphPad Prism were used. The comparison of similarities in nucleotide as well as amino acid level was conducted using the National Center for Biotechnology Information (NCBI) and Clustal Omega. For motif enrichment analysis in the promoter region of effector orthologues, STREME was used. Scales and contrast for confocal microscopy pictures were adjusted using the Leica software LAS X.Ink. For fluorescence microscopy pictures the software Nikon Ti was used. Western and Southern blots were detected and analyzed using the Bio-Rad software Image Lab 5.2. For the design of sgRNAs, ECRISP or CHOPCHOP (https://chopchop.cbu.uib.no/) were used. For the visualization of RNA-seq data, R and Venny (Oliveros, 2007-2015; https://csbg.cnb.csic.es/BioinfoGP/venny.html) were used.

6.12.2 Availability of data

All generated data in this study are available on the internal server of the working group of Prof. Dr. Gunther Döhlemann. Upon publication, raw data of the RNA-seq will be available on GEO (Gene Expression Omnibus) at NCBI and released via GEO to the general public.

6.13 References

Aichinger, C., Hansson, K., Eichhorn, H., Lessing, F., Mannhaupt, G., Mewes, W., & Kahmann, R. (2003). Identification of plant-regulated genes in *Ustilago maydis* by enhancer-trapping mutagenesis. *Molecular Genetics and Genomics*, *270*(4), 303–314. https://doi.org/10.1007/s00438-003-0926-z

Day, P. R., & Anagnostakis, S. L. (1971). Corn Smut Dikaryon in Culture. *Nature New Biology*, *231*, 1971.

Doehlemann, G., Van Der Linde, K., Aßmann, D., Schwammbach, D., Hof, A., Mohanty, A., Jackson, D., & Kahmann, R. (2009). Pep1, a secreted effector protein of *Ustilago maydis*, is required for successful invasion of plant cells. *PLoS Pathogens*, *5*(2). https://doi.org/10.1371/journal.ppat.1000290

Ghareeb, H., Zhao, Y., & Schirawski, J. (2019). *Sporisorium reilianum* possesses a pool of effector proteins that modulate virulence on maize. *Molecular Plant Pathology*, *20*(1), 124–136. https://doi.org/10.1111/mpp.12744

Kretschmer, M., Damoo, D., Sun, S., Lee, C. W. J., Croll, D., Brumer, H., & Kronstad, J. (2022). Organic acids and glucose prime late-stage fungal biotrophy in maize. *Science*, *376*(6598), 1187–1191. https://doi.org/10.1126/science.abo2401

Laemmli, U. K. (1970). 227680a0. *Nature*, *227*, 680–685.

Redkar, A., & Doehlemann, G. (2016). *Ustilago maydis* Virulence Assays in Maize. *Bio-Protocol*, *6*, 1–7. https://doi.org/10.21769/BioProtoc.1760.http

Schuster, M., Schweizer, G., Reissmann, S., & Kahmann, R. (2016). Genome editing in *Ustilago maydis* using the CRISPR-Cas system. *Fungal Genetics and Biology*, *89*, 3–9. https://doi.org/10.1016/j.fgb.2015.09.001

Southern, E. M. (1975). Detection of specific sequences among DNA fragments separated by gel electrophoresis. 1975. *Biotechnology (Reading, Mass.)*, *98*, 503–517. https://doi.org/10.1016/b978-0-12-131200-8.50041-1

Werner, J., Zuo, W., & Doehlemann, G. (2024). CRISPR / Cas9 Ribonucleoprotein- Mediated Mutagenesis in *Sporisorium reilianum*. *14*, 1–10. https://doi.org/10.21769/BioProtoc.4978.2

Zuo, W., Depotter, J. R., & Doehlemann, G. (2020). Cas9HF1 enhanced specificity in *Ustilago maydis*. *Fungal Biology*, *124*(3–4), 228–234. https://doi.org/10.1016/j.funbio.2020.02.006

References - Chapter 1 and 5

Aerts, N., Pereira Mendes, M., & Van Wees, S. C. M. (2021). Multiple levels of crosstalk in hormone networks regulating plant defense. *Plant Journal*, *105*(2), 489–504. https://doi.org/10.1111/tpj.15124

Ahuja, M. R. (1998). Genetic tumors in *Nicotiana* and other plants. *Quarterly Review of Biology*, *73*(4), 439–462. https://doi.org/10.1086/420413

Albert, I., Hua, C., Nürnberger, T., Pruitt, R. N., & Zhang, L. (2020). Surface sensor systems in plant immunity. *Plant Physiology*, *182*(4), 1582–1596. https://doi.org/10.1104/PP.19.01299

Anderson, C. M., Willits, D. A., Kosted, P. J., Ford, E. J., Martinez-Espinoza, A. D., & Sherwood, J. E. (1999). Molecular analysis of the pheromone and pheromone receptor genes of *Ustilago hordei*. *Gene*, *240*(1), 89–97. https://doi.org/10.1016/S0378-1119(99)00428-X

Andrews, D. L., Egan, J. D., Mayorga, M. E., & Gold, S. E. (2000). The *Ustilago maydis* ubc4 and ubc5 genes encode members of a MAP kinase cascade required for filamentous growth. *Molecular Plant-Microbe Interactions*, *13*(7), 781–786. https://doi.org/10.1094/MPMI.2000.13.7.781

Arnold ML (1997) Natural hybridization and evolution, Oxford series in ecology and evolution. Oxford University Press, Oxford.

Bakkeren, G., Kämper, J., & Schirawski, J. (2008). Sex in smut fungi: Structure, function and evolution of mating-type complexes. *Fungal Genetics and Biology*, *45*(SUPPL. 1). https://doi.org/10.1016/j.fgb.2008.04.005

Bakkeren, G., & Kronstad, J. W. (1994). Linkage of mating-type loci distinguishes bipolar from tetrapolar mating in basidiomycetous smut fungi. *Proceedings of the National Academy of Sciences of the United States of America*, *91*(15), 7085–7089. https://doi.org/10.1073/pnas.91.15.7085

Bakkeren, G., & Kronstad, J. W. (1996). The pheromone cell signaling components of the *Ustilago* a mating-type loci determine intercompatibility between species. *Genetics*, *143*(4), 1601–1613.

Bakkeren, G., Kronstad, J. W., & Lévesque, C. A. (2000). Comparison of AFLP fingerprints and ITS sequences as phylogenetic markers in Ustilaginomycetes. *Mycologia*, *92*(3), 510–521. https://doi.org/10.1080/00275514.2000.12061187

Bari, R., & Jones, J. D. G. (2009). Role of plant hormones in plant defence responses. *Plant Molecular Biology*, *69*(4), 473–488. https://doi.org/10.1007/s11103-008-9435-0

Barr, C. M., Neiman, M., & Taylor, D. R. (2005). Inheritance and recombination of mitochondrial genomes in plants, fungi and animals. *New Phytologist*, *168*(1), 39–50. https://doi.org/10.1111/j.1469-8137.2005.01492.x

Barton, N. H. (2001). The role of hybridization in evolution. *Molecular Ecology*, *10*(3), 551–568. https://doi.org/10.1046/j.1365-294X.2001.01216.x

Basse, C. W. (2010). Mitochondrial inheritance in fungi. *Current Opinion in Microbiology*, *13*(6), 712–719. https://doi.org/10.1016/j.mib.2010.09.003

Begerow, D., Göker, M., Lutz, M., & Stoll, M. (2004). On the evolution of smut fungi on their hosts. *Frontiers in basidiomycote mycology*, 81-98.

Behling, A. H., Winter, D. J., Ganley, A. R. D., & Cox, M. P. (2022). Cross-kingdom transcriptomic trends in the evolution of hybrid gene expression. *Evolutionary Biology*, *35*, 1126–1137.

Bell, G. D. M., Kane, N. C., Rieseberg, L. H., & Adams, K. L. (2013). RNA-seq analysis of allele-specific expression, hybrid effects, and regulatory divergence in hybrids compared with their parents from natural populations. *Genome Biology and Evolution*, *5*(7), 1309–1323. https://doi.org/10.1093/gbe/evt072

Benevenuto, J., Teixeira-Silva, N. S., Kuramae, E. E., Croll, D., & Monteiro-Vitorello, C. B. (2018). Comparative genomics of smut pathogens: Insights from orphans and positively selected genes into host specialization. *Frontiers in Microbiology*, *9*(APR), 1–17. https://doi.org/10.3389/fmicb.2018.00660

Bentham, A. R., de la Concepcion, J. C., Mukhi, N., Zdrzałek, R., Draeger, M., Gorenkin, D., Hughes, R. K., & Banfield, M. J. (2020). A molecular roadmap to the plant immune system. *Journal of Biological Chemistry*, *295*(44), 14916–14935. https://doi.org/10.1074/jbc.REV120.010852

Bindics, J., Khan, M., Uhse, S., Kogelmann, B., Baggely, L., Reumann, D., Ingole, K. D., Stirnberg, A., Rybecky, A., Darino, M., Navarrete, F., Doehlemann, G., & Djamei, A. (2022). Many ways to TOPLESS – manipulation of plant auxin signalling by a cluster of fungal effectors. *New Phytologist*, *236*(4), 1455–1470. https://doi.org/10.1111/nph.18315

Birchler, J. A., Yao, H., Chudalayandi, S., Vaiman, D., & Veitia, R. A. (2010). Heterosis. *Plant Cell*, *22*(7), 2105–2112. https://doi.org/10.1105/tpc.110.076133

Bobola, N., & Merabet, S. (2017). Homeodomain proteins in action: similar DNA binding preferences, highly variable connectivity. *Current Opinion in Genetics and Development*, *43*, 1–8. https://doi.org/10.1016/j.gde.2016.09.008

Bölker, M. (2001). *Ustilago maydis* - A valuable model system for the study of fungal dimorphism and virulence. *Microbiology*, *147*(6), 1395–1401. https://doi.org/10.1099/00221287-147-6-1395

Bölker, Michael, Genin, S., Lehmler, C., & Kahmann, R. (1995). Genetic regulation of mating and dimorphism in *Ustilago maydis*. *Canadian Journal of Botany*, *73*(S1), 320–325. https://doi.org/10.1139/b95-262

Bölker, Michael, Urban, M., & Kahmann, R. (1992). The *a* mating type locus of *U. maydis* specifies cell signaling components. *Cell*, *68*(3), 441–450. https://doi.org/10.1016/0092-8674(92)90182-C

Bortfeld, M., Auffarth, K., Kahmann, R., & Basse, C. W. (2004). The *Ustilago maydis* a2 mating-type locus genes *lga2* and *rga2* compromise pathogenicity in the absence of the mitochondrial p32 family protein Mrb1. *Plant Cell*, *16*(8), 2233–2248. https://doi.org/10.1105/tpc.104.022657

Bosch, J., Czedik-Eysenberg, A., Hastreiter, M., Khan, M., Güldener, U., & Djamei, A. (2019). Two is better than one: Studying *Ustilago bromivora-Brachypodium* compatibility by using a hybrid pathogen. *Molecular Plant-Microbe Interactions*, *32*(12), 1623–1634. https://doi.org/10.1094/MPMI-05-19-0148-R

Botet, R., & Keurentjes, J. J. B. (2020). The Role of Transcriptional Regulation in Hybrid Vigor. *Frontiers in Plant Science*, *11*(April), 1–9. https://doi.org/10.3389/fpls.2020.00410

Bourras, S., Praz, C. R., Spanu, P. D., & Keller, B. (2018). Cereal powdery mildew effectors: a complex toolbox for an obligate pathogen. *Current Opinion in Microbiology*, *46*, 26–33. https://doi.org/10.1016/j.mib.2018.01.018

Boutrot, F., & Zipfel, C. (2017). Function, Discovery, and Exploitation of Plant Pattern Recognition Receptors for Broad-Spectrum Disease Resistance. *Annual Review of Phytopathology*, *55*, 257–286. https://doi.org/10.1146/annurev-phyto-080614-120106

Brachmann, A., Weinzierl, G., Kämper, J., & Kahmann, R. (2001). Identification of genes in the bW/bE regulatory cascade in *Ustilago maydis*. *Molecular Microbiology*, *42*(4), 1047–1063. https://doi.org/10.1046/j.1365-2958.2001.02699.x

Brasier, C. (2000). The rise of the hybrid fungi. *Nature*, *405*(6783), 134–135. https://doi.org/10.1038/35012193

Brasier, C. M. (2001). Rapid evolution of introduced plant pathogens via interspecific Hybridization. *BioScience*, *51*(2), 123–133. https://doi.org/10.1641/0006-3568

Brefort, T., Tanaka, S., Neidig, N., Doehlemann, G., Vincon, V., & Kahmann, R. (2014). Characterization of the Largest Effector Gene Cluster of *Ustilago maydis*. *PLoS Pathogens*, *10*(7). https://doi.org/10.1371/journal.ppat.1003866

Callaghan, S., & Guest, D. (2015). Globalisation, the founder effect, hybrid *Phytophthora* species and rapid evolution: new headaches for biosecurity. *Australasian Plant Pathology*, *44*(3), 255–262. https://doi.org/10.1007/s13313-015-0348-5

Cheung, H. Y. K., Donaldson, M. E., Storfie, E. R. M., Spence, K. L., Fetsch, J. L. O., Harrison, M. C., & Saville, B. J. (2021). Zfp1, a putative Zn(II)2Cys6 transcription factor, influences *Ustilago maydis* pathogenesis at multiple stages. *Plant Pathology*, *70*(7), 1626–1639. https://doi.org/10.1111/ppa.13398

Christensen JJ (1963) Corn smut caused by Ustilago maydis. Am Phytopathol Soc, St. Paul, MN.

Combes, M. C., Hueber, Y., Dereeper, A., Rialle, S., Herrera, J. C., & Lashermes, P. (2015). Regulatory divergence between parental alleles determines gene expression patterns in hybrids. *Genome Biology and Evolution*, *7*(4), 1110–1121. https://doi.org/10.1093/gbe/evv057

Couto, D., & Zipfel, C. (2016). Regulation of pattern recognition receptor signalling in plants. *Nature Reviews Immunology*, *16*(9), 537–552. https://doi.org/10.1038/nri.2016.77

Cox, M. P., Dong, T., Shen, G. G., Dalvi, Y., Scott, D. B., & Ganley, A. R. D. (2014). An Interspecific Fungal Hybrid Reveals Cross-Kingdom Rules for Allopolyploid Gene Expression Patterns. *PLoS Genetics*, *10*(3). https://doi.org/10.1371/journal.pgen.1004180

D'Angiolo, M., Chiara, M. De, Yue, J., Irizar, A., Persson, K., Llored, A., Barré, B., Schacherer, J., Marangoni, R., Angiolo, M., Chiara, M. De, Yue, J., Irizar, A., Stenberg, S., Angiolo, M. D., Chiara, M. De, Yue, J., Irizar, A., & Stenberg, S. (2020). A yeast living ancestor reveals the origin of genomic introgressions. *Nature*, *587*, 420–425.

Darino, M., Chia, K. S., Marques, J., Aleksza, D., Soto-Jiménez, L. M., Saado, I., Uhse, S., Borg, M., Betz, R., Bindics, J., Zienkiewicz, K., Feussner, I., Petit-Houdenot, Y., & Djamei, A. (2021). *Ustilago maydis* effector Jsi1 interacts with Topless corepressor, hijacking plant jasmonate/ethylene signaling. *New Phytologist*, *229*(6), 3393–3407. https://doi.org/10.1111/nph.17116

De Jonge, R., Esse, H. P. Van, Kombrink, A., Shinya, T., Desaki, Y., Bours, R., Krol, S. Van Der, Shibuya, N., Joosten, M. H. A. J., & Thomma, B. P. H. J. (2010). Conserved Fungal LysM Effector Ecp6 Prevents Chitin-Triggered Immunity in Plants. *Science*, *625*(1991), 6–9.

De Jonge, R., Van Esse, H. P., Maruthachalam, K., Bolton, M. D., Santhanam, P., Saber, M. K., Zhang, Z., Usami, T., Lievens, B., Subbarao, K. V., & Thomma, B. P. H. J. (2012). Tomato immune receptor Ve1 recognizes effector of multiple fungal pathogens uncovered by genome and RNA sequencing. *Proceedings of the National Academy of Sciences of the United States of America*, *109*(13), 5110–5115. https://doi.org/10.1073/pnas.1119623109

Dean, R., Van Kan, J. A. L., Pretorius, Z. A., Hammond-Kosack, K. E., Di Pietro, A., Spanu, P. D., Rudd, J. J., Dickman, M., Kahmann, R., Ellis, J., & Foster, G. D. (2012). The Top 10 fungal pathogens in molecular plant pathology. *Molecular Plant Pathology*, *13*(4), 414–430. https://doi.org/10.1111/j.1364-3703.2011.00783.x

DeFalco, T. A., & Zipfel, C. (2021). Molecular mechanisms of early plant pattern-triggered immune signaling. *Molecular Cell*, *81*(17), 3449–3467. https://doi.org/10.1016/j.molcel.2021.07.029

Depotter, J. R. L., & Doehlemann, G. (2020). Target the core: durable plant resistance against filamentous plant pathogens through effector recognition. *Pest Management Science*, *76*(2), 426–431. https://doi.org/10.1002/ps.5677

Derbyshire, M. C., & Raffaele, S. (2023). Till death do us pair: Co-evolution of plant–necrotroph interactions. *Current Opinion in Plant Biology*, *76*, 102457. https://doi.org/10.1016/j.pbi.2023.102457

Devier, B., Aguileta, G., Hood, M. E., & Giraud, T. (2009). Ancient trans-specific polymorphism at pheromone receptor genes in basidiomycetes. *Genetics*, *181*(1), 209–223. https://doi.org/10.1534/genetics.108.093708

Djamei, A., Schipper, K., Rabe, F., Ghosh, A., Vincon, V., Kahnt, J., Osorio, S., Tohge, T., Fernie, A. R., Feussner, I., Feussner, K., Meinicke, P., Stierhof, Y. D., Schwarz, H., MacEk, B., Mann, M., & Kahmann, R. (2011). Metabolic priming by a secreted fungal effector. *Nature*, *478*(7369), 395–398. https://doi.org/10.1038/nature10454

Djamei, A., Depotter; J., Saridis, G., Prokchorchik, M., Barghahn, S., ... (2023). Modulation of Host Immunity and Development by *Ustilago maydis*. In: Scott, B., Mesarich, C. (eds) Plant Relationships. The Mycota, vol 5. Springer, Cham. https://doi.org/10.1007/978-3-031-16503-0_1

Dodds, P. N., Chen, J., & Outram, M. A. (2024). Pathogen perception and signaling in plant immunity. *The Plant Cell*, 1–17. https://doi.org/10.1093/plcell/koae020

Dodds, P. N., & Rathjen, J. P. (2010). Plant immunity: Towards an integrated view of plant-pathogen interactions. *Nature Reviews Genetics*, *11*(8), 539–548. https://doi.org/10.1038/nrg2812

Dodueva, I. E., Lebedeva, M. A., Kuznetsova, K. A., Gancheva, M. S., Paponova, S. S., & Lutova, L. L. (2020). Plant tumors: a hundred years of study. *Planta*, *251*(4), 1–28. https://doi.org/10.1007/s00425-020-03375-5

Doehlemann, G., Van Der Linde, K., Aßmann, D., Schwammbach, D., Hof, A., Mohanty, A., Jackson, D., & Kahmann, R. (2009). Pep1, a secreted effector protein of *Ustilago maydis*, is required for successful invasion of plant cells. *PLoS Pathogens*, *5*(2). https://doi.org/10.1371/journal.ppat.1000290

Doehlemann, G., Wahl, R., Horst, R. J., Voll, L. M., Usadel, B., Poree, F., Stitt, M., Pons-Kühnemann, J., Sonnewald, U., Kahmann, R., & Kämper, J. (2008). Reprogramming a maize plant: Transcriptional and metabolic changes induced by the fungal biotroph *Ustilago maydis. Plant Journal*, *56*(2), 181-195. https://doi.org/10.1111/j.1365-313X.2008.03590.x

Doehlemann, G., Wahl, R., Vranes, M., de Vries, R. P., Kämper, J., & Kahmann, R. (2008). Establishment of compatibility in the *Ustilago maydis*/maize pathosystem. *Journal of Plant Physiology*, *165*(1), 29–40. https://doi.org/10.1016/j.jplph.2007.05.016

Dutheil, J. Y., Mannhaupt, G., Schweizer, G., Sieber, C. M. K., Münsterkötter, M., Güldener, U., Schirawski, J., & Kahmann, R. (2016). A tale of genome compartmentalization: The evolution of virulence clusters in smut fungi. *Genome Biology and Evolution*, *8*(3), 681–704. https://doi.org/10.1093/gbe/evw026

Elías-Villalobos, A., Barrales, R. R., & Ibeas, J. I. (2019). Chromatin modification factors in plant pathogenic fungi: Insights from *Ustilago maydis*. *Fungal Genetics and Biology*, *129*(June 2018), 52–64. https://doi.org/10.1016/j.fgb.2019.04.006

Elías-Villalobos, A., Fernández-Álvarez, A., Moreno-Sánchez, I., Helmlinger, D., & Ibeas, J. I. (2015). The Hos2 Histone Deacetylase Controls *Ustilago maydis* Virulence through Direct Regulation of Mating-Type Genes. In *PLoS Pathogens* (Vol. 11, Issue 8). https://doi.org/10.1371/journal.ppat.1005134

FAO - News Article: New standards to curb the global spread of plant pests and diseases (2019). https://www.fao.org/news/story/en/item/1187738/icode/

Fedler, M., Luh, K. S., Stelter, K., Nieto-Jacobo, F., & Basse, C. W. (2009). The *a2* mating-type locos genes *lga2* and *rga2* direct uniparental mitochondrial DNA (mtDNA) inheritance and constrain mtDNA recombination during sexual development of *Ustilago maydis*. *Genetics*, *181*(3), 847–860. https://doi.org/10.1534/genetics.108.096859

Flor-Parra, I., Vranes, M., Kämper, J., & Pérez-Martín, J. (2006). Biz1, a zinc finger protein required for plant invasion by *Ustilago maydis*, regulates the levels of a mitotic cyclin. *Plant Cell*, *18*(9), 2369-2387. https://doi.org/10.1105/tpc.106.042754

Gabaldón, T. (2020). Hybridization and the origin of new yeast lineages. *FEMS Yeast Research*, *20*(5), 1–8. https://doi.org/10.1093/femsyr/foaa040

García-Muse, T., Steinberg, G., & Pérez-Martín, J. (2003). Pheromone-induced G2 arrest in the phytopathogenic fungus *Ustilago maydis*. *Eukaryotic Cell*, *2*(3), 494–500. https://doi.org/10.1128/EC.2.3.494-500.2003

Gehrmann, T., Pelkmans, J. F., Ohm, R. A., Vos, A. M., Sonnenberg, A. S. M., Baars, J. J. P., Wösten, H. A. B., Reinders, M. J. T., & Abeel, T. (2018). Nucleus-specific expression in the multinuclear mushroom-forming fungus *Agaricus bisporus* reveals different nuclear regulatory programs. *Proceedings of the National Academy of Sciences of the United States of America*, *115*(17), 4429–4434. https://doi.org/10.1073/pnas.1721381115

Ghareeb, H., Becker, A., Iven, T., Feussner, I., & Schirawski, J. (2011). *Sporisorium reilianum* infection changes inflorescence and branching architectures of maize. *Plant Physiology*, *156*(4), 2037–2052. https://doi.org/10.1104/pp.111.179499

Ghareeb, H., Drechsler, F., Löfke, C., Teichmann, T., & Schirawski, J. (2015). SUPPRESSOR OF APICAL DOMINANCE1 of *Sporisorium reilianum* modulates inflorescence branching architecture in maize and arabidopsis. *Plant Physiology*, *169*(4), 2789–2804. https://doi.org/10.1104/pp.15.01347

Gillissen, B., Bergemann, J., Sandmann, C., Schroeer, B., Bölker, M., & Kahmann, R. (1992). A two-component regulatory system for self/non-self recognition in *Ustilago maydis*. *Cell*, *68*(4), 647–657. https://doi.org/10.1016/0092-8674(92)90141-X

Giordano, L., Sillo, F., Garbelotto, M., & Gonthier, P. (2018). Mitonuclear interactions may contribute to fitness of fungal hybrids. *Scientific Reports*, *8*(1), 1–7. https://doi.org/10.1038/s41598-018-19922-w

Glazebrook, J. (2005). Contrasting mechanisms of defense against biotrophic and necrotrophic pathogens. *Annual Review of Phytopathology*, *43*, 205–227. https://doi.org/10.1146/annurev.phyto.43.040204.135923

Grabenstein, K. C., & Taylor, S. A. (2018). Breaking Barriers: Causes, Consequences, and Experimental Utility of Human-Mediated Hybridization. *Trends in Ecology and Evolution*, *33*(3), 198–212. https://doi.org/10.1016/j.tree.2017.12.008

Grant, M., & Lamb, C. (2006). Systemic immunity. *Current Opinion in Plant Biology*, *9*(4), 414–420. https://doi.org/10.1016/j.pbi.2006.05.013

Greig, D., Louis, E. J., Borts, R. H., & Travisano, M. (2002). Hybrid speciation in experimental populations of yeast. *Science*, *298*(5599), 1773–1775. https://doi.org/10.1126/science.1076374

Groth, J. V. (1967). Parasitism of Barley by *Ustilago hordei* (Pers.) Lagerh.: some quantitative aspects of disease expression. *PhD Thesis, University of Brithish Columbia*.

Hacquard, S., Kracher, B., Maekawa, T., Vernaldi, S., Schulze-Lefert, P., & Van Themaat, E. V. L. (2013). Mosaic genome structure of the barley powdery mildew pathogen and conservation of transcriptional programs in divergent hosts. *Proceedings of the National Academy of Sciences of the United States of America*, *110*(24), 2219–2228. https://doi.org/10.1073/pnas.1306807110

Harris, W., Kim, S., Völz, R., & Lee, Y. H. (2023). Nuclear effectors of plant pathogens: Distinct strategies to be one step ahead. *Molecular Plant Pathology*, *24*(6), 637–650. https://doi.org/10.1111/mpp.13315

Hartmann, H. A., Kahmann, R., & Bölker, M. (1996). The pheromone response factor coordinates filamentous growth and pathogenicity in *Ustilago maydis*. *EMBO Journal*, *15*(7), 1632–1641. https://doi.org/10.1002/j.1460-2075.1996.tb00508.x

He, F., Zhang, X., Hu, J., Turck, F., Dong, X., Goebel, U., Borevitz, J., & De Meaux, J. (2012). Genome-wide analysis of *cis*-regulatory divergence between species in the Arabidopsis genus. *Molecular Biology and Evolution*, *29*(11), 3385–3395. https://doi.org/10.1093/molbev/mss146

Heimel, K., Scherer, M., Schuler, D., & Kämper, J. (2010a). The *Ustilago maydis* Clp1 protein orchestrates pheromone and b-dependent signaling pathways to coordinate the cell cycle and pathogenic development. *Plant Cell*, *22*(8), 2908–2922. https://doi.org/10.1105/tpc.110.076265

Heimel, K., Scherer, M., Vranes, M., Wahl, R., Pothiratana, C., Schuler, D., Vincon, V., Finkernagel, F., Flor-Parra, I., & Kämper, J. (2010b). The transcription factor rbf1 is the master regulator for b-mating type controlled pathogenic development in *Ustilago maydis*. *PLoS Pathogens*, *6*(8), 17–18. https://doi.org/10.1371/journal.ppat.1001035

Helariutta, Y., Fukaki, H., Wysocka-Diller, J., Nakajima, K., Jung, J., Sena, G., Hauser, M. T., & Benfey, P. N. (2000). The SHORT-ROOT gene controls radial patterning of the Arabidopsis root through radial signaling. *Cell*, *101*(5), 555–567. https://doi.org/10.1016/S0092-8674(00)80865-X

Hemetsberger, C., Herrberger, C., Zechmann, B., Hillmer, M., & Doehlemann, G. (2012). The *Ustilago maydis* effector Pep1 suppresses plant immunity by inhibition of host peroxidase activity. *PLoS Pathogens*, *8*(5). https://doi.org/10.1371/journal.ppat.1002684

Hemetsberger, C., Mueller, A. N., Matei, A., Herrberger, C., Hensel, G., Kumlehn, J., Mishra, B., Sharma, R., Thines, M., Hückelhoven, R., & Doehlemann, G. (2015). The fungal core effector Pep1 is conserved across smuts of dicots and monocots. *New Phytologist*, *206*(3), 1116–1126. https://doi.org/10.1111/nph.13304

Henry, S., Dievart, A., Divol, F., Pauluzzi, G., Meynard, D., Swarup, R., Wu, S., Gallagher, K. L., & Périn, C. (2017). SHR overexpression induces the formation of supernumerary cell layers with cortex cell identity in rice. *Developmental Biology*, *425*(1), 1–7. https://doi.org/10.1016/j.ydbio.2017.03.001

Hogenhout, S. A., Van Der Hoorn, R. A. L., Terauchi, R., & Kamoun, S. (2009). Emerging concepts in effector biology of plant-associated organisms. *Molecular Plant-Microbe Interactions*, *22*(2), 115–122. https://doi.org/10.1094/MPMI-22-2-0115

Holliday, R. (2004). Early studies on recombination and DNA repair in *Ustilago maydis*. *DNA Repair*, *3*(6), 671–682. https://doi.org/10.1016/j.dnarep.2004.02.002

Horbach, R., Navarro-Quesada, A. R., Knogge, W., & Deising, H. B. (2011). When and how to kill a plant cell: Infection strategies of plant pathogenic fungi. *Journal of Plant Physiology*, *168*(1), 51–62. https://doi.org/10.1016/j.jplph.2010.06.014

Hou, S., Liu, D., & He, P. (2021). Phytocytokines function as immunological modulators of plant immunity. *Stress Biology*, *1*(1), 1–14. https://doi.org/10.1007/s44154-021-00009-y

Hovhannisyan, H., Saus, E., Ksiezopolska, E., Gabaldón, T., Krogerus, K., Arvas, M., De Chiara, M., Magalhães, F., Mattinen, L., Oja, M., Vidgren, V., Yue, J. X., Liti, G., & Gibson, B. (2020). Ploidy influences the functional attributes of de novo lager yeast hybrids. *Applied Microbiology and Biotechnology*, *100*(3), 7203–7222. https://doi.org/10.1007/s00253-016-7588-3

Irieda, H., Inoue, Y., Mori, M., Yamada, K., Oshikawa, Y., Saitoh, H., Uemura, A., Terauchi, R., Kitakura, S., Kosaka, A., Singkaravanit-Ogawa, S., & Takano, Y. (2019). Conserved fungal effector suppresses PAMP-triggered immunity by targeting plant immune kinases. *Proceedings of the National Academy of Sciences of the United States of America*, *116*(2), 496–505. https://doi.org/10.1073/pnas.1807297116

Jones, J. D., & Dangl, J. L. (2006). The plant immune system. *nature*, *444*(7117), 323-329.

Jones, J. D. G., Staskawicz, B. J., & Dangl, J. L. (2024). The plant immune system: From discovery to deployment. *Cell*, *187*(9), 2095–2116. https://doi.org/10.1016/j.cell.2024.03.045

Jurca, M. (2021). Die Charakterisierung des Transkriptionsfaktors Hdp2 und dessen Rolle in der biotrophen Phase von *Ustilago maydis*. *PhD Thesis*.

Kaffarnik, F., Müller, P., Leibundgut, M., Kahmann, R., & Feldbrügge, M. (2003). PKA and MAPK phosphorylation of Prf1 allows promoter discrimination in *Ustilago maydis*. *EMBO Journal*, *22*(21), 5817–5826. https://doi.org/10.1093/emboj/cdg554

Kahmann, R., & Bölker, M. (1996). Self/nonself recognition in fungi: Old mysteries and simple solutions. *Cell*, *85*(2), 145–148. https://doi.org/10.1016/S0092-8674(00)81091-0

Kahmann, R., Steinberg, G., Basse, C. W., Feldbrügge, M., & Kämper, J. (2000). *Ustilago maydis*, the causative agent of corn smut disease. *Fungal Pathology*, 347–371.

Kämper, J. (2004). A PCR-based system for highly efficient generation of gene replacement mutants in *Ustilago maydis*. *Molecular Genetics and Genomics*, *271*(1), 103–110. https://doi.org/10.1007/s00438-003-0962-8

Kämper, Jörg, Kahmann, R., Bölker, M., Ma, L. J., Brefort, T., Saville, B. J., Banuett, F., Kronstad, J. W., Gold, S. E., Müller, O., Perlin, M. H., Wösten, H. A. B., De Vries, R., Ruiz-Herrera, J., Reynaga-Peña, C. G., Snetselaar, K., McCann, M., Pérez-Martín, J., Feldbrügge, M., … Birren, B. W. (2006). Insights from the genome of the biotrophic fungal plant pathogen *Ustilago maydis*. *Nature*, *444*(7115), 97–101. https://doi.org/10.1038/nature05248

Kazan, K., & Lyons, R. (2014). Intervention of phytohormone pathways by pathogen effectors. *Plant Cell*, *26*(6), 2285–2309. https://doi.org/10.1105/tpc.114.125419

Kohn, L. M. (2005). Mechanisms of fungal speciation. *Annual Review of Phytopathology*, *43*(11), 279–308. https://doi.org/10.1146/annurev.phyto.43.040204.135958

Kosted, P. J., Gerhardt, S. A., Anderson, C. M., Stierle, A., & Sherwood, J. E. (2000). Structural requirements for activity of the pheromones of *Ustilago hordei*. *Fungal Genetics and Biology*, *29*(2), 107–117. https://doi.org/10.1006/fgbi.2000.1191

Krogerus, K., Arvas, M., De Chiara, M., Magalhães, F., Mattinen, L., Oja, M., Vidgren, V., Yue, J. X., Liti, G., & Gibson, B. (2016). Ploidy influences the functional attributes of de novo lager yeast hybrids. *Applied Microbiology and Biotechnology*, *100*(16), 7203–7222. https://doi.org/10.1007/s00253-016-7588-3

Kronstad, J W, & Staben, C. (1997). CSF7254037.pdf. *Annual Review of Genetics*, *31*, 275–276.

Kronstad, James W., & Leong, S. A. (1990). The *b* mating-type locus of *Ustilago maydis* contains variable and constant regions. *Genes and Development*, *4*(8), 1384–1395. https://doi.org/10.1101/gad.4.8.1384

Kroon, L. P. N. M., Brouwer, H., De Cock, A. W. A. M., & Govers, F. (2012). The genus *Phytophthora* anno 2012. *Phytopathology*, *102*(4), 348–364. https://doi.org/10.1094/PHYTO-01-11-0025

Kües, U. (2000). Life History and Developmental Processes in the Basidiomycete *Coprinus cinereus* . *Microbiology and Molecular Biology Reviews*, *64*(2), 316–353. https://doi.org/10.1128/mmbr.64.2.316-353.2000

Landry, C. R., Hartl, D. L., & Ranz, J. M. (2007). Genome clashes in hybrids: Insights from gene expression. *Heredity*, *99*(5), 483–493. https://doi.org/10.1038/sj.hdy.6801045

Lanver, D., Berndt, P., Tollot, M., Naik, V., Vranes, M., Warmann, T., Münch, K., Rössel, N., & Kahmann, R. (2014). Plant Surface Cues Prime *Ustilago maydis* for Biotrophic Development. *PLoS Pathogens*, *10*(7). https://doi.org/10.1371/journal.ppat.1004272

Lanver, D., Mendoza-Mendoza, A., Brachmann, A., & Kahmann, R. (2010). Sho1 and Msb2-related proteins regulate appressorium development in the smut fungus *Ustilago maydis*. *Plant Cell*, *22*(6), 2085–2101. https://doi.org/10.1105/tpc.109.073734

Lanver, D., Müller, A. N., Happel, P., Schweizer, G., Haas, F. B., Franitza, M., Pellegrin, C., Reissmann, S., Altmüller, J., Rensing, S. A., & Kahmann, R. (2018). The biotrophic development of *Ustilago maydis* studied by RNA-seq analysis. *Plant Cell*, *30*(2), 300–323. https://doi.org/10.1105/tpc.17.00764

Lanver, D., Tollot, M., Schweizer, G., Lo Presti, L., Reissmann, S., Ma, L. S., Schuster, M., Tanaka, S., Liang, L., Ludwig, N., & Kahmann, R. (2017). *Ustilago maydis* effectors and their impact on virulence. *Nature Reviews Microbiology*, *15*(7), 409–421. https://doi.org/10.1038/nrmicro.2017.33

Laurie, J. D., Ali, S., Linning, R., Mannhaupt, G., Wong, P., Güldener, U., Münsterkötter, M., Moore, R., Kahmann, R., Bakkeren, G., & Schirawski, J. (2012). Genome comparison of barley and maize smut fungi reveals targeted loss of RNA silencing components and species-specific presence of transposable elements. *Plant Cell*, *24*(5), 1733–1745. https://doi.org/10.1105/tpc.112.097261

Lee, B. H., Ko, J. H., Lee, S., Lee, Y., Pak, J. H., & Kim, J. H. (2009). The Arabidopsis GRF-Interacting Factor gene family performs an overlapping function in determining organ size as well as multiple. *Plant Physiology*, *151*(2), 655–668. https://doi.org/10.1104/pp.109.141838

León-Ramírez, C. G., Sánchez-Arreguín, J. A., & Ruiz-Herrera, J. (2014). *Ustilago maydis*, a Delicacy of the Aztec Cuisine and a Model for Research. *Natural Resources*, *05*(06), 256–267. https://doi.org/10.4236/nr.2014.56024

Li, G., Dulal, N., Gong, Z., & Wilson, R. A. (2023). Unconventional secretion of *Magnaporthe oryzae* effectors in rice cells is regulated by tRNA modification and codon usage control. *Nature Microbiology*, *8*(9), 1706–1716. https://doi.org/10.1038/s41564-023-01443-6

Li, H., Wang, H., Jing, M., Zhu, J., Guo, B., Wang, Y., Lin, Y., Chen, H., Kong, L., Ma, Z., Wang, Y., Ye, W., Dong, S., Tyler, B., & Wang, Y. (2018). A *Phytophthora* effector recruits a host cytoplasmic transacetylase into nuclear speckles to enhance plant susceptibility. *ELife*, *7*, 1–23. https://doi.org/10.7554/eLife.40039

Li, M., Zheng, Y., Cui, D., Du, Y., Zhang, D., Sun, W., Du, H., & Zhang, Z. (2022). GIF1 controls ear inflorescence architecture and floral development by regulating key genes in hormone biosynthesis and meristem determinacy in maize. *BMC Plant Biology*, *22*(1), 1–15. https://doi.org/10.1186/s12870-022-03517-9

Li, W., Metin, B., White, T. C., & Heitman, J. (2010). Organization and evolutionary trajectory of the mating type (MAT) locus in dermatophyte and dimorphic fungal pathogens. *Eukaryotic Cell*, *9*(1), 46–58. https://doi.org/10.1128/EC.00259-09

Lin, J. S., Happel, P., & Kahmann, R. (2021). Nuclear status and leaf tumor formation in the *Ustilago maydis*–maize pathosystem. *New Phytologist*, *231*(1), 399–415. https://doi.org/10.1111/nph.17377

Liu, W., Zhou, X., Li, G., Li, L., Kong, L., Wang, C., Zhang, H., & Xu, J. R. (2011). Multiple plant surface signals are sensed by different mechanisms in the rice blast fungus for appressorium formation. *PLoS Pathogens*, *7*(1). https://doi.org/10.1371/journal.ppat.1001261

Lo Presti, L., Lanver, D., Schweizer, G., Tanaka, S., Liang, L., Tollot, M., Zuccaro, A., Reissmann, S., & Kahmann, R. (2015). Fungal effectors and plant susceptibility. *Annual Review of Plant Biology*, *66*, 513–545. https://doi.org/10.1146/annurev-arplant-043014-114623

Ludwig, N., Reissmann, S., Schipper, K., Gonzalez, C., Assmann, D., Glatter, T., Moretti, M., Ma, L. S., Rexer, K. H., Snetselaar, K., & Kahmann, R. (2021). A cell surface-exposed protein complex with an essential virulence function in *Ustilago maydis*. *Nature Microbiology*, *6*(6), 722–730. https://doi.org/10.1038/s41564-021-00896-x

Ma, L. S., Wang, L., Trippel, C., Mendoza-Mendoza, A., Ullmann, S., Moretti, M., Carsten, A., Kahnt, J., Reissmann, S., Zechmann, B., Bange, G., & Kahmann, R. (2018). The *Ustilago maydis* repetitive effector Rsp3 blocks the antifungal activity of mannose-binding maize proteins. *Nature Communications*, *9*(1). https://doi.org/10.1038/s41467-018-04149-0

Ma, Y., & Johnson, K. (2023). Arabinogalactan proteins – Multifunctional glycoproteins of the plant cell wall. *The Cell Surface*, *9*(January), 100102. https://doi.org/10.1016/j.tcsw.2023.100102

Macho, A. P., & Zipfel, C. (2014). Plant PRRs and the activation of innate immune signaling. *Molecular Cell*, *54*(2), 263–272. https://doi.org/10.1016/j.molcel.2014.03.028

Mack, K. L., & Nachman, M. W. (2017). Gene Regulation and Speciation. *Trends in Genetics*, *33*(1), 68–80. https://doi.org/10.1016/j.tig.2016.11.003

Mallet, J. (2005). Hybridization as an invasion of the genome. *Trends in Ecology and Evolution*, *20*(5), 229–237. https://doi.org/10.1016/j.tree.2005.02.010

Mallet, J. (2007). Hybrid speciation. *Nature*, *446*(7133), 279–283. https://doi.org/10.1038/nature05706

Malumbres, M., & Barbacid, M. (2009). Cell cycle, CDKs and cancer: A changing paradigm. *Nature Reviews Cancer*, *9*(3), 153–166. https://doi.org/10.1038/nrc2602

Martínez-Espinoza, A. D., García-Pedrajas, M. D., & Gold, S. E. (2002). The Ustilaginales as plant pests and model systems. *Fungal Genetics and Biology*, *35*(1), 1–20. https://doi.org/10.1006/fgbi.2001.1301

Martinez, C., Roux, C., & Dargent, R. (1999). Biotrophic development of *Sporisorium reilianum f. sp. zeae* in vegetative shoot apex of maize. *Phytopathology*, *89*(3), 247–253. https://doi.org/10.1094/PHYTO.1999.89.3.247

Matei, A., Ernst, C., Günl, M., Thiele, B., Altmüller, J., Walbot, V., Usadel, B., & Doehlemann, G. (2018). How to make a tumour: cell type specific dissection of *Ustilago maydis*-induced tumour development in maize leaves. *New Phytologist*, *217*(4), 1681-1695.

Mayorga, M. E., & Gold, S. E. (2001). The *ubc2* gene of *Ustilago maydis* encodes a putative novel adaptor protein required for filamentous growth, pheromone response and virulence. *Molecular Microbiology*, *41*(6), 1365–1379. https://doi.org/10.1046/j.1365-2958.2001.02606.x

McQueen-Mason, S., Durachko, D. M., & Cosgrove, D. J. (1992). Two endogenous proteins that induce cell wall extension in plants. *Plant Cell*, *4*(11), 1425–1433. https://doi.org/10.1105/tpc.4.11.1425

Meyerowitz, E. M. (2002). Comparative genomics. Plants compared to animals: The broadest comparative study of development. *Science*, *295*(5559), 1482–1485. https://doi.org/10.1126/science.1066609

Misas Villamil, J. C., Mueller, A. N., Demir, F., Meyer, U., Ökmen, B., Schulze Hüynck, J., Breuer, M., Dauben, H., Win, J., Huesgen, P. F., & Doehlemann, G. (2019). A fungal substrate mimicking molecule suppresses plant immunity via an inter-kingdom conserved motif. *Nature Communications*, *10*(1). https://doi.org/10.1038/s41467-019-09472-8

Mixao, V., & Gabaldón, T. (2018). Hybridization and emergence of virulence in opportunistic human yeast pathogens. *Yeast*, 5–20. https://doi.org/10.1002/yea

Morrow, C. A., & Fraser, J. A. (2009). Sexual reproduction and dimorphism in the pathogenic basidiomycetes. *FEMS Yeast Research*, *9*(2), 161–177. https://doi.org/10.1111/j.1567-1364.2008.00475.x

Mueller, A. N., Ziemann, S., Treitschke, S., Aßmann, D., & Doehlemann, G. (2013). Compatibility in the *Ustilago maydis*-Maize Interaction Requires Inhibition of Host Cysteine Proteases by the Fungal Effector Pit2. *PLoS Pathogens*, *9*(2). https://doi.org/10.1371/journal.ppat.1003177

Müller, P., Aichinger, C., Feldbrügge, M., & Kahmann, R. (1999). The MAP kinase Kpp2 regulates mating and pathogenic development in *Ustilago maydis*. *Molecular Microbiology*, *34*(5), 1007–1017. https://doi.org/10.1046/j.1365-2958.1999.01661.x

Müller, P., Weinzierl, G., Brachmann, A., Feldbrügge, M., & Kahmann, R. (2003). Mating and Pathogenic Development of the Smut Fungus *Ustilago maydis* Are Regulated by One Mitogen-Activated Protein Kinase Cascade. *Eukaryotic Cell*, *2*(6), 1187–1199. https://doi.org/10.1128/EC.2.6.1187-1199.2003

Nakajima, K., Sena, G., Nawy, T., & Benfey, P. N. (2001). Intercellular movement of the putative transcription factor SHR in root patterning. *Nature*, *413*(6853), 307–311. https://doi.org/10.1038/35095061

Navarrete, F., Gallei, M., Kornienko, A. E., Saado, I., Khan, M., Chia, K. S., Darino, M. A., Bindics, J., & Djamei, A. (2022). TOPLESS promotes plant immunity by repressing auxin signaling and is targeted by the fungal effector Naked1. *Plant Communications*, *3*(2), 100269. https://doi.org/10.1016/j.xplc.2021.100269

Ngou, B. P. M., Ding, P., & Jones, J. D. G. (2022). Thirty years of resistance: Zig-zag through the plant immune system. *Plant Cell*, *34*(5), 1447–1478. https://doi.org/10.1093/plcell/koac041

Ngou, B. P. M., Jones, J. D. G., & Ding, P. (2022). Plant immune networks. *Trends in Plant Science*, *27*(3), 255–273. https://doi.org/10.1016/j.tplants.2021.08.012

O'Connell, R. J., Thon, M. R., Hacquard, S., Amyotte, S. G., Kleemann, J., Torres, M. F., Damm, U., Buiate, E. A., Epstein, L., Alkan, N., Altmüller, J., Alvarado-Balderrama, L., Bauser, C. A., Becker, C., Birren, B. W., Chen, Z., Choi, J., Crouch, J. A., Duvick, J. P., … Vaillancourt, L. J. (2012). Lifestyle transitions in plant pathogenic *Colletotrichum* fungi deciphered by genome and transcriptome analyses. *Nature Genetics*, *44*(9), 1060–1065. https://doi.org/10.1038/ng.2372

Ohm, R. A., De Jong, J. F., Lugones, L. G., Aerts, A., Kothe, E., Stajich, J. E., De Vries, R. P., Record, E., Levasseur, A., Baker, S. E., Bartholomew, K. A., Coutinho, P. M., Erdmann, S., Fowler, T. J., Gathman, A. C., Lombard, V., Henrissat, B., Knabe, N., Kües, U., … Wösten, H. A. B. (2010). Genome sequence of the model mushroom *Schizophyllum commune*. *Nature Biotechnology*, *28*(9), 957–963. https://doi.org/10.1038/nbt.1643

Ökmen, B., Etalo, D. W., Joosten, M. H. A. J., Bouwmeester, H. J., de Vos, R. C. H., Collemare, J., & De Wit, P. J. G. M. (2013). Detoxification of α-tomatine by *Cladosporium fulvum* is required for full virulence on tomato. *New Phytologist*, *198*(4), 1203–1214. https://doi.org/10.1111/nph.12208

Olson, Å, & Stenlid, J. (2001). Mitochondrial control of fungal hybrid virulence. *Nature*, *411*(6836), 438. https://doi.org/10.1038/35078147

Olson, Åke, & Stenlid, J. (2002). Pathogenic fungal species hybrids infecting plants. *Microbes and Infection*, *4*(13), 1353–1359. https://doi.org/10.1016/S1286-4579(02)00005-9

Perez-Nadales, E., & Di Pietro, A. (2015). The transmembrane protein Sho1 cooperates with the mucin Msb2 to regulate invasive growth and plant infection in *Fusarium oxysporum*. *Molecular plant pathology*, *16*(6), 593-603.

Priyashantha, A. K. H., Dai, D.-Q., Bhat, D. J., Stephenson, S. L., Promputtha, I., Kaushik, P., Tibpromma, S., & Karunarathna, S. C. (2023). Plant–Fungi Interactions: Where It Goes? *Biology*, *12*(6), 809. https://doi.org/10.3390/biology12060809

Redkar, A., Villajuana-Bonequi, M., & Doehlemann, G. (2015). Conservation of the *Ustilago maydis* effector See1 in related smuts. *Plant Signaling and Behavior*, *10*(12), 1–5. https://doi.org/10.1080/15592324.2015.1086855

Reineke, G., Heinze, B., Schirawski, J., Buettner, H., Kahmann, R., & Basse, C. W. (2008). Indole-3-acetic acid (IAA) biosynthesis in the smut fungus *Ustilago maydis* and its relevance for increased IAA levels in infected tissue and host tumour formation. *Molecular plant pathology*, *9*(3), 339-355.

Remick, B. C., Gaidt, M. M., & Vance, R. E. (2023). Effector-triggered immunity. *Annual Review of Immunology*, *41*, 453-481.

Renaudin, J. P., Doonan, J. H., Freeman, D., Hashimoto, J., Hirt, H., Inzé, D., Jacobs, T., Kouchi, H., Rouzé, P., Sauter, M., Savouré, A., Sorrell, D. A., Sundaresan, V., & Murray, J. A. H. (1996). Plant cyclins: A unified nomenclature for plant A-, B- and D-type cyclins based on sequence organization. *Plant Molecular Biology*, *32*(6), 1003–1018. https://doi.org/10.1007/BF00041384

Romeis, T., Brachmann, A., Kahmann, R., & Kämper, J. (2000). Identification of a target gene for the bE-bW homeodomain protein complex in *Ustilago maydis*. *Molecular Microbiology*, *37*(1), 54–66. https://doi.org/10.1046/j.1365-2958.2000.01978.x

Rooney, H. C. E., Van, J. W., t Klooster, van der Hoorn, R. A. L., Joosten, M. H. A. J., Jones, J. D. G., & de Wit, P. J. G. M. (2005). *Cladosporium* Avr2 Inhibits Tomato Rcr3 Protease Required for Cf-2-Dependent Disease Resistance. *Science*, *308*(5729), 1783 LP – 1786. http://science.sciencemag.org/content/308/5729/1783.abstract

Ruiz-Roldán, C., Pareja-Jaime, Y., González-Reyes, J. A., & Roncero, M. I. G. (2015). The transcription factor Con7-1 is a master regulator of morphogenesis and virulence in *Fusarium oxysporum*. *Molecular Plant-Microbe Interactions*, *28*(1), 55–68. https://doi.org/10.1094/MPMI-07-14-0205-R

Runemark, A., Moore, E. C., & Larson, E. L. (2024). Hybridization and gene expression: Beyond differentially expressed genes. *Molecular Ecology*, *February*, 1–18. https://doi.org/10.1111/mec.17303

Samarasinghe, H., You, M., Jenkinson, T. S., Xu, J., & James, T. Y. (2020). Hybridization Facilitates Adaptive Evolution in Two Major Fungal Pathogens. *Genes*, *11*(101), 1–21.

Savary, S., Willocquet, L., Pethybridge, S. J., Esker, P., McRoberts, N., & Nelson, A. (2019). The global burden of pathogens and pests on major food crops. *Nature Ecology and Evolution*, *3*(3), 430–439. https://doi.org/10.1038/s41559-018-0793-y

Saville, B. J., Donaldson, M. E., & Doyle, C. E. (2012). Investigating Host Induced Meiosis in a Fungal Plant Pathogen. *Meiosis - Molecular Mechanisms and Cytogenetic Diversity*, *February 2012*. https://doi.org/10.5772/30032

Schardl, C. L., & Craven, K. D. (2003). Interspecific hybridization in plant-associated fungi and oomycetes: a review. *Molecular Ecology*, *12*, 2861–2873.

Schenk, P. M., Kazan, K., Wilson, I., Anderson, J. P., Richmond, T., Somerville, S. C., & Manners, J. M. (2000). Coordinated plant defense responses in Arabidopsis revealed by microarray analysis. *Proceedings of the National Academy of Sciences of the United States of America*, *97*(21), 11655–11660. https://doi.org/10.1073/pnas.97.21.11655

Schilling, L., Matei, A., Redkar, A., Walbot, V., & Doehlemann, G. (2014). Virulence of the maize smut *Ustilago maydis* is shaped by organ-specific. *Molecular Plant Pathology*, *15*(8), 780–789.

Schirawski, J., Heinze, B., Wagenknecht, M., & Kahmann, R. (2005). Mating type loci of *Sporisorium reilianum*: Novel pattern with three a and multiple b specificities. *Eukaryotic Cell*, *4*(8), 1317–1327. https://doi.org/10.1128/EC.4.8.1317-1327.2005

Schirawski, J., Mannhaupt, G., Münch, K., Brefort, T., Schipper, K., Doehlemann, G., Di Stasio, M., Rössel, N., Mendoza-Mendoza, A., Pester, D., Müller, O., Winterberg, B., Meyer, E., Ghareeb, H., Wollenberg, T., Münsterkötter, M., Wong, P., Walter, M., Stukenbrock, E., … Kahmann, R. (2010). Pathogenicity determinants in smut fungi revealed by genome comparison. *Science*, *330*(6010), 1546–1548. https://doi.org/10.1126/science.1195330

Schulz, B., Banuett, F., Dahl, M., Schlesinger, R., Schäfer, W., Martin, T., Herkowitz, I., Kahmann, R. (1990). Erratum: The b alleles of *U. maydis*, whose combinations program pathogenic development, code for polypeptides containing a homeodomain-related motif (Cell 60, (295-306), 1990). *Cell*, *60*(3), 521. https://doi.org/10.1016/0092-8674(90)90744-y

Schurack, S., Depotter, J. R. L., Gupta, D., Thines, M., & Doehlemann, G. (2021). Comparative transcriptome profiling identifies maize line specificity of fungal effectors in the maize–*Ustilago maydis* interaction. *Plant Journal*, *106*(3), 733–752. https://doi.org/10.1111/tpj.15195

Schuster, M., Schweizer, G., Reissmann, S., & Kahmann, R. (2016). Genome editing in *Ustilago maydis* using the CRISPR-Cas system. *Fungal Genetics and Biology*, *89*, 3–9. https://doi.org/10.1016/j.fgb.2015.09.001

Seidel, D., Wurster, S., Jenks, J. D., Sati, H., Gangneux, J. P., Egger, M., Alastruey-Izquierdo, A., Ford, N. P., Chowdhary, A., Sprute, R., Cornely, O., Thompson, G. R., Hoenigl, M., & Kontoyiannis, D. P. (2024). Impact of climate change and natural disasters on fungal infections. *The Lancet Microbe*, 1-12. https://doi.org/10.1016/S2666-5247(24)00039-9

Seitner, D., Uhse, S., Gallei, M., & Djamei, A. (2018). The core effector Cce1 is required for early infection of maize by *Ustilago maydis*. *Molecular Plant Pathology*, *19*(10), 2277–2287. https://doi.org/10.1111/mpp.12698

Sharma, R., Mishra, B., Runge, F., & Thines, M. (2014). Gene Loss rather than gene gain is associated with a host jump from monocots to dicots in the smut fungus *Melanopsichium pennsylvanicum*. *Genome Biology and Evolution*, *6*(8), 2034–2049. https://doi.org/10.1093/gbe/evu148

Shen, J., Wang, M., & Wang, E. (2024). Exploitation of the microbiome for crop breeding. *Nature Plants*, *10*(April), 533–534. https://doi.org/10.1038/s41477-024-01657-4

Shi, W., Stolze, S. C., Nakagami, H., Misas Villamil, J. C., Saur, I. M. L., & Doehlemann, G. (2023). Combination of *in vivo* proximity labeling and co-immunoprecipitation identifies the host target network of a tumor-inducing effector in the fungal maize pathogen *Ustilago maydis*. *Journal of Experimental Botany*, *74*(15), 4736–4750. https://doi.org/10.1093/jxb/erad188

Shi, X., Ng, D. W. K., Zhang, C., Comai, L., Ye, W., Jeffrey Chen, Z., He, F., Zhang, X., Hu, J., Turck, F., Dong, X., Goebel, U., Borevitz, J., & De Meaux, J. (2012). *Cis*- and *trans*-regulatory divergence between progenitor species determines gene-expression novelty in Arabidopsis allopolyploids. *Nature Communications*, *3*(11), 3385–3395. https://doi.org/10.1038/ncomms1954

Singh, B. K., Delgado-Baquerizo, M., Egidi, E., Guirado, E., Leach, J. E., Liu, H., & Trivedi, P. (2023). Climate change impacts on plant pathogens, food security and paths forward. *Nature Reviews Microbiology*, *21*(10), 640–656. https://doi.org/10.1038/s41579-023-00900-7

Skibbe, D. S., Doehlemann, G., Fernandes, J., & Walbot, V. (2010). Genes in Host and Pathogen. *Science*, *328*, 89–92. https://doi.org/10.1126/science.1185775

Slewinski, T. L., Anderson, A. A., Price, S., Withee, J. R., Gallagher, K., & Turgeon, R. (2014). Short-root1 plays a role in the development of vascular tissue and Kranz anatomy in maize leaves. *Molecular Plant*, *7*(8), 1388–1392. https://doi.org/10.1093/mp/ssu036

Snetselaar, K. M., Bölker, M., & Kahmann, R. (1996). *Ustilago maydis* mating hyphae orient their growth toward pheromone sources. *Fungal Genetics and Biology*, *20*(4), 299–312. https://doi.org/10.1006/fgbi.1996.0044

Snetselaar, K. M., & Mims, C. W. (1992). Sporidial Fusion and Infection of Maize Seedlings by the Smut Fungus *Ustilago maydis*. *Mycologia*, *84*(2), 193. https://doi.org/10.2307/3760250

Spellig, T., Bölker, M., Lottspeich, F., Frank, R. W., & Kahmann, R. (1994). Pheromones trigger filamentous growth in *Ustilago maydis*. *EMBO Journal*, *13*(7), 1620–1627. https://doi.org/10.1002/j.1460-2075.1994.tb06425.x

Spellig, T., Regenfelder, E., Reichmann, M., Schauwecker, F., Bohlmann, R., Urban, M., Bölker, M., Kämper, J., & Kahmann, R. (1994). Control of mating and development in *Ustilago maydis*. *Antonie van Leeuwenhoek*, *65*(3), 191–197. https://doi.org/10.1007/BF00871946

Sriswasdi, S., Takashima, M., Manabe, R. ichiroh, Ohkuma, M., & Iwasaki, W. (2019). Genome and transcriptome evolve separately in recently hybridized *Trichosporon* fungi. *Communications Biology*, *2*(1), 1–7. https://doi.org/10.1038/s42003-019-0515-2

Steensels, J., Gallone, B., & Verstrepen, K. J. (2021). Interspecific hybridization as a driver of fungal evolution and adaptation. *Nature Reviews Microbiology*, *19*(8), 485–500. https://doi.org/10.1038/s41579-021-00537-4

Steinberg, G., & Perez-Martin, J. (2008). *Ustilago maydis*, a new fungal model system for cell biology. *Trends in Cell Biology*, *18*(2), 61–67. https://doi.org/10.1016/j.tcb.2007.11.008

Stes, E., Vandeputte, O. M., El Jaziri, M., Holsters, M., & Vereecke, D. (2011). A successful bacterial coup d'état: How *Rhodococcus fascians* redirects plant development. *Annual Review of Phytopathology*, *49*, 69–86. https://doi.org/10.1146/annurev-phyto-072910-095217

Stirnberg, A., & Djamei, A. (2016). Characterization of ApB73, a virulence factor important for colonization of *Zea mays* by the smut *Ustilago maydis*. *Molecular Plant Pathology*, *17*(9), 1467–1479. https://doi.org/10.1111/mpp.12442

Stoll, M., Begerow, D., & Oberwinkler, F. (2005). Molecular Phylogeny of *Ustilago*, *Sporisorium*, and related taxa based on combined analyses of rDNA sequences. *Mycol. Res.*, *109*(3), 342–356.

Storfie, E. R. M., & Saville, B. J. (2021). Fungal Pathogen Emergence : Investigations with an *Ustilago maydis* × *Sporisorium reilianum* Hybrid. *Journal of Fungi*, *7*(672).

Tanaka, S., Brefort, T., Neidig, N., Djamei, A., Kahnt, J., Vermerris, W., Koenig, S., Feussner, K., Feussner, I., & Kahmann, R. (2014). A secreted *Ustilago maydis* effector promotes virulence by targeting anthocyanin biosynthesis in maize. *ELife*, *3*, 1–27. https://doi.org/10.7554/elife.01355

Tanaka, S., Schweizer, G., Rössel, N., Fukada, F., Thines, M., & Kahmann, R. (2019). Neofunctionalization of the secreted Tin2 effector in the fungal pathogen *Ustilago maydis*. *Nature Microbiology*, *4*(2), 251–257. https://doi.org/10.1038/s41564-018-0304-6

Tirosh, I., Reikhav, S., Levy, A. A., & Barkai, N. (2009). A yeast hybrid provides insight into the evolution of gene expression regulation. *Science*, *324*(5927), 659–662. https://doi.org/10.1126/science.1169766

Tollot, M., Assmann, D., Becker, C., Altmüller, J., Dutheil, J. Y., Wegner, C. E., & Kahmann, R. (2016). The WOPR Protein Ros1 Is a Master Regulator of Sporogenesis and Late Effector Gene Expression in the Maize Pathogen *Ustilago maydis*. *PLoS Pathogens*, *12*(6), 1–37. https://doi.org/10.1371/journal.ppat.1005697

Uhse, S., & Djamei, A. (2018). Effectors of plant-colonizing fungi and beyond. *PLoS Pathogens*, *14*(6), 1-8. https://doi.org/10.1371/journal.ppat.1006992

Ullrich, C. I., & Aloni, R. (2000). Vascularization is a general requirement for growth of plant and animal tumours. *Journal of Experimental Botany*, *51*(353), 1951–1960. https://doi.org/10.1093/jexbot/51.353.1951

Ulrich, J. (2020). Die kombinatorische Regulation eines Transkriptions- Netzwerks reguliert die Pflanzeninfektion von *Ustilago maydis*. *PhD Thesis*.

Urban, M., Kahmann, R., & Bölker, M. (1996). Identification of the pheromone response element in *Ustilago maydis*. *Molecular and General Genetics*, *251*(1), 31–37. https://doi.org/10.1007/s004380050136

van der Burgh, A. M., & Joosten, M. H. A. J. (2019). Plant Immunity: Thinking Outside and Inside the Box. *Trends in Plant Science*, *24*(7), 587–601. https://doi.org/10.1016/j.tplants.2019.04.009

van der Linde, K., & Göhre, V. (2021). How do smut fungi use plant signals to spatiotemporally orientate on and in planta? *Journal of Fungi*, *7*(2), 1–13. https://doi.org/10.3390/jof7020107

van Kan, J. A. L. (2006). Licensed to kill: the lifestyle of a necrotrophic plant pathogen. *Trends in Plant Science*, *11*(5), 247–253. https://doi.org/10.1016/j.tplants.2006.03.005

Vatén, A., Dettmer, J., Wu, S., Stierhof, Y. D., Miyashima, S., Yadav, S. R., Roberts, C. J., Campilho, A., Bulone, V., Lichtenberger, R., Lehesranta, S., Mähönen, A. P., Kim, J. Y., Jokitalo, E., Sauer, N., Scheres, B., Nakajima, K., Carlsbecker, A., Gallagher, K. L., & Helariutta, Y. (2011). Callose Biosynthesis Regulates Symplastic Trafficking during Root Development. *Developmental Cell*, *21*(6), 1144–1155. https://doi.org/10.1016/j.devcel.2011.10.006

Venbrux, M., Crauwels, S., & Rediers, H. (2023). Current and emerging trends in techniques for plant pathogen detection. *Frontiers in Plant Science*, *14*(May), 1–25. https://doi.org/10.3389/fpls.2023.1120968

Vollmeister, E., Schipper, K., Baumann, S., Haag, C., Pohlmann, T., Stock, J., & Feldbrügge, M. (2012). Fungal development of the plant pathogen *Ustilago maydis*. *FEMS Microbiology Reviews*, *36*(1), 59–77. https://doi.org/10.1111/j.1574-6976.2011.00296.x

Vonk, P. J., & Ohm, R. A. (2018). The role of homeodomain transcription factors in fungal development. *Fungal Biology Reviews*, *32*(4), 219–230. https://doi.org/10.1016/j.fbr.2018.04.002

Walbot, V., & Skibbe, D. S. (2010). Maize host requirements for *Ustilago maydis* tumor induction. *Sexual Plant Reproduction*, *23*(1), 1–13. https://doi.org/10.1007/s00497-009-0109-0

Wang, X., Yang, B., Li, K., Kang, Z., Cantu, D., & Dubcovsky, J. (2016). A conserved *Puccinia striiformis* protein interacts with wheat NPR1 and reduces induction of pathogenesis-related genes in response to pathogens. *Molecular Plant-Microbe Interactions*, *29*(12), 977–989. https://doi.org/10.1094/MPMI-10-16-0207-R

Xia, W., Yu, X., & Ye, Z. (2020a). Smut fungal strategies for the successful infection. *Microbial Pathogenesis*, *142*(February), 104039. https://doi.org/10.1016/j.micpath.2020.104039

Xia, W., Yu, X., & Ye, Z. (2020b). Smut fungal strategies for the successful infection. *Microbial Pathogenesis*, *142*(December 2019), 104039. https://doi.org/10.1016/j.micpath.2020.104039

You, M., & Xu, J. (2021). What are the best parents for hybrid progeny? An investigation into the human pathogenic fungus *Cryptococcus*. *Journal of Fungi*, *7*(4), 8–11. https://doi.org/10.3390/jof7040299

Yu, X., Feng, B., He, P., & Shan, L. (2017). From Chaos to Harmony: Responses and Signaling upon Microbial Pattern Recognition. *Annual Review of Phytopathology*, *55*, 109–137. https://doi.org/10.1146/annurev-phyto-080516-035649

Zahiri, A., Heimel, K., Wahl, R., Rath, M., & Kämper, J. (2010). The *Ustilago maydis* forkhead transcription factor Fox1 is involved in the regulation of genes required for the attenuation of plant defenses during pathogenic development. *Molecular Plant-Microbe Interactions*, *23*(9), 1118–1129. https://doi.org/10.1094/MPMI-23-9-1118

Zeyl, C., Andreson, B., & Weninck, E. (2005). Nuclear-mitochondrial epistasis for fitness in *Saccharomyces cerevisiae. Evolution*, *59*(4), 910–914. https://doi.org/10.1111/j.0014-3820.2005.tb01764.x

Zhang, J., Coaker, G., Zhou, J. M., & Dong, X. (2020). Plant Immune Mechanisms: From Reductionistic to Holistic Points of View. *Molecular Plant*, *13*(10), 1358–1378. https://doi.org/10.1016/j.molp.2020.09.007

Zhang, Y., Gao, Y., Wang, H. L., Kan, C., Li, Z., Yang, X., Yin, W., Xia, X., Nam, H. G., Li, Z., & Guo, H. (2021). *Verticillium dahliae* secretory effector PevD1 induces leaf senescence by promoting ORE1-mediated ethylene biosynthesis. *Molecular Plant*, *14*(11), 1901–1917. https://doi.org/10.1016/j.molp.2021.07.014

Zheng, Y., Kief, J., Auffarth, K., Farfsing, J. W., Mahlert, M., Nieto, F., & Basse, C. W. (2008). The *Ustilago maydis* Cys2His2-type zinc finger transcription factor Mzr1 regulates fungal gene expression during the biotrophic growth stage. *Molecular microbiology*, *68*(6), 1450-1470.

Zhou, J. M., & Zhang, Y. (2020). Plant Immunity: Danger Perception and Signaling. *Cell*, *181*(5), 978–989. https://doi.org/10.1016/j.cell.2020.04.028

Zuo, W., Depotter, J. R., & Doehlemann, G. (2020). Cas9HF1 enhanced specificity in *Ustilago maydis*. *Fungal Biology*, *124*(3–4), 228–234. https://doi.org/10.1016/j.funbio.2020.02.006

Zuo, W., Depotter, J. R. L., Gupta, D. K., Thines, M., & Doehlemann, G. (2021). Cross-species analysis between the maize smut fungi *Ustilago maydis* and *Sporisorium reilianum* highlights the role of transcriptional change of effector orthologs for virulence and disease. *New Phytologist*. https://doi.org/10.1111/nph.17625

Zuo, W., Depotter, J. R. L., Stolze, S. C., Nakagami, H., & Doehlemann, G. (2023). A transcriptional activator effector of *Ustilago maydis* regulates hyperplasia in maize during pathogen-induced tumor formation. *Nat Commun,* 14, 6722 (2023). https://doi.org/10.1038/s41467-023-42522-w

Zuo, W., Oekmen, B., Depotter, J. R. L., Ebert, M. K., Redkar, A., Misas Villamil, J., & Doehlemann, G. (2019). Molecular Interactions between Smut Fungi and Their Host Plants. *Annual Review of Phytopathology*, *57*, 411–430. https://doi.org/10.1146/annurev-phyto-082718-100139

Supplementary data

Chapter 2

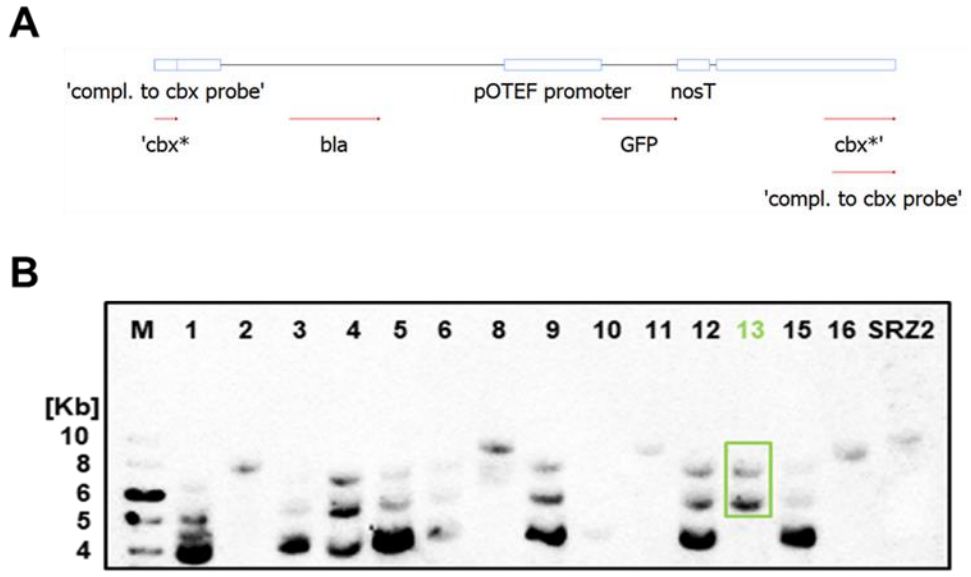

Figure S2.1: Southern blot of single integrated GFP into SRZ2 strain. (A) Construct pNEB_SrCbx_pOTEF_GFP was linearized with StuI for integration into *ip* locus of *S. reilianum* to test the efficiency of RNP-mediated transformation (Clone Manager 9). **(B)** Southern blot of pNEB_SrCbx_pOTEF_GFP in *S. reilianum* wild type strain SRZ2. Hybridization probe: Srcbx (1561 bp). Expected sizes: (i) Single integration: 7451 bp + 5740 bp, (ii) Multiple integration: 7451 bp + 5740 bp + 4348 bp, (iii) Wild type (SRZ2): 8827 bp. (Note: The efficiency of single and multiple integrations in the *ip* locus can differ between constructs. When 14 mutants are tested in Southern blot, on average 1-2 single integrations are obtained.)

Chapter 3

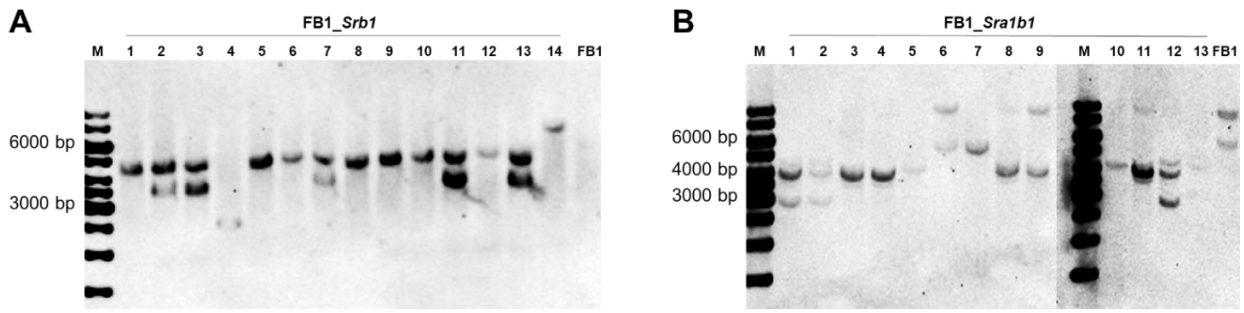

Figure S3.1: Southern blot of FB1_*Srb1* and FB1_*Sra1b1* (Um_Smt). (A) Southern blot of FB1_*Srb1*. DNA was digested with SpHI-HF and the expected sizes were: 4,820 bp (FB1_*Srb1*) and 2,813 bp (FB1). Positive transformants for glycerol: 5, 8, and 9. **(B)** Southern blot of FB1_*Sa1rb1*. FB1_*Srb1* transformant #5 was used as a background strain to integrate *Sra1.* DNA was digested with HindIII-HF and the expected sizes are 4,433 bp for FB1_*Sra1b1* and 5995 bp for the control (FB1). M: 1 kb Ladder (Thermo Fisher). Southern blots were performed by Tom Winkler under the supervision of Weiliang Zuo (AG Döhlemann).

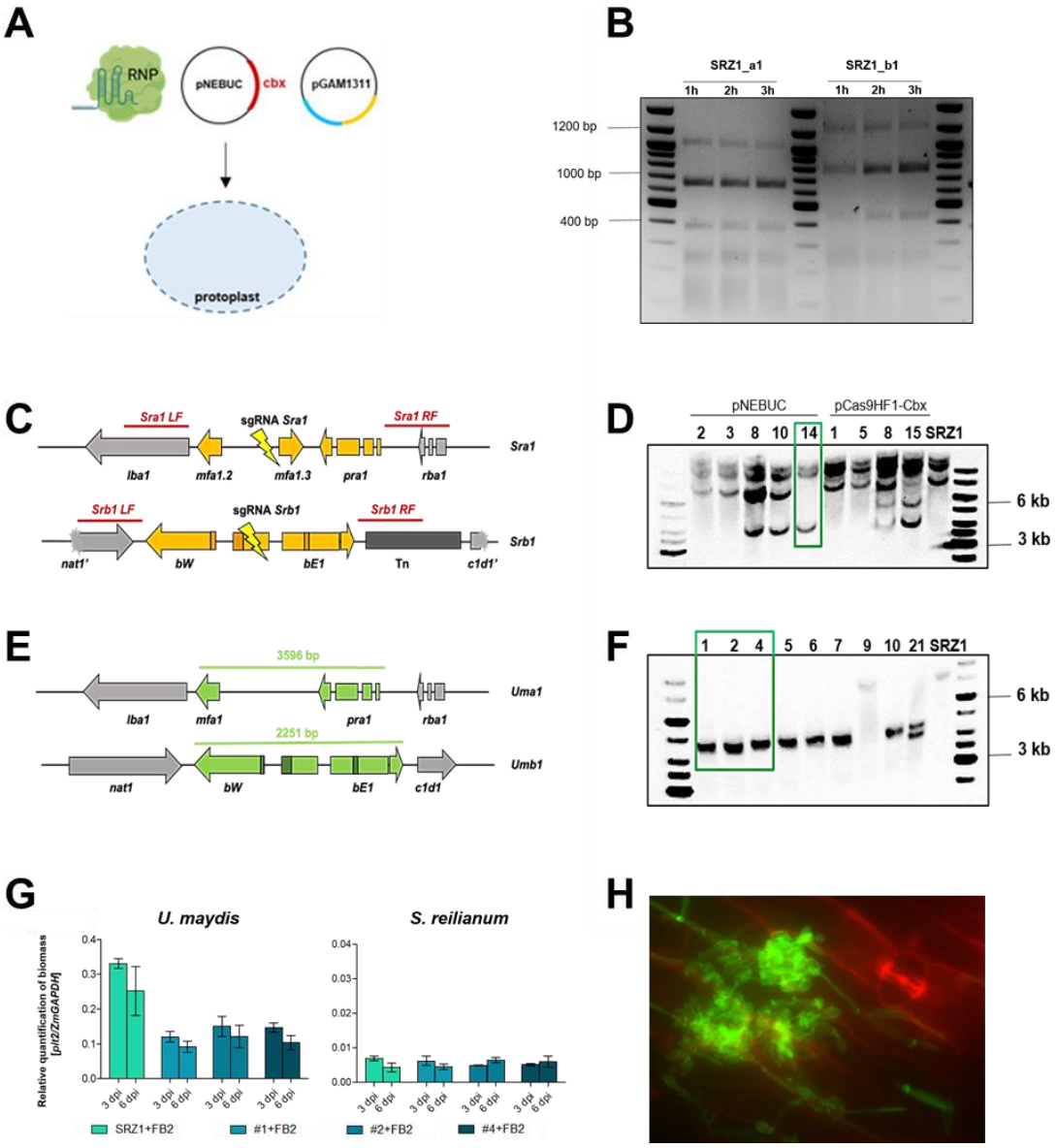

Figure S3.2: Generation and infection of Sr_Umt. (A) Sr_Umt was generated using RNP-mediated transformation with a donor template and an auto-replicating plasmid. **(B)** The sgRNAs used for the genomic loci of *Uma1* and *Umb1*, respectively, were tested in an *in vitro* cleavage assay prior to infection. **(C)** Schematic overview of the *Sra1* and *Srb1* locus. sgRNAs are indicated in yellow. 1 kb flanks used for the donor template are marked in red. **(D)** Southern blot of SRZ1_Umb1. Putative positive colonies were selected based on colony PCR (not shown). DNA was digested with BamHI-HF and the right flank of the *b1* locus was used as a probe. Expected sizes: WT: 8,961 bp, mutant: 4,640 bp. **(E)** Schematic overview of the *Uma1* and *Umb1* locus. The green line marks the region that was used for the replacement of *Sra1* and *Srb1*, respectively. **(F)** Southern blot of SRZ1_*Uma1* in SRZ1_*Umb1* background. Putative positive colonies were selected based on colony PCR (not shown). DNA of putative positive colonies was digested with SacI-HF and the left flank of the *a1* locus was used as a probe. Expected sizes: WT: 9,503 bp, mutant: 5,575 bp. Green squares represent selected positive mutant strains. M: 1 kb ladder. **(G)** qRT-PCT of SRZ1+FB2, SRZ1_*Uma1b1*#1+FB2 (#1+FB2), SRZ1_*Uma1b1*#2+FB2 (#2+FB2) and SRZ1_*Uma1b1*#4+FB2 (#4+FB2) for quantification of fungal biomass using *Umppi or Srppi*, respectively, and *GAPDH* of maize. **(H)** WGA staining of #1+FB2 at 6 dpi revealed a clump-like structure on the plant surface.

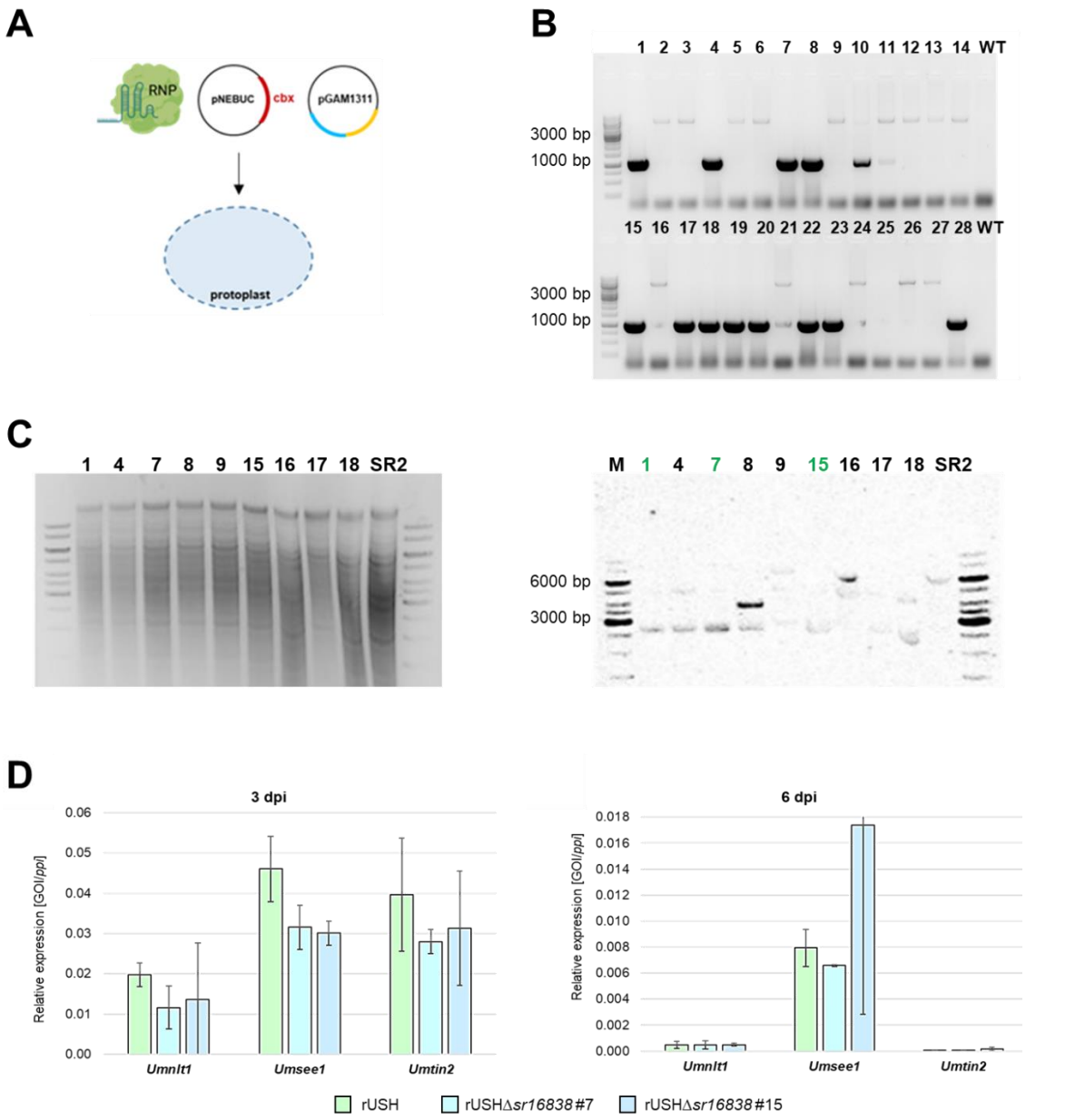

Figure S3.3: Generation of *dicer* deletion mutant strains in *S. reilianum*. (A) Schematic illustration of transformation. *sr16838* was deleted in the SRZ2 strain of *S. reilianum* to test, whether the *dicer* gene is responsible for the downregulation of *U. maydis* effector orthologues rUSH. Therefore, 1 kb upstream and 1 kb downstream of the cds were amplified and using Gibson assembly cloned into pAGM1311 linearized with XbaI and EcoRI. The resulting donor template was used together with a sgRNA cutting approximately in the middle of the cds of *sr16838* in an RNP and the autoreplicating plasmid pNEBUC. In the transformation, Cbx was used for selection. **(B)** PCR to validate deletion of *sr16838*. **(C)** Southern blot of *sr16838* deletion mutants, previously verified by PCR. PvuI was used for the digestion of the gDNA. Expected sizes of the Southern blot: WT: 8,137 bp; mutant: 3,072 bp. **(D)** Relative Expression of *Umnlt1*, *Umsee1* and *Umtin2* in rUSHΔ*sr16838*. Maize leaves were infected with rUSH, rUSHΔ*sr16838*#7, and rUSHΔ*sr16838*#15 with a final OD of 1 and addition of 0.1% Tween. After 3 dpi 4-cm leaf sections were harvested and further processed. Using qRT-PCR, gene expression was measured relative to *Umppi* (green). Error bars (standard deviation) were calculated from four biological replicates. Significant differences were calculated based on students t-test (* =p<0.05, ** =p<0.01, *** =p<0.001).

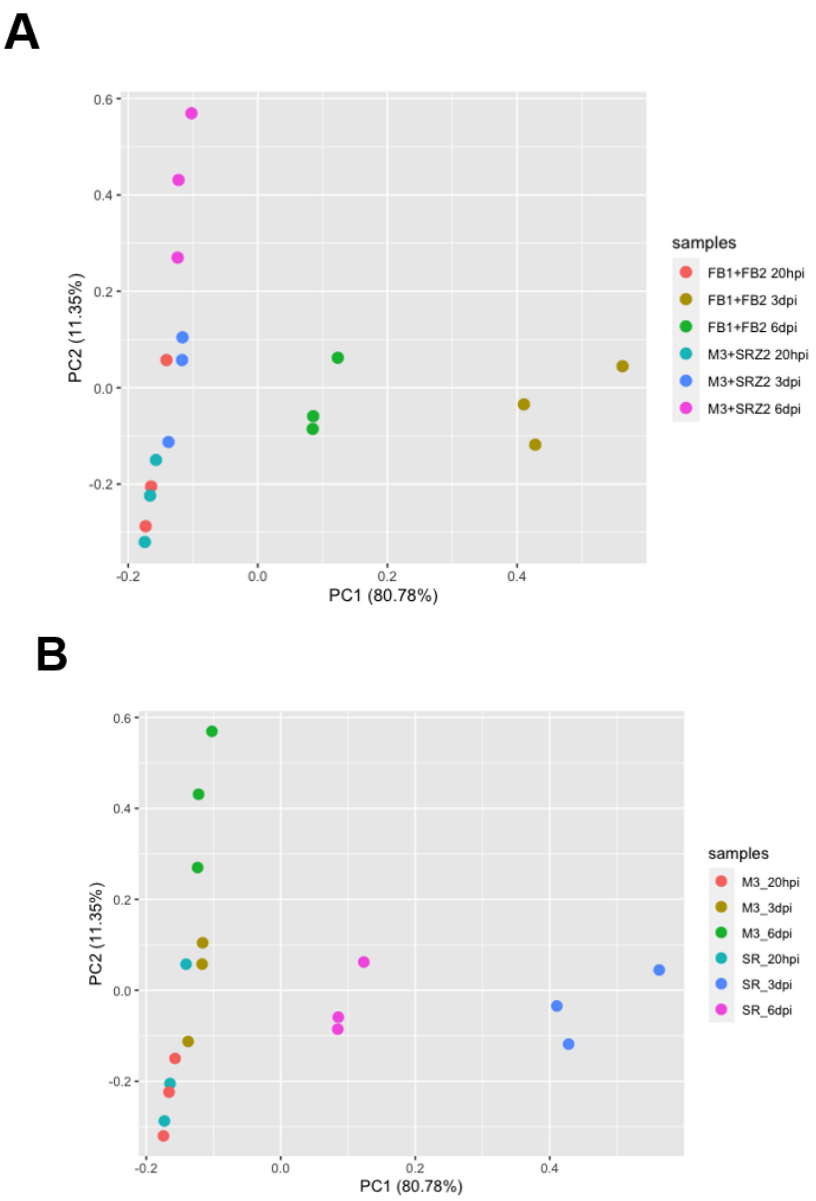

Figure S3.4: PCA plot of RNA-seq of 3 biological replicates of FB1+FB1, SRZ1+SRZ2, and hybrid-infected maize leaves at 20 hpi, 3 dpi, and 6 dpi. (A) Counts obtained from *U. maydis*. **(B)** Counts obtained from *S. reilianum*

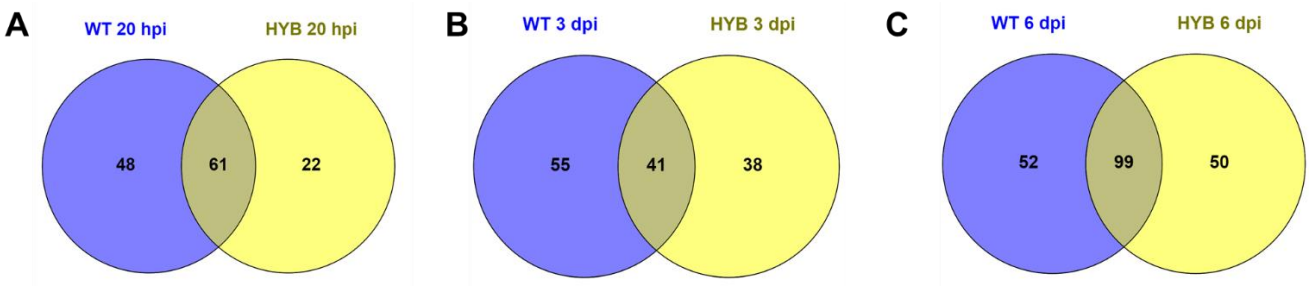

Figure S3.5: Venn diagram of differentially expressed effector genes between the *U. maydis* WT and rUSH (HYB) at 20 hpi, 3 dpi, and 6 dpi.

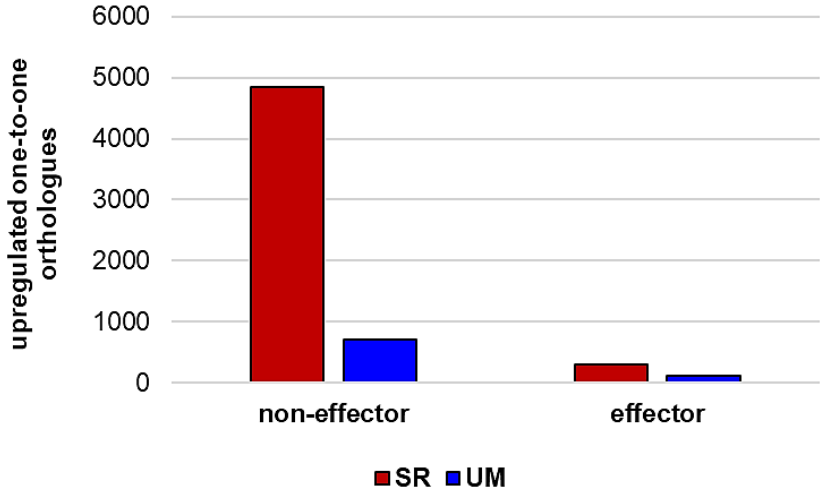

Figure S3.6: Differentially expressed one-to-one orthologues in rUSH compared to FB1+SRZ2. RNA-seq analysis was conducted as explained in chapter 3. Differentially expressed one-to-one orthologues (log_2FC >1, $p<0.05$) were grouped into effector genes and non-effector genes and compared between *U. maydis* and *S. reilianum*.

Table S3.1: Differentially expressed effector genes, exclusively found in the hybrid.

25 elements exclusively in HYB 6 dpi:		12 common elements in HYB 3 dpi and HYB 6 dpi:
UMAG_11931	UMAG_01501	UMAG_05927
UMAG_11362	UMAG_01632	UMAG_05548
UMAG_06158	UMAG_03822	UMAG_05314
UMAG_04630	UMAG_04641	UMAG_04032
UMAG_05680	UMAG_10091	UMAG_12216
UMAG_06064	UMAG_11649	UMAG_01820
UMAG_10676	UMAG_00330	UMAG_00961
UMAG_12127	UMAG_10068	UMAG_06218
UMAG_06157	UMAG_03689	UMAG_04696
UMAG_01823	UMAG_06255	UMAG_01851
UMAG_05036	UMAG_01236	UMAG_10975
UMAG_11910	UMAG_12184	UMAG_12175
UMAG_01213		

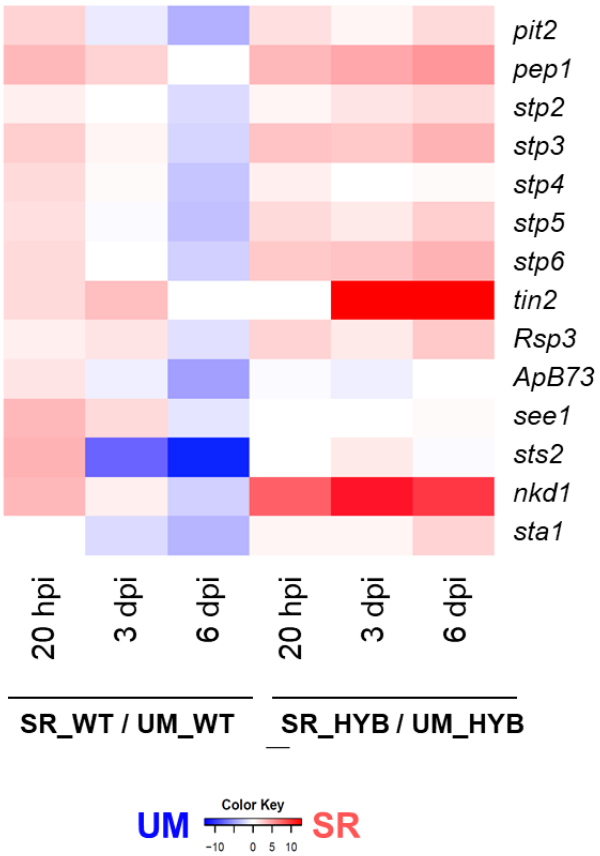

Figure S3.7: Differential expression of already characterized effector genes. Log_2FC of effector gene expression was calculated by dividing the *S. reilianum* transcripts per million (TPM) by *U. maydis* TPM of the wild types SRZ1+SRZ2 and FB1+FB2, respectively, as well as within the hybrid.

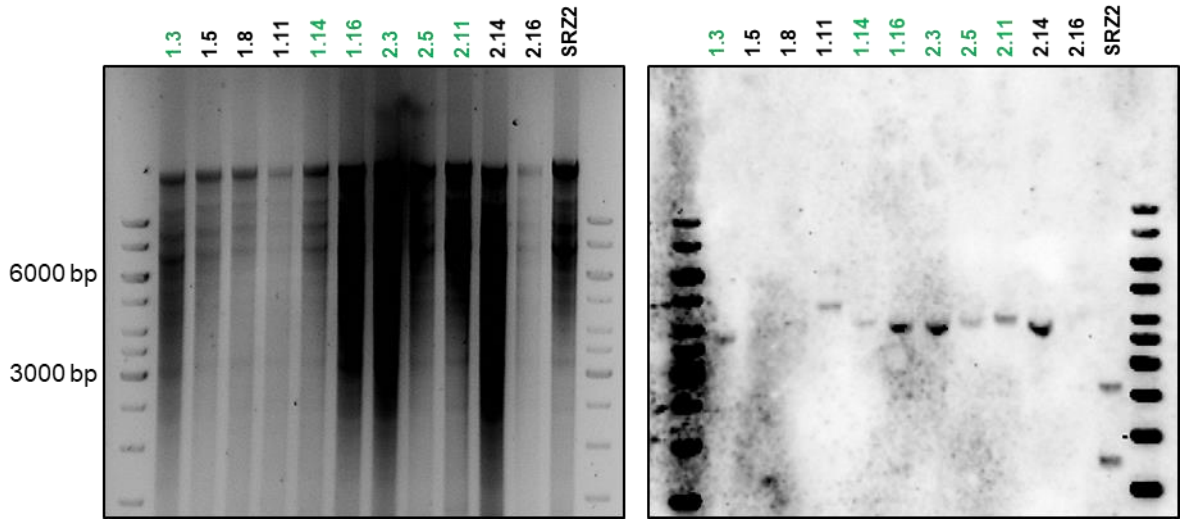

Figure S3.8: Southern blot of *S. reilianum* Δ*sr16075* in SRZ1 and SRZ2. DNA was digested using the restriction enzyme SpHI-HF. Southern blot detection indicated one band in the wild type at 2,635 bp and one band in the deletion at 4,046 bp. The DIG-labeled PCR products from the left flank and right flank were used as probe. Green-colored numbers represent selected positive mutant strains.

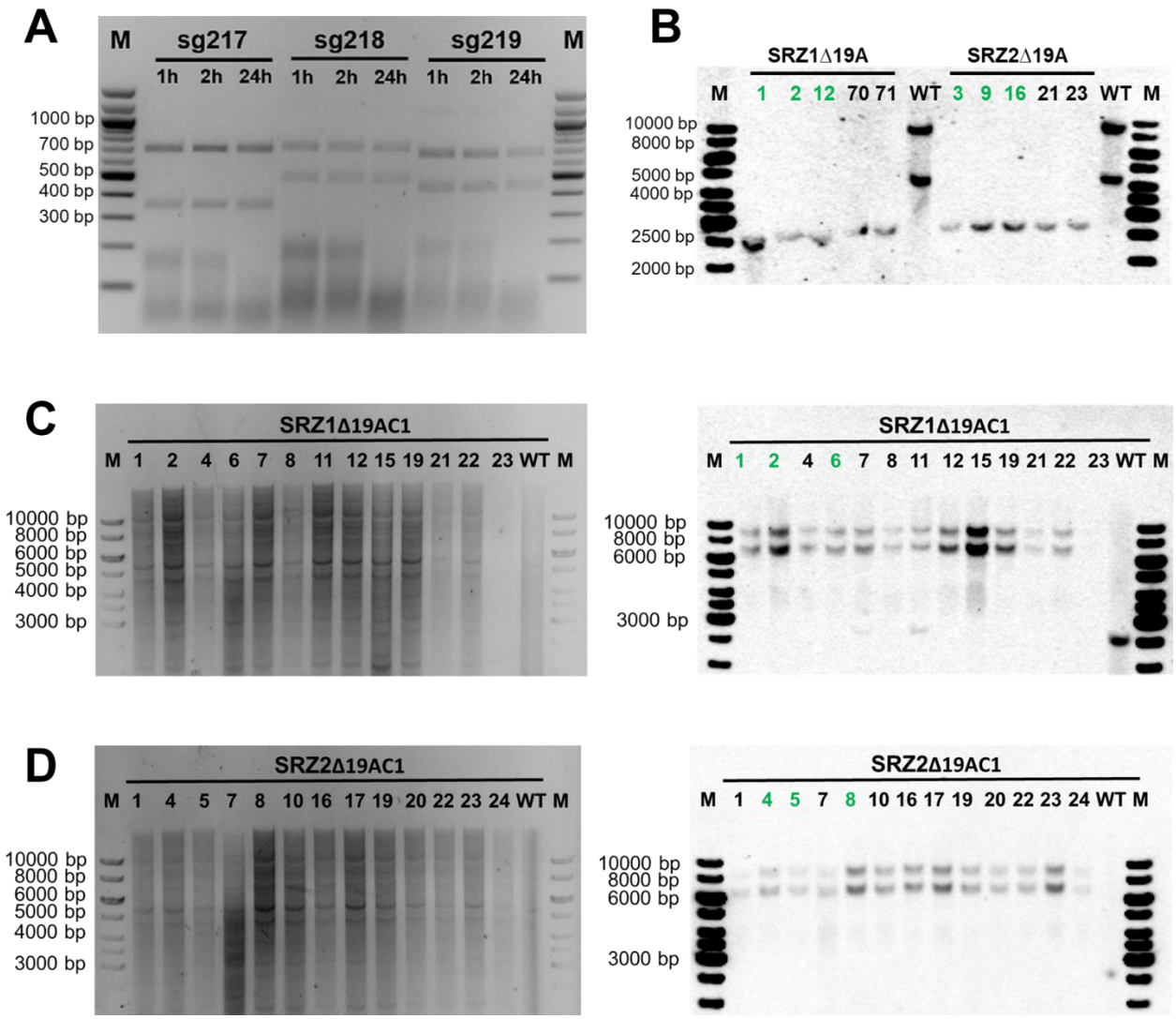

Figure S3.9: Generation of *S. reilianum* cluster 19A deletion strain and complementation 1 of *U. maydis* cluster 19A. (A) *In vitro* cleavage assay of sg217, sg218, and 219. The PCR products containing the target sequence of corresponding sgRNAs were cleaved after incubation. Expected fragment sizes after cleavage are sg217: 351+680 bp, sg218: 419+703 bp, sg219: 442+661 bp. M, 100 bp ladder. **(B)** Southern blot of *S. reilianum* Cluster 19A deletion in SRZ1 (SRZ1Δ19A) and SRZ2 (SRZ2Δ19A). Southern blot detection indicated two bands in the wild type of SRZ1 and SRZ2 at 9,373 bp and 4,409 bp, while the knock out mutant has one band around 2,809 bp. The DIG-labeled PCR products from the left flank and right flank were used as probe. Southern blot of SRZ1Δ19A#1 **(C)** and SRZ2Δ19A#3 **(D)** with complementation 1 of *U. maydis* cluster 19A. Southern blot detection indicated one band in the deletion strain of SRZ1 and SRZ2 around 2,809 bp, while the complementation mutant showed two bands at 9,152 bp and 7,050 bp. The DIG-labeled PCR products from the left flank and right flank were used as a probe. Green-colored numbers represent selected positive mutant strains. M: 1 kb ladder.

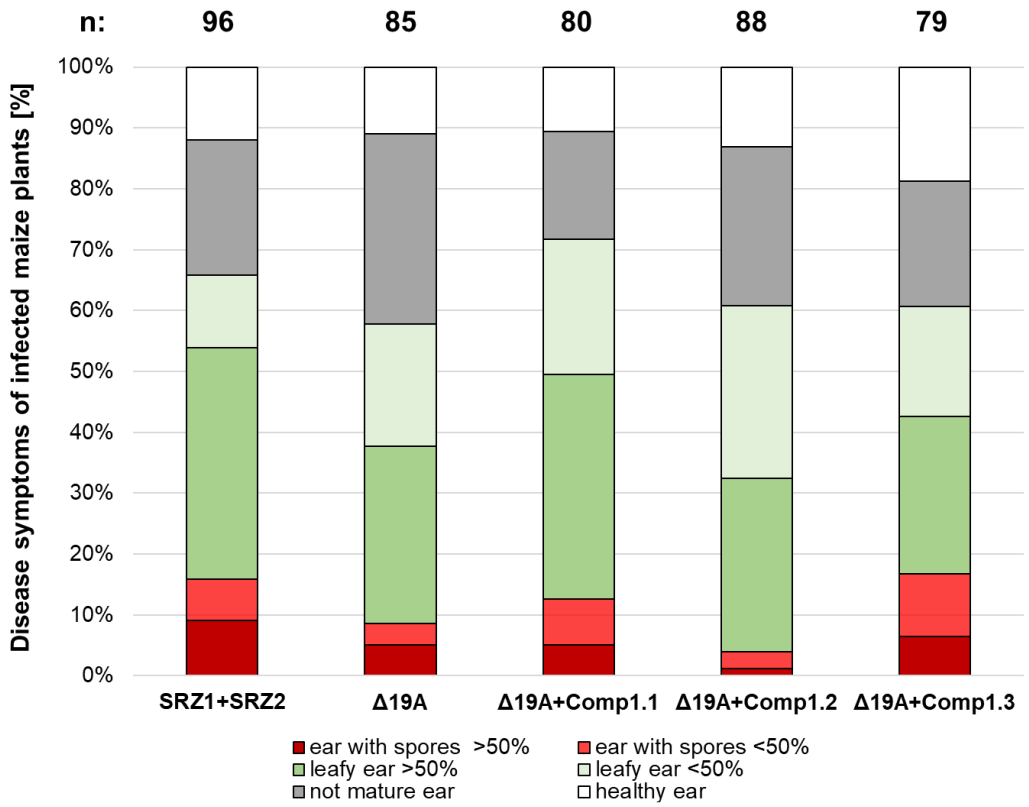

Figure S3.10: Disease symptoms of infected maize plants with WT of *S. reilianum*, *S. reilianum* cluster 19A deletion strain (Δ19A), and 3 independent complementation 1 mutants (Δ19A+Comp1.1, Δ19A+Comp1.2, Δ19A+Comp1.3). For infection the early flowering maize cultivar Gaspe Flint was used. Disease symptoms were scored 7 wpi as described by Ghareeb *et al*. (2019). N: Total number of evaluated plants.

Chapter 4

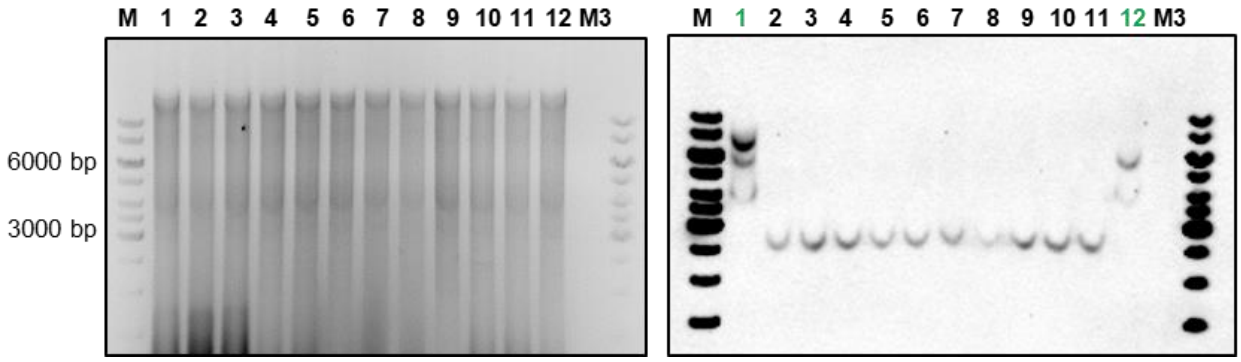

Figure S4.1: Southern blot of Um_Smt_proCmu1_*Umhdp2*-2xHA. DNA was digested with BamHI-HF and EcoRV-HF. Expected sizes: WT: 3255 bp, Single integration: 7239 bp + 4869 bp, Multiple integration: 8853 bp + 7239 bp + 4869 bp. Positive transformants are marked in green. M3: Um_Smt control.

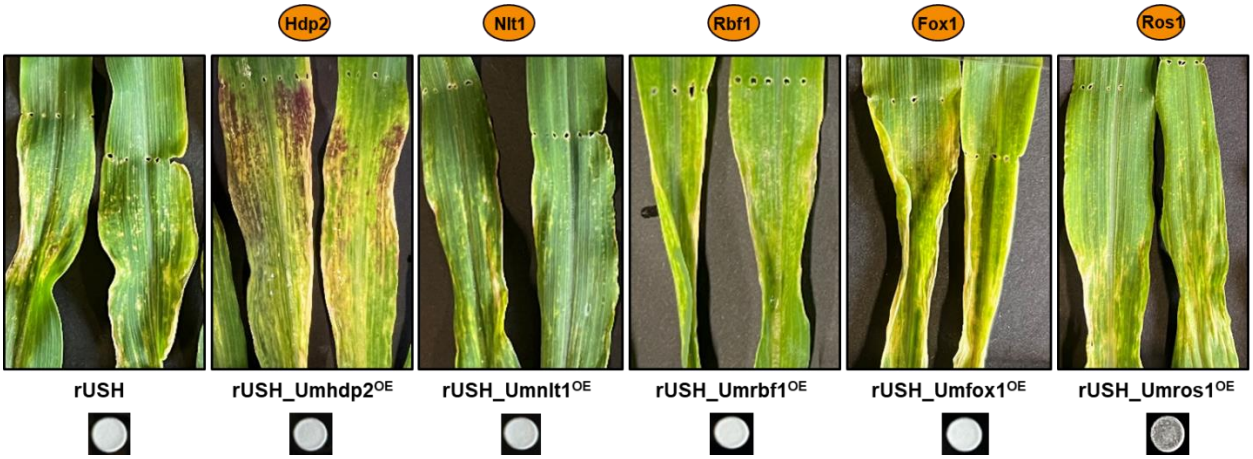

Figure S4.2: Infection assay of transcription factor overexpressions in rUSH. *hdp2*, *nlt1*, *rbf1*, *fox1,* and *ros1* were overexpressed in Um_Smt and infected together with SRZ2 (mixed 1:1, final OD of 1) in 7-days old maize seedlings. Pictures were taken at 6 dpi.

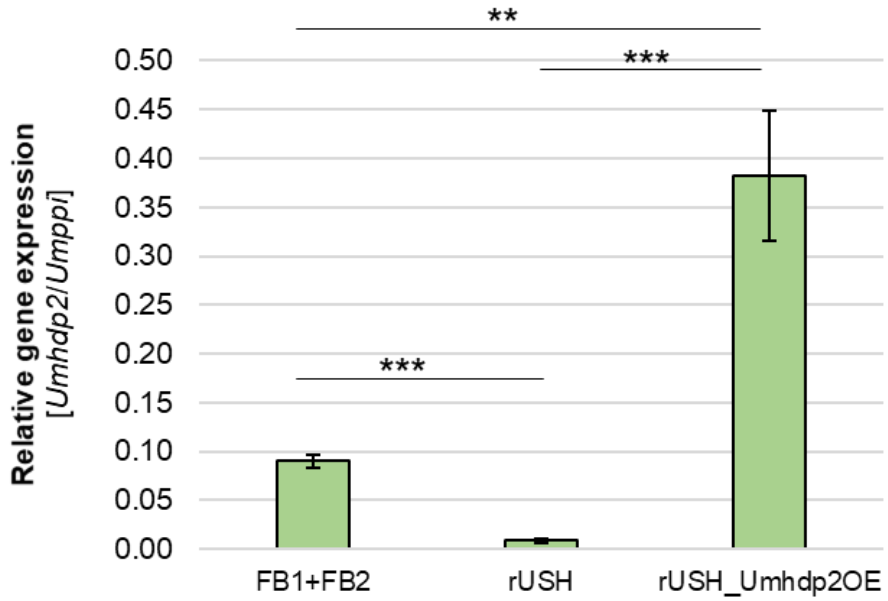

Figure S4.3: Relative expression of *Umhdp2* in *U. maydis* wild type (FB1+FB2), hybrid and HYB_Umhdp2^{OE}. qRT-PCR was conducted to compare the expression level of *Umhdp2* normalized to *Umppi* between the different strains at 3 dpi.

Table S4.1: Hdp2 motif enrichment analysis using STREME. 500 bp promoter regions of effector genes of *U. maydis* and *S. reilianum* were used to identify Hdp2 binding sites.

gene_id	ATGAA	[A,T][A,G]ATGAA	[A,T][A,C,G,T]ATGAA
***U. maydis* effector genes**			
UMAG_11060	5	1	2
UMAG_11062	5	3	4
UMAG_11417	5	2	5
UMAG_01796	5	1	5
UMAG_01689	5	1	3
UMAG_01987	5	0	3
UMAG_01820	4	2	3
UMAG_04035	4	1	1
UMAG_02097	4	0	1
UMAG_00032	4	1	1
UMAG_06179	4	2	3
UMAG_05932	4	1	2
UMAG_00940	4	1	3
UMAG_01690	4	2	4
UMAG_01734	4	1	4
UMAG_03202	3	1	2
UMAG_05731	3	3	3

UMAG_12313	3	1	2
UMAG_05781	3	2	2
UMAG_12226	3	2	2
UMAG_02139	3	0	2
UMAG_02192	3	2	2
UMAG_00715	3	3	3
UMAG_00781	3	1	3
UMAG_02537	3	0	2
UMAG_02540	3	1	3
UMAG_05856	3	2	3
UMAG_01305	3	1	2
UMAG_02854	3	1	1
UMAG_11484	3	1	2
UMAG_03650	3	0	2
UMAG_05310	3	0	2
UMAG_05311	3	1	3
UMAG_11377	3	1	1
UMAG_05090	3	0	0
UMAG_00792	3	0	0
UMAG_05027	3	1	1
UMAG_03201	3	1	2
UMAG_10067	3	1	1
UMAG_04171	3	1	1
UMAG_12257	3	2	2
UMAG_05604	3	1	1
UMAG_02821	3	1	1
UMAG_11362	3	1	2
UMAG_01779	3	1	1
UMAG_00793	2	0	0
UMAG_05694	2	0	0
UMAG_11517	2	0	1
UMAG_04039	2	1	2
UMAG_04040	2	0	1
UMAG_10707	2	1	2
UMAG_12049	2	1	1
UMAG_03343	2	1	2
UMAG_02194	2	1	1
UMAG_02231	2	1	1
UMAG_02239	2	1	1
UMAG_10156	2	1	1
UMAG_02466	2	1	1
UMAG_02477	2	0	0

UMAG_06027	2	0	1
UMAG_06126	2	2	2
UMAG_10408	2	0	0
UMAG_04248	2	0	0
UMAG_12107	2	0	0
UMAG_00273	2	0	0
UMAG_00420	2	1	1
UMAG_00629	2	1	2
UMAG_11416	2	0	0
UMAG_10315	2	1	1
UMAG_05583	2	1	1
UMAG_10587	2	1	1
UMAG_11639	2	0	0
UMAG_01375	2	2	2
UMAG_03105	2	1	1
UMAG_03747	2	1	2
UMAG_03748	2	2	2
UMAG_03867	2	1	2
UMAG_12302	2	1	1
UMAG_10555	2	0	0
UMAG_10556	2	1	2
UMAG_10557	2	0	1
UMAG_05319	2	1	1
UMAG_04508	2	1	2
UMAG_11886	2	0	0
UMAG_03467	2	0	0
UMAG_12237	2	1	2
UMAG_15018	2	0	1
UMAG_06315	2	1	1
UMAG_11250	2	1	1
UMAG_06178	2	2	2
UMAG_12197	2	2	2
UMAG_04027	2	0	1
UMAG_02474	2	2	2
UMAG_00445	2	0	2
UMAG_02523	2	2	2
UMAG_05803	2	2	2
UMAG_01202	2	0	0
UMAG_01213	2	1	2
UMAG_01301	2	1	1
UMAG_10816	2	0	1
UMAG_06332	2	1	2

UMAG_06350	2	0	0
UMAG_06180	1	0	0
UMAG_01022	1	1	1
UMAG_03392	1	0	1
UMAG_05222	1	0	0
UMAG_10724	1	1	1
UMAG_03924	1	1	1
UMAG_04057	1	0	0
UMAG_10536	1	0	0
UMAG_06394	1	0	0
UMAG_12045	1	0	1
UMAG_03138	1	0	0
UMAG_10403	1	1	1
UMAG_03231	1	0	0
UMAG_03297	1	0	0
UMAG_02092	1	0	0
UMAG_02193	1	0	0
UMAG_10076	1	0	0
UMAG_02229	1	1	1
UMAG_02230	1	0	1
UMAG_11403	1	0	0
UMAG_06113	1	0	0
UMAG_04196	1	0	1
UMAG_10006	1	0	0
UMAG_00438	1	0	0
UMAG_11831	1	1	1
UMAG_12356	1	0	0
UMAG_00811	1	0	0
UMAG_06181	1	0	0
UMAG_06185	1	1	1
UMAG_11223	1	0	1
UMAG_06221	1	0	0
UMAG_06222	1	0	0
UMAG_10975	1	1	1
UMAG_02516	1	0	0
UMAG_02538	1	1	1
UMAG_02561	1	0	0
UMAG_05528	1	1	1
UMAG_10358	1	1	1
UMAG_05824	1	0	0
UMAG_05870	1	0	0
UMAG_05930	1	0	1

UMAG_01031	1	1	1
UMAG_01210	1	1	1
UMAG_12196	1	0	0
UMAG_02852	1	1	1
UMAG_02853	1	1	1
UMAG_10323	1	0	0
UMAG_02981	1	1	1
UMAG_10476	1	0	0
UMAG_03746	1	0	1
UMAG_03752	1	1	1
UMAG_10554	1	1	1
UMAG_10208	1	0	1
UMAG_04514	1	0	0
UMAG_01499	1	0	0
UMAG_01637	1	0	0
UMAG_11370	1	1	1
UMAG_03449	1	0	0
UMAG_03553	1	0	0
UMAG_05227	1	0	1
UMAG_10766	1	0	0
UMAG_03642	1	0	0
UMAG_11562	1	1	1
UMAG_10387	1	0	0
UMAG_10823	1	0	0
UMAG_03381	1	1	1
UMAG_11397	1	0	0
UMAG_02430	1	1	1
UMAG_04104	1	1	1
UMAG_04145	1	0	0
UMAG_12258	1	1	1
UMAG_10418	1	0	0
UMAG_00081	1	0	0
UMAG_00144	1	0	0
UMAG_11637	1	1	1
UMAG_06157	1	0	1
UMAG_02727	1	0	1
UMAG_11931	1	0	0
UMAG_05799	1	0	1
UMAG_04816	1	0	1
UMAG_00961	1	1	1
UMAG_01300	1	0	0
UMAG_02921	1	0	0

UMAG_01788	1	0	1
***S. reilianum* effector genes**			
sr10996.2	5	2	3
sr13375	5	2	2
sr14944	5	2	4
sr10075	4	1	3
sr13898	4	2	4
sr10916.2	4	3	3
sr13495	4	2	3
sr15334	4	1	2
sr15147	4	1	3
sr11009	3	0	1
sr20006	3	0	1
sr11238	3	1	2
sr11472	3	0	1
sr11947	3	1	3
sr12809	3	1	2
sr12879	3	1	1
sr13344	3	1	3
sr14449	3	0	3
sr10079	3	3	3
sr13904	3	2	2
sr14223	3	0	1
sr14368	3	2	3
sr14941	3	0	0
sr10433	3	0	1
sr10292	3	2	3
sr12210	3	2	2
sr16780	3	2	2
sr15146	3	1	1
sr15399	3	2	2
sr10982	3	1	1
sr11603	3	0	0
sr12856	3	0	0
sr12947	3	2	2
sr11400	2	0	0
sr12086	2	2	2
sr11002.2	2	0	0
sr10995.2	2	0	0
sr13835	2	0	1
sr11237	2	0	0
sr11235.2	2	0	1

sr10105	2	1	2
sr12085	2	2	2
sr12105	2	1	1
sr12072	2	1	1
sr11585	2	1	2
sr16835	2	1	1
sr10767	2	1	2
sr13382	2	0	2
sr13342	2	0	1
sr16559	2	0	0
sr13341	2	1	1
sr16691	2	1	1
sr10069	2	1	2
sr10077	2	0	0
sr10073	2	0	2
sr16335	2	1	2
sr14040	2	1	1
sr13900	2	1	2
sr13901	2	0	1
sr13903	2	2	2
sr13869	2	0	0
sr10921	2	1	2
sr13615	2	0	0
sr13525	2	2	2
sr16476	2	2	2
sr02613	2	0	1
sr14220	2	1	1
sr14226	2	1	1
sr12315	2	1	1
sr16075	2	2	2
sr15127	2	1	2
sr15393	2	0	0
sr13834	2	2	2
sr11101	2	1	2
sr15092	2	0	2
sr14709	2	0	1
sr12902	2	0	1
sr13522	2	2	2
sr10848	2	1	1
sr14380	2	0	1
sr15026	2	0	0
sr15050	2	1	1

sr02614	1	1	1
sr14274	1	0	0
sr12318	1	0	0
sr11006	1	1	1
sr20007	1	1	1
sr10998.2	1	0	0
sr13836	1	1	1
sr11008.2	1	1	1
sr15840	1	1	1
sr15865	1	0	0
sr14685	1	0	0
sr06433	1	1	1
sr12705	1	0	0
sr12751	1	0	0
sr10605	1	0	0
sr12761	1	1	1
sr16880	1	1	1
sr16881	1	1	1
sr16555	1	0	0
sr13420	1	0	0
sr13434	1	1	1
sr16553	1	1	1
sr16558	1	1	1
sr13312	1	0	0
sr13418	1	1	1
sr16560	1	1	1
sr14387	1	0	0
sr14546	1	0	0
sr16211	1	1	1
sr16207	1	0	0
sr16204	1	0	1
sr10052.2	1	0	0
sr10057	1	0	0
sr10060	1	1	1
sr13897	1	0	1
sr13494	1	0	0
sr11102	1	0	1
sr15335	1	1	1
sr14946	1	1	1
sr15676	1	1	1
sr10318	1	0	0
sr10287	1	1	1

sr12175	1	0	0
sr12398	1	0	1
sr10286	1	1	1
sr15134	1	0	0
sr13102	1	0	1
sr13184	1	1	1
sr13081	1	1	1
sr15478	1	1	1
sr15533	1	0	0
sr10957	1	0	0
sr15890	1	1	1
sr14589	1	0	0
sr16823	1	1	1
sr16292	1	1	1
sr14083	1	1	1
sr13927	1	1	1
sr13976	1	0	0
sr16461	1	0	0
sr13458	1	0	0
sr13523	1	0	1
sr14797	1	1	1
sr15608	1	1	1
sr10289	1	0	0
sr13229	1	1	1
sr13007	1	1	1

Table S4.2: Expression pattern of one-to-one effector orthologues between *U. maydis* and *S. reilianum* in the hybrid (Sr_HYB/Um_HYB) and between the wild type (Sr_WT/Um_WT) were clustered at 3 dpi and 6 dpi into 8 distinct clusters (G1-G8).

Group	UMAG_id	SR_id	WT_3dpi	WT_6dpi	HYB_3dpi	HYB_6dpi
G1	UMAG_05704	sr16037	0.0	3.7	0.0	0.0
G1	UMAG_05222	sr13130	0.0	1.2	0.0	0.0
G1	UMAG_04114	sr14996	0.0	2.8	0.0	0.0
G1	UMAG_02727	sr13783	0.0	3.4	0.0	0.0
G1	UMAG_02080	sr13302	0.0	2.2	0.0	0.0
G1	UMAG_02006	sr12968	0.0	4.4	0.0	0.0
G1	UMAG_12356	sr12076	0.0	1.7	0.0	0.0
G1	UMAG_01937	sr10683	0.0	1.0	0.0	0.0
G1	UMAG_11839	sr12171	0.0	3.0	0.0	0.0
G1	UMAG_11562	sr15890	0.0	1.7	0.0	0.0
G1	UMAG_11403	sr13484	0.0	1.8	0.0	0.0
G1	UMAG_10881	sr12878	0.0	2.0	0.0	0.0

G1	UMAG_10657	sr14327	0.0	2.1	0.0	0.0
G1	UMAG_10640	sr11116	0.0	2.2	0.0	0.0
G1	UMAG_10514	sr15283	0.0	1.4	0.0	0.0
G1	UMAG_10208	sr16353	0.0	1.9	0.0	0.0
G1	UMAG_06456	sr16897	0.0	4.8	0.0	0.0
G1	UMAG_06119	sr16758	0.0	3.0	0.0	0.0
G1	UMAG_06118	sr16762	0.0	1.6	0.0	0.0
G1	UMAG_06112	sr16735	0.0	4.4	0.0	0.0
G1	UMAG_05774	sr16106	0.0	4.2	0.0	0.0
G1	UMAG_05303	sr20012	0.0	4.3	0.0	0.0
G1	UMAG_04740	sr15615	0.0	1.3	0.0	0.0
G1	UMAG_03065	sr14124	0.0	1.7	0.0	0.0
G1	UMAG_03024	sr14076	0.0	4.0	0.0	0.0
G1	UMAG_02922	sr13977	0.0	1.6	0.0	0.0
G1	UMAG_02212	sr10799	0.0	2.3	0.0	0.0
G1	UMAG_01854	sr10554	0.0	2.4	0.0	0.0
G1	UMAG_01604	sr12670	0.0	2.9	0.0	0.0
G1	UMAG_12316	sr13431	1.1	1.2	0.0	0.0
G1	UMAG_11765	sr00094.2	1.1	0.0	0.0	0.0
G1	UMAG_05227	sr13136	1.3	0.0	0.0	0.0
G1	UMAG_06027	sr16652	1.4	0.0	0.0	0.0
G1	UMAG_01802	sr12879	1.5	1.1	0.0	0.0
G1	UMAG_11464	sr13312	1.6	0.0	0.0	0.0
G1	UMAG_03923	sr14828	1.8	1.4	0.0	0.0
G1	UMAG_00446	sr10116	1.9	2.4	0.0	0.0
G1	UMAG_04044	sr14951	1.9	0.0	0.0	0.0
G1	UMAG_01888	sr10607	1.9	1.6	0.0	0.0
G1	UMAG_10587	sr12255	2.1	0.0	0.0	0.0
G1	UMAG_02231	sr13420	2.1	0.0	0.0	0.0
G1	UMAG_02071	sr13292	2.2	2.3	0.0	0.0
G1	UMAG_00567	sr11845	2.3	1.9	0.0	0.0
G1	UMAG_05708	sr16040	2.5	3.0	0.0	0.0
G1	UMAG_04145	sr14084	2.8	0.0	0.0	0.0
G1	UMAG_04557	sr13615	3.1	0.0	0.0	0.0
G1	UMAG_00876	sr12165	4.4	4.2	0.0	0.0
G1	UMAG_02758	sr13813	4.9	4.4	0.0	0.0
G2	UMAG_03807	sr14709	0.0	3.7	0.0	-1.0
G2	UMAG_01022	sr12315	0.0	1.1	0.0	-1.4
G2	UMAG_10632	sr14171	0.0	1.6	0.0	-2.6
G2	UMAG_00723	sr12012	0.0	1.0	-1.5	0.0
G2	UMAG_03860	sr14762	1.3	0.0	0.0	-1.1
G2	UMAG_10221	sr16409	2.5	2.2	0.0	-1.9

G2	UMAG_01204	sr10279	3.3	0.0	0.0	-2.3
G3	UMAG_10554	sr10052.2	-10.3	0.0	0.0	0.0
G3	UMAG_11417	sr11000.2	-7.5	-6.6	0.0	0.0
G3	UMAG_02294	sr13491	-6.6	0.0	0.0	0.0
G3	UMAG_02295	sr13492	-5.8	-5.2	0.0	0.0
G3	UMAG_05318	sr10075	-5.4	-9.4	0.0	0.0
G3	UMAG_03232	sr14226	-4.4	-2.8	0.0	0.0
G3	UMAG_05964	sr16592	-4.2	-4.5	0.0	0.0
G3	UMAG_06075	sr16700	-3.6	0.0	0.0	0.0
G3	UMAG_02119	sr13344	-2.6	-5.8	0.0	0.0
G3	UMAG_10055	sr13345	-2.3	-3.4	0.0	0.0
G3	UMAG_02473	sr10916.2	-2.0	-3.7	0.0	0.0
G3	UMAG_05780	sr16112	-1.9	-3.3	0.0	0.0
G3	UMAG_00411	sr11775	-1.9	-7.2	0.0	0.0
G3	UMAG_05731	sr16064	-1.9	-2.7	0.0	0.0
G3	UMAG_00628	sr11908	-1.8	-3.6	0.0	0.0
G3	UMAG_05931	sr16555	-1.4	0.0	0.0	0.0
G3	UMAG_01297	sr10429.2	-1.3	-3.4	0.0	0.0
G3	UMAG_11763	sr15573	0.0	-2.8	0.0	0.0
G3	UMAG_11540	sr15523	0.0	-1.1	0.0	0.0
G3	UMAG_12197	sr13927	0.0	-2.1	0.0	0.0
G3	UMAG_11715	sr11032	0.0	-1.7	0.0	0.0
G3	UMAG_11586	sr16119	0.0	-1.9	0.0	0.0
G3	UMAG_10831	sr14293	0.0	-1.4	0.0	0.0
G3	UMAG_05926	sr16549	0.0	-2.9	0.0	0.0
G3	UMAG_05781	sr16113	0.0	-2.0	0.0	0.0
G3	UMAG_05528	sr16207	0.0	-1.0	0.0	0.0
G3	UMAG_05319	sr10073	0.0	-5.6	0.0	0.0
G3	UMAG_05301	sr10055	0.0	-7.9	0.0	0.0
G3	UMAG_04816	sr15690	0.0	-3.0	0.0	0.0
G3	UMAG_04318	sr15204	0.0	-1.5	0.0	0.0
G3	UMAG_03563	sr14557	0.0	-4.5	0.0	0.0
G3	UMAG_03201	sr11100	0.0	-3.0	0.0	0.0
G3	UMAG_02981	sr14040	0.0	-1.6	0.0	0.0
G3	UMAG_02921	sr13976	0.0	-1.3	0.0	0.0
G3	UMAG_02239	sr13434	0.0	-1.1	0.0	0.0
G3	UMAG_02011	sr12972	0.0	-3.5	0.0	0.0
G3	UMAG_01957	sr10711.2	0.0	-2.0	0.0	0.0
G3	UMAG_01014	sr12321	0.0	-1.8	0.0	0.0
G3	UMAG_00154	sr11500	0.0	-2.4	0.0	0.0
G4	UMAG_02538	sr20007	-12.1	-6.6	0.0	4.7
G4	UMAG_05306	sr10059	-6.7	-7.0	4.9	3.9

G4	UMAG_03751	sr11236.2	-6.3	-5.0	0.0	2.2
G4	UMAG_04815	sr15688	-6.1	-5.7	0.0	4.8
G4	UMAG_10553	sr10051	-5.9	-5.6	0.0	1.7
G4	UMAG_02535	sr10996.2	-5.1	-3.4	8.2	7.9
G4	UMAG_05312	sr20014	-3.6	-4.5	0.0	4.0
G4	UMAG_03749	sr11234.2	-3.6	-6.3	5.2	2.3
G4	UMAG_03154	sr14196	-3.5	-2.2	2.7	0.0
G4	UMAG_10556	sr10060	-3.4	-4.1	0.0	2.0
G4	UMAG_02297	sr13494	-3.2	-2.2	4.0	6.0
G4	UMAG_02533	sr10994.2	-3.2	-2.0	4.6	4.5
G4	UMAG_01237	sr10312	-3.1	-2.3	2.7	3.2
G4	UMAG_02298	sr13495	-2.5	-3.2	0.0	4.0
G4	UMAG_02135	sr13361	-2.1	-1.2	5.5	3.2
G4	UMAG_05295	sr10050	-1.6	-1.9	3.2	4.4
G4	UMAG_11193	sr16445	-1.5	-2.4	0.0	2.6
G4	UMAG_04038	sr14940	-1.5	-3.1	6.0	4.7
G4	UMAG_12226	sr14368	-1.4	-2.6	0.0	1.6
G4	UMAG_00027	sr00846.2	-1.2	-1.7	0.0	1.1
G4	UMAG_03105	sr14168	-1.2	-3.0	1.1	1.2
G4	UMAG_11060	sr14941	-1.1	-2.5	1.8	2.9
G4	UMAG_02299	sr13496	0.0	-1.7	7.2	6.4
G4	UMAG_02851	sr13902	0.0	-1.4	4.4	4.0
G4	UMAG_02296	sr13493	0.0	-2.9	3.4	3.8
G4	UMAG_00054	sr11385	0.0	-1.0	2.8	2.5
G4	UMAG_01977	sr12937	0.0	-1.2	2.3	2.8
G4	UMAG_10030	sr11472	0.0	-1.5	2.2	2.7
G4	UMAG_01945	sr10702	0.0	-1.8	2.1	1.9
G4	UMAG_10756	sr16171	0.0	-1.1	2.0	2.7
G4	UMAG_00715	sr12002	0.0	-1.5	2.0	2.7
G4	UMAG_00781	sr12072	0.0	-1.4	1.9	4.1
G4	UMAG_01301	sr10432.2	0.0	-1.8	1.9	1.2
G4	UMAG_00538	sr11817	0.0	-2.2	1.7	1.7
G4	UMAG_01829	sr12911	0.0	-2.1	1.7	2.3
G4	UMAG_01130	sr12431	0.0	-1.7	1.7	2.1
G4	UMAG_12330	sr16778	0.0	-2.0	1.6	2.0
G4	UMAG_03223	sr14220	0.0	-2.6	1.5	1.7
G4	UMAG_05046	sr15930	0.0	-2.2	1.4	0.0
G4	UMAG_05097	sr12999	0.0	-3.9	1.1	1.1
G4	UMAG_11940	sr17138	0.0	-2.9	0.0	1.0
G4	UMAG_11415	sr20006	0.0	-1.7	0.0	5.6
G4	UMAG_10067	sr10759	0.0	-1.4	0.0	1.4
G4	UMAG_10000	sr06444	0.0	-1.7	0.0	1.7

G4	UMAG_04422	sr15309	0.0	-1.3	0.0	1.6
G4	UMAG_04343	sr15230	0.0	-1.9	0.0	1.1
G4	UMAG_04039	sr14946	0.0	-1.4	0.0	3.3
G4	UMAG_03274	sr14274	0.0	-1.2	0.0	1.9
G4	UMAG_02826	sr13869	0.0	-1.1	0.0	1.6
G4	UMAG_01375	sr10529	0.0	-3.0	0.0	1.4
G4	UMAG_01299	sr10431.2	0.0	-2.3	0.0	1.3
G4	UMAG_01241	sr10318	0.0	-1.9	0.0	1.3
G5	UMAG_11002	sr16823	0.0	4.8	7.0	7.0
G5	UMAG_11070	sr14401	0.0	2.6	5.3	3.8
G5	UMAG_10536	sr15342	0.0	1.8	0.0	3.0
G5	UMAG_01640	sr12708	0.0	1.8	0.0	1.2
G5	UMAG_01377	sr10532	1.2	0.0	0.0	1.8
G5	UMAG_11062	sr14948	1.2	0.0	1.5	2.5
G5	UMAG_01774	sr12852	1.2	0.0	0.0	1.4
G5	UMAG_01788	sr12866	1.4	0.0	1.3	1.7
G5	UMAG_10493	sr14660	1.5	1.1	0.0	1.1
G5	UMAG_03615	sr11165	1.5	0.0	1.9	1.5
G5	UMAG_01690	sr12761	1.6	-1.0	2.1	1.6
G5	UMAG_01987	sr12947	1.6	0.0	3.0	3.6
G5	UMAG_00695	sr11983	1.6	0.0	1.9	2.5
G5	UMAG_10972	sr16775	1.6	0.0	2.9	3.7
G5	UMAG_02430	sr10848	1.7	0.0	2.7	1.9
G5	UMAG_02853	sr13904	1.7	0.0	1.3	3.1
G5	UMAG_00795	sr12087	1.8	-1.3	2.8	3.2
G5	UMAG_04040	sr14947	1.8	0.0	4.4	4.1
G5	UMAG_12313	sr16075	1.9	2.1	3.6	5.3
G5	UMAG_01547	sr12619	2.0	2.0	2.2	1.4
G5	UMAG_02510	sr10957	2.1	1.7	0.0	1.8
G5	UMAG_01855	sr10555	2.3	2.5	1.4	1.1
G5	UMAG_01734	sr12809	2.3	1.1	3.2	4.1
G5	UMAG_05302	sr10057	2.4	0.0	9.1	9.2
G5	UMAG_02740	sr13799	2.4	2.7	0.0	1.2
G5	UMAG_04247	sr15137	2.4	0.0	2.3	0.0
G5	UMAG_05861	sr16482	2.5	1.2	3.9	4.4
G5	UMAG_05223	sr13131	2.6	0.0	2.4	3.1
G5	UMAG_01234	sr10308	2.7	2.4	1.9	3.0
G5	UMAG_06050	sr16674	2.7	1.7	0.0	1.5
G5	UMAG_05229	sr13138	2.7	1.9	0.0	1.2
G5	UMAG_12233	sr14508	2.8	3.2	2.3	4.2
G5	UMAG_00064	sr11394	4.0	5.2	2.1	2.7
G5	UMAG_05562	sr16247	4.0	2.1	0.0	1.8

G5	UMAG_10816	sr12627	4.1	2.0	3.1	2.3
G5	UMAG_10186	sr13060	4.1	5.6	0.0	1.3
G5	UMAG_06440	sr16877	4.7	2.8	4.4	4.1
G5	UMAG_02111	sr13333	5.1	6.0	0.0	2.9
G5	UMAG_04433	sr15320	6.9	5.0	0.0	4.7
G5	UMAG_03551	sr14544	7.7	6.4	5.8	5.9
G6	UMAG_05300	sr10054	-10.6	-10.6	0.0	-6.0
G6	UMAG_05928	sr16551	-8.4	-10.3	0.0	-4.2
G6	UMAG_02196	sr10770	-5.6	-7.9	-1.6	-1.3
G6	UMAG_03381	sr14380	-5.3	-5.3	0.0	-8.0
G6	UMAG_02229	sr13418	-5.0	-7.3	-4.8	-3.0
G6	UMAG_05104	sr13007	-4.9	-6.6	0.0	-7.8
G6	UMAG_06073	sr16703	-4.9	-3.4	0.0	-3.8
G6	UMAG_04503	sr15386	-4.3	-3.9	0.0	-1.5
G6	UMAG_00182	sr11530	-3.9	-1.7	0.0	-2.5
G6	UMAG_03023	sr14075	-3.7	-2.2	-3.1	-5.0
G6	UMAG_01302	sr20001	-3.2	-4.7	-1.8	-1.4
G6	UMAG_15089	sr12886	-3.2	-4.2	-4.3	-5.5
G6	UMAG_06120	sr16757	-3.0	-2.1	0.0	-2.3
G6	UMAG_03416	sr12115	-3.0	-2.1	0.0	-2.0
G6	UMAG_04248	sr15138	-3.0	-2.9	0.0	-3.9
G6	UMAG_10418	sr15147	-2.7	-4.6	-2.5	-1.3
G6	UMAG_04400	sr15288	-2.4	-3.1	-2.3	-3.8
G6	UMAG_01750	sr12826	-2.1	-2.2	-3.7	-4.8
G6	UMAG_00913	sr12211	-1.9	-3.4	-2.0	-1.4
G6	UMAG_00837	sr12124	-1.9	-1.9	0.0	-2.5
G6	UMAG_02852	sr13903	-1.3	-3.3	0.0	-2.3
G6	UMAG_02293	sr13490	-1.2	-4.4	-1.1	0.0
G6	UMAG_12123	sr12271	0.0	-1.1	0.0	-1.3
G6	UMAG_11317	sr10537	0.0	-1.2	0.0	-1.9
G6	UMAG_06190	sr11305	0.0	-3.3	0.0	-3.3
G6	UMAG_05305	sr10058	0.0	-12.7	0.0	-5.8
G6	UMAG_04533	sr15417	0.0	-1.4	0.0	-2.6
G6	UMAG_03947	sr14853	0.0	-1.0	0.0	-1.7
G6	UMAG_03924	sr14829	0.0	-4.4	0.0	-4.8
G6	UMAG_03392	sr14504	0.0	-4.7	0.0	-3.7
G6	UMAG_03246	sr14242	0.0	-1.8	0.0	-1.8
G6	UMAG_02597	sr13637	0.0	-2.4	0.0	-2.6
G6	UMAG_00144	sr11488	0.0	-1.7	0.0	-1.9
G6	UMAG_00102	sr11441	0.0	-1.1	0.0	-5.8
G6	UMAG_04708	sr15584	0.0	-3.2	-1.1	0.0
G6	UMAG_03977	sr14879	0.0	-1.1	-1.2	-1.9

G6	UMAG_01298	sr10430.2	0.0	-3.5	-1.2	0.0
G6	UMAG_06332	sr13229	0.0	-2.1	-1.4	-2.4
G6	UMAG_04309	sr15193	0.0	-3.1	-1.7	-2.8
G6	UMAG_10274	sr10650	0.0	-1.4	-1.9	-4.1
G6	UMAG_12007	sr15758	0.0	-2.2	-2.8	-2.6
G6	UMAG_12258	sr15146	0.0	-7.0	-4.0	-4.3
G6	UMAG_05604	sr16292	0.0	-5.1	-4.0	-4.3
G6	UMAG_03382	sr14381	0.0	-4.6	-7.1	-5.6
G7	UMAG_05927	sr16550	0.0	0.0	8.8	7.0
G7	UMAG_05548	sr16230	0.0	0.0	4.5	6.0
G7	UMAG_05314	sr10069	0.0	0.0	4.3	5.0
G7	UMAG_03585	sr00798.2	0.0	0.0	3.6	1.3
G7	UMAG_04032	sr14937	0.0	0.0	2.8	4.1
G7	UMAG_12216	sr14222	0.0	0.0	2.4	3.6
G7	UMAG_02523	sr10982	0.0	0.0	1.3	1.9
G7	UMAG_01820	sr12897	0.0	0.0	1.2	2.5
G7	UMAG_04915	sr15792	0.0	0.0	1.1	0.0
G7	UMAG_06158	sr11265	0.0	0.0	0.0	1.0
G7	UMAG_11931	sr13816	0.0	0.0	0.0	6.6
G7	UMAG_11362	sr12780	0.0	0.0	0.0	2.6
G8	UMAG_12184	sr13456	0.0	0.0	0.0	-2.3
G8	UMAG_10676	sr15597	0.0	0.0	0.0	-1.6
G8	UMAG_10091	sr11646	0.0	0.0	0.0	-1.5
G8	UMAG_06064	sr16690	0.0	0.0	0.0	-1.2
G8	UMAG_04641	sr15529	0.0	0.0	0.0	-1.5
G8	UMAG_03822	sr14724	0.0	0.0	0.0	-1.4
G8	UMAG_01823	sr12902	0.0	0.0	0.0	-1.9
G8	UMAG_01501	sr12557	0.0	0.0	0.0	-1.3
G8	UMAG_00235	sr11587	0.0	0.0	0.0	-2.2
G8	UMAG_12127	sr12428	0.0	0.0	0.0	-1.7
G8	UMAG_11910	sr13265	0.0	0.0	0.0	-2.0
G8	UMAG_11649	sr12452	0.0	0.0	0.0	-1.6
G8	UMAG_10068	sr10755	0.0	0.0	0.0	-2.6
G8	UMAG_06255	sr16785	0.0	0.0	0.0	-4.1
G8	UMAG_06157	sr11263	0.0	0.0	0.0	-1.8
G8	UMAG_05703	sr16036	0.0	0.0	0.0	-1.4
G8	UMAG_05680	sr16013	0.0	0.0	0.0	-1.1
G8	UMAG_05036	sr15917	0.0	0.0	0.0	-2.0
G8	UMAG_04630	sr15514	0.0	0.0	0.0	-1.1
G8	UMAG_04508	sr15393	0.0	0.0	0.0	-1.5
G8	UMAG_03689	sr14635	0.0	0.0	0.0	-2.8
G8	UMAG_03411	sr14403	0.0	0.0	0.0	-3.2

G8	UMAG_03076	sr14135	0.0	0.0	0.0	-1.6
G8	UMAG_02611	sr13650	0.0	0.0	0.0	-1.6
G8	UMAG_01786	sr12864	0.0	0.0	0.0	-1.0
G8	UMAG_01632	sr12700	0.0	0.0	0.0	-1.4
G8	UMAG_01236	sr10311	0.0	0.0	0.0	-5.6
G8	UMAG_01213	sr10289	0.0	0.0	0.0	-2.3
G8	UMAG_00330	sr11681	0.0	0.0	0.0	-2.6
G8	UMAG_11915	sr13303	0.0	0.0	-1.1	0.0
G8	UMAG_00961	sr12257	0.0	0.0	-1.2	-1.7
G8	UMAG_12205	sr14091	0.0	0.0	-1.3	0.0
G8	UMAG_06218	sr11346	0.0	0.0	-1.4	-1.8
G8	UMAG_04696	sr15575	0.0	0.0	-1.4	-1.1
G8	UMAG_11303	sr10270	0.0	0.0	-1.5	0.0
G8	UMAG_01851	sr12933	0.0	0.0	-1.5	-2.8
G8	UMAG_10975	sr16780	0.0	0.0	-1.8	-2.3
G8	UMAG_10861	sr16576	0.0	0.0	-1.8	-1.2
G8	UMAG_12175	sr10635.2	0.0	0.0	-3.3	-2.0

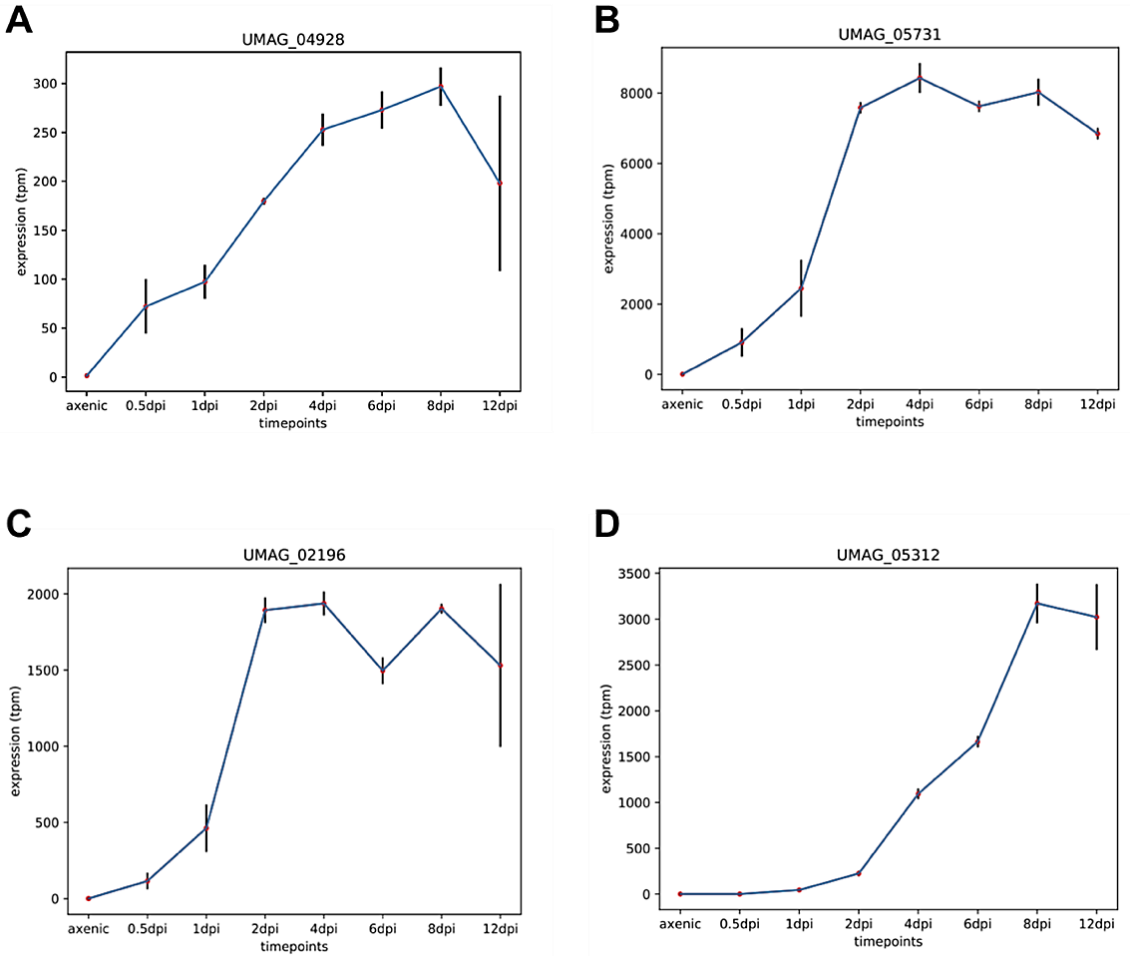

Figure S4.4: Expression patterns of different *U. maydis* promoters for the overexpression of *hdp2*. **(A)** Expression pattern of *Umhdp2*, **(B)** *Umcmu1,* and two effector genes, **(C)** *UMAG_02196* and **(D)** *UMAG_05312.*

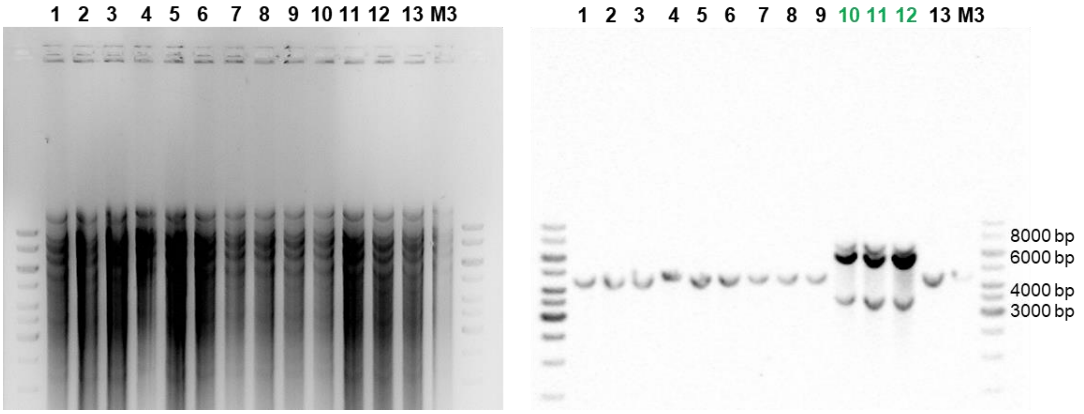

Figure S4.5: Southern blot of Um_Smt_proCmu1_*Srhdp2*_2xHA. DNA was digested with SacI. Expected sizes: WT: 3255 bp, Single integration: 7381 bp + 3652 bp, Multiple integration: 7381 bp + 6277 bp + 3652 bp. Positive transformants are marked in green. M3: Um_Smt control.

Publication Licenses – Figures

49 Spadina Ave. Suite 200
Toronto ON M5V 2J1 Canada
www.biorender.com

Confirmation of Publication and Licensing Rights

June 16th, 2024
Science Suite Inc.

Subscription: *Lab*
Agreement number: *DZ26Y5P5FD*
Journal name: *PhD thesis*

To whom this may concern,

This document is to confirm that Gunther Doehlemann has been granted a license to use the BioRender content, including icons, templates and other original artwork, appearing in the attached completed graphic pursuant to BioRender's Academic License Terms. This license permits BioRender content to be sublicensed for use in journal publications.

All rights and ownership of BioRender content are reserved by BioRender. All completed graphics must be accompanied by the following citation: "Created with BioRender.com".

BioRender content included in the completed graphic is not licensed for any commercial uses beyond publication in a journal. For any commercial use of this figure, users may, if allowed, recreate it in BioRender under an Industry BioRender Plan.

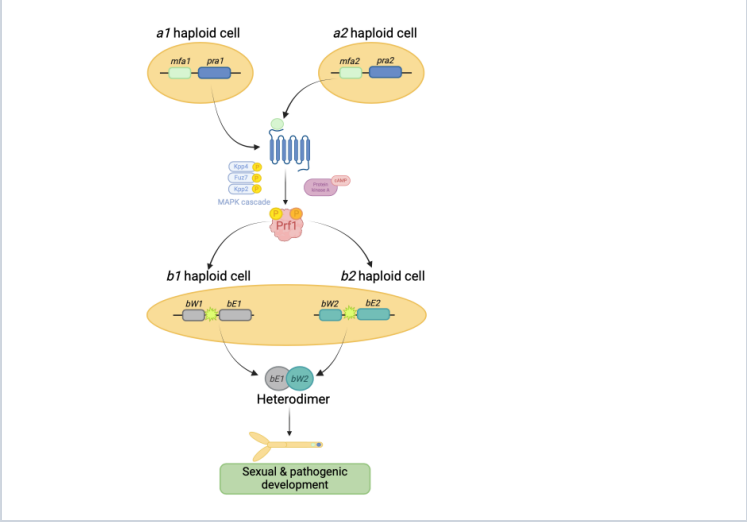

For any questions regarding this document, or other questions about publishing with BioRender refer to our BioRender Publication Guide, or contact BioRender Support at support@biorender.com.

49 Spadina Ave. Suite 200
Toronto ON M5V 2J1 Canada
www.biorender.com

Confirmation of Publication and Licensing Rights

June 16th, 2024
Science Suite Inc.

Subscription:	*Lab*
Agreement number:	*QP26Y5PAPD*
Journal name:	*PhD thesis*

To whom this may concern,

This document is to confirm that Gunther Doehlemann has been granted a license to use the BioRender content, including icons, templates and other original artwork, appearing in the attached completed graphic pursuant to BioRender's Academic License Terms. This license permits BioRender content to be sublicensed for use in journal publications.

All rights and ownership of BioRender content are reserved by BioRender. All completed graphics must be accompanied by the following citation: "Created with BioRender.com".

BioRender content included in the completed graphic is not licensed for any commercial uses beyond publication in a journal. For any commercial use of this figure, users may, if allowed, recreate it in BioRender under an Industry BioRender Plan.

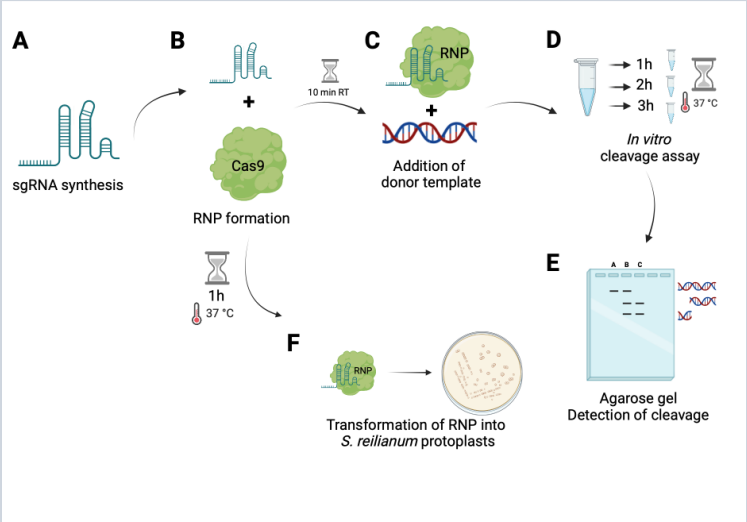

For any questions regarding this document, or other questions about publishing with BioRender refer to our BioRender Publication Guide, or contact BioRender Support at support@biorender.com.

49 Spadina Ave. Suite 200
Toronto ON M5V 2J1 Canada
www.biorender.com

Confirmation of Publication and Licensing Rights

June 16th, 2024
Science Suite Inc.

Subscription:	*Lab*
Agreement number:	*QH26Y4MHUW*
Journal name:	*PhD thesis*

To whom this may concern,

This document is to confirm that Gunther Doehlemann has been granted a license to use the BioRender content, including icons, templates and other original artwork, appearing in the attached completed graphic pursuant to BioRender's Academic License Terms. This license permits BioRender content to be sublicensed for use in journal publications.

All rights and ownership of BioRender content are reserved by BioRender. All completed graphics must be accompanied by the following citation: "Created with BioRender.com".

BioRender content included in the completed graphic is not licensed for any commercial uses beyond publication in a journal. For any commercial use of this figure, users may, if allowed, recreate it in BioRender under an Industry BioRender Plan.

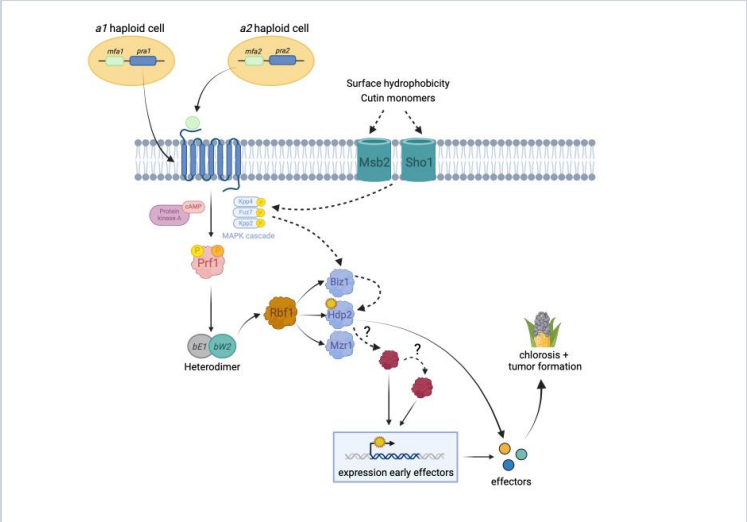

For any questions regarding this document, or other questions about publishing with BioRender refer to our BioRender Publication Guide, or contact BioRender Support at support@biorender.com.

49 Spadina Ave. Suite 200
Toronto ON M5V 2J1 Canada
www.biorender.com

Confirmation of Publication and Licensing Rights

June 16th, 2024
Science Suite Inc.

Subscription:	*Lab*
Agreement number:	*JM26Y58ZSC*
Journal name:	*PhD thesis*

To whom this may concern,

This document is to confirm that Gunther Doehlemann has been granted a license to use the BioRender content, including icons, templates and other original artwork, appearing in the attached completed graphic pursuant to BioRender's Academic License Terms. This license permits BioRender content to be sublicensed for use in journal publications.

All rights and ownership of BioRender content are reserved by BioRender. All completed graphics must be accompanied by the following citation: "Created with BioRender.com".

BioRender content included in the completed graphic is not licensed for any commercial uses beyond publication in a journal. For any commercial use of this figure, users may, if allowed, recreate it in BioRender under an Industry BioRender Plan.

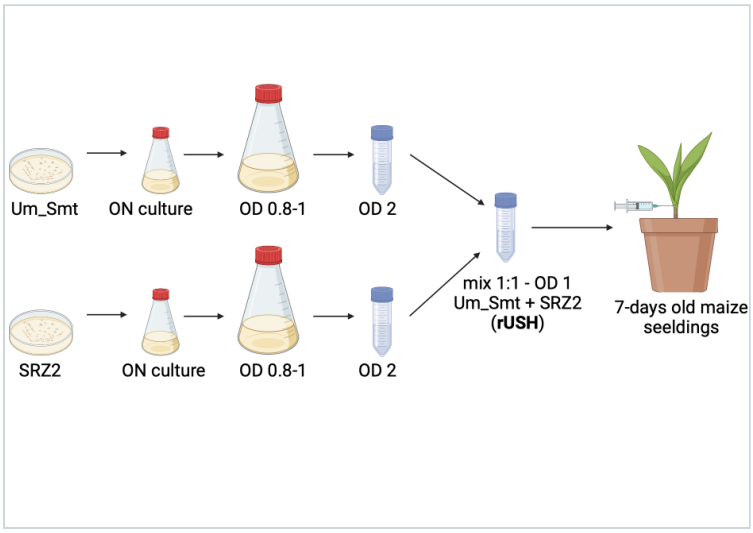

For any questions regarding this document, or other questions about publishing with BioRender refer to our BioRender Publication Guide, or contact BioRender Support at support@biorender.com.

49 Spadina Ave. Suite 200
Toronto ON M5V 2J1 Canada
www.biorender.com

Confirmation of Publication and Licensing Rights

June 16th, 2024
Science Suite Inc.

Subscription:	*Lab*
Agreement number:	*XO26Y5PCZF*
Journal name:	*PhD thesis*

To whom this may concern,

This document is to confirm that Gunther Doehlemann has been granted a license to use the BioRender content, including icons, templates and other original artwork, appearing in the attached completed graphic pursuant to BioRender's Academic License Terms. This license permits BioRender content to be sublicensed for use in journal publications.

All rights and ownership of BioRender content are reserved by BioRender. All completed graphics must be accompanied by the following citation: "Created with BioRender.com".

BioRender content included in the completed graphic is not licensed for any commercial uses beyond publication in a journal. For any commercial use of this figure, users may, if allowed, recreate it in BioRender under an Industry BioRender Plan.

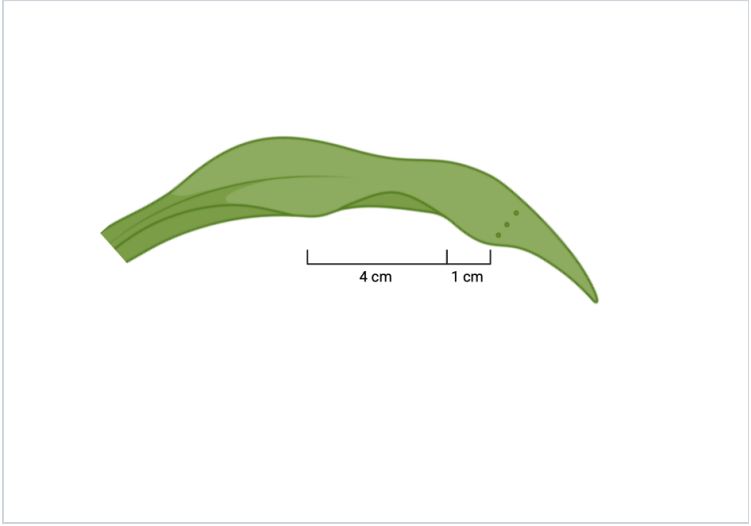

For any questions regarding this document, or other questions about publishing with BioRender refer to our BioRender Publication Guide, or contact BioRender Support at support@biorender.com.

List of Figures

Chapter 1

Chapter 2

Chapter 3

Chapter 4

Chapter 5

Chapter 6

Delimitation of own contribution

- **Dr. Weiliang Zuo** generated the Um_Smt mutants (FB1_*Sra1b1* #1 and FB1_*Sra1b1* #2) (Chapter 3) and performed the Southern blot of the SRZ2 strain harboring the single integration of pro^{OTEF}-GFP in the *ip* locus of *S. reilianum* (see Chapter 2).
- **Dr. Georgios Saridis** performed the phylogenetic analysis for Hdp2 and conducted the motif enrichment analysis (Chapter 4).
- **Samodya K. Jayasinghe** helped to clone the cluster 19A complementation 2 construct (Chapter 3).
- **Maurice König** helped with the identification of maize genes in the RNA-seq data of Hdp2 (Chapter 4).
- **Novogene** conducted the bioinformatical analysis of the Hdp2 RNA-seq experiment (Chapter 4)

During the course of my dissertation, I was responsible for the supervision of the following students, whose final theses contributed to this thesis:

Bachelor theses:

- **Katharina Fleckenstein (2021):** Optimization of CRISPR/Cas9 for genome editing in *Sporisorium reilianum*

Katharina Fleckenstein helped with the generation of the plasmid SRZ2_pOTEF_GFP, used for the single integration of GFP into the *ip* locus of *S. reilianum* (Chapter 2).

- **Kerstin R. Lehnen (2023):** Analysis of *Ustilago maydis* transcription factors and their role in fungal pathogenicity

Kerstin Lehnen generated three pCas9HF1 plasmids for the TF KOs in *U. maydis* (Chapter 3).

- **Katharina Stein (2024):** Regulation of Effector Gene Expression by Transcription Factor Hdp2 in *Ustilago maydis* and *Sporisorium reilianum*

Katharina Stein generated the *U. maydis* mutants for *Umhdp2* OE in the hybrid using the promoters of the effector genes *UMAG_02196* and *UMAG_05312* (Chapter 4).

Master thesis:

- **Vanessa Volz (2023):**
  Deletion and recombinant complementation of effector gene cluster 19A in *Sporisorium reilianum* using CRISPR/Cas9

Vanessa Volz generated the cluster 19A deletion and the complementation 1 plasmid for the *U. maydis* cluster 19A complementation in *S. reilianum*. She generated the KO of cluster 19A in *S. reilianum* and conducted the first complementation of Um19A in *S. reilianum*.

Danksagung

Zuerst möchte ich mich ganz herzlich bei Prof. Dr. Gunther Döhlemann für die Möglichkeit bedanken, meine Doktorarbeit in seinem Labor durchzuführen. Danke Gunther für deine ständige Hilfe, dein Vertrauen und die Möglichkeit, in den letzten 4,5 Jahren an verschiedenen Projekten zu arbeiten. Ich freue mich auf die kommenden Jahre!
Weiterhin würde ich gerne Prof. Dr. Bart Thomma danken, der die Zweitkorrektur meiner Dissertation übernimmt. Danke Bart für deine Ideen und die Diskussionen bezüglich meines Projektes in den TAC Meetings. Danke auch an Prof. Dr. Kay Hofmann für die Leitung der Prüfungskommision meiner Disputation.
Gerne möchte ich mich herzlich bei der gesamten AG Döhlemann für die tolle Arbeitsatmosphäre und die freundliche Aufnahme in die Arbeitsgruppe bedanken. Danke an Johana, Ute, Rapha und Jan, die für die Organisation des Labors unentbehrlich sind. Außerdem möchte ich mich bei meinen Studentinnen Kathi, Kerstin, Vanessa und Katharina bedanken. Ihr habt mit euren Abschlussarbeiten wesentlich zum Gelingen der Arbeit beigetragen.
Mein besonderer Dank gilt Weiliang, meiner wandelnden Wissensquelle! Danke Weiliang für deine Betreuung während meiner Promotion, deine Hilfe im Laboralltag, die Korrektur meiner Dissertation und danke für deine Freundschaft! Deine Unterstützung hat wesentlich zum Erfolg dieses Projektes beigetragen. Für die Unterstützung bei bioinformatischen Fragen würde ich gerne Jasper und Georgios danken. Von ganzem Herzen möchte ich mich bei meiner Kollegin und Freundin Sina bedanken! Danke für deine Hilfe im Laboralltag, aber noch mehr für die gemeinsamen Kaffeepausen, Organisationen sowie unsere „Dinner Dates“, Sis. Du hast die letzten 4 Jahre im Labor besonders gemacht! Danke auch an Sina’s bessere Hälfte – Philipp! Dank dir habe ich mein erstes FC Spiel im Kölner Stadion gesehen! Danke auch an Ruchi für unsere MadFungi Diskussionen, die gemeinsamen Mittagspausen sowie die lustigen Gespräche im Labor. Yoon Joo möchte ich besonders danken für die witzigen Momente im Labor, die gemeinsame Zeit auf der Konferenz in Asilomar sowie unseren Kurzurlaub in San Fransciso – Wir werden Tenderloin nie vergessen! Weiterhin würde ich mich gerne bei Daniel für seine positive Art, die Organisation von unseren Lab Hike’s sowie seine last minute Hilfe bei R bedanken!
Von Herzen würde ich mich gerne bei Anna und Andrea bedanken. Ihr habt die Doktorandenzeit - egal ob auf der Arbeit oder privat - unvergesslich gemacht! Danke auch an meine neuen labmates: Zarah und Niklas. Ein ganz besonderer Dank gilt Sarah, für das nächtliche Korrekturlesen meiner Arbeit sowie die Snacks während des Schreibens.

Last but not least, back to the roots! Ich möchte mich von ganzem Herzen bei meinen Freunden und bei meiner Familie in der Pfalz bedanken! Besonders bei Julian, Mike, Chris und Tanja!
Auch wenn wir uns in den letzten Jahren aufgrund der Distanz zu Köln weniger sehen konnten, habt ihr mich immer unterstützt, von der Schulzeit bis heute! Was soll man auch sagen...

#annerschdwoisannerschdunhaldnedwieindepalz

Besonders möchte ich meinen Eltern für ihre Unterstützung sowie ihre unendliche Liebe danken. Ich durfte immer meinen eigenen Weg gehen ohne Einschränkungen. Weiterhin möchte ich von Herzen meiner Schwester Meike danken, du bist schon immer ein Vorbild für mich und bist immer für mich da. Danke auch an meinen kleinen Sonnenschein Thorin, du machst jeden Tag mit deinem Lächeln etwas besser!
Abschließend möchte ich Maurice für seine positive Art, seine Unterstützung in allen Lebenslagen sowie seine Loyalität von Herzen danken. Du hast mein Leben in den letzten zwei Jahren maßgeblich bereichert und motivierst mich jeden Tag.

DANKE ❤️

Curriculum Vitae

Janina Werner

born on the 25th of June 1994 in Kaiserslautern, Germany

Education

02/2020 – 2024 **PhD program:** GSfBS – University of Cologne
Thesis: "A smut hybrid provides insights into the regulation of effector genes contributing to tumor formation of *Ustilago maydis*"
Supervisor: Prof. Dr. Gunther Döhlemann

07/2019 – 12/2019 Research Assistant, Technical University of Kaiserslautern

08/2019 – 10/2019 Collaboration Project at Aristoteles University of Thessaloniki
Supervisor: Prof. Dr. Matthias Hahn & Prof. Dr. George Karaoglanidis

03/2018 – 04/2018 Laboratory internship – Lebosol® Dünger GmbH, Sembach

10/2017 - 06/2019 **Master program:** Plant and Microbial Biotechnology, Technical University of Kaiserslautern
Thesis: „Etablierung von CRISPR/Cas9 für die Mutagenese in *Botrytis cinerea*"
Supervisor: Prof. Dr. Matthias Hahn

09/2017-11/2017 Research Assistant, Technical University of Kaiserslautern

10/2013 – 05/2017 **Bachelor program:** Biowissenschaften, Technical University of Kaiserslautern
Thesis: „Untersuchungen zur Funktion und Lokalisierung von VELVET--Proteinen in *Botrytis cinerea*"
Supervisor: Prof. Dr. Matthias Hahn

Publications

1. **Werner, J.**, Zuo, W. and Doehlemann, G. (2024). CRISPR/Cas9 Ribonucleoprotein-Mediated Mutagenesis in *Sporisorium reilianum*. Bio-protocol 14(8): e4978. DOI: 10.21769/BioProtoc.4978

2. Leisen, T., **Werner, J**., Pattar, P., Safari, N., Ymeri, E., Sommer, F., Schroda, M., Suárez, I., Collado, I. G., Scheuring, D., & Hahn, M. (2022). Multiple knockout mutants reveal a high redundancy of phytotoxic compounds contributing to necrotrophic pathogenesis of *Botrytis cinerea*. PLoS pathogens, 18(3), e1010367. https://doi.org/10.1371/journal.ppat.1010367

3. Leisen, T., Bietz, F., **Werner, J**., Wegner, A., Schaffrath, U., Scheuring, D., Willmund, F., Mosbach, A., Scalliet, G., & Hahn, M. (2020). CRISPR/Cas with ribonucleoprotein complexes and transiently selected telomere vectors allows highly efficient marker-free and multiple genome editing in *Botrytis cinerea*. PLoS pathogens, 16(8), e1008326. https://doi.org/10.1371/journal.ppat.1008326

References

1. Prof. Dr. Gunther Döhlemann
2. Prof. Dr. Matthias Hahn
3. Prof. Dr. George Karaoglanidis